

**Evolution of developmental regulation
in a simple multicellular life cycle**

Dissertation

in fulfilment of the requirements for the degree of

Doctor rerum naturalium (Dr. rer. nat.)

of the Faculty of Mathematics and Natural Sciences
at the Christian-Albrecht University of Kiel

Submitted by

Joanna Amelia Summers

Department of Microbial Population Biology
Max Planck Institute for Evolutionary Biology

Plön, 2023

First examiner: Prof. Dr. Paul Rainey

Second examiner: Prof. Dr. Tal Dagan

Date of the oral examination: 4th July 2023

Declaration:

I, *Joanna Amelia Summers*, hereby declare that apart from the guidance of my supervisors Prof. Dr. Paul Rainey and Dr. David Rogers, that the content and design of this thesis is entirely my own work. The design of a new life cycle experiment (Chapter III) was additionally carried out with the guidance of Postdoctoral researcher Dr. Daniel Rexin. The large-scale life cycle experiment (Chapter IV) was completed with assistance from technician Norma Rivera. This research work has not yet been published, and was not submitted partially or wholly as part of a doctoral degree to another examining body. The thesis was prepared with regard to the Rules of Good Scientific Practice of the German Research Foundation. I have not had any academic degree withdrawn.

Date: 23.05.2023

Signature:

A handwritten signature in black ink, appearing to be 'J. Summers', written in a cursive style.

Abstract

The evolution of multicellularity involved a transition in individuality from the level of the cell to the new hierarchical level of the collective, allowing the multicellular group to become a unit of selection in its own right. This transition required the emergence of Darwinian properties at the group-level (variation, reproduction & heredity), which cannot be assumed to simply transfer from the lower level. Most pertinent is the origin of a mechanism for collective-level reproduction, that may be envisioned with a nascent two-phase life cycle that transitions between the collective (soma-like) and individual cell (germ-like) dispersal phases. The bacterial model *Pseudomonas fluorescens* SBW25 has previously been used to demonstrate the experimental evolution of such a life cycle. When grown in a spatially structured environment the ancestral ‘smooth’ (SM) type colonises the broth, and rapidly diversifies to produce ‘wrinkly spreader’ (WS) mutants that colonise the surface. These WS types form a mat (or biofilm) at the air-liquid interface by the cooperative overproduction of a cellulosic polymer. The life cycle experiment (LCE) selected for lineages able to repeatedly transition between the SM individual & WS collective phases, and therefore the evolution of a developmental program. By virtue of a selective regime that used colony morphology as a proxy for adaptation to each phase, lineages were forced to transition by mutations that generated a stable phenotype outside of the selective environment. In this thesis, I investigate the potential for the evolution of a life cycle that relies on developmental regulation – that is a mechanism for transitioning between phenotypic states that does not rely on mutation.

As a first step, in Chapter II, I characterise an environmentally-responsive strain, that changes colony phenotype as observed with a shift in temperature: SM at 28°C & WS at 20°C. Having previously sequenced this strain, I reconstructed the mutations to identify those responsible for the ability to switch phenotype in response to the environment. This required minimal genetic manipulation, the phenotype switch occurred with only three point mutations – therefore is readily accessible to selection. I next worked to modify the LCE to allow for the evolution of developmental regulation. Chapter III describes the production of a revised experimental regime that eliminates use of the colony morphology proxy, with new methods of selection based on mat formation and dispersal by swimming motility. Results are provided from a pilot experiment, demonstrating rapid adaptation to the life cycle and the evolution of different strategies to transition – mutational, generalism & developmental. In Chapter IV the results of a large-scale experiment using the revised LCE regime are

presented, in which a decrease in extinction rate and major improvements to mat formation & motility were observed after only five life cycle generations. Sequencing of evolved lines revealed a number of unique strategies for developmental regulation of the life cycle. I show that certain evolved lineages had increased lineage fitness with no associated decrease to cell fitness; this trade-off breaking can be attributed to the capacity to modulate phenotype in response to the environment. This thesis highlights possible mechanisms of collective-level reproduction in nascent multicellular groups, and the evolution of developmental regulation of a simple life cycle by tuning the activation threshold of existing regulatory pathways, causing modification to environmental interactions.

Zusammenfassung

Die Evolution der Mehrzelligkeit beinhaltet einen Übergang von der Individualität einzelner Zellen zur neuen hierarchischen Ebene einer Gruppe, um es mehrzelligen Gruppen zu ermöglichen, eine eigenständige Selektionseinheit zu werden. Dieser Übergang erfordert die Entstehung darwinistischer Eigenschaften auf Gruppenebene (Variation, Fortpflanzung und Vererbung), von denen nicht angenommen werden kann, dass sie einfach von niedriger gestellten Evolutionstufen übernommen werden können. Am wichtigsten ist die Entwicklung eines Mechanismus für die Fortpflanzung auf Gruppenebene, die man sich mit einem im Entstehen begriffenen zweiphasigen Lebenszyklus vorstellen kann, der zwischen der kollektiven (soma-ähnlich) und der individuellen Zellausbreitungsphase (keim-ähnlich) hin und her wechselt. Das bakterielle Modellsystem *Pseudomonas fluorescens* SBW25 wurde bereits früher dazu verwendet, die experimentelle Evolution eines solchen Lebenszyklus zu zeigen. In einer räumlich strukturierten Umgebung kolonisiert der ursprüngliche „Smooth“ (SM) Typ sein Nährmedium und diversifiziert sich schnell zu „Wrinkly Spreader“ (WS) Mutanten, die die Oberfläche besiedeln können. Die WS-Typen bilden an der Schnittstelle zwischen Luft und Nährmedium eine Matte (oder Biofilm) aus, die aus der kooperativen Überproduktion von Zellulosepolymeren resultiert. Das Lebenszyklusexperiment (LCE) selektiert auf Abstammungslinien, die in der Lage sind, wiederholt zwischen der individuellen SM und der kollektiven WS Phase zu wechseln, und untersucht somit die Entstehung eines Entwicklungsprogramms. Auf Grund eines Selektionsregimes, das die Koloniemorphologie als indirektes Maß für die Anpassung an jede Phase verwendet, wurden die Abstammungslinien zu Übergängen durch Mutation gezwungen, die zu einem stabilen Phänotypen außerhalb der selektiven Umgebung führen. In dieser Doktorarbeit untersuche ich das Potenzial für die Evolution eines Lebenszyklus, der auf Entwicklungsregulierung basiert, das heißt, einen Mechanismus für den Übergang zwischen phänotypischen Zuständen, der nicht auf Mutation beruht.

In einem ersten Schritt charakterisiere ich in Kapitel II einen auf Umwelteinflüsse reagierenden Stamm, dessen Koloniephänotyp sich mit Temperaturverlagerungen verändert: SM bei 28°C und WS bei 20°C. Nach vorheriger Sequenzierung dieses Stammes habe ich die Mutationen rekonstruiert, die für die Fähigkeit verantwortlich sind, den Phänotyp als Reaktion auf die Umwelt zu verändern. Dies erforderte nur minimale genetische Manipulation, da sich der Phänotypwechsel mit nur drei Punktmutationen reproduzieren ließ

und somit für Selektion leicht zugänglich war. Als nächstes habe ich daran gearbeitet, das LCE zu modifizieren, um die Evolution der Entwicklungsregulation zu ermöglichen. In Kapitel III beschreibe ich ein überarbeitetes Versuchsregime, das die Verwendung der Koloniemorphologie als indirektes Maß eliminiert und eine neue Selektionsmethode basierend auf der Mattenbildung und der Ausbreitung durch Schwimmbewegung verwendet. Ergebnisse eines Pilotexperiments zeigen eine schnelle Anpassung an den Lebenszyklus und die Entwicklung verschiedener Übergangsstrategien: Mutationen, Generalismus und Entwicklung. In Kapitel IV werden die Ergebnisse eines groß angelegten Experiments unter Verwendung des überarbeiteten LCE Regimes vorgestellt, in welchem nach nur fünf Generationen ein Rückgang der Aussterberate und erhebliche Verbesserungen in der Mattenausbildung und Motilität beobachtet wurden. Die Sequenzierung der evolvierten Abstammungslinien ergab eine Reihe einzigartiger Strategien zur Entwicklungsregulierung des Lebenszyklus. Ich zeige, dass bestimmte evolvierte Abstammungslinien eine erhöhte Linienfitness aufweisen, ohne dass dies mit einer Verringerung der Zellfitness einherging. Das Überwinden dieses „Trade-offs“ kann auf die Fähigkeit zurückgeführt werden, den Phänotyp als Reaktion auf die Umwelt zu modulieren. Diese Doktorarbeit beleuchtet die möglichen Mechanismen der Reproduktion auf Gemeinschaftsebene in entstehenden multizellulären Gruppen und die Evolution der Entwicklungsregulation eines einfachen Lebenszyklus durch Einstellen der Aktivierungsschwelle bereits existierender Regulationspfade, was zu einer Veränderung der Interaktion mit der Umwelt führt.

Translated from English by Manuela Spagnuolo and Michael Sieber

Table of Contents

Abstract.....	2
Table of Contents.....	6
Chapter I: Introduction	
1.1 Evolution by natural selection.....	11
1.1.1 Darwinian populations.....	11
1.1.2 Hierarchical levels of organisation.....	11
1.1.3 Transitions in individuality.....	12
1.1.4 Major evolutionary transitions.....	12
1.2 The evolution of multicellular life.....	13
1.2.1 Advantages of multicellularity.....	14
1.2.2 Cooperation and conflict mediation.....	15
1.2.3 Nascent life cycles.....	16
1.2.4 The evolution of development.....	16
1.2.5 Ecological scaffolding.....	18
1.3 <i>Pseudomonas fluorescens</i> SBW25 model.....	18
1.3.1 Phenotypic cycling as a nascent life cycle.....	19
1.3.2 Basis of the WS phenotype.....	20
1.3.2.1 Wsp pathway.....	21
1.3.2.2 Aws pathway.....	23
1.3.2.3 Mws pathway.....	23
1.3.2.4 Alternative pathways & regulators.....	24
1.3.3 The life cycle experiment.....	24
1.3.3.1 Fitness decoupling.....	26
1.3.3.2 Evolution of a genetic switch.....	27
1.4 Aims of the current study.....	27
Chapter II: Characterisation of an environmentally-responsive genotype	
2.1 Environmentally-responsive strain – TSS-f6.....	29
2.1.1 Origin of TSS-f6.....	29
2.1.2 Phenotypic characterisation.....	30
2.2 Suppressor analysis of TSS-f6.....	32
2.2.1 <i>wsp</i> & <i>wss</i> operons and MMR system.....	33
2.2.2 <i>wspE</i> gene.....	33
2.2.3 <i>pflu5960</i> gene.....	35

2.2.4 <i>amrZ</i> gene.....	35
2.2.5 <i>pflu0479</i> gene.....	36
2.3 Mutational history of TSS-f6.....	37
2.3.1 TSS-f6 – <i>wspA</i> mutation.....	38
2.3.1.1 WspA conserved residues.....	38
2.3.1.2 Environmental sensing by WspA.....	39
2.3.1.3 Reversion of TSS-f6 <i>wspA</i> mutation.....	40
2.3.2 TSS-f6 – <i>dipA</i> mutation.....	41
2.3.3 f2 ancestor – <i>wspA</i> & <i>wspE</i> mutations.....	41
2.3.4 L17-mutS-WT ancestor – <i>wsp</i> mutations.....	42
2.3.4.1 WspF methylesterase.....	42
2.3.4.2 WspB scaffold protein.....	43
2.4 Deletion of identified candidate genes.....	43
2.4.1 WspE histidine kinase.....	44
2.4.1.1 Suppressor analysis of TSS-f6 <i>wspE</i> mutant.....	45
2.4.2 Cellulose synthase operon.....	47
2.4.3 Colonic acid operon.....	48
2.4.4 Pflu5960 PDE enzyme.....	50
2.4.4.1 Mutation of EAL motif.....	51
2.4.5 Suppressor analysis of <i>pflu5960</i> deletion mutants.....	52
2.4.5.1 WS phenotype suppression.....	52
2.4.5.2 Restoration of phenotype switch.....	55
2.4.5.3 SM phenotype suppression.....	56
2.4.6 AmrZ transcriptional regulator.....	59
2.4.7 Suppressor analysis of <i>amrZ</i> deletion mutants.....	60
2.4.7.1 WS phenotype suppression.....	61
2.4.7.2 Restoration of phenotype switch.....	63
2.5 Recreation of TSS-f6 mutations.....	65
2.5.1 f2 ancestor – <i>wspA</i> mutation.....	66
2.5.2 L17-mutS-WT – <i>wspE</i> & <i>wspA</i> mutations.....	67
2.5.3 SBW25 – <i>wspA</i> , <i>wspE</i> & <i>wspF</i> mutations.....	68
2.5.4 Combination of mutations.....	70
2.6 Revised model for TSS-f6 phenotype switch.....	71
2.6.1 SM phenotype at 28°C.....	73
2.6.2 WS phenotype at 20°C.....	74
2.6.3 Prospects for testing the model.....	74

Chapter III: Development of a new life cycle experiment

3.1 Motivation for revised life cycle experiment.....	76
--	-----------

3.1.1 Life cycle proceeding by mutation.....	76
3.1.2 Significance of environmentally-responsive strain.....	76
3.1.3 Two-phase life cycle in natural environment.....	77
3.1.4 Mat formation & swimming motility.....	78
3.1.3.1 Regulation by c-di-GMP signalling.....	79
3.2 New selective methods based on mat formation & motility.....	79
3.2.1 Mat formation screen.....	79
3.2.2 Swimming motility screen.....	80
3.2.2.1 Testing the efficiency of motility plates.....	82
3.3 Revised experimental regime.....	84
3.3.1 Phase I: Collective.....	84
3.3.2 Phase II: Dispersal.....	86
3.4 Trial experiment using the new regime.....	86
3.4.1 Genealogy over five generations.....	87
3.4.2 Extinction rate & seed phenotype.....	88
3.4.3 Phase I – phenotypic analysis.....	89
3.4.4 Phase II – phenotypic analysis.....	90
3.5 Strategies to transition through the life cycle.....	91
3.5.1 Mutational strategy.....	93
3.5.2 Non-mutational strategies.....	94
3.5.2.1 Generalist strategy.....	95
3.5.2.2 Developmental strategy.....	96
3.6 Analysis of select evolved lines.....	98
3.6.1 Phenotypic characterisation.....	99
3.6.2. Level of c-di-GMP in different environments.....	101
3.6.3 Lineage-level fitness.....	104
3.6.3.1 Mutations obtained during additional generation.....	105
3.7 Conclusions from the trial experiment.....	106

Chapter IV: Evolution of developmental regulation in a simple multicellular life cycle

4.1 Large-scale life cycle experiment.....	109
4.1.1 Genealogy over five generations.....	109
4.1.2 Rapid decrease in extinction rate.....	111
4.1.2.1 Extinction rate within replicate racks.....	112
4.1.3 Improvement in collective & individual traits.....	113
4.1.4 Fixation of high fitness lineages.....	114
4.2 Strategies to transition through the life cycle.....	116

4.2.1 Geneology of different strategies.....	118
4.2.2 Mutational strategy.....	119
4.2.3 Hypermutation strategy.....	121
4.2.4 Developmental strategy – single mutant genotypes.....	121
4.2.4.1 <i>bifA</i> mutations.....	122
4.2.4.2 <i>awsR</i> & <i>awsX</i> mutations.....	124
4.2.5 Developmental strategy – double & triple mutant genotypes.....	127
4.2.5.1 <i>awsR-pflu0956</i> mutant.....	128
4.2.5.2 <i>awsR-mwsR</i> mutants.....	129
4.2.5.3 <i>awsR-mwsR-dipA</i> mutant.....	131
4.2.5.4 <i>awsX-awsR-mwsR</i> mutant.....	133
4.2.5.5 <i>sadB-awsX</i> & <i>sadB-awsR</i> mutants.....	134
4.2.5.6 <i>pflu0185-wspA</i> mutant.....	136
4.2.6 Concluding remarks.....	137
4.3 Analysis of select evolved lines.....	138
4.3.1 Measuring fitness.....	139
4.3.2 Lineage-level fitness.....	140
4.3.3 Individual-level fitness.....	141
4.3.4 Trade-off breaking observations.....	144
4.3.5 Level of c-di-GMP in different environments.....	144
4.4 Mutational steps to rack-21 genotype.....	147
4.4.1 Lineage & individual-level fitness.....	149
4.4.2 Level of c-di-GMP in different environments.....	150
4.4.3 Conclusions regarding trade-off breaking.....	151
4.5 Mutations obtained during additional generation.....	152
4.5.1 WT SBW25 mutations.....	154
4.5.2 Mutational strategy rack-23 mutations.....	155
4.5.3 Developmental strategy mutations.....	156
4.6 Conclusions.....	158
4.6.1 Future perspectives.....	162

Chapter V: Materials & Methods

5.1 Bacterial strains, culturing & reagents.....	164
5.1.1 <i>P. fluorescens</i> strains.....	164
5.1.2 <i>E. coli</i> strains.....	172
5.1.3 Plasmids and transposons.....	172
5.1.4 Primers.....	174
5.1.5 Culture medium.....	177
5.1.6 Antibiotics & reagents.....	178

5.1.7 Enzymes & kits.....	179
5.2 Phenotypic analysis.....	180
5.2.1 Colony morphology.....	180
5.2.2 Mat formation.....	181
5.2.3 Swimming motility.....	181
5.3 Polymerase Chain Reaction.....	181
5.3.1 Standard PCR.....	181
5.3.2 Strand Overlap Extension.....	183
5.3.3 FastCloning.....	184
5.3.4 Arbitrary Primed-PCR.....	184
5.3.5 Gel electrophoresis.....	186
5.4 Bacterial transformation.....	186
5.4.1 Bi-parental conjugation.....	187
5.4.2 Tri-parental conjugation.....	187
5.4.3 Electroporation.....	187
5.5 Transposon mutagenesis.....	188
5.6 Site-directed mutagenesis.....	188
5.6.1 Ligation into pGem-T & pUIC3.....	189
5.6.2 Gibson assembly into pUIC3-mini.....	190
5.6.3 Allelic exchange.....	191
5.7 DNA extraction & sequencing.....	192
5.7.1 Sanger sequencing.....	192
5.7.2 Whole-genome sequencing.....	193
5.8 Life cycle experiment with new selective methods.....	193
5.9 Phenotypic assessment of evolved lines.....	196
5.9.1 c-di-GMP assay using pCdrA reporter.....	196
5.9.2 Lineage fitness approximation.....	197
5.9.3 Competitive fitness assays.....	198
5.10 Graphing and statistical analysis.....	198
Supplementary A.....	199
Supplementary B.....	199
Acknowledgements.....	200
Bibliography.....	201

Chapter I: Introduction

1.1 Evolution by natural selection

Darwin (1859) proposed the theory of evolution by natural selection with the intention of explaining the diversity of life and its adaptation to the natural world, as witnessed on a survey expedition aboard the H.M.S. *Beagle*. In the publication *On the Origin of Species*, Darwin (1859) describes the ‘struggle for existence’ in which individuals in an exponentially growing population compete for survival under limited natural resources. As a result of variation in heritable traits, some individuals in the population will have a higher probability of survival and thus more opportunity for reproduction (Mayr, 1982; Gould, 2002). Therefore natural selection will act to accumulate advantageous variants in a population, allowing for the gradual adaptation of organisms to the local environment.

1.1.1 Darwinian populations

Lewontin (1970) outlined three principles that a population must uphold to participate in evolution by natural selection: (1) Variation – individuals differ from one another in a phenotypic trait, (2) Differential fitness – differences in phenotype result in unequal survival rates and reproduction in different environments, and (3) Heritable fitness – individuals form a new generation in which the offspring fitness correlates with that of the parent. Using this framework predictions can be made regarding the ‘unit of selection’, whether individuals at each level of a biological system satisfy these properties determines if selection may operate to produce evolutionary change at that level (Lewontin, 1970). Godfrey-Smith (2009) elaborates on this concept, defining the minimal ‘Darwinian population’ as a collection of interacting individuals that fulfil the Darwinian properties of variation, inheritance & differential reproduction; while marginal cases only approximate these properties, and paradigm cases include the rare evolving Darwinian populations in which adaptive novelty and complexity may arise.

1.1.2 Hierarchical levels of organisation

Buss (1987) emphasises the hierarchical organisation of life – populations (or species) containing organisms, organisms composed of cells, cells having genomes, and genomes with genes. It is increasingly evident that Darwinian populations may exist at multiple hierarchical levels of biological organisation, and therefore each may be units of selection in their own

right (Gould & Lloyd, 1999; Calcott & Sterelny, 2011; Godfrey-Smith, 2009). This would allow for ‘de-Darwinization’, in which natural selection acting at the higher level (e.g. multicellular organisms) suppresses evolution at the lower level (e.g. cells); while independent evolution at the lower level can also cause conflict or subversion of the higher level (e.g. cancer) (Godfrey-Smith, 2009). In the formation of a new hierarchical level of organisation, the interaction of the lower level and the external environment is altered (within the context of the higher level), with the higher level favouring variants that both maximise their interaction with the environment and minimise further modification or variation at the lower level (Buss, 1987). For example, in the origin of multicellular organisms, the sequestration of the germ-line benefited both the lower level by reducing conflict between cells, and the higher level by limiting the production of variation for the next generation (Buss, 1987; Michod, 1996). Godfrey-Smith (2009) describes this reproductive specialisation as resulting in de-Darwinization of the lower level of the cell, and shifts the collective level towards the paradigm case.

1.1.3 Transitions in individuality

The evolutionary history of life is punctuated by ‘transitions in individuality’, in which Darwinian properties emerge at a new level of biological organisation, and the unit of selection shifts from the lower level to the higher level (Godfrey-Smith, 2009; Buss, 1987; Michod, 1997). Within the multi-level selection framework, this may be represented as a transformation from MLS1 in which the collective fitness is a product of the lower level fitness (interaction between cooperating particles), to MLS2 where the fitness of the collective is defined by the production of offspring irrespective of particle fitness (Okasha, 2005; Sober & Wilson, 1998). Transitions in individuality allow for selection to act on higher level collective traits, and therefore the evolution of more complex life forms over time; though the emergence of Darwinian properties at a new hierarchical level cannot be assumed, and requires evolutionary explanation (Griesemer, 2000).

1.1.4 Major evolutionary transitions

Szathmáry & Maynard Smith (1995) outline the ‘major evolutionary transitions’ during the origin of complex life, broadly defined by the occurrence of innovation in the storage and transmission of heritable information. These significant events included origin of the following: compartmentalisation of replicating molecules, chromosomes, the genetic code (from RNA enzymes to DNA encoding proteins), eukaryotic cells (endosymbiosis involving

ancestral eubacterial and archaeobacterial cells), sexual populations, multicellular organisms (from unicellular ancestors), eusocial animal groups, and human societies with language (Maynard Smith & Szathmáry, 1995; West et al., 2015). The major evolutionary transitions may also be characterised by individual entities coming together to form a higher-level cooperative group, where the lower-level individuals have division of labour and are no longer capable of independent replication (Calcott & Sterelny, 2011; Maynard Smith & Szathmáry, 1995; Griesemer, 2000).

Furthermore, Queller (1997) made the distinction between ‘fraternal’ and ‘egalitarian’ transitions; the former involving cooperation between genetically similar individuals, with division of labour evolving afterwards by epigenesis (e.g. multicellularity); and the later where unrelated individuals form a higher-level group, having pre-evolved distinct functions (e.g. the eukaryotic cell). Szathmáry (2015) later updated this theoretical framework, to combine the origin of compartmentalisation and chromosomes to that of the protocell, and demote sexual reproduction by meiosis to be included in the origin of the eukaryotic cell. The origin of plastids (e.g. photosynthetic chloroplasts) was also added as an additional major transition, and emphasis made on the importance of horizontal gene transfer in the origin of the prokaryotic genome (Szathmáry, 2015).

1.2 The evolution of multicellular life

The evolution of multicellular life is a prime example of a fraternal transition, in which individual cells of a unicellular ancestor came together to form a multicellular group or organism (Maynard Smith & Szathmáry, 1995). Multicellularity originated numerous times across the tree of life, including in eukaryotes (e.g. fungi, green algae & slime molds), bacteria (e.g. myxobacteria & cyanobacteria), and archaea (Bonner, 2000). When considering all basic forms of cellular aggregation, this evolved in at least 25 independent lineages (Rose & Hammerschmidt, 2021); Grosberg & Strathmann (2007) therefore referring to the evolution of multicellularity as a ‘minor major’ transition.

Under Godfrey-Smith’s (2009) Darwinian population framework, the early stages of the evolution of multicellularity involved a transition in individuality to the new hierarchical level of the multicellular group, requiring the derived properties of variation, reproduction & heredity (Libby & Rainey, 2013a). This would allow for the unit of selection to shift from the lower-level of the individual cell to the higher-level of the cell group (or collective), and the

nascent multicellular organism to become more than just a sum of its constituent cells (Godfrey-Smith, 2009; Lewontin, 1970). Cooperation between cells was also necessary, to acquire the fitness advantage of residing in a multicellular group; though it is unclear how this was maintained in the face of internal genetic conflict (Michod, 1996; Rainey & De Monte, 2014). Upon establishment of Darwinian individuality in the multicellular group, natural selection may then act on collective traits that improve fitness of the group, allowing for an increase in complexity and further adaptation to the environment (Buss, 1987; Rose & Hammerschmidt, 2021). Although the emergence of Darwinian properties at the group level requires explanation, and cannot be assumed to simply transfer from the lower level (Libby & Rainey, 2013a; Griesemer, 2000). Most pertinent is exactly how a mechanism of collective-level reproduction came about (Rainey & Kerr, 2010). De Monte & Rainey (2014) suggest that for nascent multicellular groups it may be useful to relax the strict requirement of Darwinian properties, and rather focus on the genealogical connection and recurrence of defined collectives through time (instead of reproduction). Consideration of this marginal case of simple collectives could shine light on the initial shift in Darwinian individuality to the higher level, and early origins of collective-level reproduction and development (De Monte & Rainey, 2014; Godfrey-Smith, 2009).

1.2.1 Advantages of multicellularity

The transition from unicellular to multicellular life provided a number of advantages, resulting from the increase in organism size (Grosberg & Strathmann, 2007). Bonner (2000) introduces the concept of ‘size niches’, explaining that organisms evolve to increase or decrease size to fill ecological niches imposed by the environment. It has been predicted that a larger size may minimise predation by physically preventing grazing upon by other organisms, as well as enabling faster movement to escape predators and forage for nutrients (Bonner, 1998, 2000; Michod & Roze, 1999). Herron et al. (2019) have demonstrated this experimentally, observing the evolution of simple multicellular structures in the green alga *Chlamydomonas reinhardtii* in response to a filter feeding predator. Multicellularity also allows for the division of labour and spatial differentiation of cell types, and therefore the production of a more efficient and functionally complex organism (Bonner, 2004; Grosberg & Strathmann, 2007). For example, division of labour is observed in *Volvox carteri*, with the large gonidia cells (used in asexual reproduction) surrounded by a layer of flagellated somatic cells that are specialised for motility (Kirk, 2001). The formation of an internal environment may also provide the advantages of protecting germline cells from the external environment,

storage of nutrients under limiting conditions, and the control of local metabolic gradients (Bonner, 1998; Pfeiffer & Bonhoeffer, 2003).

1.2.2 Cooperation and conflict mediation

Cooperative interactions between cells were essential for the transition to multicellularity, these providing benefits to the multicellular group though costly to the individual cell (Michod & Roze, 2001; West et al., 2015). Numerous theories have been put forward to explain this altruistic behaviour including mechanisms based on – reciprocity, in which individuals mutually benefit from cooperation; kin selection, where related individuals cooperate to increase the frequency of their own genes in the next generation; and group selection, deducing that groups composed of altruistic individuals will be selected over selfish ones in certain settings (Godfrey-Smith, 2009; Sachs et al., 2004). There has been extensive debate around the significance of the opposing kin selection (Maynard Smith, 1964; Hamilton, 1964) and group selection (Wilson, 1975), though the nuances of this will not be discussed further (Nowak et al., 2010).

With cooperation also comes the issue of evolution of defectors (or ‘cheaters’) – selfish individuals that reap the benefit of cooperating without reciprocation, and favour their own reproduction at the expense of others; this may lead to destabilisation of the multicellular group and inhibit the establishment of a new unit of selection at the higher-level of the group (Michod, 1996, 1997; Michod & Roze, 1999, 2001; Rainey & De Monte, 2014). As asserted by Maynard Smith & Szathmáry (1995), the mediation of conflicts at the lower-level is an important factor to consider for the origin of multicellularity. The passage through a single-cell bottleneck was likely required during the development of multicellular organisms, resulting in a reduced mutational load and therefore minimal conflict between clonal cells (Queller, 2000; Grosberg & Strathmann, 1998; Bonner, 2000). Buss (1987) rather had proposed that sequestration of the germ-line would reduce the appearance of defectors, allowing early isolation of reproductive cells and exclusion of the passage of somatic mutations to the next generation (Michod, 1996; Grosberg & Strathmann, 2007). Other suggested methods of conflict mediation include: small propagule sizes, self/non-self recognition, mutual policing of defectors (Frank, 1995), programmed cell death, and power asymmetry including maternal control during early development (Queller, 2000; Grosberg & Strathmann, 2007).

1.2.3 Nascent life cycles

The life cycle of an organism describes the process in which it develops, grows and reproduces; a nascent life cycle must have been present for the reproduction of simple multicellular groups (Ratcliff et al., 2017). Michod & Roze (2001) outline three potential reproductive modes for group formation – fragmentation: small groups grow to form larger groups, that fragment to produce group offspring; aggregation: different cells that are potentially unrelated come together to form a group, producing single cell offspring; and clonal development: an individual cell (e.g. zygote or spore) divides and grows to form a clonal group, with production of unicellular propagules (Grosberg & Strathmann, 2007). These types of multicellular development differ in the size of propagule and amount of genetic variation passed to the next generation. Aggregation results in higher within-group variation and therefore allows for conflict; only observed to occur in a few simple terrestrial organisms, for example slime molds (Michod & Roze, 1999, 2001; Bonner, 2000). Clonal development includes passage through a single-cell bottleneck that reduces genetic variation in offspring, thus minimising conflict and purging deleterious mutations (Grosberg & Strathmann, 1998; Queller, 2000).

A number of models have demonstrated the positive group fitness effect of reproduction with a small size propagule or single-cell (Michod & Roze, 1999, 2001; Pichugin et al., 2017; Ratcliff et al., 2017). Furthermore, the majority of multicellular life forms are observed to have a single-cell stage in the life cycle, and complex multicellularity with distinct specialisation of germ-line and somatic cells (Bonner, 2000; Buss, 1987). Wolpert & Szathmary (2002) emphasise that a unicellular bottleneck is both important to minimise inter-group conflict, as well as enabling the establishment of developmental signalling processes for cell differentiation. The evolution of a developmental program would unify the activities of the single-cell and multicellular group stages of the life cycle, allowing for genetically identical cells to perform diverse functions, and therefore greater complexity (Libby & Rainey, 2013b; Hammerschmidt et al., 2014; Wolpert & Szathmary, 2002)

1.2.4 The evolution of development

As stated by Wolpert (1994), ‘The evolution of development is intimately linked to the origin of multicellular forms’. Development refers to the processes that produce variation in a phenotypic trait, in response to input from both the genome and environment (West-Eberhard, 2003). Oster & Alberch (1982) explain that such developmental processes may generate

diverse phenotypes, as a result of simple rules that constrain the mechanical or chemical interaction between cells. For the early origins of development in nascent multicellular organisms, Bonner (2000) outlines the fundamental properties of polarity and cellular differentiation. Polarity refers to the directional orientation of an organism, allowing for spatial or temporal localisation of gene expression, and metabolic gradients for pattern formation (Bonner, 2000; Wolpert, 1994; Kaiser, 2001). Once polarity is established cell differentiation may follow, resulting from the response of cells to different local environments; for example in *Dictyostelium* slime molds, environmental oxygen gradients induce the production of anterior stalk cells for dispersal from posterior spore cells (Bonner, 2000). Wolpert (1994) suggests that cell patterning initially in response to an environmental signal may become genetically encoded into a developmental program, therefore enabling autonomous regulation and coordination of cellular differentiation. As introduced by Waddington (1942), the genetic assimilation (or ‘canalization’) of developmental pathways will provide a selective advantage by allowing the reliable production of phenotype regardless of environmental conditions (Waddington, 1959; Wolpert, 1994).

Development programs were required for the heritable reproduction of simple multicellular groups; though it is difficult to explain the evolutionary origin of this adaptive group-level trait, without assuming the existence of the Darwinian property of reproduction at the level of the multicellular group (Rainey & Kerr, 2010; Griesemer, 2000). Early forms of developmental regulation were likely the product of simple signal-response systems and the interaction of cells with their external environment; for example in cellular slime molds, cell differentiation is controlled by the extracellular cyclic AMP molecule (Bonner, 2000). Selection may then act to refine the functions of both signalling molecules (e.g. size & concentration) and their receptors (e.g. spatial distribution, activation threshold & specific response), resulting in more complex signalling pathways (Bonner, 2000). Those response pathways that allow for the environmentally induced expression of alternative phenotypes, if adaptive, may then stabilise by coming under the control of genes (Minelli & Fusco, 2010; Moczek et al., 2011). Rainey and Kerr (2010) propose that proto-life cycles in which ecological conditions favour cycling between distinct phenotypes, could provide a basis for the evolution of developmental regulation and more complex multicellular life cycles.

1.2.5 Ecological scaffolding

For the emergence of group-level reproduction in the transition to multicellularity, an alternate solution considers that Darwinian properties can be imposed on simple groups by virtue of the structure of the external environment (Rainey et al., 2017; Black et al., 2020). Rainey et al. (2017) explain this using the analogy of 'Darwinian pond scum' or microbial mats growing on reeds in a pond – the reed provides a structure in which bacteria may colonise to form mats, with discrete variation between reeds; upon the collapse of a mat, another may disperse and recolonise this reed, allowing for group-level reproduction; and the offspring mat resembles the parent, thus variation. This 'ecological scaffolding' may therefore enable selection to act on the longer timescale of the collective generation, rather than just the shorter timescale of the doubling of individual cells (Black et al., 2020). While the Darwinian properties are initially exogenously imposed by the environment, these may become endogenously determined by the evolution of a developmental program (Rainey et al., 2017; Okasha, 2021; Bourrat, 2022). Hammerschmidt et al. (2014) demonstrated that this was possible with experimental populations of *Pseudomonas fluorescens*, observing the evolution of a simple genetic switch to transition between the soma- and germ-like phases of the life cycle.

1.3 *Pseudomonas fluorescens* SBW25 model

For experimental evolution, a bacterial model organism is preferred due to the benefits of a large population size and short generation time, as well as the relatively small genome size that lowers the cost of whole-genome sequencing. The gram-negative bacterium *Pseudomonas fluorescens* SBW25 (*P. fluorescens* SBW25; hence referred as SBW25) was first isolated from the phyllosphere of a sugar beet plant (Bailey et al., 1995). This plant-colonising bacterium is an obligate aerobe and saprophytic; the genome having been previously mapped and extensively annotated (Rainey & Bailey, 1996; Silby et al., 2009). *P. fluorescens* SBW25 is non-pathogenic and has been shown to promote plant growth; though is closely related to other species members *Pseudomonas putida*, and the pathogens *Pseudomonas aeruginosa* (*P. aeruginosa*) & *Pseudomonas syringae*, making for an ideal model system (Rainey, 1999; Rainey & Bailey, 1996).

Furthermore, when grown in a spatially structured environment *P. fluorescens* SBW25 rapidly diversifies, with the evolution of adaptive variants specialised to occupy different

niches (Rainey & Travisano, 1998). The ancestral ‘smooth morphology’ (SM) colonises the broth phase of the static microcosm, while the mutant types ‘wrinkly spreader’ (WS) and ‘fuzzy spreader’ (FS) colonise the broth surface; this niche preference also corresponding with distinct colony morphology phenotypes on agar plates (Rainey & Travisano, 1998; Ferguson et al., 2017), as shown in *Figure 1.1* below. The WS type forms a self-supporting mat (or biofilm) at the interface between the broth and the air, as a result of a mutation that causes overproduction of an adhesive polymer, allowing cells to stick to one another; this cooperative behaviour is costly to the individual cell but benefits the group by providing access to oxygen at the surface (Rainey & Rainey, 2003).

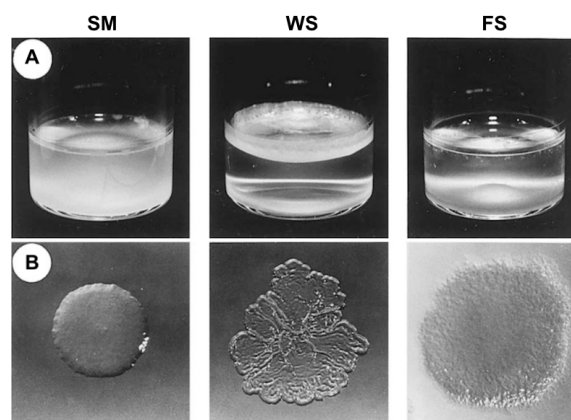


Figure 1.1. Diversification of SBW25 in a spatially structured environment. The ancestral SBW25 colonises the broth phase (A), and displays the ‘smooth morphology’ (SM) phenotype on agar plates (B). While the evolved mutant ‘wrinkly spreader’ (WS) & ‘fuzzy spreader’ (FS) types colonise the air-liquid interface, and display the distinctive wrinkly and fuzzy colony morphology. Adapted from Rainey & Travisano, 1998.

1.3.1 Phenotypic cycling as a nascent life cycle

Cycling is observed between the WS and SM phenotypes in the static broth environment, by simple virtue of the spatial structure imposing a competitive trade-off between niche specialists, and the resulting negative frequency dependent selection (Rainey & Travisano, 1998). As shown in *Figure 1.2* below, the ancestral smooth (SM) type colonises the broth phase, with the depletion of nutrients over time producing an oxygen gradient (O_2 highest at the surface). The competition for access to oxygen at the air-liquid interface (ALI) drives the evolution of wrinkly spreader (WS) mutants that colonise the new niche at the broth surface, forming a mat due to overproduction of an acetylated cellulosic polymer that acts as a cell-cell glue (Rainey & Rainey, 2003; Spiers et al., 2003). Upon formation of the cooperative collective mat, revertant mutant SM types (or ‘cheaters’) soon evolve that reap the benefit of existing in the collective without paying the cost of glue production, these cheating types

compromise the structural integrity of the mat and eventually lead to its collapse (Rainey & Rainey, 2003).

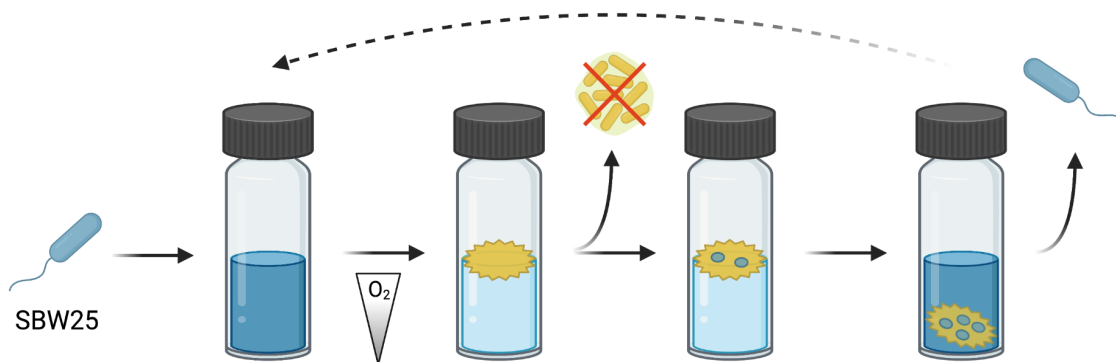


Figure 1.2. Cycling between SM & WS phenotype in static broth resembles a nascent life cycle. Ancestral SBW25 with the SM phenotype (blue) colonises the broth upon inoculation into a static microcosm. Over time nutrients deplete and an oxygen gradient forms, competition driving the evolution of WS mutants (yellow-orange) that colonise the ALI, and form a collective mat by overproduction of a cell-cell glue. SM revertant ‘cheater’ types will soon come about that selfishly benefit from being in the collective without paying the costs, eventually leading to collapse of the mat (Rainey & Rainey, 2003). While the WS collective itself is an evolutionary dead end, the SM cheater may be utilised as a single-cell propagule to seed the next generation of the collective (Rainey & Kerr, 2010). Created with BioRender.

Rather than focusing on the need for conflict mediation in the collective mat and ways to suppress the evolution of cheating types, Rainey & Kerr (2010) propose that the cheaters may instead act as a single-cell propagule capable of dispersal to seed the next generation of the collective. Based on this a nascent two-phase life cycle is envisioned, that transitions between the WS multicellular collective phase (‘somatic body’) and SM individual cell dispersal phase (‘germ-line’) (Rainey & Kerr, 2010; Hammerschmidt et al., 2014). This simple multicellular life cycle in *P. fluorescens* SBW25 is an ideal model system to investigate the early origins of multicellularity, and the emergence of mechanisms for group-level reproduction and development that were required for the transition in individuality.

1.3.2 Basis of the WS phenotype

The structural basis and mutational pathways to the WS phenotype have been extensively characterised. Spiers et al. (2003) determined that the main structural component is an acetylated cellulosic polymer, with the cellulose synthase machinery encoded by ten genes of the *wss* operon (*wssA-wssJ*). The proteins WssB, WssC & WssE are predicted to form core subunits of the cellulose synthase complex, in association with the WssD cellulase; while WssG, WssH & WssI are predicted to function in the acetylation of cellulose, and WssA &

WssJ involved in spatial localisation (Spiers et al., 2002). The primary mutational pathways to the WS phenotype were identified as the *wsp*, *aws*, & *mws* operons; these all include genes encoding di-guanylate cyclase (DGC) enzymes (McDonald et al., 2009). DGCs contain the conserved GGDEF domain and catalyse the synthesis of c-di-GMP, while phosphodiesterase (PDE) enzymes with the EAL domain break down c-di-GMP (Römling et al., 2005; Hengge, 2009). The secondary messenger bis-(3'-5')-cyclic-dimeric-guanosine monophosphate (c-di-GMP) has been previously identified as an allosteric activator of cellulose biosynthesis enzymes (Ross et al., 1987; D'Argenio & Miller, 2004). Therefore the WS phenotype is most commonly the result of mutational activation of the DGC enzymes WspR, AwsR or MwsR, causing an increase in c-di-GMP level, that results in activation of transcription of the *wss* operon, and overproduction of a cellulosic polymer (McDonald et al., 2009). The regulatory network underpinning the WS phenotype is even more complex, with the SBW25 genome encoding another 36 putative DGC enzymes, as well as a number of regulatory proteins that have been shown to control expression of the *wss* operon (McDonald et al., 2009; Giddens et al., 2007).

1.3.2.1 Wsp pathway

The *wsp* (*wrinkly spreader phenotype*) operon contains the seven genes *wspABCDEF* (*pflu1219-1224*) & *wspR* (*pflu1225*); mutation in the negative regulator WspF was previously observed to result in activation of the DGC WspR and therefore the WS phenotype (Spiers et al., 2002; Goymer et al., 2006; Bantinaki et al., 2007). In *P. aeruginosa* PAO1, disruption of the *wspF* gene (PA3703) was shown to increase levels of c-di-GMP, resulting in cell aggregation and biofilm formation; while mutation to the remaining *wsp* operon caused suppression of the wrinkly phenotype (Hickman et al., 2005; D'Argenio et al., 2002). *wspR* ([pflu1225](#)) encodes the putative GGDEF response regulator protein WspR (length: 333 amino acids), with 73.3% sequence identity to the diguanylate cyclase WspR in *P. aeruginosa* PAO1 ([PA3702](#); BLASTP *E*-value: $2e-176$). WspR contains a CheY-like response regulator receiver (REC) domain ([PF00072](#); residue: 18-130; *E*-value: $1.1e-18$), and GGDEF domain ([PF00990](#); residue: 169-329; *E*-value: $4.1e-49$) with an intact GGEEF motif. Malone et al. (2007) carried out a mutational scan of the *wspR* gene (in-frame insertions of five amino acids), identifying activating mutations clustered within the N-terminal REC domain & linker region; this confirming the DGC activity of WspR and importance of sequence conservation in the RYGGEEF motif (residues 246-252).

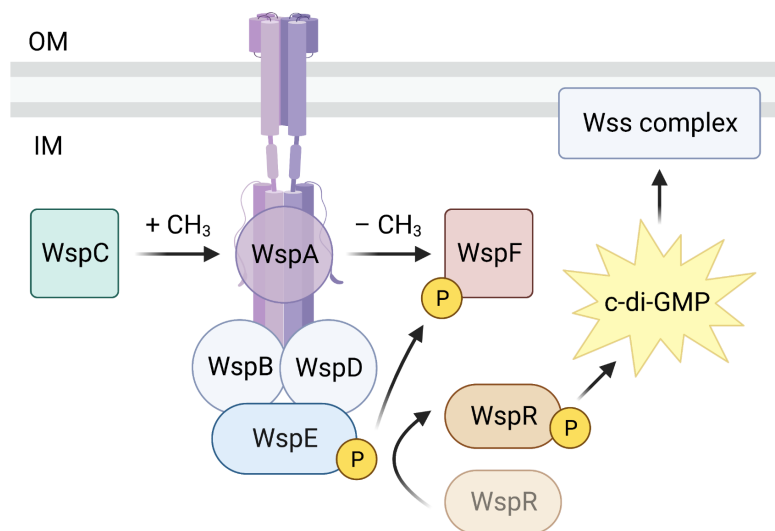


Figure 1.3. Regulation of c-di-GMP level by the Wsp signal transduction pathway. Model of the Wsp pathway based on the Che pathway in *E. coli*, as adapted from Bantinaki et al. (2007). The WspA MCP protein forms a signalling complex with the CheW-like scaffold proteins WspB & WspD, and the CheA-like histidine kinase WspE. The WspE kinase activity is controlled by addition & removal of methyl groups by the CheR-like methyltransferase WspC & CheB-like methylesterase WspF; methylation of the MCP conserved glutamate residues by WspC causes WspE to undergo autophosphorylation. The activated WspE kinase then phosphorylates WspF (inactivating the Wsp complex) and the WspR DGC enzyme, activating the synthesis of the secondary messenger c-di-GMP. High levels of intracellular c-di-GMP result in activation of the Wss cellulose synthase complex, overproduction of the cellulosic polymer, and formation of a mat in static broth.

Based on homology with the Che chemosensory pathway in *Escherichia coli* (*E. coli*), Bantinaki et al. (2007) proposed a model for the regulation of the Wsp pathway, as summarised in *Figure 1.3* above. The WspA methyl-accepting chemotaxis protein (MCP) receives a signal from the environment, likely associated with cell growth on a surface or membrane stress (O'Connor et al., 2012; O'Neal et al., 2022). WspA forms a membrane-bound receptor signalling complex with the WspB & WspD scaffold proteins, and the WspE histidine kinase/response regulator. The WspC methyltransferase adds methyl groups to the WspA methylation sites, while the WspF methylesterase removes methyl groups; this controls the activation state of the Wsp complex, with methylation of the WspA MCP resulting in autophosphorylation of the WspE kinase (Bantinaki et al., 2007). WspE, when activated, phosphorylates the WspR diguanylate cyclase/response regulator, as well as WspF (causing inactivation of the Wsp complex). The phosphorylated WspR DGC synthesises c-di-GMP, which results in activation of the Wss cellulose synthase complex, overproduction of the cellulose adhesive polymer, and thus the WS phenotype & mat formation in static broth (Bantinaki et al., 2007). From this model, mutations in the *wspF*

gene are predicted to cause a decrease in WspF methyltransferase activity, resulting in constitutive activation of the Wsp system, phosphorylation of the WspR DGC, and overproduction of c-di-GMP & cellulose (Bantinaki et al., 2007; Güvener & Harwood, 2007).

1.3.2.2 *Aws* pathway

The *aws* (*alternative wrinkly spreader*) operon contains the three genes *awsO* (*pflu5209*), *awsR* (*pflu5210*) & *awsX* (*pflu5211*); mutations were observed in the negative regulator *AwsX*, resulting in the WS phenotype, likely due to activation of the DGC *AwsR* (McDonald et al., 2009; Giddens et al., 2007). *awsR* ([pflu5210](#)) encodes the putative signalling protein *AwsR* (length: 420 amino acids), with 61.7% sequence identity to the diguanylate cyclase *YfiN* (also known as *TpbB*) in *P. aeruginosa* PAO1 ([PA1120](#); BLASTP *E*-value: $8e-172$). *AwsR* contains a CHASE8 periplasmic sensor domain ([PF17152](#); residue: 41-142; *E*-value: $1.3e-28$), and GGDEF domain ([PF00990](#); residue: 245-398; *E*-value: $1.0e-46$) with an intact GGDEF motif. Various studies in *P. aeruginosa* have demonstrated that *YfiN* functions as a membrane-bound DGC enzyme in the production of c-di-GMP, under control of the regulatory proteins *YfiR* & *YfiB* (orthologs of *AwsX* & *AwsO*, respectively); deletion of the *yfiR* gene resulting in activation of the *YfiN* DGC, increase in production of the Pel exopolysaccharide, and the small-colony variant phenotype (Ueda & Wood, 2009; Malone et al., 2010, 2012). Malone et al. (2010) propose a model for function of the *YfiBNR* complex – the inner-membrane localised *YfiN* is under repression of the small periplasmic protein *YfiR*; the outer-membrane lipoprotein *YfiB* is predicted to sequester the *YfiR* repressor from the inner membrane in response to cell envelope stress, causing activation of the *YfiN* DGC and an increase in c-di-GMP levels (Malone et al., 2012). The *Aws* pathway of SBW25 likely has analogous function; mutations in the *awsX* gene resulting in relief of repression of the *AwsR* DGC enzyme by the *AwsX* periplasmic protein.

1.3.2.3 *Mws* pathway

The *mws* (*Mike's wrinkly spreader*) pathway contains one large gene *mwsR* (*pflu5329*), with mutations observed in the C-terminal EAL domain producing the WS phenotype, predicted to cause activation of DGC activity (McDonald et al., 2009). *mwsR* ([pflu5329](#)) encodes the putative sensory box GGDEF/EAL dual-domain protein *MwsR* (length: 1283 amino acids), with 67.2% sequence identity to the motility regulator *MorA* in *P. aeruginosa* PAO1 ([PA4601](#); BLASTP *E*-value: 0.0). *MwsR* contains a PAS fold ([PF08447](#); residue: 478-569; *E*-value: $5.8e-9$), two PAS sensory domains ([PF13426](#); residue: 600-714 & 735-836; *E*-value:

3.0e-5 & 2.5e-16), a GGDEF domain ([PF0090](#); residue: 848-1009; *E*-value: 4.7e-50), and EAL domain ([PF00563](#); residue: 1029-1264; *E*-value: 1.0e-76); with both GGDEF & EAL motifs intact. Previous studies in *Pseudomonas* species have shown that MorA functions as both a PDE & DGC enzyme in the synthesis and hydrolysis of c-di-GMP; with *morA* gene knockout strains displaying improvement to swimming motility and impairment of biofilm formation (Phippen et al., 2014; Choy et al., 2004; Kulasakara et al., 2006). McDonald et al. (2009) found in SBW25 that deletion of the entire *mwsR* gene resulted in suppression of the WS phenotype, indicating that the MwsR DGC activity is under negative regulation by the internal PDE activity.

1.3.2.4 Alternative pathways & regulators

The SBW25 genome encodes a total of 39 putative DGC enzymes, though the experimental evolution of the WS phenotype has primarily been observed as a result of mutations in the Wsp, Aws & Mws pathways (McDonald et al., 2009). Lind et al. (2015) deleted the *wsp*, *aws* & *mws* operons, and subsequently identified 13 additional mutational routes to the WS phenotype of similar fitness. The alternative pathways include – single mutations in *pflu0085*, *pflu0956*, *pflu3448*, *pflu3571* & *pflu5960*; promoter activating mutations in *pflu0956*, *pflu5898* & *pflu1349*; gene fusions of *pflu0184-0183*, *pflu4305-4306* & *pflu4308-4313*; double mutations in *dipA/amrZ* & *dipA/pflu0621*; and the triple mutant *amrZ/fleQ/pflu4414* (Lind et al., 2015). These rare mutational pathways were predicted to result in an increase in c-di-GMP levels by activation of DGC catalytic activity, disruption of PDE activity, or alteration to the function of transcriptional regulatory proteins. In comparison, the common pathways all involved loss-of-function mutation to a negative regulator (encoded by *wspF*, *awsX* & *mwsR* genes) (Lind et al., 2015). Giddens et al. (2007) also established the involvement of a number of regulatory proteins in expression of the cellulose synthase-encoding *wss* operon in the plant environment, including WspF, AwsR & AwsX, as well as the transcriptional activators FleQ & AmrZ.

1.3.3 The life cycle experiment

To explore the origins of multicellularity, Rainey and Kerr (2010) hypothesised a means of collective-level reproduction in a nascent life cycle that embraces the SM ‘cheater’ type as a single-cell propagule for a new generation of the collective mat (as discussed in [Section 1.3.1](#)). The life cycle experiment (LCE) was previously conducted by Hammerschmidt et al. (2014), recreating this simple two-phase life cycle in *P. fluorescens* SBW25, transitioning

between the WS collective ('soma') and SM individual cell ('germ-line') phases. The cheat-embracing regime of this experiment evolved replicate lineages of SBW25 (initially clonal) through ten life cycle generations – 120 total lines, divided into 15 metapopulations (with 8 replicate lines each). Each lineage was seeded with a single-cell WS bottleneck each cycle, and required during Phase I to have an intact WS mat after 6 days static incubation, as well as produce SM propagules with screening based on colony morphology on agar plates. For Phase II, each lineage was then inoculated with a pool of SM cells, and required to produce WS types after 3 days growth, also screened based on colony phenotype. Extinctions occurred when lineages were unable to make the WS mat or produce the respective wrinkly or smooth colony phenotype; these were then replaced by another viable line within the metapopulation, allowing for reproduction of the collective (Hammerschmidt et al., 2014); as displayed in *Figure 1.4* below.

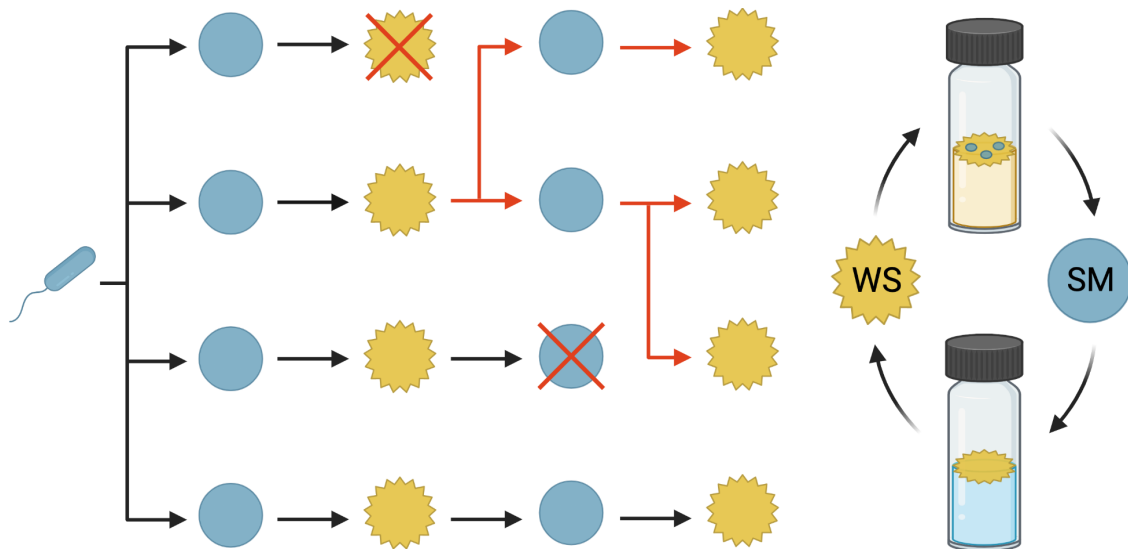


Figure 1.4. Life cycle experiment with collective-level reproduction. Replicate lineages of SBW25 were evolved in a two-phase life cycle, transitioning between the WS collective and SM individual cell phases, with selection based on the WS or SM colony morphology on agar plates (Hammerschmidt et al., 2014). Shown is an example of lineage selection within a small metapopulation (four replicate lines inoculated with the ancestral SBW25) over two life cycle generations, cycling between the WS (yellow-orange) and SM (blue) colony phenotype. Due to an extinction event in two lines (no WS or SM colonies produced), one remaining viable lineage is able to undergo collective-level reproduction (red arrows), resulting in the production of three offspring lineages (originating from a single parental line).

The LCE imposes selection on two different time scales – the shorter time scale of the growth of cells, and the longer time scale of persistence of lineages across generations, this requiring the repeated and reliable ability to switch between the WS and SM phenotypic states

(Hammerschmidt et al., 2014; Rose et al., 2020; Black et al., 2020). Therefore this selects for the evolution of a developmental program: some form of epigenetic regulation that would allow transitioning between the soma- and germ-like phases of the life cycle, thus unifying the activity of the two phases and mediating the shift in the unit of selection to the collective level (Hammerschmidt et al., 2014). This experimental life cycle bestows Darwinian properties on nascent multicellular groups – lineages have variation in phenotype as a result of spontaneous mutation and strong selection for adaptation to the spatially structured environment (under negative frequency dependent selection), this variation is partitioned by virtue of the ecological scaffold of the glass microcosm; group-level reproduction is enforced by a process of death and birth of lineages, over the longer time scale of the life cycle generation; and heritability imposed due to the genealogical connection between parent & offspring lineages, and the passage through single-cell bottlenecks (Rainey & Kerr, 2010; Rainey et al., 2017). The approximation of these Darwinian properties may enable the transition in individuality to the higher hierarchical level of the multicellular group, and therefore natural selection to act on collective-level traits and improve group fitness (Godfrey-Smith, 2009; Libby & Rainey, 2013a).

1.3.3.1 Fitness decoupling

Hammerschmidt et al. (2014) observed in the two-phase cheat-embracing regime after ten generations, the ‘decoupling’ of group fitness from the constituent cell fitness – improvement to the fitness of evolved lineages (increased ability to leave mat offspring), and a corresponding decrease in individual cell fitness (fewer cells in the mat). Fitness decoupling was previously theorised to be an indicator of an evolutionary transition in individuality, with selection having shifted to the higher level allowing for improvement to collective-level fitness and the mediation of conflict at the lower level of the individual cell (Michod & Nedelcu, 2003). While in the single-phase regime (cheat-purging control, with no SM bottleneck) decoupling was not observed to occur – the increase in lineage fitness correlated with an enhancement of individual cell fitness (Hammerschmidt et al., 2014; Rose et al., 2020). Further experiments by Rose et al. (2020) also revealed the importance of the ecology & metapopulation structure; the mixing of SM propagules between replicate lineages resulted in selection favouring improvement to individual cell growth rate rather than group fitness, with no evidence of fitness decoupling observed.

1.3.3.2 Evolution of a genetic switch

The fittest lineage of the life cycle experiment, Line 17, was found to have evolved a simple genetic switch that enabled semi-reliable switching between the WS and SM phenotypic states and therefore the transition through the life cycle (Hammerschmidt et al., 2014). This genetic switch was dependent on a mutation in the DNA mismatch repair-encoding gene *mutS* (protein change (p.) Y497P), which likely resulted in an increase in mutation rate (Oliver et al., 2002). Furthermore, Line 17 was shown to achieve this switch in phenotype by the expansion and contraction of a tract of guanine residues (nucleotides 742-748) in the DGC-encoding *wspR* gene; the frameshift mutations in the RYGGEEF conserved motif predicted to activate/inactivate the WspR DGC activity, therefore turning on/off the WS phenotype (Hammerschmidt et al., 2014; Malone et al., 2007; De et al., 2008). Although this *mutS*-dependent genetic switch still required mutational change to transition through each phase of the life cycle. Hypermutability also resulted in an accumulation of disruptive mutations across the genome – this is clearly not an ideal solution, and a far cry from a developmentally regulated life cycle.

1.4 Aims of the current study

- I. To characterise the environmentally-responsive strain TSS-f6 that evolved from a continuation of the LCE, continuing on work from my Masters (Summers, 2018). Use site-directed mutagenesis to delete candidate genes & operons previously found to be involved in the phenotype switch, including *wspE*, the *wss* operon, *pflu5960* & *amrZ*. Followed by recreation of the mutations identified in the *wsp* pathway of TSS-f6, to reproduce the environmentally-responsive phenotype in the ancestral SBW25 background.
- II. To design a revised experimental regime for the LCE that eliminates the use of the SM & WS colony morphology proxy, and may allow for the evolution of developmental regulation of the life cycle. Establish new selective methods based on the collective trait of mat-formation & individual trait of dispersal by swimming motility; and then test this new regime with a small-scale trial experiment. After five generations, explore the different strategies that have emerged to mediate the transition through phenotypic states, and identify those that do not require mutation.

- III. To run a large-scale life cycle experiment using the new selective regime, with 24 replicate metapopulations (total 192 lines) taken through five life cycle generations. Characterise the genetic basis of the various developmental strategies acquired for evolved lineages to regulate the life cycle. For select lines, measure the cell fitness (using competitive fitness assays), lineage-level fitness (approximate with survival rate of replicate lines during an additional generation), and level of c-di-GMP in the static broth, motility plate & shaken broth environments.
- IV. To investigate the trade-off breaking observation in the evolved line rack-21, that displays an increase in lineage & cell fitness, as well as modulation of c-di-GMP level in response to the environment. Characterise the mutational steps to the rack-21 genotype (cycle-1, cycle-2 & cycle-5), with measurements of cell fitness, lineage fitness, and c-di-GMP level in different environments.

Chapter II: Characterisation of an environmentally-responsive strain

2.1 Environmentally-responsive strain – TSS-f6

The environmentally-responsive strain TSS-f6 was evolved from a continuation of the life cycle experiment, displaying a switch in phenotype on agar plates from the SM to WS colony morphology at lower incubation temperatures. This chapter carries on from the work completed during my Master's thesis (Summers, 2018), characterising the genetic basis of this TSS-f6 phenotype switch.

2.1.1 Origin of TSS-f6

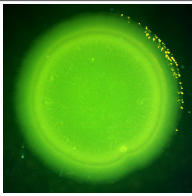
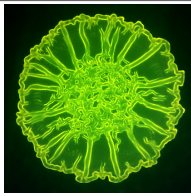
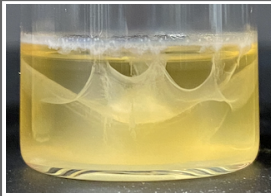
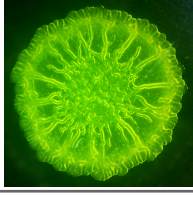
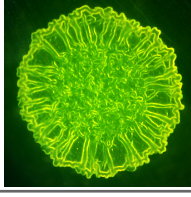
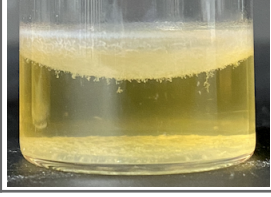
The LCE of Hammerschmidt et al. (2014) selected for the evolution of a developmental program, to mediate the transition through a simple two-phase life multicellular cycle in *P. fluorescens* SBW25; discussed in further detail in [Section 1.3.3](#). After ten generations 'fitness decoupling' was observed – an increase in fitness of evolved lineages, at the cost of individual cell fitness; the most fit lineage Line 17, was found to achieve this by the evolution of a simple genetic switch, that allowed for reliable production of the WS or SM phenotype by expansion and contraction of a guanine tract (G tract) in the DGC-encoding *wspR* gene (Hammerschmidt et al., 2014; Rose et al., 2020). Although this switch still required mutational change to transition through the life cycle, and was found to be dependent on the hypermutability resulting from disruption of the DNA mismatch repair-encoding *mutS* gene. Replicate lineages of Line 17 with *mutS* restored to wild-type (L17-*mutS*-WT) were taken through additional life cycle generations, and after seven cycles an interesting observation was made in the replicate line-f6 – colonies had switched from the SM phenotype at 28°C to the WS phenotype at room temperature (P. Remigi & D. Rixin, unpublished). While the immediate ancestor line-f2 from cycle 6 (f2 ancestor) & L17-*mutS*-WT did not demonstrate this phenotype switch, both displaying the WS phenotype at either incubation temperature. This environmentally-responsive strain was named TSS-f6 (temperature sensitive switcher – line-f6), and given to Summers (2018) for characterisation.

The significance of TSS-f6 lies in its potential to transition through the SM & WS phenotypic states in response to the environment (observed as temperature), therefore representing a possible solution to developmental regulation of the life cycle. However this lineage went extinct in the next generation as it always displayed the SM phenotype on agar plates at

28°C; so while TSS-f6 was adaptive in the context of the static broth environment, it was non-adaptive within the experimental regime enforced by Hammerschmidt et al. (2014). This observation further emphasised the limitations of the original LCE selective regime – the use of the colony morphology proxy for niche preference in static broth was likely precluding discovery of a developmental program to transition through the life cycle. Nevertheless, understanding the genetic basis of the TSS-f6 phenotype switch was still of great interest.

2.1.2 Phenotypic characterisation

Summers (2018) previously carried out extensive characterisation of TSS-f6, as well as the ancestral strains f2, L17-*mutS*-WT & the wild-type SBW25. The colony morphology and mat formation phenotypes of TSS-f6 (MPB13890), f2 (MPB13893), L17-*mutS*-WT (MPB13896) & SBW25 (MPB14218), are shown in *Table 2.1* below. TSS-f6 demonstrates an environmentally-responsive change to colony morphology, observed with incubation temperature – the SM phenotype at 28°C & WS phenotype at 20°C (or room temperature). This phenotype switch was also observed to be very stable, with multiple successive restreaks made from single colonies grown at either temperature, always displaying the colony phenotype of SM at 28°C & WS at 20°C (Summers, 2018). The stability of the TSS-f6 phenotype switch indicates that it is not a result of mutational change (or hypermutability), but rather an epigenetic mechanism of regulating gene expression in response to the environment. While for the ancestral strains the phenotype switch was not observed – f2 & L17-*mutS*-WT displaying the WS colony morphology at both 28°C & 20°C, and SBW25 the SM phenotype at either incubation temperature.

Strain	MPB	Colony morphology spot		Mat formation: 28°C
		28°C	20°C	
TSS-f6	13890			
f2 ancestor	13893			

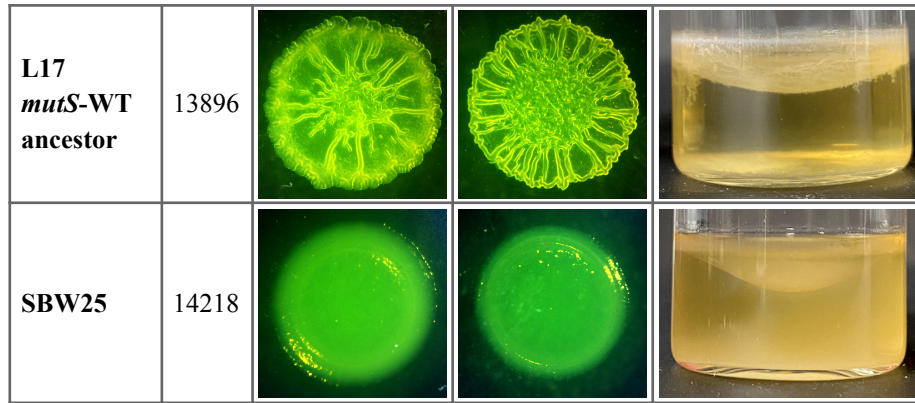


Table 2.1. TSS-f6 phenotype switch observed with incubation temperature. Phenotypic images & MPB number (unique strain storage number) provided for the strains TSS-f6, f2, L17-*mutS*-WT & SBW25. Colony morphology spot (imaged with Axiocam) – 5 μ L overnight culture spotted on a KBA plate and incubated for 1 day at 28°C or 20°C. Mat formation (imaged with iPhone 11) – 6 μ L overnight culture inoculated into a 6 mL KB microcosm (10^{-3} dilution) and incubated under static conditions for 24 hours at 28°C.

In the static broth environment, at 28°C TSS-f6 forms a thin ‘milky’ mat with colonisation of the broth phase, and at room temperature a thick ‘webbed’ mat with minimal broth growth (Summers, 2018). At 28°C, the unstable TSS-f6 mat is also prone to falling (see image in Table 2.1 above). The f2 & L17-*mutS*-WT ancestral strains both form a substantial mat at the air-liquid interface, with minimal growth of cells throughout the broth phase. While the wild-type SBW25 primarily colonises the broth phase, forming only a very thin & feeble mat that droops into the centre and is often disconnected from the walls of the microcosm, resulting in a tendency for mat collapse.

These phenotypic results suggest that the TSS-f6 strain has evolved the capacity to sense some signal present in the static broth and agar plate environment, that is amplified by a decrease in incubation temperature (e.g. from 28°C to 20°C). In response to this environmental signal, cells trigger the overproduction of an adhesive polymer (e.g. cellulose), resulting in the formation of a mat at the broth surface and the WS colony morphology at 20°C. The ancestral SBW25 displays a primitive ability to activate biofilm formation at the surface of the static broth environment; this is not surprising given the ecological role of the *P. fluorescens* SBW25 bacterium in colonisation of the plant phyllosphere (Rainey & Bailey, 1996). While the f2 & L17-*mutS*-WT ancestors do not demonstrate the phenotype switch, instead having constitutive activation of cellulose production and the WS phenotype. The TSS-f6 phenotype switch is likely dependent on mutational rewiring of the regulatory network underpinning the WS phenotype (McDonald et al., 2009), that allows for responsive gene expression and change to colony phenotype in response to the environmental conditions.

2.2 Suppressor analysis of TSS-f6

Summers (2018) performed suppressor analysis on the TSS-f6 genotype for the SM phenotype at 28°C or WS phenotype at 20°C, to gain insight into the regulatory genes underpinning the environmentally-responsive phenotype. This was achieved by mutagenesis of TSS-f6 (MPB13890) using the IS-Ω-km/hah transposon, with transposon mutants screened for loss of the phenotype switch on agar plates, and insertion locations identified by AP-PCR & Sanger sequencing (Giddens et al., 2007; Manoil, 2000). The results of these two mutagenesis screens are summarised in *Table 2.2* below, detailing the genes in which independent transposon insertions in TSS-f6 resulted in suppression of the SM phenotype at 28°C or WS phenotype at 20°C (with no phenotype switch observed).

Suppress	Ins.	Gene name	PFLU	Putative product	Size	Ortholog (PAO1)	Seq. identity	E-value
TSS-f6: SM at 28°C	17	<i>pflu5960</i>	5960	EAL/GGDEF domain protein	554	ProE	74.8%	0.0
	6	<i>amrZ</i>	4744	DNA-binding protein	108	AmrZ	85.0%	2e-60
	1	<i>fuzZ</i>	0479	glycosyl transferase	293	WapR	63.2%	1e-136
	3	<i>wspE</i>	1223	chemotaxis-related two-component system, sensor kinase	755	WspE	71.6%	0.0
5								
TSS-f6: WS at 20°C	2	<i>wspD</i>	1222	chemotaxis-like protein	232	WspD	62.4%	4e-89
	1	<i>wspA</i>	1219	methyl-accepting chemotaxis protein	540	WspA	69.7%	0.0
	3	<i>mutL</i>	0518	DNA mismatch repair protein	633	MutL	81.6%	0.0
	1	<i>mutY</i>	0323	A/G-specific adenine glycosylase	355	MutY	80.0%	0.0
	1	<i>wssB</i>	0301	cellulose synthase catalytic subunit	739	-	-	-
	1	<i>wssE</i>	0304	cellulose synthase protein C	1279	-	-	-

Table 2.2. Genes involved in TSS-f6 phenotype switch identified by suppressor analysis. Summary of select genes disrupted by transposon insertion in TSS-f6 (MPB13890), suppressing the SM phenotype at 28°C or WS phenotype at 20°C (Summers, 2018). Suppressor analysis was achieved by mutagenesis with the IS-Ω-km/hah transposon, and insertion locations identified by AP-PCR & Sanger sequencing (Giddens et al., 2007). Provided for each gene: Ins. (number of independent transposon insertions), Gene name, PFLU locus number (link to *Pseudomonas* Genome DB entry), Putative protein product, Size (number of amino acids), Ortholog in *P. aeruginosa* PAO1 (link to *Pseudomonas* Genome DB entry), Sequence identity (%) with *P. aeruginosa* PAO1 protein, and E-value (BLASTP search).

Suppressor analysis revealed that the SM phenotype of TSS-f6 at 28°C was dependent on the genes: *pflu5960* (x17 independent transposon insertions), *amrZ* (x6), *pflu0479* (x1) & *wspE*

(x3). While the WS phenotype at 20°C required the genes: *wspE* (x5), *wspD* (x2), *wspA* (x1), *mutL* (x3), *mutY* (x1), *wssB* (x1) & *wssE* (x1) (Summers, 2018).

2.2.1 *wsp* & *wss* operons and MMR system

In TSS-f6, suppression of the WS phenotype at 20°C was achieved primarily by transposon insertions in the *wsp* & *wss* operons, as well as genes of the DNA mismatch repair (MMR) system (Summers, 2018). The involvement of the Wsp pathway and Wss cellulose synthase pathway was to be expected, based on extensive knowledge of the WS phenotype in SBW25 (Spiers et al., 2002; Spiers et al., 2003; Bantinaki et al., 2007; McDonald et al., 2009). This confirms for TSS-f6 that expression of the WS phenotype at 20°C is the result of activation of the Wsp system (encoded by the *wsp* operon), production of c-di-GMP by the diguanylate cyclase enzyme WspR, and overproduction of acetylated cellulose by the *wss*-encoded cellulose synthase complex (Spiers et al., 2003). Transposon insertions were also observed in the genes *mutL* (*pflu0518*) & *mutY* (*pflu1323*), that encode proteins of the DNA mismatch-repair (MMR) system, responsible for the repair of base mismatches during DNA replication (Modrich, 1991). Disruption to the MMR system is predicted to cause elevation of mutation rate (Oliver et al., 2002). This may then result in secondary mutations (e.g. in the *wsp* operon) that cause suppression of the WS phenotype in TSS-f6; making it unlikely that MutL & MutY are directly involved in the environmentally-responsive phenotype.

2.2.2 *wspE* gene

Paradoxically, during the mutagenesis screen of TSS-f6, transposon insertions in the *wspE* gene resulted in suppression of both the WS and SM phenotype (Summers, 2018). *wspE* ([pflu1223](#)) encodes the putative sensor kinase/response regulator protein WspE (length: 755 amino acids), with 71.6% sequence identity to WspE in *P. aeruginosa* PAO1 ([PA3704](#); BLASTP *E*-value: 0.0). WspE contains a histidine phosphotransfer (Hpt) domain ([PF01627](#); residue: 11-100; *E*-value: $4.7e-13$), histidine kinase ATPase domain ([PF02518](#); residue: 332-472; *E*-value: $2.1e-11$), CheW-like domain ([PF01584](#); residue: 479-607; *E*-value: $5.9e-17$), and CheY-like response regulator receiver (REC) domain ([PF00072](#); residue: 634-745; *E*-value: $5.8e-25$). Within the Wsp receptor signalling complex, the WspE kinase is predicted to function in phosphorylation of the WspR DGC (and WspF methylesterase, inactivating the signalling cascade), resulting in activation of c-di-GMP synthesis and cellulose production (Bantinaki et al., 2007; Güvener & Harwood, 2007). Previous studies in *P. aeruginosa* PAO1 demonstrated that disruption of WspE results in suppression of the

wrinkled phenotype (in the *wspF* mutant background), with *wspE* deletion mutants displaying no cell aggregation or biofilm formation (D'Argenio et al., 2002; Hickman et al., 2005). Therefore the observation of TSS-f6 transposon mutants with suppression of the WS phenotype at 20°C, due to insertions throughout the WspE protein (residue 171, 81, 469, 741 & 379), is consistent with previous literature. This likely resulted in loss of WspE kinase activity, preventing activation of the WspR DGC and synthesis of c-di-GMP, and thus the SM phenotype (Bantinaki et al., 2007). While transposon insertions suppressing the SM phenotype at 28°C, were located within a particular region of the C-terminal REC domain in WspE (residue 660, 618 & 688), the effect of which is unclear.

To further investigate the WS & SM phenotype TSS-f6 *wspE* transposon mutants, two representatives were selected – TSS-f6 WS Tn-*wspE* (MPB13591; insertion at residue 660) & TSS-f6 SM Tn-*wspE* (MPB13588; insertion at residue 81). For these genotypes, Summers (2018) carried out Cre-mediated excision of the transposon, leaving a 189 bp scar at the insertion site (Bailey & Manoil, 2002); the resulting strains TSS-f6-WspE*(WS) (MPB13598) & TSS-f6-WspE*(SM) (MPB13596) displayed no change to colony morphology. Therefore the observation of the TSS-f6 *wspE* mutants with opposite phenotypes cannot be explained by polar effects of the transposon on nearby genes (e.g. *wspF* downstream). Summers (2018) also performed a second round of suppressor analysis with the cre-deleted WspE mutants, and found for TSS-f6-WspE* (WS) that transposon insertions in *wspE* (7 independent insertions) resulted in suppression of the WS phenotype. This result confirms that the initial insertions in *wspE* (at residue 618-688) must not have caused complete loss of function to WspE, and instead may have activated kinase activity. A number of studies in *Pseudomonas* species observed mutations in the REC domain of WspE (e.g. D638G in SBW25, and D648G in PAO1), which resulted in activation of the WspR DGC, overproduction of c-di-GMP and the WS phenotype (McDonald et al., 2009; Kim et al., 2016; Kessler & Kim., 2022). In conclusion, for TSS-f6 the WspE kinase is important for the WS phenotype at 20°C; the *wspE* transposon mutants suppressing the SM phenotype can be explained as an artefact of the insertion activating protein function.

2.2.3 *pflu5960* gene

For the TSS-f6 phenotype switch, the genes *pflu5960*, *amrZ* & *pflu0479* were found to be required for maintenance of the SM phenotype at 28°C (Summers, 2018). [pflu5960](#) encodes the putative GGDEF/EAL domain protein Pflu5960 (length: 554 amino acids), with 74.8%

sequence identity to the phosphodiesterase ProE in *P. aeruginosa* PAO1 ([PA5295](#); BLASTP *E*-value: 0.0). Pflu5960 contains a GGDEF-like domain ([PF00990](#); residue: 125-274; *E*-value: $4.4e-31$), and EAL domain ([PF00563](#); residue: 298-533; *E*-value: $1.9e-75$). This protein lacks the conserved GGDEF motif required for DGC activity (instead with GSDEF), but contains an intact EAL motif, indicating that Pflu5960 functions as a PDE in the breakdown of c-di-GMP (Hengge, 2009). In SBW25, Lind et al. (2015) identified *pflu5960* mutants with the WS phenotype, and hypothesised that mutation within the GGDEF domain caused activation of Pflu5960 DGC catalytic activity. However this conclusion does not fit with the previous literature in *P. aeruginosa* (Kulasakara et al., 2006; Ha et al., 2014b). In PAO1, Feng et al. (2020) have shown that ProE is a highly active phosphodiesterase enzyme able to degrade c-di-GMP, negatively regulating production of the Pel & Psl exopolysaccharides. Deletion of the *proE* gene in both PA14 & PAO1, resulted in the wrinkly colony morphology, though no difference in biofilm formation or swimming/swarming motility as compared to the wild-type (Ha et al., 2014b; Feng et al., 2020). Therefore in TSS-f6, the Pflu5960 protein likely functions as a PDE enzyme, degrading the low levels of c-di-GMP produced by the Wsp system (or other DGC enzymes), to maintain the SM phenotype at 28°C.

2.2.4 *amrZ* gene

amrZ ([pflu4744](#)) encodes the putative DNA-binding protein AmrZ (length: 108 amino acids), predicted to localise in the cytoplasm, with 85.0% sequence identity to AmrZ (also known as AlgZ) in *P. aeruginosa* PAO1 ([PA3385](#); BLASTP *E*-value: $2e-60$). AmrZ contains an Arc-like DNA binding domain ([PF03869](#); residue: 11-60; *E*-value: $2.2e-26$). The AmrZ protein has been demonstrated to regulate alginate synthesis by activation of *algD* transcription (Baynham et al., 1999), and twitching motility, with deletion of the *amrZ* gene resulting in no detectable type IV pili on the cell surface (Baynham et al., 2006). Tart et al. (2006) have also shown that AmrZ inhibits flagellum production and expression of the flagellar regulatory protein FleQ, by specific binding at the *fleQ* promoter. In *P. aeruginosa* PAO1, the AmrZ transcriptional regulator represses production of the Psl exopolysaccharide, by direct binding to the *pslA* promoter region (Jones et al., 2013); deletion of *amrZ* resulting in an increase in Psl production & c-di-GMP, and formation of structured biofilms containing larger microcolonies (Jones et al., 2014). Furthermore, Jones et al. (2014) attributed the regulation of c-di-GMP levels using ChIP-Seq & RNA-Seq analysis, to the binding of AmrZ to numerous DGC-encoding genes, including *gcbA* ([PA4843](#); ortholog of *pflu0621* in

SBW25). In SBW25, AmrZ was shown to negatively regulate the *wss* operon and therefore cellulose production (Giddens et al., 2007). Lind et al. (2015) also observed mutations in *amrZ* (in combination *dipA* or *pflu4414* & *fleQ*), resulting in the WS phenotype.

Therefore in TSS-f6, AmrZ likely acts as a suppressor of the cellulose synthase complex, by binding to the *wss* operon promoter region, thus preventing cellulose production and suppressing the WS phenotype at 28°C. It is also possible that AmrZ regulates the transcription of other DGC-encoding genes related to the WS phenotype, with the binding and repression of a number of genes observed in *P. aeruginosa* PAO1 (Jones et al., 2014). The Pflu5960 PDE and AmrZ transcriptional regulator are both important in TSS-f6 for maintenance of the SM phenotype at 28°C, though it is unclear whether these proteins are inactive at lower temperatures or just overpowered by the high levels of c-di-GMP produced from the activate Wsp pathway & WspR DGC.

2.2.5 *pflu0479* gene

fuzZ ([pflu0479](#)) encodes the putative glycosyl transferase FuzZ (length: 293 amino acids), predicted to localise in the inner membrane, with 63.2% sequence identity to WapR in *P. aeruginosa* PAO1 ([PA5000](#); BLASTP *E*-value: 1e-136). In *P. aeruginosa* PAO1, WapR was shown to function as a rhamnosyltransferase enzyme, capping outer core oligosaccharides (OS) in the lipopolysaccharide (LPS) layer of the outer membrane with an O-antigen chain; deletion of the *wapR* gene resulting in uncapped and truncated LPS core OS (Poon et al., 2008). LPS deficiency due to disruption of WapR was also shown to increase cell adhesion to glass and cell-cell cohesion during early biofilm development, and formation of a biofilm with reduced thickness as compared to the wild-type PAO1 (Lau et al., 2009). In SBW25, the locus *pflu0475-pflu0479* was previously shown to be essential for the WS phenotype, identified in suppressor analysis screens with both the LSWS *wspF* mutant & AWS *awsX* mutant (McDonald et al., 2009). Ferguson et al. (2013) termed the genes *pflu0475-pflu0479* as the ‘fuzzy spreader’ locus *fuzVWXYZ*; disruption of *pflu0478* (*fuzY*) resulting in the fuzzy spreader phenotype, and formation of a weak mat in static broth composed of transient cell ‘rafts’. In TSS-f6, FuzZ is likely important for LPS modification, though it is not obvious how this relates to maintenance of the SM phenotype at 28°C.

2.3 Mutational history of TSS-f6

Whole-genome sequencing was previously completed of TSS-f6 (MPB13890) and the ancestral strains f2 (MPB13893) & L17-*mutS*-WT (MPB13896), to determine the mutational basis of the phenotype switch (Summers, 2018). The unique mutations identified in TSS-f6 & f2, and those in the *wsp* operon for L17-*mutS*-WT, are summarised in *Table 2.3* below. TSS-f6 obtained two final mutations – a substitution in WspA (V441G), and small in-frame duplication in DipA (470_472 dupNLT). The f2 ancestor had only two unique mutations – a substitution in WspA (T104N) & WspE (H70L). And the L17-*mutS*-WT ancestor contained three existing mutations in the Wsp pathway – a substitution in WspA (D253Y) & WspF (I295S), and small in-frame deletion in WspB (37_39delAEV). The details of all mutations in the L17-*mutS*-WT background are provided by Summers (2018) (see *Appendix 1 - Table 3*).

Strain	Gene name	PFLU	Putative product	Nucleotide change	Amino acid change	Protein domain	E-value
TSS-f6	<i>wspA</i>	1219	methyl-accepting chemotaxis protein	1321T>G	V441G	MCPsignal	5.0e-34
	<i>dipA</i>	0458	hypothetical protein	1408_1416dup TTGGACTGG	470_472 dupNLT	GGDEF	1.0e-38
f2 ancestor	<i>wspA</i>	1219	methyl-accepting chemotaxis protein	311C>A	T104N	4HB MCP	1.1e-20
	<i>wspE</i>	1223	two-component system, sensor kinase	209A>T	H70L	Hpt	4.7e-13
L17 <i>mutS</i> -WT ancestor	<i>wspA</i>	1219	methyl-accepting chemotaxis protein	757G>T	D253Y	HAMP	2.2e-11
	<i>wspB</i>	1220	chemotaxis-like protein	109_117del GCCGAAGTG	37_39 delAEV	CheW	3.5e-24
	<i>wspF</i>	1224	chemotaxis-specific methyltransferase	884T>G	I295S	CheB methylest	6.5e-55

Table 2.3. Unique mutations identified in TSS-f6 and the f2 & L17-*mutS*-WT ancestors. The unique coding sequence variation is given for the strains TSS-f6 (MPB13890) & f2 (MPB13893), and the mutations in the *wsp* operon for L17-*mutS*-WT (MPB13896) (Summers, 2018). Provided for each mutation: Gene name, PFLU locus number (link to *Pseudomonas* Genome DB entry), Putative protein product, Nucleotide sequence change, Amino acid sequence change, Protein domain the mutation is located within (link to InterPro entry), and E-value (Pfam database search).

2.3.1 TSS-f6 – *wspA* mutation

For the TSS-f6 phenotype switch, the final WspA substitution V441G was considered of great interest, due to the role of WspA as a chemoreceptor (Summers, 2018). *wspA* ([pflu1219](#)) encodes the putative methyl-accepting chemotaxis protein (MCP) WspA,

predicted to localise in the inner membrane, with 69.7% sequence identity to WspA in *P. aeruginosa* PAO1 ([PA3708](#); BLASTP *E*-value: 0.0). WspA contains a four-helix bundle (4HB) MCP sensory module ([PF12729](#); residue: 3-181; *E*-value: $1.1e-20$) flanked by two transmembrane helices, a HAMP regulatory domain ([PF00672](#); residue: 208-259; *E*-value: $2.2e-11$), and MCP signalling domain ([PF00015](#); residue: 324-503; *E*-value: $5.0e-34$). Models of the *wsp* pathway in SBW25 predict the formation of a receptor signalling complex (bound to the inner membrane), containing the WspA MCP, WspB & WspD scaffold proteins, and the WspE kinase; the kinase activity is controlled by the addition & removal of methyl groups by the WspC methyltransferase & WspF methylesterase, altering the phosphorylation state of the WspR DGC (Bantinaki et al., 2007). The WspA receptor therefore receives some environmental signal, that is transduced along the Wsp pathway, causing activation of the WspR DGC enzyme that synthesises c-di-GMP, resulting in overproduction of cellulose and the WS phenotype (Bantinaki et al., 2007). Hickman et al. (2005) found that deletion of the *wspA* gene in *P. aeruginosa* PAO1 had no effect on colony morphology, surface attachment, or biofilm formation (only the deletion of *wspF*).

2.3.1.1 WspA conserved residues

Ortega et al. (2017) predicted in *P. aeruginosa* the interaction between the WspA MCP and histidine kinase (CheA) or adaptor (CheW) proteins of the Wsp pathway; identifying the conserved motif LLSxxxxIExEK in WspA (residue 388-399), and the corresponding motif LAHIERM in the WspE kinase (residue 506-512). The conserved methylation sites were also predicted in heptad C14 of WspA (residue E496, Q497 & Q500), and the binding region of the CheR-like WspC methyltransferase (residue 21-35) (Ortega et al., 2017). Additionally, Xu et al. (2021) identified the methylation sites E280 & E294 in WspA, with deletion of this region (residue 280-307) observed in environmental strains of *P. aeruginosa* isolated from crude oil. The loss of these methylation sites in the WspA chemoreceptor resulted in constitutive activation of the Wsp system, an increase in c-di-GMP level and the hyper-biofilm phenotype; although deletion of the *wspF* gene resulted in even higher levels of c-di-GMP (Xu et al., 2021). Kim et al. (2016) observed the evolution of *P. fluorescens* Pf0-1 mutants containing an in-frame deletion (residues 283-311) in this same region of WspA, conferring the WS phenotype. In TSS-f6, the WspA substitution V441G is located within the MCP signalling domain, with no obvious connection to any of the predicted kinase binding or methylation sites. Therefore this mutation is unlikely to result in constitutive

activation or disruption of the Wsp system, but rather alter the sensing or transduction of environmental signals by the WspA MCP.

2.3.1.2 Environmental sensing by WspA

Previous studies in *P. aeruginosa* PAO1 have shown that the WspA protein localises in unstable polar/lateral clusters within the cell, as compared to standard chemoreceptors that are found at the cell poles; this localisation being dependent on the C-terminal signalling domain, but not the N-terminal periplasmic ligand-binding domain (Güvener & Harwood, 2007; O'Connor et al., 2012). O'Connor et al. (2012) speculate that WspA is able to sense a signal associated with cell growth on a surface (e.g. mechanical stress), activating the production of c-di-GMP by the WspR DGC. Chen et al. (2014) found that ethanol (produced by the fungus *Candida albicans*) stimulated an increase in c-di-GMP level and biofilm formation on plastic surfaces, this effect was dependent on both WspR & WspA. The presence of ethanol may cause an increase in membrane rigidity, by altering the lipid composition of the inner membrane (Dombek & Ingram, 1984; Chen et al., 2014). In a recent study, perturbation of the cell envelope by exposure to chemical compounds (including SDS, ethanol, lysozyme & glycerol), was observed to result in the unfolding of proteins in the periplasm, and activation of the Wsp pathway, including an increase in c-di-GMP levels (O'Neal et al., 2022). Based on this result, O'Neal et al. (2022) suggest that upon surface contact the WspA receptor senses cell envelope stress (e.g. unfolded periplasmic proteins or change to membrane fluidity), inducing structural change to WspA that activates the Wsp system, and triggers biofilm formation.

In TSS-f6 the final *wspA* mutation may therefore change the sensitivity of the WspA receptor to an environmental signal related to cell envelope stress (O'Neal et al., 2022), which may also correlate with temperature. Exposure of bacterial cells to low temperatures has been demonstrated to increase membrane rigidity, which may then cause activation of membrane-bound sensors or other proteins (Shivaji & Prakash, 2010). For example, Bouffartigues et al. (2020) observed in *P. aeruginosa* the activation of the ECF sigma factor SigX in response to cold shock or chemical induction of membrane stress (using valinomycin), with SigX upregulating the downstream *cfrX* & *cmpX* genes. Vásquez-Ponce et al. (2017) also identified an environmental strain of *Pseudomonas mandelii*, that overproduces the biofilm component alginate at low temperatures, likely due to downregulation of the anti-sigma factor MucA (negative regulator of the *alg* operon). The

TSS-f6 phenotype switch could be underpinned by an analogous system sensitive to temperature that utilises the Wsp pathway.

2.3.1.3 Reversion of TSS-f6 *wspA* mutation

To investigate whether the final TSS-f6 *wspA* mutation (p.V441G) was required for the phenotype switch, this mutation was reverted to wild-type by site-directed mutagenesis, producing the strain TSS-f6-*wspA*-mut1-WT (MPB16047). The phenotypic effect of reversion of this mutation in TSS-f6 is displayed in *Table 2.4* below. I found that this resulted in loss of the phenotype switch and restoration of mat formation capacity, with the WS colony morphology phenotype observed at both 28°C & 20°C. TSS-f6-*wspA*-mut1-WT resembles the phenotype of the f2 ancestor, except that at 28°C the colony texture is slightly less wrinkly, and some broth colonisation is observed in the static broth environment. This result confirms that the substitution V441G in the WspA MCP is essential for the TSS-f6 environmentally-responsive phenotype.

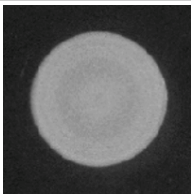
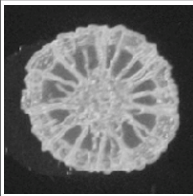
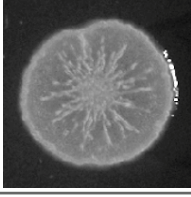
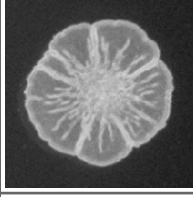
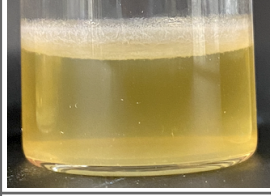
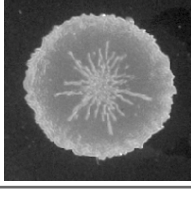
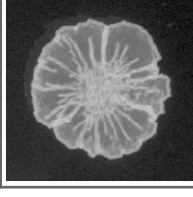
Strain	MPB	Genotype	Colony morphology spot		Mat formation: 28°C
			28°C	20°C	
TSS-f6	13890	Evolved			Refer to Table 2.1
TSS-f6 <i>wspA</i> - mut1-WT	16047	Evolved <i>wspA</i> - G441V			
f2 ancestor	13893	Evolved			Refer to Table 2.1

Table 2.4. Loss of phenotype switch by reversion of final TSS-f6 *wspA* mutation. Phenotypic images, MPB number & Genotype (Evolved in experiment or Wild-type (WT), and relevant mutation) provided for the strains TSS-f6, TSS-f6-*wspA*-mut1-WT & f2 ancestor. Colony morphology spot (imaged with ChemiDoc) & Mat formation as described in [Table 2.1](#) legend.

2.3.2 TSS-f6 – *dipA* mutation

The other unique mutation observed in TSS-f6 was the in-frame duplication 470_472dupNLT in DipA (Summers, 2018). The *dipA* ([pflu0458](#)) gene encodes the hypothetical protein DipA (length: 894 amino acids), with predicted localisation to the inner membrane, and 71.3% sequence identity to DipA in *P. aeruginosa* PAO1 ([PA5017](#); BLASTP *E*-value: 0.0). DipA contains a GAF regulatory domain ([PF01590](#); residue: 193-328; *E*-value: $3.4e-12$), PAS sensor domain ([PF13426](#); residue: 352-454; *E*-value: $7.0e-13$), GGDEF domain ([PF0090](#); residue: 466-619; *E*-value: $1.0e-38$), and EAL domain ([PF00563](#); residue: 640-875; *E*-value: $2.6e-73$). The DipA protein has a degenerate GGDEF motif, with the intact EAL motif indicating likely function as a PDE in the degradation of c-di-GMP (Hengge, 2009). This is supported by previous studies in *P. aeruginosa*, demonstrating that DipA has PDE enzymatic activity (no DGC activity was detected), and reduces c-di-GMP levels in response to environmental conditions that induce dispersal (Li et al., 2007; Roy et al., 2012). Deletion of the *dipA* gene in PAO1 or PA14, resulted in greater production of the Psl exopolysaccharide, an increase in biofilm biomass (but no change to thickness or architecture), and reduction in swarming motility (Roy et al., 2012). In SBW25, the silencing of *dipA* gene expression with CRISPRi, resulted in a more densely structured biofilm, although no increase in thickness was observed as compared to the wild-type control (Noirot-Gros et al., 2019). Lind et al. (2015) also identified loss-of-function mutations in *dipA* (in combination with mutation to *amrZ* or *pflu0621*), as an alternate mutational pathway to the WS phenotype. In TSS-f6, the DipA duplication is located within the inactive GGDEF domain; this likely caused a decrease in the PDE activity of DipA, resulting in higher levels of c-di-GMP and the WS phenotype.

2.3.3 f2 ancestor – *wspA* & *wspE* mutations

The f2 ancestral strain obtained only two mutations over the six life cycle generations (refer to [Section 2.1.1](#)) – the substitution T104N in WspA & H70L in WspE (Summers, 2018). The observation of so few mutations implies that the f2 ancestor was transitioning between the WS & SM phenotypes by reversible mutation to a single locus (e.g. expansion/contraction of a guanine tract in the *wsp* operon). The WspA substitution T104N is located within the 4HB MCP sensory domain (see discussion of *wspA* in [Section 2.3.1](#)). For the response of the Wsp system to environmental surface contact, sequence conservation of this N-terminal periplasmic domain was shown to be inessential, indicating that ligand binding is not required for WspA to sense the environment (O'Connor et al., 2012; O'Neal et al., 2022). Therefore

the effect of this f2 *wspA* mutation is unclear, but it likely resulted in the turning on/off of the WS phenotype, with the *wspE* mutation presumably having the opposite effect. While the WspE kinase substitution H70L is located in the Hpt domain (see discussion of *wspE* in [Section 2.2.2](#)), with the effect on kinase activity & phosphorylation state of the WspR DGC unknown. Kessler & Kim (2022) identified a number of evolved *wspE* mutants of *P. fluorescens* Pf0-1; all missense mutations in WspE (e.g. R58W) were found to increase c-di-GMP production, and nonsense or frameshift mutations to decrease c-di-GMP levels. As the f2 *wspE* mutation cannot be loss-of-function (WspE was shown to be active in TSS-f6, refer to [Section 2.2.2](#)), it is more likely that this mutation resulted in activation of c-di-GMP production by the WspR DGC, and thus the WS phenotype. It is not evident whether either of these mutations obtained by the f2 ancestor are necessary for the TSS-f6 phenotype switch, or were just acquired to turn the WS phenotype on/off for transitioning through the life cycle.

2.3.4 L17-*mutS*-WT ancestor – *wsp* mutations

The L17-*mutS*-WT ancestor contains a total of 75 pre-existing mutations, as a result of the period of time that Line 17 spent as a hypermutator, due to disruption of the *mutS* gene & MMR system (refer to [Section 1.3.3.2](#)) (Hammerschmidt et al., 2014; Summers, 2018). This complicates the mutational history of TSS-f6, and may therefore make it difficult to disentangle the exact mutations required for the environmentally-responsive phenotype. I previously showed that alteration to the WspA MCP was necessary for the TSS-f6 phenotype switch (see [Section 2.3.1.3](#)); based on this result, focusing on the L17-*mutS*-WT mutations in the *wsp* operon seemed the most reasonable way to proceed. L17-*mutS*-WT obtained three mutations in the Wsp pathway – the substitution D253Y in the HAMP domain of WspA, substitution I295S in the methylesterase domain of WspF, and an in-frame deletion (37_39delAEV) in the CheW-like domain of WspB (Summers, 2018). As with the f2 *wspA* mutation, the L17-*mutS*-WT *wspA* mutation is also located in the non-essential N-terminal region, so the effect of this mutation is unclear (O'Connor et al., 2012).

2.3.4.1 WspF methylesterase

wspF ([pflu1224](#)) encodes the methylesterase protein WspF (length: 336 amino acids), with 75.8% identity to WspF in *P. aeruginosa* PAO1 ([PA3703](#); BLASTP *E*-value: 0.0). WspF contains a CheY-like REC domain ([PF00072](#); residue: 3-102; *E*-value: 1.2e-16), and CheB-like methylesterase domain ([PF01339](#); residue: 154-330; *E*-value: 6.5e-55). The WspF methylesterase has been predicted to function in removal of methyl groups from the WspA

MCP, controlling the activation state of the Wsp signalling complex (together with the WspC methyltransferase); mutation to the *wspF* gene providing the main mutational route to the WS phenotype (Bantinaki et al., 2007). In *P. aeruginosa*, deletion of *wspF* resulted in an increase in c-di-GMP production by the WspR DGC enzyme, and elevated biofilm formation (Hickman et al., 2005). Therefore the L17-*mutS*-WT *wspF* mutation (p.I295S) likely disrupted methylesterase activity, causing activation of the Wsp pathway & WspR DGC, and therefore the WS phenotype. Bantinaki et al. (2007) previously identified a number of similar mutations in the *wspF* gene (including p.S301R & p.G275C), that produced the WS phenotype in SBW25.

2.3.4.2 WspB scaffold protein

While *wspB* ([pflu1220](#)) encodes the putative chemotaxis protein WspB (length: 170 amino acids), with 60.7% identity to WspB in *P. aeruginosa* PAO1 ([PA3707](#); BLASTP *E*-value: $2e-57$). WspB contains a CheW-like coupling domain ([PF01584](#); residue: 19-156; *E*-value: $3.5e-24$), and is predicted to function as a scaffold protein for the formation of the Wsp receptor signalling complex (Bantinaki et al., 2007). In *P. aeruginosa* PAO1, O'Connor et al. (2012) observed that deletion of the *wspB* or *wspD* gene caused disruption to WspA subcellular localisation, demonstrating the importance of these scaffold proteins in the function of the Wsp complex. Mutations in *wspB* have not been previously identified to influence the WS phenotype in SBW25; although in *P. fluorescens* Pf0-1, mutations in WspB (e.g. L135P) were found to decrease c-di-GMP levels and suppress the WS phenotype (Kessler & Kim, 2022). Therefore the effect of the L17-*mutS*-WT *wspB* mutation is unclear, but was unlikely to have caused major disruption to the Wsp pathway.

2.4 Deletion of identified candidate genes

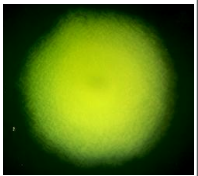
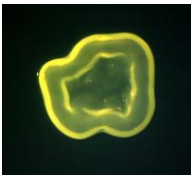
A number of candidate genes were identified by suppressor analysis, indicating involvement in the TSS-f6 environmentally-responsive phenotype, as previously discussed in [Section 2.2](#). The *wsp* & *wss* operons were found to be important for maintenance of the WS phenotype at 20°C, and the genes *wspE*, *pflu5960* & *amrZ* for the SM phenotype at 28°C (Summers, 2018). To further investigate the role of these genes in the TSS-f6 phenotype switch, each gene (or operon) was deleted in the TSS-f6 and wild-type SBW25 background by site-directed mutagenesis, and the phenotypic effect examined. Mutation constructs were first assembled by SOE-PCR & ligation into pUIC3 (see [Section 5.6.1](#)) or by PCR & Gibson

assembly in the pUIC3-mini vector (see [Section 5.6.2](#)). Each deletion was then introduced into TSS-f6 (MPB13890) & SBW25 (MPB14218), as well as the f2 ancestor (MPB13893) where applicable, by allelic exchange (see [Section 5.6.3](#)). The presence of all mutations were confirmed by colony PCR and Sanger sequencing of the mutation construct and flanking regions. This section will present the results of deletion of each gene or operon in TSS-f6 & SBW25, including the effect on the colony morphology and mat formation phenotypes.

2.4.1 *WspE* histidine kinase

wspE ([pflu1223](#)) encodes the histidine kinase/response regulator protein WspE, with disruption of kinase activity resulting in phosphorylation of the WspR DGC, overproduction of c-di-GMP & cellulose, and the WS phenotype (Bantinaki et al., 2007). Transposon insertions in *wspE* were observed to suppress both the SM phenotype at 28°C and WS phenotype at 20°C in TSS-f6 (Summers, 2018); see previous discussion in [Section 2.2.2](#). It was hypothesised that insertion in the C-terminal REC domain of WspE resulted in activation of kinase activity. To confirm this, the entire *wspE* gene was deleted in the two selected representative TSS-f6 *wspE* mutants (MPB13598 & MPB13596), producing the strains: TSS-f6-WspE*(WS)- Δ *wspE* (MPB14105) & TSS-f6-WspE*(SM)- Δ *wspE* (MPB14106). I found that both of these *wspE* deletion mutants displayed the SM phenotype, therefore confirming that the transposon insertion causing suppression of the SM phenotype in TSS-f6, was indeed a consequence of protein activation.

The *wspE* gene was also deleted in the TSS-f6 & WT SBW25 background, producing the strains: TSS-f6- Δ *wspE* (MPB14083) & SBW25- Δ *wspE* (MPB14082); with the effect on single colony morphology shown in [Table 2.5](#) below. As was expected, I observed that removal of the WspE kinase in TSS-f6 caused suppression of the WS phenotype and loss of the phenotype switch in response to temperature. While in SBW25, the deletion of *wspE* resulted in no change to colony morphology, with the SM phenotype displayed at both incubation temperatures.

Strain	MPB	Genotype	Colony morphology	
			28°C	20°C
TSS-f6	13890	Evolved		

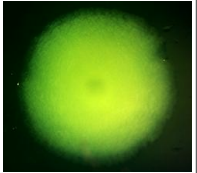
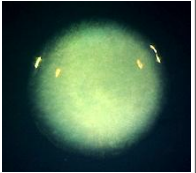
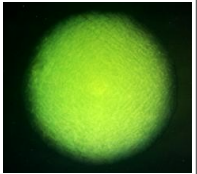
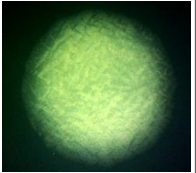
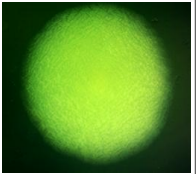
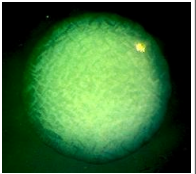
TSS-f6 <i>ΔwspE</i>	14083	Evolved <i>ΔwspE</i>		
SBW25	14218	WT		
SBW25 <i>ΔwspE</i>	14082	WT <i>ΔwspE</i>		

Table 2.5. Deletion of *wspE* suppresses the WS phenotype in TSS-f6. Colony images, MPB number & Genotype (Evolved in experiment or WT, and relevant mutation) provided for the strains TSS-f6, TSS-f6-*ΔwspE*, SBW25 & SBW25-*ΔwspE*. Colony morphology (imaged with AxioCam) – single colonies from an overnight culture spread on a KBA plate and incubated for 2 days at 28°C or 20°C.

These results confirm that the Wsp system is required for the environmentally-responsive phenotype in TSS-f6. The WspE kinase is functionally active at 20°C, mediating the phosphorylation of the WspR DGC, with DGC activity resulting in an increase in c-di-GMP levels and thus the WS phenotype. Loss of WspE causes disruption of signal transduction along the Wsp pathway, preventing activation of the WspR DGC, and therefore generating the fixed SM phenotype (Bantinaki et al., 2007). In SBW25, the Wsp complex is already in an inactive state (e.g. WspR DGC with low activity), so deletion of the *wspE* gene did not generate any change to colony phenotype.

2.4.1.1 Suppressor analysis of TSS-f6 *wspE* mutant

Summers (2018) also carried out a second round of suppressor analysis with the TSS-f6 *wspE* mutant TSS-f6-WspE*(SM) (MPB13596; Cre-deletion leaving 189 bp scar at residue 81), with transposon insertions identified that suppress the SM phenotype at 20°C; the results are summarised in Table 2.6 below. The WS phenotype was restored by insertion in the following genes – *pflu5960* (x21), *amrZ* (x1), *wspA* (x1), *wspR* (x1) & *pflu5574* (x1).

Suppress	Ins.	Gene name	PFLU	Putative product	Size	Ortholog (PAO1)	Seq. identity	E-value
TSS-f6 WspE*: SM	21	<i>pflu5960</i>	5960	EAL/GGDEF domain protein	554	ProE	74.8%	0.0
	1	<i>amrZ</i>	4744	DNA-binding protein	108	AmrZ	85.0%	2e-60

1	<i>wspA</i>	1219	methyl-accepting chemotaxis protein	540	WspA	69.7%	0.0
1	<i>wspR</i>	1225	chemotaxis-related two component system response regulator	333	WspR	73.3%	2e-176
1	<i>pflu5574</i>	5574	phosphotransferase	341	PA0596	67.8%	1e-168

Table 2.6. Disruption of *pflu5960* & *amrZ* restores the WS phenotype in TSS-f6 *wspE* mutant. Summary of genes disrupted by transposon insertions in TSS-f6-WspE*(SM) (MPB13596), suppressing the SM phenotype at 20°C (Summers, 2018). Details as described in [Table 2.2](#) legend.

In TSS-f6, transposon insertions were also observed in *pflu5960* & *amrZ*, resulting in suppression of the SM phenotype at 28°C (Summers, 2018) (see [Section 2.2](#)). Pflu5960 likely functions as a PDE enzyme in the breakdown of c-di-GMP (Feng et al., 2020), while AmrZ is a DNA-binding transcriptional regulator that suppresses cellulose production by the *wss* operon (Giddens et al., 2007); as previously discussed in [Section 2.2.3](#) & [2.2.4](#). For the TSS-f6 *wspE* mutant, disruption of the WspE kinase was predicted to inactivate the Wsp signalling complex, and prevent the synthesis of c-di-GMP by the WspR DGC (Bantinaki et al., 2007). The observation of transposon insertions in *pflu5960* & *amrZ* restoring the WS phenotype, indicates that the Pflu5960 PDE & AmrZ regulator remain active in this background to maintain the SM phenotype. Therefore either the Wsp system & WspR DGC are still semi-functional, or c-di-GMP is being synthesised by other active DGC enzymes.

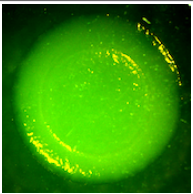
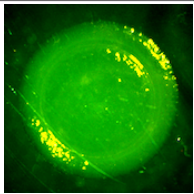
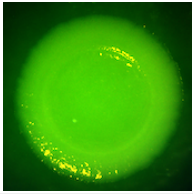
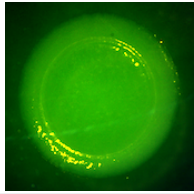
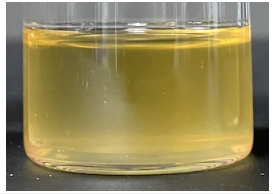
Summers (2018) also observed for TSS-f6-WspE*(SM), transposon insertions in *wspA* (residue 116), *wspR* (residue 37) & *pflu5574* that suppressed the SM phenotype. For the *wspR* transposon mutant, the SM phenotype was restored after Cre-mediated excision of the transposon, indicating polar effects on the upstream *wspF* gene (Summers, 2018). The restoration of the WS phenotype by transposon insertion in the *wsp* operon, further implies that the Wsp system is functional in this TSS-f6 *wspE* mutant. The disruption of the WspA chemoreceptor or WspR (likely polar effect on WspF methylesterase) may have caused activation of the Wsp complex, though exactly how is unclear.

While [pflu5574](#) encodes the putative phosphotransferase protein Pflu5574, with 67.8% sequence identity to AmgK in *P. aeruginosa* PAO1 ([PA0596](#); BLASTP *E*-value: 1e-168). In *Pseudomonas* species, AmgK has been shown to function in the phosphorylation of polysaccharide sugars (MurNAc & GlcNAc), for peptidoglycan biosynthesis and recycling (Gisin et al., 2013). *amgK* transposon mutants were also identified in *P. aeruginosa* PA14, conferring an increase in resistance to penicillin-class antibiotics (Dötsch et al., 2009). In

TSS-f6-WspE*(SM) the transposon insertion in *pflu5574* may inhibit synthesis of the cell wall peptidoglycan layer, and therefore activate the Wsp system (or other membrane-bound pathways containing a DGC enzyme), resulting in the WS phenotype. O’Neal et al. (2022) observed in PAO1, the Wsp-dependent increase in c-di-GMP levels in response to the antibiotic bleomycin that inhibits peptidoglycan synthesis.

2.4.2 Cellulose synthase operon

The *wss* operon was found to be essential for the WS phenotype of TSS-f6 at 20°C, with transposon insertions in *wssB* ([pflu0301](#)) & *wssE* ([pflu0304](#)) resulting in the SM phenotype (Summers, 2018); see discussion in [Section 2.2.1](#). This operon is composed of ten genes *wssA-wssJ* ([pflu0300-pflu0309](#)), encoding the cellulose synthase machinery required for production of an acetylated cellulosic polymer (Spiers et al., 2002; Spiers et al., 2003). Spiers et al. (2002) have previously shown that overproduction of cellulose underpins the wrinkly colony morphology & biofilm formation in evolved WS mutants of SBW25. For TSS-f6, suppression of the WS phenotype by transposon insertions in the *wss* operon indicates that cellulose is the basis of the WS phenotype at 20°C and main component of the biofilm matrix. To confirm this role of the cellulose synthase pathway in TSS-f6, the entire *wss* operon (*wssA-wssJ*) was deleted in SBW25, TSS-f6 & the f2 ancestor, producing the strains: SBW25- Δwss (MPB14424), TSS-f6- Δwss (MPB14425) & f2- Δwss (MPB14426). These deletion mutants were made using the *wssKO1* mutation construct (MPB12616), courtesy of Jenna Gallie (Gallie, 2010). The phenotypic effect of loss of the cellulose synthase pathway is displayed in [Table 2.7](#) below.

Strain	MPB	Genotype	Colony morphology spot		Mat formation: 28°C
			28°C	20°C	
SBW25	14218	WT			Refer to Table 2.1
SBW25 Δwss	14424	WT $\Delta wssA-wssJ$			

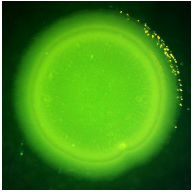
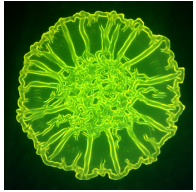
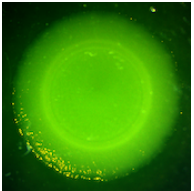
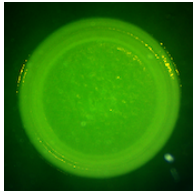
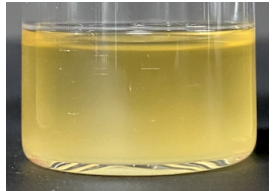
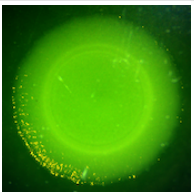
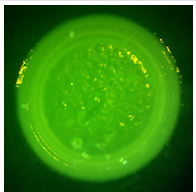
TSS-f6	13890	Evolved			Refer to Table 2.1
TSS-f6 Δwss	14425	Evolved $\Delta wssA-wssJ$			
f2 Δwss	14426	Evolved $\Delta wssA-wssJ$			

Table 2.7. Deletion of *wss* operon suppresses the WS phenotype & mat formation. Phenotypic images, MPB number & Genotype (Evolved in experiment or WT, and relevant mutation) provided for the strains SBW25, SBW25- Δwss , TSS-f6, TSS-f6- Δwss & f2- Δwss . Phenotypes as described in [Table 2.1](#) legend.

I found that deletion of the *wss* operon produced the SM colony morphology at both 28°C & 20°C for all genetic backgrounds (SBW25, TSS-f6 & f2). In the static broth environment, the wild-type SBW25 forms a feeble mat at the surface; removal of the cellulose synthase pathway resulted in only broth colonisation and no surface growth (see image in [Table 2.7](#)). This result is consistent with previous analysis by Ardre et al. (2019) of SBW25 growing at the ALI, in which the production of cellulose and formation of surface microcolonies was observed (regulated by the *Wsp*, *Aws* & *Mws* pathways). TSS-f6- Δwss also displays loss of mat formation capacity, with cell growth only in the broth phase, confirming that the biofilm matrix is composed of the cellulose polymer. These results support that the WS phenotype of TSS-f6 at 20°C is due to activation of the *Wsp* pathway, and the high levels of c-di-GMP causing overproduction of acetylated cellulose by the *wss* operon (Spiers et al., 2003).

2.4.3 Colonic acid operon

Summers (2018) observed the formation of a ‘lumpy’ mucoid coating covering the wrinkly colonies of TSS-f6, when grown on KBA plates at 20°C for 6 days. Based on the visual similarity to colonic acid based capsules in SBW25 (Beaumont et al., 2009), this coating was hypothesised to be the colonic acid-like polymer. In *P. fluorescens* SBW25, Gallie et al. (2015) identified the *wcaJ-wzb* locus (*pflu3658-3678*), with strong resemblance to the *E. coli* K12 gene cluster responsible for colonic acid biosynthesis (Stevenson et al., 1996). Deletion

of this *wcaJ-wzb* colonic acid (CA) operon resulted in translucent colonies (instead of opaque), and loss of cell capsulation (Gallie, 2010; Gallie et al., 2015). To confirm that the TSS-f6 mucoid coating was indeed colonic acid, I proceeded to delete the CA operon in SBW25 & TSS-f6, producing the strains: SBW25- Δ CA (MPB14478) & TSS-f6- Δ CA (MPB14479). These deletion mutants were made using the *wcaJ-wzb*KO construct (MPB00460), courtesy of Jenna Gallie (Gallie et al., 2015). The effect of removal of the colonic acid biosynthetic pathway on colony morphology is shown in *Table 2.8* below.

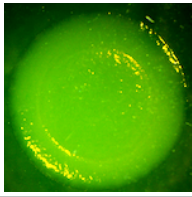
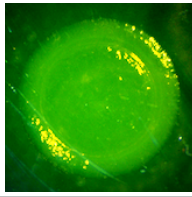
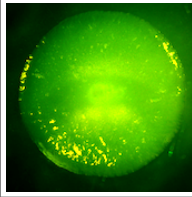
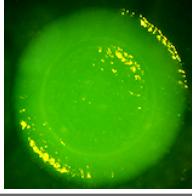
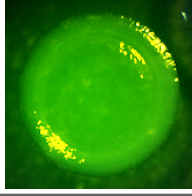
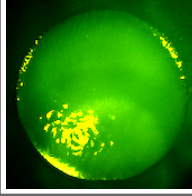
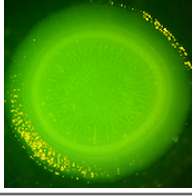
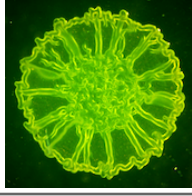
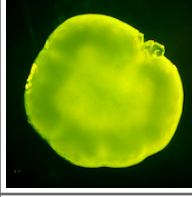
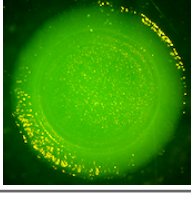

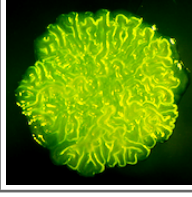
Strain	MPB	Genotype	Colony morphology spot		Colony 6d: 20°C
			28°C	20°C	
SBW25	14218	WT			
SBW25 Δ CA	14478	WT Δ <i>wcaJ-wzb</i>			
TSS-f6	13890	Evolved			
TSS-f6 Δ CA	14479	Evolved Δ <i>wcaJ-wzb</i>			

Table 2.8. Mucooid colony coating in TSS-f6 confirmed to be colonic acid. Colony images, MPB number & Genotype (Evolved in experiment or WT, and relevant mutation) provided for the strains SBW25, SBW25- Δ CA, TSS-f6 & TSS-f6- Δ CA. Colony morphology spot as described in [Table 2.1](#) legend. Colony 6d (imaged with Axioacam) – single colonies spread on a KBA plate and incubated for 6 days at 20°C.

Deletion of the *wcaJ-wzb* CA operon in SBW25 caused no change to colony phenotype; consistent with the ancestral capsulation state described previously (Gallie et al., 2015). In TSS-f6, I found that loss of the colonic acid operon had no effect on the phenotype switch, but did eliminate formation of the mucooid colony coating after incubation on plates for 6 days at 20°C; confirming that this coating was indeed the colonic acid polymer. However it is not apparent why the TSS-f6 genotype is producing colonic acid at low temperatures. In *E. coli*,

the exopolysaccharide CA likely functions in cell persistence under adverse environmental conditions (for example desiccation), with osmotic shock demonstrated to induce the synthesis of colonic acid (Ophir & Gutnick, 1994; Sledjeski & Gottesman, 1996). Therefore the formation of this colonic acid coating by TSS-f6 at 20°C may reflect that the cells are under stress from the environment.

2.4.4 Pflu5960 PDE enzyme

The [pflu5960](#) gene was found to be critical for the SM phenotype of TSS-f6 at 28°C (Summers, 2018). Pflu5960 likely functions as a PDE enzyme in the degradation of c-di-GMP, negatively regulating production of exopolysaccharides that constitute the biofilm matrix (Feng et al., 2020). In TSS-f6, Pflu5960 is predicted to have PDE enzymatic activity, important at 28°C for the breakdown of c-di-GMP and suppression of the WS phenotype; as discussed in [Section 2.2.3](#). To investigate the role of Pflu5960, the entire *pflu5960* gene was deleted in SBW25, TSS-f6 & f2, producing the strains: SBW25- Δ 5960 (MPB14084), TSS-f6- Δ 5960 (MPB14085) & f2- Δ 5960 (MPB14634); the effect shown in [Table 2.9](#) below.

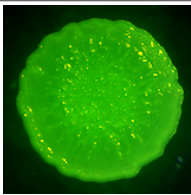
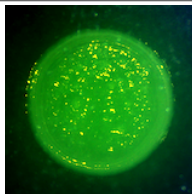
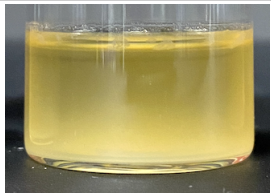


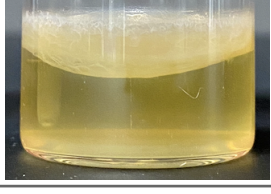
Strain	MPB	Genotype	Colony morphology spot		Mat formation: 28°C
			28°C	20°C	
SBW25 Δ 5960	14084	WT Δ pflu5960			
TSS-f6 Δ 5960	14085	Evolved Δ pflu5960			

Table 2.9. Deletion of *pflu5960* produces a wrinkled colony phenotype at 28°C incubation. Phenotypic images, MPB number & Genotype (Evolved in experiment or WT, and relevant mutation) provided for the strains SBW25- Δ 5960 & TSS-f6- Δ 5960. Phenotypes as described in [Table 2.1](#) legend.

I found that the removal of Pflu5960 in TSS-f6 resulted in suppression of the SM phenotype and loss of the phenotype switch, as was expected based on the mutagenesis screen. TSS-f6- Δ 5960 displays a strong wrinkly colony morphology at both incubation temperatures, and forms a substantial mat in the static broth environment (see images in [Table 2.9](#)). Deletion of *pflu5960* in the f2 ancestor produced no observable change to phenotype, while in SBW25 there was subtle phenotypic effect. SBW25- Δ 5960 displays a semi-wrinkly colony

texture (semi-WS) at 28°C, and only slightly wrinkled at 20°C (more closely resembling the SM phenotype); in static broth this deletion mutant does not demonstrate the capacity to form a mat, with only minor clumping of cells at the surface (as visible at the upper edge of the meniscus). This result implies that Pflu5960 has minimal activity in ancestral SBW25, while in TSS-f6 it is necessary for maintenance of the SM phenotype at 28°C.

2.4.4.1 Mutation of EAL motif

Phosphodiesterase (PDE) enzymatic activity is dependent on the conserved EAL motif, for c-di-GMP binding and degradation (Henнге, 2009; Schmidt et al., 2005). Therefore, to investigate whether Pflu5960 has PDE activity, I proceeded to mutate this EAL motif to an inactive form (residue 328: EAL→AAL) using site-directed mutagenesis. If the EAL mutation (E328A) produces the same phenotypic effect as deletion of *pflu5960*, this provides support for the role of Pflu5960 as a functional PDE enzyme. This mutation was recreated in SBW25, TSS-f6 & f2, producing the strains: SBW25-5960-EAL-mut (MPB14627), TSS-f6-5960-EAL-mut (MPB14628) & f2-5960-EAL-mut (MPB14629); the phenotypic effect shown in *Table 2.10* below.

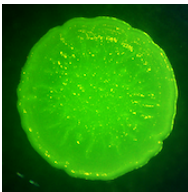
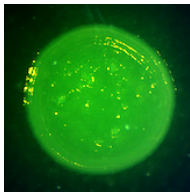
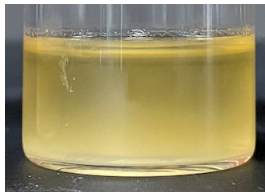
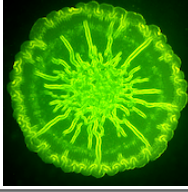

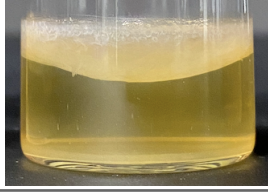
Strain	MPB	Genotype	Colony morphology spot		Mat formation: 28°C
			28°C	20°C	
SBW25 5960- EAL-mut	14627	WT <i>pflu5960</i> - E328A			
TSS-f6 5960- EAL-mut	14628	Evolved <i>pflu5960</i> - E328A			

Table 2.10. PDE activity of Pflu5960 confirmed by mutation of EAL motif. Phenotypic images, MPB number & Genotype (Evolved in experiment or WT, and relevant mutation) provided for the strains SBW25-5960-EAL-mut & TSS-f6-5960-EAL-mut. Phenotypes as described in [Table 2.1](#) legend.

In all genetic backgrounds, I observed that the *pflu5960* EAL mutation produced the exact same effect on phenotype as the gene deletion (see previous [Section 2.4.4](#)). SBW25-5960-EAL-mut displayed the semi-WS phenotype with no mat formation, and TSS-f6-5960-EAL-mut the WS phenotype with a thick mat forming in static broth (see images in *Table 2.10*). This result confirms that Pflu5960 does function as a PDE enzyme in

the degradation of c-di-GMP; though only low levels of activity were observed in ancestral SBW25 (especially at lower temperatures). For the TSS-f6 phenotype switch, at 28°C the PDE activity of Pflu5960 is essential to maintain the SM phenotype, likely required for breaking down excess c-di-GMP in the cell (produced in low levels by WspR, or other DGC enzymes). While at 20°C, Pflu5960 is either inactive, or just unable to degrade the high levels of c-di-GMP produced by the active Wsp system & WspR DGC.

2.4.5 Suppressor analysis of pflu5960 deletion mutants

To further explore the role of the Pflu5960 PDE and its interaction with other proteins relating to the WS phenotype, a second round of suppressor analysis was carried out with the *pflu5960* deletion mutants TSS-f6- Δ 5960 (MPB14085) & SBW25- Δ 5960 (MPB14084). This was achieved by mutagenesis with the IS- Ω -km/hah transposon, and the location of insertions mapped using AP-PCR & Sanger sequencing (Giddens et al., 2007); refer to methods [Section 5.5](#). For TSS-f6- Δ 5960, I screened ~12,000 colonies, and identified 17 transposon mutants with suppression of the WS phenotype at 28°C – Tn1-17 (MPB14801-14817). And for SBW25- Δ 5960, I screened ~9,700 colonies, identifying 23 transposon mutants suppressing the semi-WS phenotype – Tn1-23 (MPB14833-14855); as well as 25 transposon mutants with further suppression of the SM phenotype – Tn24-48 (MPB14856-14880). Further detail of each transposon mutant is available in [Supplementary A-3](#).

2.4.5.1 WS phenotype suppression

For the *pflu5960* deletion mutants, transposon insertions that resulted in suppression of the WS or semi-WS phenotype are summarised in [Table 2.11](#) below. I observed a number of independent insertions in the *wss* operon – for TSS-f6- Δ 5960: *wssA* (x1), *wssB* (x2), *wssC* (x2), *wssD* (x1) & *wssE* (x3); and for SBW25- Δ 5960: *wssB* (x2), *wssC* (x4), *wssD* (x1) & *wssE* (x4). This result indicates that in both TSS-f6 & SBW25, Pflu5960 functions as a negative regulator of the cellulose synthase operon, likely due to PDE enzymatic activity and the degradation of c-di-GMP (an allosteric activator of the *wss* operon) (Ross et al., 1987). Notably, no transposons insertions were observed in the *wsp* operon; this may be explained by the small scale of the mutagenesis screen, or indicate that the Wsp pathway & WspR DGC are not responsible for production of c-di-GMP in the *pflu5960* mutants (although no alternative DGC enzyme was identified).

Suppress	Ins.	Gene name	PFLU	Putative product	Size	Ortholog (PA01)	Seq. identity	E-value
TSS-f6 $\Delta 5960$: WS	1	<i>wssA</i>	0300	cell morphology-like protein	344	-	-	-
	2	<i>wssB</i>	0301	cellulose synthase catalytic subunit	739	-	-	-
	2	<i>wssC</i>	0302	cellulose synthase regulator protein	755	-	-	-
	1	<i>wssD</i>	0303	endo-1,4-D-glucanase	398	-	-	-
	3	<i>wssE</i>	0304	cellulose synthase protein C	1279	-	-	-
	2	<i>pflu0888</i>	0888	ABC transporter ATP-binding protein	269	PA4456	85.1%	$3e-171$
	1	<i>pflu0889</i>	0889	ABC transporter membrane protein	265	PA4455	84.9%	$8e-163$
	2	<i>pflu3655</i>	3655	hypothetical protein	243	-	-	-
	1*	<i>pflu3542</i>	3542	serine/threonine-protein kinase	281	Stk1	62.2%	$1e-116$
	1*	<i>pflu5402</i>	5402	hypothetical protein	184	PA3978	74.5%	$1e-98$
SBW25 $\Delta 5960$: semi- WS	2	<i>wssB</i>	0301	cellulose synthase catalytic subunit	739	-	-	-
	4	<i>wssC</i>	0302	cellulose synthase regulator protein	755	-	-	-
	1	<i>wssD</i>	0303	endo-1,4-D-glucanase	398	-	-	-
	4	<i>wssE</i>	0304	cellulose synthase protein C	1279	-	-	-
	1	<i>rpoN</i>	0882	RNA polymerase factor sigma-54	497	RpoN	85.3%	0.0
	1	<i>pflu0888</i>	0888	ABC transporter ATP-binding protein	269	PA4456	85.1%	$3e-171$
	1	<i>mutS</i>	1164	DNA mismatch repair protein MutS	863	MutS	84.3%	0.0
	1	<i>pflu3541</i>	3541	hypothetical protein	109	-	-	-
	2	<i>fabF1</i>	4703	3-oxoacyl-(acyl carrier protein) synthase II	414	FabF1	83.3%	0.0
	1	<i>pflu5081</i>	5081	hypothetical protein	225	-	-	-
	2	<i>pstC</i>	6047	phosphate ABC transporter membrane protein	763	PstC	75.8%	0.0
1	<i>pstS</i>	6048	phosphate ABC transporter substrate-binding protein	328	PstS	84.3%	0.0	

Table 2.11. Suppressor analysis of WS phenotype in *pflu5960* deletion mutants. Summary of genes disrupted by transposon insertion in TSS-f6- $\Delta 5960$ (MPB14085) & SBW25- $\Delta 5960$ (MPB14084), suppressing the WS or semi-WS phenotype at 28°C. Details as described in [Table 2.2](#) legend; * indicates restoration of the phenotype switch (SM at 28°C & WS at 20°C).

Insertions were also observed in the genes *pflu0888* (x3) & *pflu0889* (x1), suppressing the WS phenotype in the *pflu5960* deletion mutants. [pflu0888](#) encodes the putative ABC transporter ATP-binding protein Pflu0888, with 85.1% sequence identity to Ttg2A (or YrbF)

in *P. aeruginosa* PAO1 ([PA4456](#); BLASTP *E*-value: $3e-171$). And [pflu0889](#) encodes the putative ABC transporter membrane protein Pflu0889, with 85.9% sequence identity to Ttg2B (or YrbE) in *P. aeruginosa* PAO1 ([PA4455](#); BLASTP *E*-value: $8e-163$). In *Pseudomonas putida*, García et al. (2010) demonstrated that the Ttg2ABC transporter is involved in toluene solvent tolerance and multidrug resistance (including antibiotics, heavy metals & oxidative stress). In *P. aeruginosa*, the ABC transporter encoded by *PA4456-4452* is predicted to function in the export of antibiotics from the cell; Chen & Duan (2016) observed that disruption of *PA4456* resulted in antibiotic sensitivity and accumulation of intracellular tetracycline (though no detectable change to membrane stability). Deletion of the *PA4455* gene in PAO1, was also shown to cause sensitivity to acidified nitrite & the membrane stressor EDTA, with *PA4455* predicted to be important for membrane stability (McDaniel et al., 2016).

Furthermore, Yero et al. (2021) provide evidence of phospholipid binding to the periplasmic protein Ttg2D ([PA4453](#)), with deletion of *ttg2D* resulting in an increased susceptibility to certain antibiotics related to the permeability barrier of the outer membrane. From this a model of the Ttg2 system was proposed, in which the Ttg2D phospholipid binding protein (together with the Ttg2ABCE complex bound to the inner membrane) transports glycerophospholipids across the periplasm, thus controlling permeability of the outer membrane (Yero et al., 2021). Therefore in the *pflu5960* deletion mutants, the proteins Pflu0888 & Pflu0889 may function in the regulation of membrane fluidity; it is possible that disruption of these genes alters the rigidity of the membrane and therefore the activity of other membrane-bound proteins (e.g. the Wsp system), resulting in suppression of biofilm formation (Yero et al., 2021; O'Neal et al., 2022).

In TSS-f6- $\Delta 5960$, transposon insertions in *pflu3655* (x2) also resulted in suppression of the WS phenotype. [pflu3655](#) encodes the hypothetical protein Pflu3655, predicted to activate transcription of the colonic acid biosynthesis operon *wcaJ-wzb* (Gallie et al., 2015). In SBW25, the transcriptional regulator Pflu3655 was shown to be required for production of colonic acid-based capsules, with bistability in capsulation state observed due to competition between ribosomes and the proteins CsrA/RsmA for binding to *pflu3655* mRNA (Beaumont et al., 2009; Gallie et al., 2015; Remigi et al., 2019). The connection between disruption to the Pflu3655 colonic acid regulator and suppression of the WS phenotype in TSS-f6- $\Delta 5960$ is unclear. In TSS-f6, deletion of the colonic acid operon (*wcaJ-wzb*) did not affect the phenotype switch or WS colony morphology, but did prevent formation of the mucoid

coating on colonies incubated at 20°C for 6 days (see [Section 2.4.3](#)). For SBW25- Δ 5960, the semi-WS phenotype was also suppressed by transposon insertion in the genes – *rpoN* ([pflu0882](#)) (x1), *mutS* ([pflu1164](#)) (x1), *fabF1* ([pflu4703](#)) (x2), *pstC* ([pflu6047](#)) & *pstS* ([pflu6048](#)); though these genes will not be discussed in further detail.

2.4.5.2 Restoration of phenotype switch

Intriguingly, for the TSS-f6 *pflu5960* deletion mutant, transposon insertions in the genes *pflu3542* (at residue 106) & *pflu5402* (residue 5) were observed to restore the environmentally-responsive phenotype (refer to [Table 2.11](#)). These TSS-f6- Δ 5960 transposon mutants display the colony morphology of SM at 28°C & WS at 20°C – resembling the TSS-f6 phenotype switch, as shown in [Table 2.12](#) below.

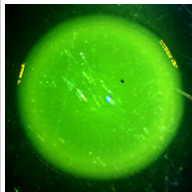
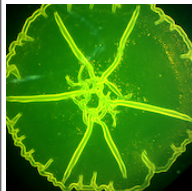
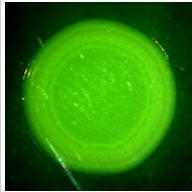
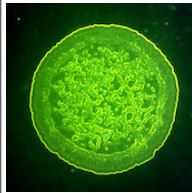
Strain	MPB	Genotype	Colony morphology spot	
			28°C	20°C
TSS-f6 Δ 5960: Tn3	14803	Evolved Δ <i>pflu5960</i> <i>pflu3542</i> *		
TSS-f6 Δ 5960: Tn12	14812	Evolved Δ <i>pflu5960</i> <i>pflu5402</i> *		

Table 2.12. TSS-f6- Δ 5960 transposon mutants with restoration of phenotype switch. Colony images, MPB number & Genotype (Evolved in experiment or WT, and relevant mutation) provided for the strains TSS-f6- Δ 5960: Tn3 & Tn12. Colony morphology spot as described in [Table 2.1](#) legend.

[pflu3542](#) encodes the putative serine/threonine-protein kinase Pflu3542, with 62.2% sequence identity to Stk1 in *P. aeruginosa* PAO1 ([PA1671](#); BLASTP *E*-value: $1e-116$). In *P. aeruginosa*, Stk1 was shown to undergo autophosphorylation, as well as phosphorylate the eukaryotic histone H1; this indicating the potential to target the regulatory protein AlgP ([PA5253](#); ortholog of *pflu5927* in SBW25) involved in alginate production (Mukhopadhyay et al., 1999; Kato et al., 1990). Zhu et al. (2020) found that deletion of the *stk1* gene in PAO1 resulted in deficiency in twitching motility, with transcriptomic analysis revealing differential expression of a large number of proteins relating to biofilm formation, including significant downregulation of *amrZ* and genes involved in type IV pilus assembly (including *fimU* & the *pil* operon). Therefore in TSS-f6, the Pflu3542 kinase may function in the phosphorylation of

proteins related to the WS phenotype, for example the AmrZ negative regulator of the cellulose synthase operon (Giddens et al., 2007). Though it is not obvious how the transposon insertion in *pflu3542* resulted in restoration of the phenotype switch in TSS-f6- Δ 5960.

While [pflu5402](#) encodes the hypothetical protein Pflu5402, with 74.5% sequence identity to PA3978 in *P. aeruginosa* PAO1 ([PA3978](#); BLASTP *E*-value: $1e-98$); containing two Sell-like tetratricopeptide repeats ([PF08238](#); residue: 63-98 & 99-130; *E*-value: $2.4e-5$ & 0.0011). Alvarez-Ortega et al. (2010) identified PA3978 mutants of *P. aeruginosa* PAO1 that demonstrated an increased susceptibility to β -lactam antibiotics (that interfere with peptidoglycan biosynthesis). The transposons insertion in *pflu5402* may therefore result in alteration to membrane permeability, though it is also unclear how this restored the TSS-f6 phenotype switch.

2.4.5.3 SM phenotype suppression

For SBW25- Δ 5960, I also identified transposon insertions that further suppress the SM phenotype; the results provided in *Table 2.13* below. Unsurprisingly, insertions were found in the genes *wspF* (at residue 218), *pflu0183* (at residue 45) & *bifA* (at residue 379 & 658); representative colony images are later displayed in *Table 2.14*. The WspF methylesterase is a negative regulator of the WspR DGC, with spontaneous mutations in *wspF* observed to be the primary mutational route to the WS phenotype (Bantinaki et al., 2007; McDonald et al., 2009). Therefore in SBW25- Δ 5960, the transposon insertion in *wspF* likely caused activation of the WspR DGC, an increase in c-di-GMP levels and thus WS phenotype.

Suppress	Ins.	Gene name	PFLU	Putative product	Size	Ortholog (PA01)	Seq. identity	<i>E</i> -value
SBW25 Δ 5960: SM	1	<i>wspF</i>	1224	chemotaxis-specific methylesterase	336	WspF	75.8%	0.0
	1	<i>pflu0183</i>	0183	hypothetical protein	335	PA0290	61.4%	$2e-145$
	2	<i>bifA</i>	4858	signaling protein	683	BifA	81.6%	0.0
	1	<i>motY</i>	1155	exported flagellar protein	302	MotY	66.9%	$9e-137$
	2	<i>fleN</i>	4418	ParA family ATPase	277	FleN	91.2%	$4e-177$
	2	<i>flhA</i>	4420	flagellar biosynthesis protein FlhA	709	FlhA	83.1%	0.0
	1	<i>flhB</i>	4422	flagellar biosynthesis protein FlhB	378	FlhB	67.4%	0.0
	1	<i>fliP</i>	4425	flagellar biosynthesis protein FliP	247	FliP	83.8%	$7e-135$
	1	<i>fliM</i>	4428	flagellar motor switch protein FliM	322	FliM	89.4%	0.0
	2	<i>fliH</i>	4437	flagellar assembly protein H	254	PA1103	59.5%	$3e-104$

2	<i>fliF</i>	4439	flagellar MS-ring protein	593	FliF	76.5%	0.0
1	<i>fliE</i>	4440	flagellar hook-basal body protein FliE	109	FliE	75.2%	4e-57
2	<i>fliC</i>	4448	flagellin	485	FliC	53.1%	3e-147
1	<i>flgK</i>	4451	flagellar hook-associated protein FlgK	682	FlgK	38.7%	1e-133
1	<i>flgF</i>	4456	flagellar basal body rod protein FlgF	246	FlgF	67.6%	8e-128
2	<i>flgE</i>	4728	flagellar hook protein FlgE	434	FlgE	43.1%	3e-113
1	<i>flgA</i>	4734	flagellar basal body P-ring biosynthesis protein FlgA	236	PA3350	57.1%	2e-95

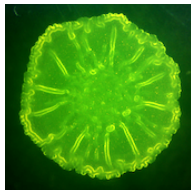
Table 2.13. Disruption of flagella genes suppresses SM phenotype in SBW25 *pflu5960* deletion mutant. Summary of genes disrupted by transposon insertion in SBW25- Δ 5960 (MPB14084), further suppressing the SM phenotype at 28°C. Details as described in [Table 2.2](#) legend

[pflu0183](#) encodes the hypothetical protein Pflu0183, with 61.4% sequence identity to PA0290 in *P. aeruginosa* PAO1 ([PA0290](#); BLASTP *E*-value: 2e-145). Pflu0183 contains a PAS fold ([PF08447](#); residue: 69-156; *E*-value: 1.1e-19), and GGDEF domain ([PF00990](#); residue: 174-331; *E*-value: 1.5e-41) with an intact GGEEF motif. In *P. aeruginosa* PAO1, PA0290 was shown to function as a DGC enzyme, important in maintenance of the basal levels of c-di-GMP; deletion of this gene resulting in decrease in biofilm formation and Psl production (Wei et al., 2019). In SBW25, Lind et al. (2015) identified mutations in *pflu0183* (gene fusion to the upstream *pflu0184*) causing the WS phenotype, predicted to activate the DGC activity of Pflu0183. The SBW25- Δ 5960 transposon mutant with insertion at the start of *pflu0183* likely activated the Pflu0183 DGC, resulting in an increase in c-di-GMP production, and the WS phenotype. While *bifA* ([pflu4858](#)) encodes the putative signalling protein BifA, with 81.6% sequence identity to BifA in *P. aeruginosa* PAO1 ([PA4367](#); BLASTP *E*-value: 0.0). BifA contains a GGDEF-like domain ([PF00990](#); residue: 250-407; *E*-value: 7.2e-36) with a degenerate motif, and EAL domain ([PF00563](#); residue: 427-662; *E*-value: 2.7e-76). Studies in *P. aeruginosa* have demonstrated that BifA functions as a PDE enzyme, degrading intracellular c-di-GMP (Kuchma et al., 2007). Therefore in SBW25- Δ 5960, insertion in the *bifA* gene likely disrupted the PDE activity of BifA, causing an increase in the level of c-di-GMP and further suppression of the SM phenotype.

Surprisingly, I also observed the WS phenotype in the SBW25 *pflu5960* deletion mutant as a result of transposon insertions in a number of genes related to flagella production, including *flaN*, *motY*, and the *flh*, *fli* & *flg* operons (see details in [Table 2.13](#), and representative colony

images in *Table 2.14*). O’Toole & Kolter (1998) previously found that flagellar mutants of *P. aeruginosa* (e.g. mutation in *flgK*) were also defective in biofilm formation, attributed to issues with initial attachment at an abiotic surface. It therefore seems counterintuitive that disruption of flagella structural genes in SBW25- $\Delta 5960$ caused further suppression of the SM phenotype. *fleN* ([pflu4418](#)) encodes the ParA family ATPase FleN, with 91.2% sequence identity to the flagellar synthesis regulator FleN in *P. aeruginosa* PAO1 ([PA1454](#); BLASTP *E*-value: $4e-177$). In PAO1, FleN was demonstrated to regulate the number of flagella, by binding to the transcriptional regulator FleQ; deletion of the *fleN* gene resulting in multiple flagella and reduced motility (Dasgupta et al., 2000; Dasgupta & Ramphal, 2001). Dasgupta et al. (2003) have also shown that FleQ activates expression of flagella biosynthesis genes, including *fliC* and the operons *fliEFGHIJ*, *fliLMNOPQR*, *flhAB*, *flgBCDE* & *flgFGHIJKL*. Therefore in SBW25- $\Delta 5960$, transposon insertion in FleN (at residues 128 & 220) likely resulted in loss of the inhibition of FleQ, and thus activation of the expression of genes producing flagella structural components.

Hickman & Harwood (2008) have shown that FleQ represses genes involved in production of the Pel exopolysaccharide, with the binding of FleQ to the *pel* promoter region inhibited by c-di-GMP. In response to the presence of c-di-GMP, the FleQ protein undergoes conformational change, that is predicted to result in a transition in the function of the FleQ regulator, from a repressor to activator of Pel expression (Baraquet et al., 2012; Matsuyama et al., 2015). SBW25- $\Delta 5960$ likely has high levels of c-di-GMP due to the lack of Pflu5960 PDE activity; disruption of FleN may have therefore caused FleQ to switch to activation of exopolysaccharide synthesis genes (e.g. cellulose production by the *wss* operon). This may explain the WS phenotype observed in the *fleN* transposon mutants – refer to colony images of SBW25- $\Delta 5960$:Tn42 (MPB14874) in *Table 2.14* below. Although this effect does seem to be unique to the SBW25 *pflu5960* mutant background; the deletion of *fleN* was previously observed to lower the expression of *pel* & *psl* genes in *P. aeruginosa*, and inhibit biofilm development in *P. putida* (Hickman & Harwood, 2008; Navarrete et al., 2019).

Strain	MPB	Genotype	Colony spot: 28°C
SBW25 $\Delta 5960$: Tn34	14866	WT $\Delta pflu5960$ <i>pflu0183</i> *	

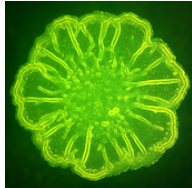
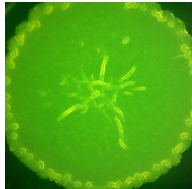
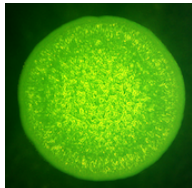
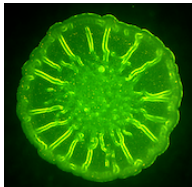
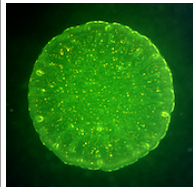
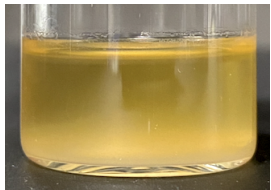
SBW25 Δ5960: Tn43	14875	WT <i>Δpflu5960</i> <i>bifA*</i>	
SBW25 Δ5960: Tn36	14868	WT <i>Δpflu5960</i> <i>flhA*</i>	
SBW25 Δ5960: Tn42	14874	WT <i>Δpflu5960</i> <i>fleN*</i>	

Table 2.14. Transposon mutants of SBW25-Δ5960 with WS phenotype. Colony images, MPB number & Genotype (Evolved in experiment or WT, and relevant mutation) provided for the strains SBW25-Δ5960: Tn34, Tn43, Tn36 & Tn42. Colony morphology spot as described in [Table 2.1](#) legend.

2.4.6 *AmrZ* transcriptional regulator

amrZ ([pflu4744](#)) was also identified to be involved in the TSS-f6 phenotype switch, with transposon insertions suppressing the SM phenotype at 28°C (Summers, 2018). AmrZ (or AlgZ) is a DNA-binding protein, shown to negatively regulate transcription of the *wss* operon and therefore cellulose production (Giddens et al., 2007). This global regulator protein has also been demonstrated to activate alginate production & twitching motility (Baynham et al., 1999; Baynham et al., 2006), and repress swimming motility & Psl exopolysaccharide production (Tart et al. 2006; Jones et al., 2013). In TSS-f6, AmrZ likely functions in the transcriptional regulation of the *wss* operon (and potentially other WS-related genes), thus suppressing the production of cellulose at 28°C; see previous discussion in [Section 2.2.4](#). To investigate this claim, I deleted the entirety of the *amrZ* gene in SBW25 & TSS-f6, producing the strains: SBW25-Δ*amrZ* (MPB14246) & TSS-f6-Δ*amrZ* (MPB14247); the phenotypic effect is shown in [Table 2.15](#) below.

Strain	MPB	Genotype	Colony morphology spot		Mat formation: 28°C
			28°C	20°C	
SBW25 Δ<i>amrZ</i>	14246	WT <i>Δpflu4744</i>			

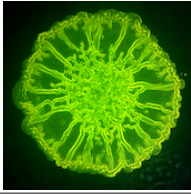
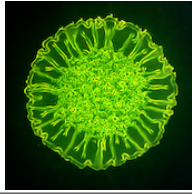
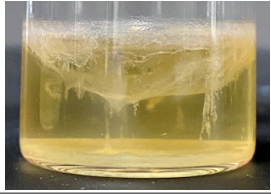
TSS-f6 $\Delta amrZ$	14247	Evolved $\Delta pflu4744$			
-------------------------	-------	------------------------------	---	--	---

Table 2.15. Deletion of *amrZ* produces the WS colony morphology. Phenotypic images, MPB number & Genotype (Evolved in experiment or WT, and relevant mutation) provided for the strains SBW25- $\Delta amrZ$ & TSS-f6- $\Delta amrZ$. Phenotypes as described in [Table 2.1](#) legend.

I found that the deletion of *amrZ* in TSS-f6, as anticipated, resulted in loss of the phenotype switch, with the WS colony morphology observed at both incubation temperatures. TSS-f6- $\Delta amrZ$ also demonstrated improvement in mat formation capacity at 28°C, though only a relatively thin mat was observed as compared to the thick mat of TSS-f6- $\Delta 5960$ (see [Section 2.4.4](#)). The removal of AmrZ in SBW25 produced the WS colony morphology at 28°C, and semi-WS phenotype at 20°C; this effect on phenotype being more pronounced than in the *pflu5960* deletion. Although SBW25- $\Delta amrZ$ does not form a mat in the static broth environment (see image in [Table 2.15](#) above). These results indicate that the AmrZ transcriptional regulator plays an essential role in TSS-f6 at 28°C, suppressing cellulose production by the *wss* operon for maintenance of the SM phenotype. In the SBW25 ancestor, AmrZ also functions in negative regulation of the cellulose synthase operon (either directly or indirectly), but in its absence the c-di-GMP level is not high enough to allow for formation of a mat in static broth. The effect of deleting *amrZ* & *pflu5960* in SBW25 was also found to depend on incubation temperature, with only a minor change to colony morphology observed at lower temperatures. Therefore in the wild-type background AmrZ & Pflu5960 are most active at 28°C in suppression of the WS phenotype, and either inactivate at 20°C, or less essential due to low levels of intracellular c-di-GMP.

2.4.7 Suppressor analysis of *amrZ* deletion mutants

To further understand the function of the AmrZ regulator, a second round of suppressor analysis was carried out with the *amrZ* deletion mutants TSS-f6- $\Delta amrZ$ (MPB14247) & SBW25- $\Delta amrZ$ (MPB14246); with transposon mutagenesis as previously described in [Section 2.4.5](#). For TSS-f6- $\Delta amrZ$, I screened ~5,500 colonies, and identified 13 transposon mutants with suppression of the WS phenotype at 28°C – Tn1-13 (MPB14788-14800). And for SBW25- $\Delta amrZ$, I screened ~28,200 colonies, identifying 44 transposon mutants

suppressing WS – Tn1-44 (MPB14818-14825 & MPB15018-15053). Further information regarding each transposon mutant is also available in *Supplementary A-3*.

2.4.7.1 WS phenotype suppression

For the *amrZ* deletion mutants, the transposon insertions that resulted in suppression of the WS phenotype are summarised in *Table 2.16* below. As with the *pflu5960* mutants (see *Section 2.4.5.1*), I observed numerous insertions in the *wss* operon – for TSS-f6- Δ *amrZ*: *wssB* (x1), *wssC* (x1) & *wssE* (x4); and for SBW25- Δ *amrZ*: *wssA* (x3), *wssB* (x6), *wssC* (x3), *wssD* (x3) & *wssE* (x13). This result further confirms the role of AmrZ in negative regulation of the *wss* operon; in absence of the *amrZ* gene, the *wss*-encoded cellulose synthase machinery is active in the overproduction of acetylated cellulose (Spiers et al., 2003). For SBW25- Δ *amrZ*, transposon mutants with the SM phenotype were also observed as a result of insertion in a number of other genes, including *pflu3655* (x1), *mwsR* (x1) & *galU* (x4), and the flagella-related genes *fleQ* (x4), *flhF* (x1) & *fliT* (x1); these will not be discussed in further detail. *pflu3655* encodes the Pflu3655 regulator of colonic acid biosynthesis (Gallie et al., 2015), disruption also observed to suppress the WS phenotype in TSS-f6- Δ 5960 (refer to previous discussion in *Section 2.4.5.1*).

Suppress	Ins.	Gene name	PFLU	Putative product	Size	Ortholog (PA01)	Seq. identity	E-value
TSS-f6 Δ <i>amrZ</i> : WS	1	<i>wssB</i>	0301	cellulose synthase catalytic subunit	739	-	-	-
	1	<i>wssC</i>	0302	cellulose synthase regulator protein	755	-	-	-
	4	<i>wssE</i>	0304	cellulose synthase operon protein C	1279	-	-	-
	3*	<i>rlpA</i>	5420	lipoprotein	334	RlpA	63.6%	4e-148
	1*	<i>ampG</i>	4993	beta-lactamase induction signal transducer AmpG	510	AmpG	56.9%	0.0
	1*	<i>pflu5545</i>	5545	peptidase	472	MepM	60.1%	0.0
	1*	<i>anmK</i>	5546	anhydro-N-acetylmuramic acid kinase	363	AnmK	67.2%	3e-180
SBW25 Δ <i>amrZ</i> : WS	3	<i>wssA</i>	0300	cell morphology-like protein	344	-	-	-
	6	<i>wssB</i>	0301	cellulose synthase catalytic subunit	739	-	-	-
	3	<i>wssC</i>	0302	cellulose synthase regulator protein	755	-	-	-
	3	<i>wssD</i>	0303	endo-1,4-D-glucanase	398	-	-	-
	13	<i>wssE</i>	0304	cellulose synthase operon protein C	1279	-	-	-
	1	<i>pflu3655</i>	3655	hypothetical protein	243	-	-	-

1	<i>mwsR</i>	5329	sensory box GGDEF/EAL domain-containing protein	1283	MorA	67.2%	0.0
4	<i>galU</i>	2985	UTP-glucose-1-phosphate uridylyltransferase	279	GalU	83.8%	6e-179
4	<i>fleQ</i>	4443	two-component system response regulator nitrogen regulator protein	491	FleQ	84.2%	0.0
1	<i>fliT</i>	4444	hypothetical protein	98	PA1096	46.9%	2e-24
1	<i>flhF</i>	4419	flagellar biosynthesis regulator FlhF	438	FlhF	67.8%	0.0
1	<i>pflu4548</i>	4548	methyl-accepting chemotaxis protein	541	PA1608	50.4%	3e-151
1	<i>ribE</i>	5472	riboflavin synthase subunit alpha	220	RibC	82.2%	3e-134
1	<i>gbdR</i>	5678	AraC family transcriptional regulator	367	GbdR	86.4%	0.0

Table 2.16. Suppressor analysis of WS phenotype in *amrZ* deletion mutants. Summary of genes disrupted by transposon insertion in TSS-f6- $\Delta amrZ$ (MPB14247) & SBW25- $\Delta amrZ$ (MPB14246), suppressing the WS phenotype at 28°C. Details as described in [Table 2.2](#) legend; * indicates restoration of the phenotype switch (SM at 28°C & WS at 20°C).

mwsR ([pflu5329](#)) encodes the putative sensory box GGDEF/EAL dual-domain protein MwsR, predicted to localise to the inner membrane, with 67.2% sequence identity to the motility regulator MorA in *P. aeruginosa* PAO1 ([PA4601](#); BLASTP *E*-value: 0.0). MwsR contains a PAS fold ([PF08447](#); residue: 478-569; *E*-value: 5.8e-9), two PAS sensory domains ([PF13426](#); residue: 600-714 & 735-836; *E*-value: 3.0e-5 & 2.5e-16), a GGDEF domain ([PF0090](#); residue: 848-1009; *E*-value: 4.7e-50), and EAL domain ([PF00563](#); residue: 1029-1264; *E*-value: 1.0e-76); with intact GGDEF & EAL motifs. Previous studies in *Pseudomonas* species, found that disruption of the *morA* gene resulted in improvement to swimming motility and impairment of biofilm formation (Choy et al., 2004). Phippen (2014) further demonstrated in PAO1 that MorA functions as both a PDE & DGC enzyme in the synthesis and degradation of c-di-GMP. In SBW25, McDonald et al. (2009) identified mutations in the EAL domain of MwsR producing the WS phenotype, predicted to result in reduction of PDE function and activation of DGC enzymatic activity. While deletion of the entire *mwsR* gene resulted in the SM phenotype (McDonald et al., 2009). Therefore for SBW25- $\Delta amrZ$, the transposon insertion in MwsR (at residue 357) likely caused loss of DGC activity, decrease in c-di-GMP levels and thus the SM phenotype.

While *galU* ([pflu2985](#)) encodes the UTP--glucose-1-phosphate uridylyltransferase GalU, with 83.8% identity to GalU in *P. aeruginosa* PAO1 ([PA2023](#); BLASTP *E*-value: 6e-179). In

P. aeruginosa, GalU was shown to function in production of UDP-glucose, a precursor required for the synthesis of LPS core oligosaccharides in the outer membrane; mutants of *galU* display truncation of the LPS outer core (Dean & Goldberg, 2002). The deletion of *galU* in PAO1 was also observed to cause defects in surface attachment and loss of Psl exopolysaccharide production (Byrd et al., 2009). The role of GalU in LPS biosynthesis shows parallels with the Pflu0479 glycosyl transferase, which was found to be necessary for the SM phenotype of TSS-f6 at 28°C (see [Section 2.2.5](#)). In SBW25, Spiers & Rainey (2005) previously demonstrated the importance of LPS expression in development of the WS biofilm, the LPS predicted to interact with cellulose fibres in the biofilm matrix. Therefore in TSS-f6- Δ *amrZ*, transposon insertions in the *galU* gene (at residue 44, 31, 158 & 145) likely caused truncation of the LPS core, altering the interactions in the cellulose biofilm matrix (produced by the active *wss* operon), resulting in suppression of the WS phenotype.

fleQ ([pflu4443](#)) encodes the transcriptional regulator FleQ, with 84.2% sequence identity to FleQ in *P. aeruginosa* PAO1 ([PA1097](#); BLASTP *E*-value: 0.0). As previously discussed in [Section 2.4.5.3](#), FleQ inversely regulates the expression of flagella & exopolysaccharide biosynthesis genes, in response to levels of intracellular c-di-GMP (Dasgupta et al., 2003; Hickman & Harwood, 2008). In PAO1, the binding of FleQ has been observed to the *pel*, *psl* & *cdrAB* promoters, with c-di-GMP mediating the conversion of FleQ from a repressor to activator of exopolysaccharide synthesis (Baraquet et al., 2012; Baraquet & Harwood, 2016). Giddens et al. (2007) found in SBW25 that FleQ functions as a negative regulator of the *wss* operon, predicted to result from interaction with the genes *amrZ* & *algR*. Therefore in TSS-f6- Δ *amrZ*, it is not obvious how transposon insertions in *fleQ* (at residue 187, 288, 408 & 462) & the upstream gene *fliT* (at residue 95) produced the SM phenotype. The deletion of *amrZ* in TSS-f6 resulted in derepression of the *wss* cellulose synthase operon, with the strong WS phenotype suggesting that c-di-GMP levels are high; in the absence of AmrZ, the FleQ transcriptional regulator must rather be activating the expression of other genes related to cellulose production. Using the conserved FleQ binding motif (GTCAATnnATTGAC) identified in *P. aeruginosa* by Baraquet & Harwood (2016), I searched for potential targets in the SBW25 genome. From this, possible binding sites were identified upstream of the genes *fleQ* (-145 bp: GTCAAATTTATGAC), *amrZ* (-150 bp: GTCACAGAATTGAC) & *wssA* (-134 bp: GTCAGTATTTTGAT); indicating that FleQ may bind directly to the *wss* operon.

2.4.7.2 Restoration of phenotype switch

A number of TSS-f6- $\Delta amrZ$ transposon mutants were observed that had restoration of the phenotype switch, colonies displaying the SM phenotype at 28°C & WS phenotype at 20°C; see images of representative mutants in *Table 2.17* below. This resulted from transposon insertion in the following genes – *rlpA* (at residue 45, 85 & 81), *ampG* (residue 277), *pflu5545* (residue 2) & *anmK* (*pflu5545*) (residue 328); as detailed in previous *Table 2.16*.

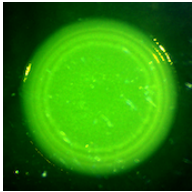
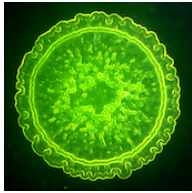
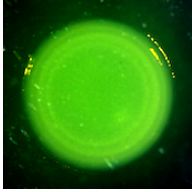

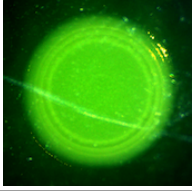

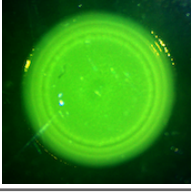

Strain	MPB	Genotype	Colony morphology spot	
			28°C	20°C
TSS-f6 $\Delta amrZ$: Tn10	14797	Evolved $\Delta amrZ$ <i>ampG</i> *		
TSS-f6 $\Delta amrZ$: Tn13	14800	Evolved $\Delta amrZ$ <i>rlpA</i> *		
TSS-f6 $\Delta amrZ$: Tn7	14794	Evolved $\Delta amrZ$ <i>anmK</i> *		
TSS-f6 $\Delta amrZ$: Tn12	14799	Evolved $\Delta amrZ$ <i>pflu5545</i> *		

Table 2.17. TSS-f6- $\Delta amrZ$ transposon mutants with restoration of phenotype switch. Colony images, MPB number & Genotype (Evolved in experiment or WT, and relevant mutation) provided for the strains TSS-f6- $\Delta amrZ$: Tn10, Tn13, Tn7 & Tn12. Colony morphology spot as described in *Table 2.1* legend.

rlpA ([pflu5420](#)) encodes the putative lipoprotein RlpA, with 63.6% identity to RlpA in *P. aeruginosa* PAO1 ([PA4000](#); BLASTP *E*-value: 4e-148). In *P. aeruginosa*, RlpA was shown to function as a membrane-bound lytic transglycosylase, preferentially digesting peptidoglycans that lack stem peptides; with *rlpA* mutants defective in daughter cell separation during cell division, and displaying the chaining phenotype (Jorgenson et al., 2014). Lamers et al. (2015) also found that the removal of lytic transglycosylases resulted in an increase in outer membrane permeability, as well as sensitivity to β -lactam antibiotics & enhancement to

biofilm formation. Therefore in TSS-f6- $\Delta amrZ$, the transposon insertion in *rlpA* likely caused alteration to membrane fluidity; though how this restored the environmentally-responsive phenotype is unclear.

ampG ([pflu4993](#)) encodes the beta-lactamase induction signal transducer AmpG, with 56.9% sequence identity to AmpG in *P. aeruginosa* PAO1 ([PA4393](#); BLASTP *E*-value: 0.0); containing an acetyl-CoA transporter-like domain ([PF13000](#); residue: 20-161; *E*-value: $9.6e-7$). In *E. coli*, the inner membrane-localised AmpG permease was shown to facilitate the transport of mucopeptides (containing GlcNAc-anhMurNAc) into the cytoplasm, during cell wall recycling (Cheng & Park, 2002). The deletion of *ampG* in *P. aeruginosa* was observed to significantly reduce the resistance to β -lactam antibiotics, indicating the importance of AmpG in membrane permeability (Zhang et al., 2010). While *anmK* ([pflu5546](#)) encodes the anhydro-N-acetylmuramic acid kinase AnmK, with 67.2% identity to AnmK in *P. aeruginosa* PAO1 ([PA0666](#); BLASTP *E*-value: $3e-180$). In *P. aeruginosa*, the AnmK kinase functions in the hydrolysis and phosphorylation of the peptidoglycan intermediate anhMurNAc, during recycling of the cell wall (Bacik et al., 2010). For TSS-f6- $\Delta amrZ$, it is unclear how transposon insertion in the genes *ampG* & *anmK* (or the nearby *pflu5545*) resulted in restoration of the phenotype switch; though it must somehow relate to their function in peptidoglycan recycling and an effect on stability of the cell membrane. In the TSS-f6 WspE mutant, transposon insertion in *amgK* ([pflu5574](#)) resulted in suppression of the SM phenotype, with the AmgK kinase also involved in cell wall recycling (Gisin et al., 2013); see [Section 2.4.1.1](#). It is evident that there is a strong connection between the TSS-f6 phenotype switch and membrane permeability; this supports the hypothesis of O'Neal et al. (2022) that the Wsp system senses and responds to cell envelope stress.

2.5 Recreation of TSS-f6 mutations

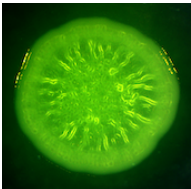
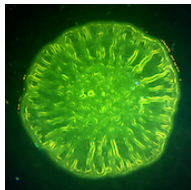
The mutational history of TSS-f6 revealed a number of mutations in the Wsp pathway, that may be required for the environmentally-responsive phenotype – SM at 28°C & WS at 20°C (Summers, 2018); see discussion in [Section 2.3](#). I previously showed that the final TSS-f6 *wspA* mutation (p.V441G) was essential, with reversion of the mutation resulting in abolition of the phenotype switch (refer to [Section 2.3.1.3](#)). This substitution in the MCPsignal domain of WspA was hypothesised to alter the sensitivity of the receptor to an environmental signal (e.g. membrane stress induced by low temperatures), and therefore the activation state of the Wsp system and biofilm formation (O'Neal et al., 2022). TSS-f6 also contains an in-frame

duplication in *dipA*, predicted to reduce the PDE activity of DipA (see [Section 2.3.2](#)). The f2 ancestor obtained only two mutations, SNPs in *wspA* (p.T104N) & *wspE* (p.H70L); the effect of alteration to the WspA chemoreceptor was unclear, while mutation to the WspE kinase was predicted to increase activity of the WspR DGC (see [Section 2.3.3](#)). While the L17-*mutS*-WT ancestor contained a total of three mutations in the *wsp* operon – in *wspA* (p.D253Y), *wspF* (p.I295S), & *wspB* (p.37_39delAEV). Disruption of the WspF methyltransferase was predicted to activate the WspR DGC, and increase c-di-GMP levels (Bantinaki et al., 2007); while the effect of mutation to the WspB scaffold protein & WspA was not obvious (see [Section 2.3.4](#)).

To fully dissect the genetic basis of the TSS-f6 phenotype switch, each of the described mutations in the *wsp* operon were recreated in the relevant ancestral strain f2 (MPB13893) or L17-*mutS*-WT (MPB13896), and in the wild-type SBW25 (MPB14218). This was achieved by site-directed mutagenesis & allelic exchange (as described in [Section 2.4](#)). The next section will describe the phenotypic effect of each mutation, as well as the combination of mutations that was observed to reproduce the environmentally-responsive phenotype in the wild-type SBW25 background.

2.5.1 f2 ancestor – *wspA* mutation

The final *wspA* mutation (p.V441G; referred to by *wspA*-mut1) was recreated in the f2 ancestor background, producing the strain: f2-*wspA*-mut1 (MPB14133); the effect on colony morphology is shown in [Table 2.18](#) below. I found that insertion of the TSS-f6 *wspA* mutation in the f2 ancestor resulted in reproduction of the phenotype switch, with f2-*wspA*-mut1 displaying the SM phenotype at 28°C & WS phenotype at 20°C. This is consistent with the effect of reversion of this mutation in TSS-f6 (see [Section 2.3.1.3](#)); confirming the necessity of the V441G substitution in the WspA MCP. Furthermore, this result also suggests that the other TSS-f6 mutation in the *dipA* gene (p.470_472dupNLT) is not required for the environmentally-responsive phenotype.

Strain	MPB	Genotype	Colony morphology spot	
			28°C	20°C
f2 ancestor	13893	Evolved		

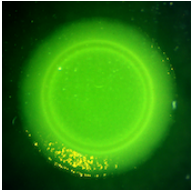
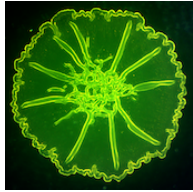
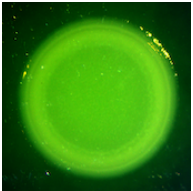
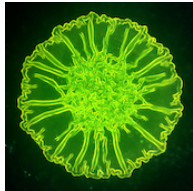
f2 ancestor <i>wspA</i>-mut1	14133	Evolved <i>wspA</i> -V441G		
TSS-f6	13890	Evolved		

Table 2.18. Phenotype switch reproduced in f2 ancestor by insertion of TSS-f6 *wspA* mutation. Colony images, MPB number & Genotype (Evolved in experiment or WT, and relevant mutation) provided for the strains f2, f2-*wspA*-mut1 & TSS-f6. Colony morphology spot as described in [Table 2.1](#) legend.

2.5.2 L17-*mutS*-WT – *wspE* & *wspA* mutations

The two mutations unique to the f2 ancestor, the substitution in *wspA* (p.T104N; referred to by *wspA*-mut2) & *wspE* (p.H70L; referred to by *wspE*-mut), were each recreated in the L17-*mutS*-WT background. Producing the strains: L17-*mutS*-WT-*wspA*-mut2 (MPB14610) & L17-*mutS*-WT-*wspE*-mut (MPB14626); the effect shown in [Table 2.19](#) below.

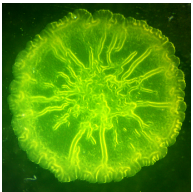
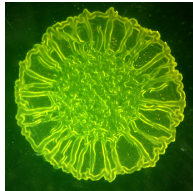
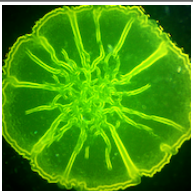

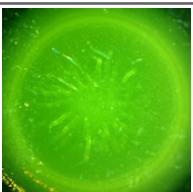
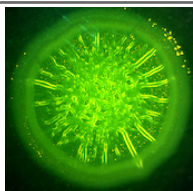
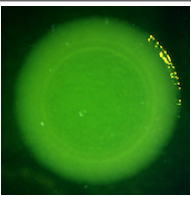
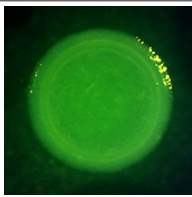
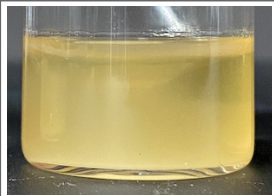
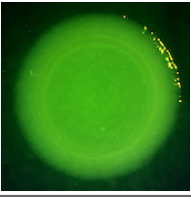
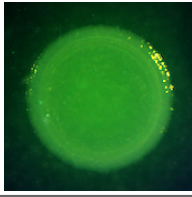
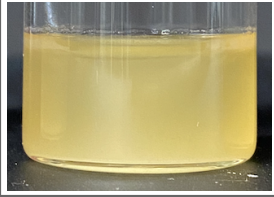
Strain	MPB	Genotype	Colony morphology spot	
			28°C	20°C
L17 <i>mutS</i>-WT	13896	Evolved <i>mutS</i> -WT		
L17 <i>mutS</i>-WT <i>wspA</i>-mut2	14610	Evolved <i>mutS</i> -WT <i>wspA</i> -T104N		
L17 <i>mutS</i>-WT <i>wspE</i>-mut	14626	Evolved <i>mutS</i> -WT <i>wspE</i> -H70L		

Table 2.19. Phenotypic analysis of f2 *wspE* & *wspA* mutation inserted in L17 *mutS*-WT ancestor. Colony images, MPB number & Genotype (Evolved in experiment or WT, and relevant mutation) provided for the strains L17-*mutS*-WT, L17-*mutS*-WT-*wspA*-mut2 & L17-*mutS*-WT-*wspE*-mut. Colony morphology spot as described in [Table 2.1](#) legend.

I found that insertion of the f2 *wspA* mutation did not have a major effect on colony morphology in L17-*mutS*-WT, with only a slight decrease in the wrinkled texture of colonies grown at 28°C. While the *wspE* mutation resulted in a significant change to colony phenotype – L17-*mutS*-WT-*wspE*-mut displaying the SM phenotype (with a semi-wrinkly centre) at 28°C & WS phenotype (with smooth edge) at 20°C (see images in *Table 2.19*). This result confirms that the WspE substitution H70L does not cause complete loss of kinase activity, as the Wsp system & WspR DGC must still be partially active to allow for cellulose production and the WS phenotype (Bantinaki et al., 2007). In comparison, I previously showed that deletion of the entire *wspE* gene in TSS-f6 resulted in complete suppression of the WS phenotype (see *Section 2.4.1*). D’Argenio et al. (2002) previously identified a transposon insertion in *wspE*, that caused only partial suppression of the WS phenotype in the SBW25 *wspF* mutant; this transposon mutant displayed the WS phenotype at 23°C, and SM phenotype at higher temperatures. Therefore the f2 *wspE* mutation may have a similar effect, causing inactivation of the Wsp system & WS phenotype at high temperatures.

2.5.3 SBW25 – *wspA*, *wspE* & *wspF* mutations

To gain better understanding of the TSS-f6 *wsp* operon mutations, each was also recreated in the wild-type SBW25 background – *wspA*-V441G from TSS-f6; *wspA*-T104N & *wspE*-H70L from the f2 ancestor; and *wspF*-I295S & *wspA*-D253Y from L17-*mutS*-WT. The following strains were produced: SBW25-*wspA*-mut1 (MPB14131), SBW25-*wspA*-mut2 (MPB14609), SBW25-*wspE*-mut (MPB14624), SBW25-*wspF*-mut (MPB14625) & SBW25-*wspA*-mut3 (MPB14623). The effect of these mutations on colony morphology and mat formation are summarised in *Table 2.20* below.

Strain	MPB	Genotype	Colony morphology spot		Mat formation: 28°C
			28°C	20°C	
SBW25 <i>wspA</i> - mut1	14131	WT <i>wspA</i> -V441G			
SBW25 <i>wspA</i> - mut2	14609	WT <i>wspA</i> -T104N			

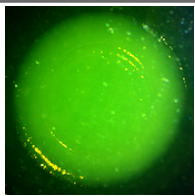
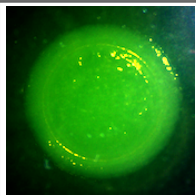

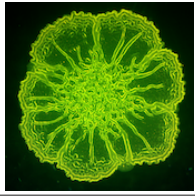
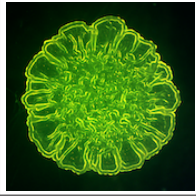
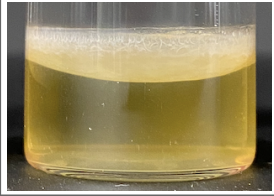
SBW25 <i>wspE</i> -mut	14624	WT <i>wspE</i> -H70L			
SBW25 <i>wspF</i> -mut	14625	WT <i>wspF</i> -I295S			

Table 2.20. Phenotypic analysis *wspA*, *wspF* & *wspE* mutations in wild-type SBW25. Phenotypic images, MPB number & Genotype (Evolved in experiment or WT, and relevant mutation) provided for the strains SBW25-*wspA*-mut1, SBW25-*wspA*-mut2, SBW25-*wspE*-mut & SBW25-*wspF*-mut. Phenotypes as described in [Table 2.1](#) legend.

I found that the insertion of each TSS-f6 *wspA* mutation produced no phenotypic effect; SBW25-*wspA*-mut1 & SBW25-*wspA*-mut2 displayed the SM phenotype at both temperatures, with colonisation of the broth phase and no improvement to mat formation as compared to SBW25. This result demonstrates that although the substitution V441G in the WspA MCP is essential for the environmentally-responsive phenotype of TSS-f6, in the wild-type SBW25 it is not sufficient to produce the effect.

The f2 *wspE* mutation also caused no change to colony phenotype, with SBW25-*wspE*-mut displaying the SM phenotype at 28°C & 20°C, indistinguishable from SBW25. Therefore the temperature-sensitive effect observed when recreating this mutation in L17-*mutS*-WT (colony with WS centre at low temperatures; see [Section 2.5.2](#)), must be dependent on other mutations present in this background. While I observed that recreation of the L17-*mutS*-WT *wspF* mutation in SBW25, resulted in the WS phenotype and formation of a substantial mat at the surface of the static broth (see images in [Table 2.20](#)). The effect of this substitution I295S in the WspF methylesterase was exactly as predicted, resulting in activation of the WspR DGC, overproduction of c-di-GMP, and the WS phenotype (Bantinaki et al., 2007). It is possible that no phenotypic change was observed for mutations in the WspA chemoreceptor & WspE kinase, as this required the underlying Wsp system to be in an active state (e.g. by disruption of WspF). Therefore the L17-*mutS*-WT *wspF* mutation may also be necessary for the TSS-f6 phenotypic switch, to prevent suppression of WspR by the WspF methylesterase activity, thus allowing for activation of the Wsp system.

2.5.4 Combination of mutations

Based on the phenotypic effects of each TSS-f6 *wsp* mutation, I proceeded to recreate different combinations of these mutations in the SBW25 background, in an attempt to reproduce the environmentally-responsive phenotype. Due to the complex mutational history of TSS-f6, this was considered an improbable task; it is possible that any number of the pre-existing mutations in the L17-*mutS*-WT ancestor (containing 75 total mutations) would be required for the phenotype switch. Regardless, the following strains were produced: SBW25-*wspA*-mut1&2 (MPB14611), SBW25-*wspA*-mut1-*wspF*-mut (MPB14990), SBW25-*wspA*-mut2-*wspF*-mut (MPB16050) & SBW25-*wspA*-mut1&2-*wspF*-mut (MPB16051). The colony morphology and mat formation phenotype of the combination of mutations are shown in *Table 2.21* below.

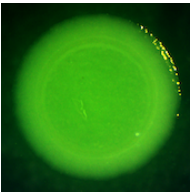
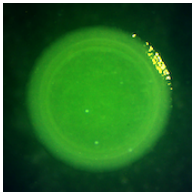
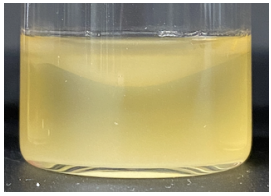
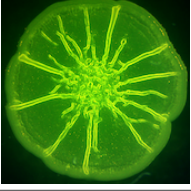
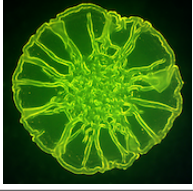
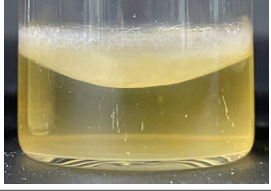
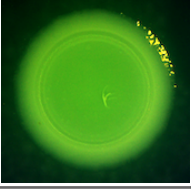
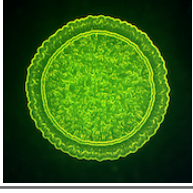
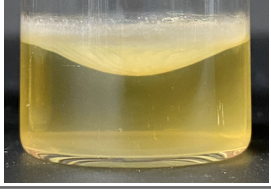
Strain	MPB	Genotype	Colony morphology spot		Mat formation: 28°C
			28°C	20°C	
SBW25 <i>wspA</i> - mut1&2	14611	WT <i>wspA</i> -V441G <i>wspA</i> -T104N			
SBW25 <i>wspA</i> - mut1 <i>wspF</i> -mut	14990	WT <i>wspA</i> -V441G <i>wspF</i> -I295S			
SBW25 <i>wspA</i> - mut1&2 <i>wspF</i> -mut	16051	WT <i>wspA</i> -V441G <i>wspA</i> -T104N <i>wspF</i> -I295S			

Table 2.21. Phenotype switch reproduced in SBW25 with three mutations in the *wsp* operon. Phenotypic images, MPB number & Genotype (Evolved in experiment or WT, and relevant mutation) provided for the strains SBW25-*wspA*-mut1&2, SBW25-*wspA*-mut1-*wspF*-mut & SBW25-*wspA*-mut1&2-*wspF*-mut. Phenotypes as described in [Table 2.1](#) legend.

The insertion of both the TSS-f6 & f2 *wspA* mutations (p.V441G & p.T104N) produced no visible phenotypic effect in SBW25, as was expected based on the individual effect of each mutation (see [Section 2.5.3](#)); SBW25-*wspA*-mut1&2 displayed the SM colony morphology, and no improvement to mat formation. While the combination of the L17-*mutS*-WT *wspF* mutation (p.I295S) and either *wspA* mutation in SBW25, resulted in the WS phenotype at

both temperatures, and formation of a thick mat in the static broth environment (see images in *Table 2.2.1*). Although the SBW25-*wspA*-mut1-*wspF*-mut does present a slightly more pronounced wrinkled colony texture at 20°C, and the colony edge resembling the semi-WS phenotype at 28°C; this result implying that these two mutations may confer some capacity for phenotypic change in response to the environment. Remarkably, I found that the combination of both *wspA* mutations and the *wspF* mutation resulted in reproduction of the phenotype switch in the wild-type SBW25. SBW25-*wspA*-mut1&2-*wspF*-mut (*wspA*-V441G-T104N & *wspF*-I295S) displays the SM phenotype at 28°C and WS phenotype at 20°C, as observed for the TSS-f6 genotype (see images in *Table 2.21*). Although the triple mutant in SBW25 does differ from TSS-f6 in mat formation capacity, as it is able to form a decent mat in the static broth environment at 28°C.

I was relatively surprised that the environmentally-responsive phenotype of TSS-f6 could be reconstituted with only three mutations, and that it was not dependent on any other mutations in the L17-*mutS*-WT ancestral background. This phenotype switch is possible as a result of simple rewiring of the Wsp pathway, including disruption to the WspF methylesterase (negative regulator of the WspR DGC), and two substitutions in the WspA MCP altering the sensitivity of the membrane-bound Wsp complex to the environment. Based on these results, a new model may be devised for the TSS-f6 phenotype switch, updating from that previously described by Summers (2018).

2.6 Revised model for TSS-f6 phenotype switch

The evolved strain TSS-f6 displays an environmentally-responsive colony phenotype, observed with change to incubation temperature – SM at 28°C & WS at 20°C (Summers, 2018). I have shown that the SM phenotype at 28°C is dependent on the PDE activity of Pflu5960 and negative regulation of the *wss* operon by the AmrZ transcriptional regulator (see *Section 2.4.4* & *2.4.6*). While the WS phenotype at 20°C relies on an intact WspE kinase, the Wsp pathway, and cellulose synthase machinery encoded by the *wss* operon (see *Section 2.4.1* & *2.4.2*). Furthermore, I was able to reproduce the phenotype switch with only three point mutations – the substitution V441G & T104N in the WspA MCP, and I295S in the WspF methylesterase (see *Section 2.5.4*). From these results, I propose a revised model for the TSS-f6 phenotype switch, summarised in *Figure 2.1* below; this is based on models previously described for the Wsp pathway by Bantinaki et al. (2007), O'Connor et al. (2012) & O'Neal et al. (2022).

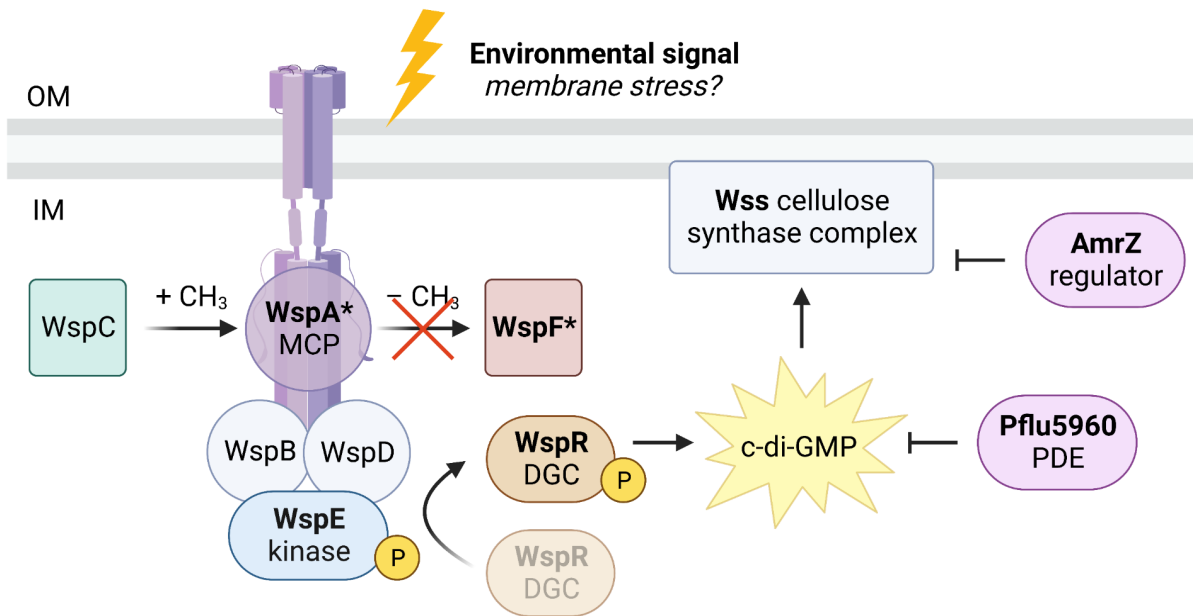


Figure 2.1. Model for regulation of the TSS-f6 phenotype switch. The Wsp signalling complex forms between the membrane-bound WspA receptor, WspB & WspD scaffold proteins, and WspE kinase. The WspA* MCP senses an environmental signal related to membrane stress, with mutations altering the sensitivity of the receptor. The WspC methyltransferase adds methyl groups (CH₃) to methylation sites on WspA, while the disrupted WspF* methyl-esterase does not remove them, therefore the Wsp complex remains in an active methylated state. In response to membrane rigidification at low temperatures, the methylated WspA* MCP transduces a signal along the Wsp pathway, resulting in autophosphorylation of the WspE kinase. The WspE kinase phosphorylates the WspR DGC, causing synthesis of c-di-GMP, activation of the Wss cellulose synthase complex and the WS phenotype. While at high temperatures the WspA* MCP is inactive; the Pflu5960 PDE actively degrades the low levels of c-di-GMP and the negative regulator AmrZ represses the *wss* operon, resulting in the SM phenotype. Model adapted from Bantinaki *et al.* (2007).

The Wsp receptor signalling complex is composed of the WspA methyl-accepting chemotaxis protein (MCP), WspB & WspD scaffold proteins, and WspE histidine kinase/response regulator (Bantinaki *et al.*, 2007). The membrane-bound WspA receptor senses an environmental signal related to cell envelope stress and surface contact, for example unfolded proteins in the periplasm or alteration to membrane fluidity (O’Neal *et al.*, 2022). In response to the environment the WspA MCP undergoes a conformational change, that results in signal transduction along the Wsp pathway and autophosphorylation of WspE; the active WspE kinase then phosphorylates the WspR DGC, activating the synthesis of c-di-GMP (O’Connor *et al.*, 2012). The Wsp complex signalling is reset by a change in methylation state of the WspA MCP; this is controlled by the opposing activities of the WspC methyltransferase & WspF methyl-esterase, that respectively add & remove methyl groups (CH₃) from the conserved glutamate residues (Hickman *et al.*, 2005; Güvener & Harwood,

2007). While Pflu5960 functions as a PDE enzyme in the degradation of intracellular c-di-GMP (Feng et al., 2020); and the AmrZ transcriptional regulator inhibits expression of the cellulose synthase complex, either directly by binding to the promoter region of the *wss* operon (or *fleQ*), or indirectly by binding to other DGC-encoding genes (e.g. *pflu0621*, ortholog of *gcbA* in PAO1) (Giddens et al., 2007; Jones et al., 2014). The secondary messenger c-di-GMP then activates the Wss cellulose synthase complex, causing the overproduction of the cellulosic polymer, and thus the WS phenotype (Bantinaki et al., 2007).

For the TSS-f6 phenotype switch, the disruptive mutation to WspF (I295S) results in no WspF* methyltransferase activity; while the constitutively active WspC methyltransferase adds methyl groups to the WspA MCP, resulting in the Wsp signalling complex remaining in the active methylated state. Mutations in the C-terminal MCP signalling domain (V441G) & N-terminal 4HB periplasmic domain (T104N) of WspA alters the sensitivity of the receptor to an environmental signal, hypothesised to be membrane stress associated with surface attachment. The methylated WspA* MCP is therefore only active in stressful environmental conditions that trigger membrane rigidification (decrease in membrane fluidity), observed with the lowering of incubation temperature.

2.6.1 SM phenotype at 28°C

At 28°C, the high membrane fluidity causes inactivation of the WspA* MCP. This results in no signal transduction along the Wsp pathway or phosphorylation of WspE; the inactive WspE kinase cannot phosphorylate WspR, therefore c-di-GMP is not synthesised by the WspR DGC. The intracellular c-di-GMP levels are further reduced by the activity of Pflu5960, with the Pflu5960 PDE enzyme active at 28°C in the degradation of c-di-GMP. The AmrZ transcriptional regulator is also active at 28°C inhibiting expression of the *wss* operon. Therefore no cellulose is produced due to the low levels of c-di-GMP & suppression of the Wss cellulose synthase complex, resulting in reduction to mat formation and the SM colony morphology phenotype.

2.6.2 WS phenotype at 20°C

At 20°C, the low temperature triggers cell membrane stress and an increase in membrane rigidity, causing activation of the WspA* MCP; this may be explained by induction of structural change to the membrane-bound WspA or Wsp signalling complex. The WspC methyltransferase adds methyl groups to the WspA methylation sites, while the WspF*

methylesterase is inactive, consequently the Wsp complex remains in an active state. The methylated WspA* MCP therefore transduces the signal along the Wsp pathway, which results in autophosphorylation of the WspE kinase & phosphorylation of WspR. The phosphorylated WspR DGC synthesises c-di-GMP; while the Pflu5960 PDE is either inactive at 20°C, or unable to degrade the large quantities of c-di-GMP produced by the active WspR. High levels of intracellular c-di-GMP cause activation of the Wss cellulose synthase complex, and overproduction of the cellulose; the AmrZ negative regulator is also either inactive at 20°C, or the activity diminished by the high c-di-GMP level. Therefore production of the adhesive cellulosic polymer causes cells to stick together, formation of a mat at the surface of static broth, and observation of the WS colony morphology phenotype.

2.6.3 Prospects for testing the model

Based on the revised model of the TSS-f6 phenotype switch, there are a number of predictions that could be tested with further experimentation. The first thing I would like to investigate is the nature of the environmental signal being sensed by the WspA receptor. If the signal is associated with cell envelope stress as hypothesised, then it should be possible in TSS-f6 to activate or inactivate the Wsp pathway by perturbation of membrane permeability (O'Neal et al., 2022). This could be achieved by the addition of chemical chelators (e.g. EDTA), surfactants (e.g. SDS & Tween 80), antimicrobial compounds (e.g. lysozyme, polymyxin B & carbenicillin), or alcohols (e.g. ethanol & benzyl alcohol) (Vaara, 1992).

Furthermore, I am most interested in exploring the effect of the two mutations identified in WspA (V441G & T104N), and figuring out exactly how they alter the sensitivity of the WspA MCP to the environment. Although I did not observe a phenotypic effect upon recreation of each *wspA* mutation in the wild-type background, further screening of these single mutants would be useful, for example measurements of c-di-GMP level and cell fitness. The specificity of these WspA mutations is also unclear – whether alteration of these specific residues was required, or other combinations of mutations in the MCPsignal & 4HB domains would also reproduce the environmentally-responsive phenotype. Performing a deep mutational scan of WspA would be highly informative, and reveal the structure-function relationship of the WspA MCP; this was previously carried out for the WspF protein (Malone et al., 2007). Of particular interest is the C-terminal signalling domain of WspA, shown to be essential for subcellular localisation and function of the Wsp system (O'Connor et al., 2012).

Another prediction of the model that I could easily test is the c-di-GMP level of TSS-f6 grown at the different incubation temperatures – assumed to be high at 20°C due to activity of the WspR DGC enzyme (WS phenotype), and low at 28°C as a result of inactivation of the Wsp system & degradation by the Pfl5960 PDE (SM phenotype). The level of c-di-GMP may be measured using the pCdrA-GFP fluorescence-based reporter, in combination with flow cytometry (Rybtke et al., 2012). This reporter could also be used to further characterise each reconstructed mutant and gene deletion (in the TSS-f6 & SBW25 backgrounds), and investigate the contribution of the respective proteins to c-di-GMP signalling.

Transcriptomic analysis of TSS-f6 would be most informative, and reveal the genes differentially expressed in the two environments & phenotypic states. I have actually already carried out this experiment, sequencing RNA extracted from colony spots of TSS-f6, TSS-f6-*wspA*-mut1-WT & SBW25 incubated at either 28°C or 20°C. Although for the scope of this thesis I did not include analysis of the dataset, I expect that it will further clarify the activity of each protein as proposed in the model of the TSS-f6 phenotype switch. For example, it would be intriguing to examine whether *pfl5960* & *amrZ* are downregulated at 20°C, or if there is differential expression of other DGC & PDE-encoding genes depending on temperature. The other experiment I would like to complete is insertion of the f2 *wspE* mutation (p.H70L) into the triple mutant SBW25-*wspA*-mut1&2-*wspF*-mut; recreation of this mutation in L17-*mutS*-WT resulted in an interesting effect, with partial suppression of the WS colony phenotype especially at higher incubation temperatures. As I still observed some phenotypic differences between the triple mutant & TSS-f6 (e.g. mat formation capacity), it is possible that the f2 *wspE* mutation is what is missing for complete realisation of the TSS-f6 environmentally-responsive phenotype.

Chapter III: Design of a new life cycle experiment

3.1 Motivation for revised life cycle experiment

This chapter outlines the motivation for redesign of the life cycle experiment (LCE), to remove the reliance on the colony morphology proxy for niche preference in static broth. The revised selective regime is described, including new methods for selection on the collective trait of mat formation and individual trait of dispersal by swimming motility. To demonstrate the efficiency of the new experimental regime, the results of a small-scale pilot experiment are also presented, which further emphasises the importance of avoiding selection for the life cycle based on colony morphology.

3.1.1 Life cycle proceeding by mutation

Hammerschmidt et al. (2014) previously recreated a simple multicellular life cycle in *P. fluorescens* SBW25, that transitioned between the WS collective and SM individual cell phases; refer to previous discussion in [Section 1.3.3](#). This experiment utilised selective methods based on colony morphology on agar plates (WS or SM), as a proxy for the niche preference behaviour in the static broth environment (colonisation of the air-liquid interface or broth). The two-phase life cycle was enforced by the passage of evolved populations through bottlenecks at the end of each phase, the propagules chosen by assessment of colony morphology – SM phenotype in Phase I & WS phenotype in Phase II (Hammerschmidt et al., 2014). This was problematic for a number of reasons, firstly because it required personal judgement to distinguish between ‘wrinkly’ & ‘smooth’ colonies; this distinction becoming blurred in evolved lineages over time, with many displaying an intermediate phenotype. More significantly, this LCE regime applied selection outside of the static broth environment where adaptation occurred, instead forcing lineages to switch between two distinct phenotypes on agar plates – this requiring mutation. Therefore it is relatively unsurprising that Hammerschmidt et al. (2014) observed hypermutation emerging as the best strategy to transition through the life cycle, the elevation of mutation rate allowing for rapid generation of the two phenotypic states.

3.1.2 Significance of environmentally-responsive strain

By virtue of the selective regime the LCE precluded the evolution of developmental regulation of the life cycle, as it excluded any genotypes that would alter phenotype in

response to a signal present in the static broth environment. As explored in Chapter II, the environmentally-responsive strain TSS-f6 is the perfect example of a possible solution. The line TSS-f6 was evolved from a continuation of the life cycle experiment, and demonstrates the capacity to switch between the WS & SM phenotype in response to the environment, observed with incubation temperature (Summers, 2018). Furthermore, I have shown that this phenotype switch could be reproduced in SBW25 with only three point mutations (see [Section 2.5.4](#)) – therefore this capacity is readily accessible to selection. The mutations conferred a simple rewiring of the Wsp pathway, that was predicted to alter the sensitivity of the WspA receptor to an environmental signal (likely associated with membrane stress), allowing for environmentally-responsive activation of the Wsp signalling complex (O’Neal et al., 2022). TSS-f6 originated from the LCE, so must be adaptive in the static broth environment; though due to the strict selective regime this line quickly went extinct, as it only displayed the SM phenotype on agar plates incubated at 28°C. It is therefore possible that developmental regulation of the life cycle had been evolving right under our noses, except that we had been unintentionally purging it. There is an apparent need for the design of a new life cycle experiment, that applies selection in the ecologically relevant static broth environment and without use of the colony morphology proxy.

3.1.3 Two-phase life cycle in natural environment

For the revised LCE, instead of transitioning between the two distinct phenotypic states as assessed by colony phenotype on an agar plate, I wanted to focus on selecting directly on the collective-level trait of mat formation and individual-level trait of dispersal by swimming motility. To better understand the motivation for this, consider a basic two-phase life cycle existing in the natural environment – shown in *Figure 3.1* below. As proposed by Rainey et al. (2017), the reeds within a pond provide an ecological scaffold in which bacteria may colonise, and form a collective mat at the surface (e.g. WS mat), by the cooperative production of an adhesive polymer (see [Section 1.2.5](#) & [1.3.1](#)). By virtue of the ecology, the discrete reeds partition variation between collectives; and upon the collapse of a mat, this reed (or niche) becomes available for colonisation by another collective. Each collective is itself considered an ‘evolutionary dead end’, as it lacks a means of group-level reproduction or dispersal to the available reed (Rainey et al., 2017). But if the collective produces single-cell motile propagules (e.g. SM revertant or ‘cheater’ types), these individual cells may become liberated from the mat and disperse by swimming through the pond, thus allowing for reproduction of the collective (Rainey & Kerr, 2010). Therefore we have a

simple multicellular life cycle that transitions through a soma-like mat-forming collective state, and a germ-like individual motile cell state for dispersal (Rainey et al., 2017; Hammerschmidt et al., 2014).

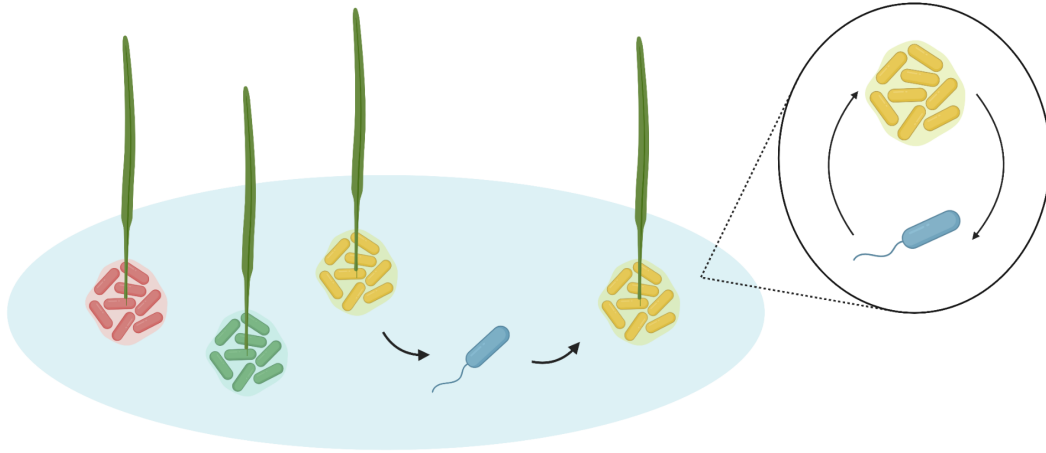


Figure 3.1. A simple two-phase multicellular life cycle in nature. This pond contains four reeds, the three on the left occupied by collective mats with discrete variation from one another (red, green & yellow). The right reed undergoes mat collapse, and the niche becomes available for colonisation – the yellow collective achieves this by production of the motile individual cell (blue) that swims through the pond to the available reed, and reforms the collective mat. By virtue of the ecology, this results in a simple two-phase multicellular life cycle that transitions between the collective mat (yellow) state, and individual motile cell state (blue) for dispersal. Adapted from the ‘Darwinian pond scum’ analogy of Rainey et al. (2017).

3.1.4 Mat formation & swimming motility

Based on this simple life cycle observed in nature, I chose the traits of mat formation and swimming motility, to apply selection on the collective and individual phases of the new LCE regime. The formation of a biofilm mat at the air-liquid interface in static broth is a collective-level behaviour, requiring cells to cooperate by the overproduction of a cellulosic polymer that acts as an adhesive glue (Rainey & Rainey, 2003). While dispersal by swimming motility involves the flagella-dependent movement of individual cells through a liquid environment (agar concentration less than 0.3%) (Ha et al., 2014a). Other forms of bacterial motility include – swarming of multicellular groups (cell rafts) along a solid surface (>0.3% agar) using multiple rotating flagella; twitching of individual cells on a surface by extension & retraction of the type IV pili; as well as the surface movements of cells by active gliding (involving adhesion complexes), and passive sliding by growth (requiring surfactants) (Kearns, 2010). I specifically focused on swimming motility as this is an individual-level

behaviour, and can be selected for by lowering the concentration of agar in the media (allowing exclusion of multicellular swarming motility, and other surface movements).

3.1.3.1 Regulation by c-di-GMP signalling

Furthermore, numerous studies in *P. aeruginosa* have demonstrated the inverse regulation of biofilm formation and dispersal by swimming or swarming motility; this under the control of intracellular levels of the secondary messenger c-di-GMP (Caiazza et al., 2007; Verstraeten et al., 2008; Guttenplan & Kearns, 2013). The c-di-GMP signalling pathway regulates the transition of bacteria from the motile to sessile (biofilm) lifestyle, with low levels of c-di-GMP associated with motility and high levels with biofilm formation (Ha & O’Toole, 2015; Hengge, 2009; Römling et al., 2013). c-di-GMP is synthesised from two molecules of GTP by diguanylate cyclase (DGC) enzymes that contain the conserved GGDEF domain, while it is degraded by phosphodiesterases (PDE) with an EAL domain (Römling et al., 2005). In *P. aeruginosa*, the level of c-di-GMP has been shown to dictate the activity of the FleQ-FleN complex – in the absence of c-di-GMP the FleQ transcriptional regulator activates flagella production, and represses the *pel* & *psl* genes by binding at the promoter region; while at high levels, c-di-GMP binds to FleQ, causing the conversion in function from a repressor to an activator of *pel* & *psl* expression, resulting in production of the exopolysaccharide biofilm matrix (Hickman & Harwood, 2008; Baraquet et al., 2012; Yan et al., 2017). Understanding of the c-di-GMP regulatory network underpinning the traits of mat formation & motility may reveal potential mechanisms for the evolution of a developmentally regulated life cycle.

3.2 New selective methods based on mat formation & motility

I designed new selective methods for the revised LCE regime that eliminates use of the colony morphology proxy (see [Section 1.3.3](#)), by directly screening for mat formation capacity (instead of the WS phenotype) and swimming motility (instead of SM phenotype).

3.2.1 Mat formation screen

For the collective phase of the life cycle, I screened for mat formation on a large-scale using 96-well plates – each well approximating the static broth microcosm environment. At the start of the life cycle generation for each replicate lineage a KB microcosm was inoculated by a single motile cell, and incubated for four days under static conditions to allow for the

evolution of mat-forming types (corresponding to Phase II of the Hammerschmidt et al., 2014 regime). Each evolved lineage was then diluted and spread onto an agar plate to obtain single colonies; at this point Hammerschmidt et al. (2014) carried out screening based on the WS colony morphology phenotype. The new mat formation screen instead involved the inoculation of random individual colonies (disregarding the colony phenotype) into each well of a 96-well plate containing a small volume of KB; with 6-12 colonies inoculated per replicate lineage. These plates were incubated under static conditions for 24 hours, and then the mat formation capacity within each well was assessed; see example image in *Figure 3.2 (left)* below. Mat formation was assessed for each lineage using the following criteria – at least one of the respective wells (6-12 colonies) must contain a mat that covers the surface of the broth (including connection with the walls of the well), with no fallen mat visible at the bottom. From this screen, each replicate lineage was marked as a mat former (1) or non-mat former (0), and the first mat forming well (from a random single colony) was passed to the next phase of the life cycle. Depending on the number of colonies screened per lineage, this new screening method also required the evolved populations to be comprised of at minimum 8-17% mat forming individuals.

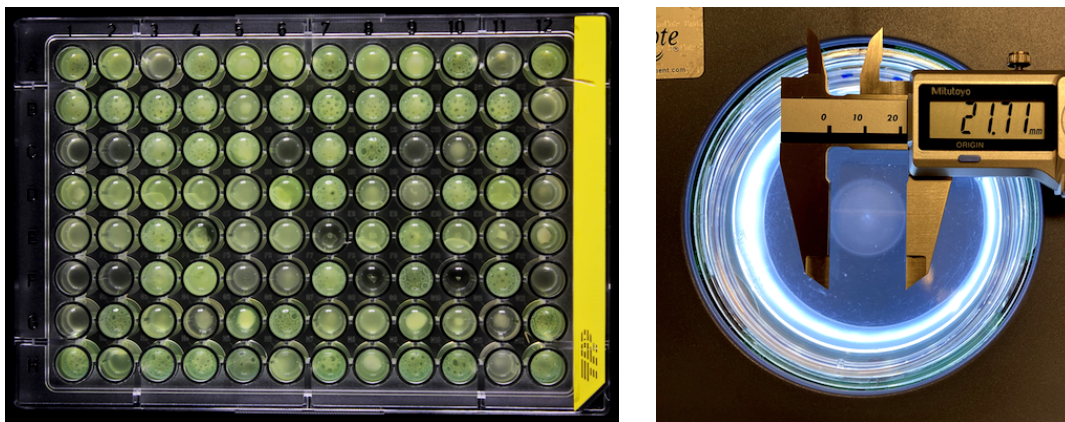


Figure 3.2. Screening methods for mat-formation and swimming motility. Left: example of mat formation screen in 96-well plate, each well inoculated with a random colony from a 6 day evolved culture of SBW25. Representative example wells containing: mat formers = D7, E3 & G6; fallen mats = D6, E4 & G5; and non-mat formers = D9, E7 & G1. Right: example of swimming motility screen, semi-solid agar plate (0.25% agar & 1% KB) inoculated with 6 day evolved culture of SBW25. The diameter of migration was measured as 21.7 mm.

3.2.2 *Swimming motility screen*

For the dispersal phase of the life cycle, I screened for swimming motility using low-nutrient semi-solid agar (SSA) plates; this protocol was adapted from the standard assay for *P. aeruginosa* swimming motility described by Ha et al. (2014a). I thoroughly tested different

combinations of nutrient composition & agar percentage, and found that motility plates containing 0.25% agar & 1% KB were most effective in screening for swimming motility. The low viscosity of 0.25% agar was chosen to encourage swimming and to minimise multicellular swarming behaviour on the surface (see previous discussion in *Section 3.1.4*); the use of any lower agar percentage resulted in unstable plates that were difficult to transport, and irreproducibility across replicates. The nutrient of KB was used to maintain consistency with the KB broth environment, and the low nutrient content of 1% to discourage growth on the surface, forcing individual cells to swim through the agar to access nutrients. The method for preparing SSA plates was also important, to maintain the uniform distribution of agar within each plate as well as between replicate plates. This was achieved using a plate pouring machine when possible (rather than pouring by hand); SSA plates were also prepared the day before use, and after the agar set, plates were left to dry in stacks of maximum 8 plates at room temperature overnight. These motility plates (0.25% agar & 1% KB) provided reliable measurements of swimming motility (diameter of migration) across replicate cultures and for different evolved genotypes; an example of this is provided in *Section 3.2.2.1*.

During the second phase of the life cycle, each replicate lineage was inoculated by a single mat-forming type, and incubated static for six days, allowing for the evolution of dispersing propagules in the collective mat (corresponding to Phase I of the old regime). Each evolved lineage was thoroughly vortexed and then inoculated directly into a motility plate; this was achieved by dipping the tip of a sterile toothpick into the vortexed culture (1-2 mm deep), and then stabbing this into the centre of an SSA plate (to the base of the agar layer). Motility plates were incubated upright for 30 hours in a temperature-controlled incubator with only natural air convection (to minimise uneven evaporation on the plate surface). Swimming motility distance was then assessed for each lineage by measuring the diameter of migration, with a minimal threshold applied of 10-15 mm; see example image in *Figure 3.2 (right)* above. The motility distance was recorded, and each replicate lineage marked as motile (≥ 15 mm), or non-motile (< 15 mm). For the surviving motile lineages, the most motile individual from the evolved population was obtained by streaking directly from the SSA plate; this was achieved by stabbing a sterile toothpick into the agar at the edge of migration, and streaking this to a new agar plate. A random single colony from the streak plate was chosen (representing the individual cell in the population that swam the furthest on the motility plate), and this motile cell used to seed the next generation of the life cycle. In comparison to the mat formation screen, this motility screen allows for the evolved populations to contain

motile individuals at a low frequency (as many cells are inoculated into the SSA plate and allowed to swim).

3.2.2.1 Testing the efficiency of motility plates

Before use in the LCE, a number of experiments were carried out to test the efficiency of the newly designed motility plates (0.25% agar & 1% KB) in assessment of swimming motility. I first observed that they were highly effective at distinguishing between a classic SM and WS type – SBW25 displaying a motility distance of ~22 mm & LSWS (*wspF* mutant) ~7 mm. While flagella mutants (*fleQ* & *fliA* mutant) were unable to swim through the agar, with a motility distance of less than 1 mm. Based on these measurements, the minimal threshold was initially set at 10 mm, to ensure selection for true motile types with a reasonable capacity for dispersal by swimming motility. The longer incubation period of 30 hours was also used, as this allowed for the strongest distinction between the SM & WS type (without the plates becoming overgrown).

Furthermore, I tested the capacity of the new motility plates to purify for low frequency motile individuals in a mixed population. For this experiment I inoculated replicate KB microcosms with a single colony of diverse WS genotypes (LSWS & WS pathways 1-16; from Lind et al., 2015 & McDonald et al., 2009) or the ancestral SBW25, and incubated the cultures under static conditions for 6 days to allow for the evolution of motile types (resembling the dispersal phase of the LCE; see [Section 3.3.2](#)). Each evolved culture was then inoculated into four replicate SSA plates (as previously described), as well as diluted and spread onto an agar plate to examine the initial distribution of colony phenotypes. The SSA plates were incubated for 30 hours, then the swimming motility distance was measured (diameter of migration), and streaks made from the edge of migration to a new agar plate to examine the final distribution of phenotypes. This experiment aimed to compare the initial phenotypes present in the evolved culture (seeded by a diverse genotype), against the final phenotypes of individual cells that had migrated through the agar of the motility plate. The results are provided in *Table 3.1* below.

Strain	MPB	Genotype	Motility (mm)	Motile?	SM phenotype (%)		Effective
					Initial	Final	
SBW25	14218	Wild-type	21.63	Yes	20.34	99.25	Yes
LSWS	13887	<i>wspF</i>	22.38	Yes	9.09	99.75	Yes
WS-1	15442	<i>pflu4308-4313</i>	25.75	Yes	32.50	96.25	Yes

WS-2	15443	<i>pflu0956</i>	31.75	Yes	33.82	100.00	Yes
WS-3	15444	<i>pflu1349</i>	25.13	Yes	5.33	57.50	Semi
WS-4	15445	<i>pflu3448</i>	14.00	No	0.00	0.00	-
WS-5	15446	<i>pflu5960</i>	25.25	Yes	24.62	0.00	No
WS-6	15447	<i>pflu0085</i>	10.38	No	0.00	28.75	-
WS-7	15448	<i>pflu4305-4306</i>	18.63	Yes	1.68	55.00	Semi
WS-8	15449	<i>pflu3571</i>	17.63	Yes	0.00	100.00	Yes
WS-9	15450	<i>pflu5698</i>	19.38	Yes	0.00	90.00	Yes
WS-10	15451	<i>dipA-pflu0621</i>	17.50	Yes	0.46	99.50	Yes
WS-11	15452	<i>dipA-amrZ</i>	14.50	No	0.38	99.75	Yes
WS-12	15453	<i>pflu4414-fleQ-amrZ</i>	0.00	No	0.00	10.00	-
WS-13	15454	<i>pflu0184-0183</i>	22.25	Yes	18.93	97.75	Yes
WS-14	15455	<i>wspF</i>	21.88	Yes	2.06	68.75	Semi
WS-15	15456	<i>awsX</i>	24.63	Yes	93.75	100.00	Yes
WS-16	15457	<i>mwsR</i>	15.38	Yes	0.00	28.75	Semi

Table 3.1. New motility plates successfully purify for the SM phenotype from evolved populations. The diverse genotypes of SBW25, LSWS, & WS pathways 1-16 (Lind et al., 2015; McDonald et al., 2009) were evolved for 6 days in the static KB microcosm, then inoculated into four replicate SSA plates (0.25% agar & 1% KB), as well as diluted & spread onto an agar plate (for initial distribution of phenotypes). Motility distance was measured after 30 hours, and streaks made from the edge of motility plate migration to an agar plate (final distribution of phenotypes). Provided for each strain: MPB number, Genotype (genes with mutation), Motility distance (mean migration diameter in mm), Motile (whether motility is greater than the 15 mm threshold), SM phenotype (percentage of colonies with the smooth phenotype on agar plates) of the Initial & Final samples, and Effective (whether the motility plate successfully purified for the SM phenotype).

I found that for the majority of evolved genotypes with a motility distance over the 15 mm threshold (including SBW25, LSWS, WS- 1, 2, 8, 9, 10, 13, & 15), that the motility plates were successful in selecting for individuals with the SM colony phenotype from a mixed population. Actually in many cases the SSA plates were highly efficient, achieving a final percentage of SM cells greater than 90%, from an initial percentage as low as 1% for the evolved culture (see strains WS- 8 & 10 in *Table 3.1* above). There were some genotypes in which this was less effective (WS- 3, 5, 7, 14, 16); though this may be explained by the swimming motility capacity not necessarily corresponding with the SM phenotype on agar plates. For example the genotype WS-5 (*pflu5960* mutant) displays the semi-wrinkled colony morphology, but achieves a motility distance greater than 15 mm, so is considered motile. The evolved genotypes with a motility distance less than 15 mm (including WS- 4, 6, 11, &

12) were far less effective in purification for the SM phenotype, which was to be expected and corresponds with the classification of these genotypes as non-motile (and setting of the final motility threshold at 15 mm).

3.3 Revised experimental regime

The new life cycle experiment was adapted from the cheat-embracing regime of Hammerschmidt et al. (2014). Although instead of screening using SM and WS colony morphology on agar plates, I used the new selective methods based on the individual trait of swimming motility and collective trait of mat formation; as detailed in the previous *Section 3.2*. The new LCE involves a simple two-phase life cycle that resembles that observed in the natural environment (see *Section 3.1.3*). Each life cycle generation required two weeks, and transitioned between the collective mat-forming phase (Phase I; *yellow*) and dispersal motile phase (Phase II; *blue*) – the experimental regime summarised in *Figure 3.3* below. The new regime was developed in collaboration with postdoctoral researcher Daniel Rexin from the MPI Plön. Further detail is also provided in the methods *Section 5.8*.

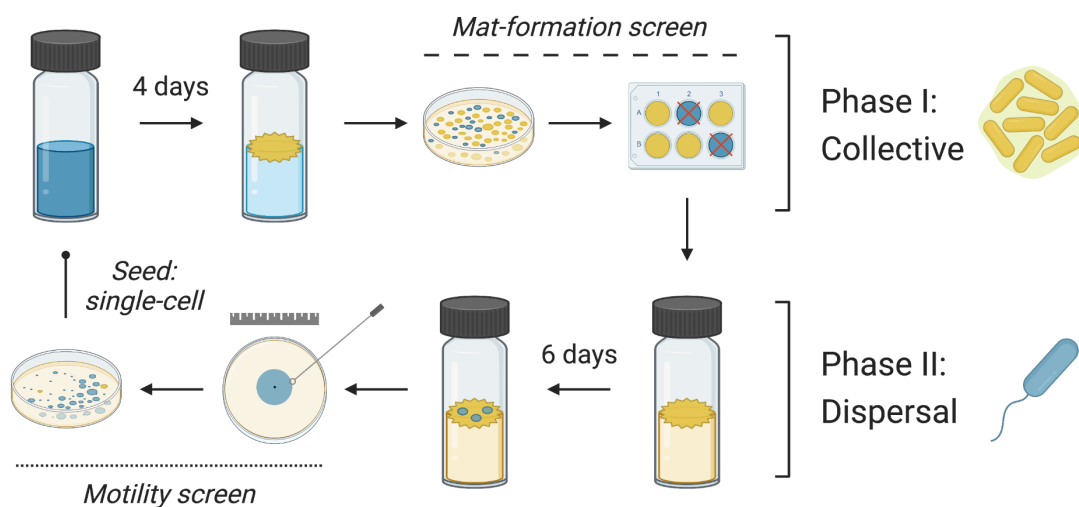


Figure 3.3. Experimental regime for two-phase life cycle with mat-formation and motility screening.

3.3.1 Phase I: Collective

To begin the experiment, replicate racks (or metapopulations) each containing 8 replicate lines were initially inoculated with the ancestral SBW25 (Rainey & Bailey, 1996). During Phase I (PI), for each replicate lineage a KB microcosm was inoculated with a single-cell motile seed (blue). Microcosms were incubated under static conditions for 4 days; the spatially structured ecology driving selection within each lineage for the evolution mat

forming types (yellow), that are able to colonise the air-liquid interface by production of an adhesive polymer. Mat-formation screening was then applied to obtain for each evolved lineage a single mat-forming individual, to pass on to the next phase of the life cycle. For this screen, each replicate microcosm was resuspended by vortexing, then diluted & spread onto a KBA plate, and plates incubated overnight. Individual colonies were then selected at random (6-12 colonies per lineage), and assessed for mat formation in a 96-well plate format (as detailed in *Section 3.2.1*). The first individual in each replicate lineage able to form a mat (likely to be the mat-forming genotype of highest frequency in the population), was then passed to the next phase of the life cycle. Inter-lineage selection was also enforced: lines that did not pass the mat formation screen (none of the 6-12 selected colonies formed a mat) were marked as extinct, and replaced by another random viable line within their rack. *Figure 3.4* below provides an example of the extinction and replacement of lines in one rack over a single life cycle generation. In the case of an entire rack extinction (all 8 replicates extinct) – eight surviving racks were randomly chosen, and a random viable line from each was used to replace the extinct rack. This allowed for inter-rack competition, where lineages evolved in independent racks were able to compete to take over this rack.

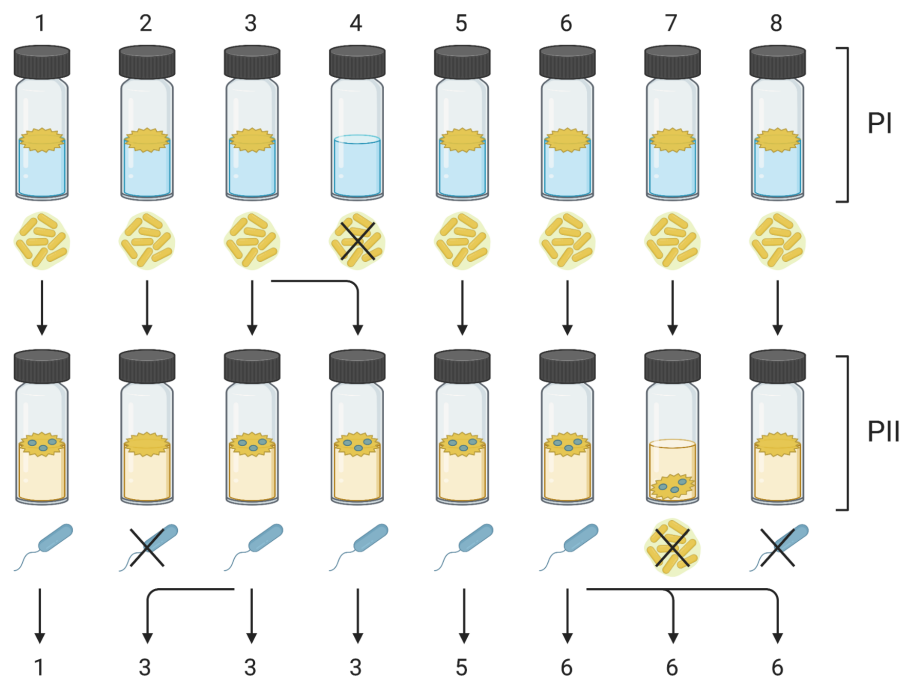


Figure 3.4. Lineage selection within rack during one life cycle generation. This hypothetical example shows the extinction and replacement of replicate lines (1-8) within a rack, over one life cycle generation using the new LCE regime. During PI (Collective) the replicate line 4 goes extinct as it does not produce mat forming types (failing the mat-formation screen), and line 3 is randomly selected as replacement. During PII (Dispersal) the replicate line 7 has a fallen mat and is replaced by line 6; while lines 2 & 8 both do not produce motile

individuals (failing the motility screen) so are replaced by lines 3 and 6 respectively. Over one generation, the extinction of four lineages allowed those surviving to undergo group-level reproduction – the parental lines 3 & 6 were able to leave three offspring lineages each, while lines 1 & 5 only left a single offspring each.

3.3.2 Phase II: Dispersal

During Phase II (PII), for each lineage a fresh KB microcosm was inoculated with the random mat-forming individual (from the respective well of the mat formation screen), and incubated under static conditions for 6 days. The longer growth phase selects for maintenance of the collective mat, as well as the production of non-mat forming types (no adhesive polymer produced) within the collective, that have the capacity to disperse by swimming motility. Motility screening was then carried out, by inoculating each evolved lineage directly into a motility plate (0.25% agar & 1% KB), with the population of cells given 30 hours to migrate through the semi-solid agar (as detailed in [Section 3.2.2](#)). The motility distance (diameter of migration) was then measured; lineages that did not reach the specified motility threshold of 10-15 mm were marked as extinct, as well as those that did not have an intact collective mat after 6 days. Motile individual cells were then obtained from the evolved population by streaking from the edge of migration on the motility plate to a new KBA plate, and these plates incubated overnight – this step selecting for the fastest swimming individual in the population, not necessarily the most common in the population. For each replicate lineage a random motile individual colony was chosen from the streak plate to seed the next life cycle generation; extinct lines were also replaced using the same method described for PI (refer to [Section 3.3.1](#)). The same colony was also inoculated into an overnight shaken culture, this then used for the storage of a freezer stock to keep a record of each line at the end of each life cycle generation.

3.4 Trial experiment using the new regime

As a final test of the new LCE regime & selective methods, I carried out a small-scale trial experiment. This was composed of four replicate metapopulation racks (A, B, C & D; with 8 replicates each – total of 32 lines), initially inoculated with the ancestral SBW25 (MPB14218). Each lineage was taken through five life cycle generations, and freezer stocks stored at the end of cycle 5 (MPB19884-19915). For this pilot experiment I applied a more lenient selective regime – for the mat-formation screen 12 colonies were examined per replicate line, and for the motility screen the threshold of 10 mm was used. Additionally, I made a record of various phenotypic measurements during the experiment. This included the

frequency of colony phenotypes present in evolved lineages during each phase of the life cycle; achieved by screening the morphology of multiple individual colonies on agar plates (classified as SM, semi-SM, WS or semi-WS). The colony phenotype of the single-cell motile seed from the end of each cycle was also recorded (this used to seed the next generation). Furthermore, I documented during the PI mat formation screen the proportion of mat-forming individuals (number of wells containing a mat from 12 random colonies), and during the PII motility screen the motility distance (migration diameter in mm) of each evolved lineage. Additional data from this trial experiment is available in *Supplementary A-7*.

3.4.1 Genealogy over five generations

Using the records of extinction & replacement of evolved lineages, I reconstructed the genealogical tree of the trial experiment (Doulcier, 2019); this is displayed in *Figure 3.5* below, with the coalescence of final lines highlighted (PI in *yellow* & PII in *blue*). From this genealogy, each final line from the end of cycle 5 may be traced back to the respective parental lineage from the start of the experiment, for example replicate lines 1-8 in rack D all originate from line D5. *Figure 3.5* also illustrates the decrease in extinction rate over five generations (note: decline in number of extinct end nodes, with more nodes connected by parallel opaque lines & fewer transparent lines).

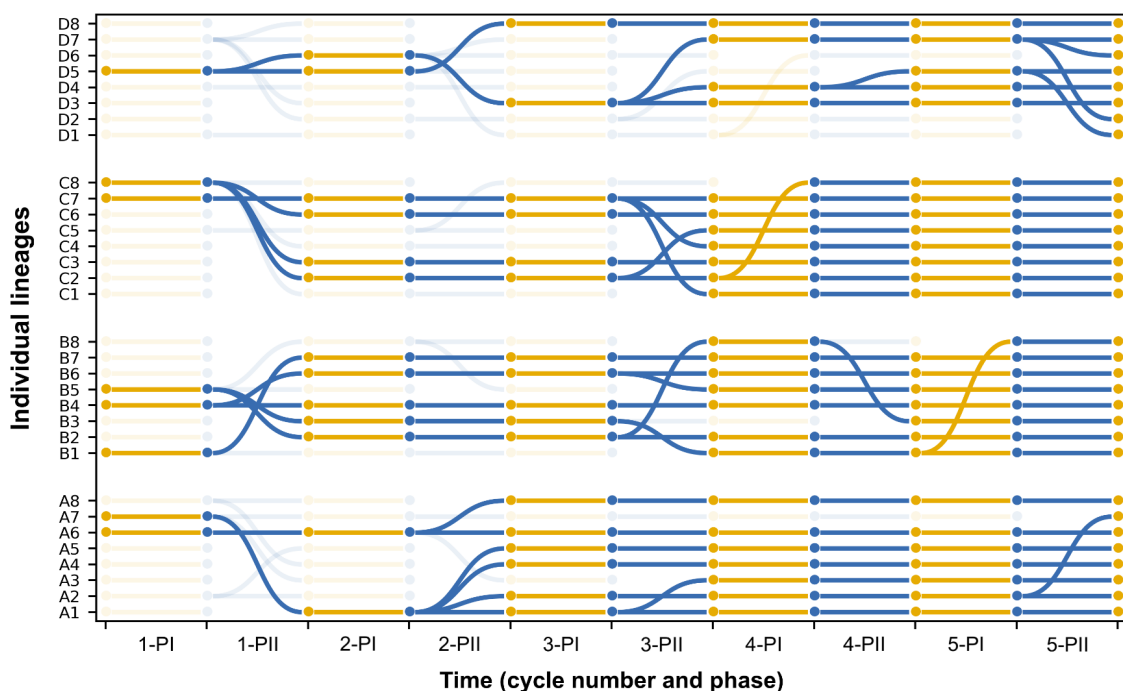


Figure 3.5. Genealogical tree of trial experiment with new LCE regime. Each row displays the genealogy of an individual lineage from the LCE trial (grouped in racks A, B, C & D, with replicates 1-8 each), over time for five life cycle generations (and phases PI & PII). The circle nodes represent a single lineage in time, and the

connections between each node show the history of extinction & replacement during the life cycle phases – an extinction event is illustrated by an end node having no connections, and a group-level reproduction event by a single node having multiple branching connections. For example, during cycle 1-PII the line D6 goes extinct and is replaced by line D5. The colour shows the phases PI: Collective (●) & PII: Dispersal (●), as well as demonstrating the coalescence of final lines – opaque nodes & connections highlight lineages that survived until the end of cycle 5 (and all parental lines), while transparent nodes & connections show extinct lineages. Figure made using Colgen (Doulcier, 2019).

3.4.2 Extinction rate & seed phenotype

During the LCE trial, I observed a rapid decrease in extinction rate over five generations, as shown in *Figure 3.6 (left)* below. This was most evident for the PI dispersal phase, in which the extinction rate dropped from 56.25% during cycle 1, to 12.5% in cycle 5. In general, there was a relatively low number of extinctions observed – only a small number of lines extinct during PI as a result of the mat-formation screen (only in the later cycles), and a few in PII due to the falling of mats (mostly in the early cycles); the majority of extinctions resulted from failing the motility screen, but this decreased over time as the experiment progressed. This result indicates that lineages were easily able to pass the mat formation screening, and quickly adapted to increase swimming motility for the motility screen; perhaps the selective regime was not strict enough, particularly for the collective phase.

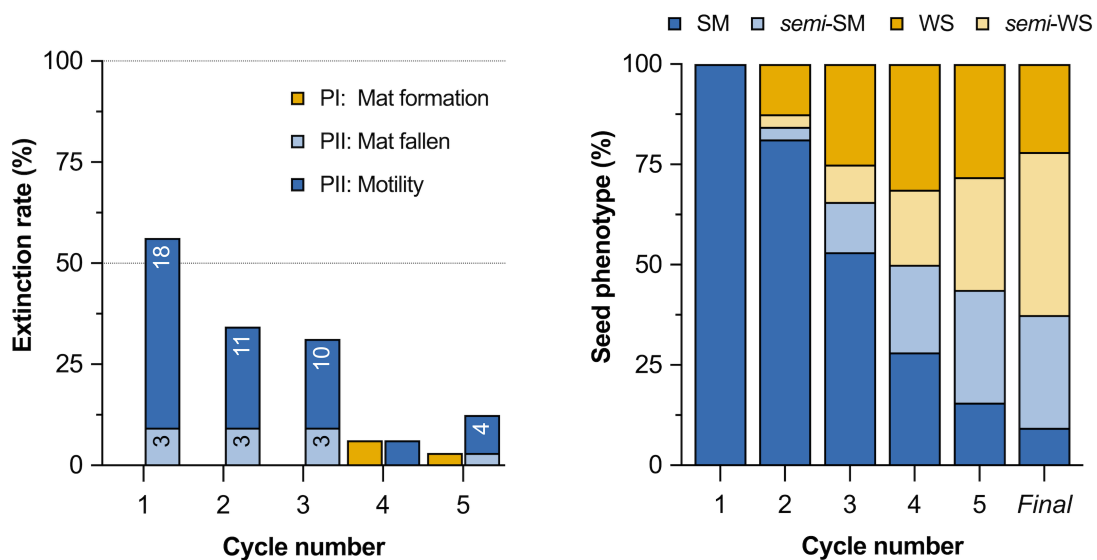


Figure 3.6. Extinction rate & seed colony phenotype over five generations. Data is shown for the 32 replicate lines of the LCE trial, across life cycle numbers 1-5; summarised with a bar graph (made in Prism 9). Left: Extinction rate (percentage of lines; number provided within bar), lines extinct as a result of – mat formation during PI (failure in mat-formation screen), mat fallen during PII, or motility during PII (failure in motility screen). Right: Seed phenotype (percentage of lines with each colony phenotype), with colony

morphology assessed on agar plates (SM, semi-SM, WS, & semi-WS) of the single-cell seed used to inoculate each line at the start of PI each cycle, as well as of final surviving lines at the end of cycle 5.

The colony phenotype of the single-cell motile seeds, used to inoculate each replicate line over the five life cycle generations, are summarised in *Figure 3.6 (right)* above. I observed a clear shift in the colony morphology of seeds – from the SM phenotype dominating in cycles 1 & 2, to the observation of diverse phenotypes in the later cycles, including WS, and the intermediate semi-SM & semi-WS phenotypes. At the start of the experiment, for cycle 1 each replicate lineage was inoculated with ancestral SBW25, which displays the SM phenotype. During cycle 2 & 3, the seed phenotype for the majority of lines displayed the SM colony morphology (81.3% & 53.1%, respectively). By cycle 3, a constant proportion of ~20-30% of lines displayed the WS phenotype; and over time an increasing proportion with the intermediate semi-SM or semi-WS phenotype (up to >25% each). For the final surviving lines at the end of cycle 5, I observed that very few displayed the classic SM phenotype on agar plates. This result demonstrates that for the new LCE regime, colony morphology on agar plates does not at all reflect the swimming motility capacity of evolved lineages. The considerable increase of evolved lines with an intermediate seed phenotype also further highlights the difficulty in screening based on colony morphology – it is near impossible to distinguish colonies using the strict categories of wrinkly & smooth.

3.4.3 Phase I – phenotypic analysis

For Phase I (Collective) of the experiment, I observed improvement to the collective trait of mat formation over five generations, as shown in *Figure 3.7 (left)* below. During the first cycle, in the mat formation screen there was a wide distribution in the percentage of colonies able to form a mat for evolved lineages, with a median of 33.3% (4 of the 12 random individuals). This distribution shifted initially in both directions – in cycle 3 some lines had a majority of mat-forming colonies (up to 100%), but most lines had a minority (<40%), with few having an intermediate proportion. By cycle 5, most evolved lineages had a high percentage of mat-forming colonies, and a median of 100% was observed; though some lines remained that had a lesser proportion of mat-forming individuals, these likely still proceeded through the life cycle using mutation. I also found that the improvement to mat formation in evolved lineages corresponded with a decrease in variation of colony phenotype, as displayed in *Figure 3.7 (right)*. During cycle 1, all replicate lines had variation in colony morphology on agar plates, with the median of 69.9% of individuals with the WS phenotype (within each

evolved lineage) – this corresponds with the rapid diversification of the ancestral SBW25 in the static broth environment. As the experiment progressed, more evolved lineages displayed a single colony phenotype (e.g. 100% of colonies with WS phenotype, or other); this decrease in phenotypic variation implies a lack of genetic diversity, and perhaps that lineages had fixed a single mutant type that was capable of developmental regulation of the life cycle (therefore no further mutation required to transition between the collective & dispersal phases). This result also highlights that the improvement to mat formation in evolved lineages does not necessarily require the WS colony morphology; by cycle 5, a number of replicates had fixed a non-WS phenotype, with the median of 68% of colonies with the WS phenotype observed (and mean of 54%). Therefore mat formation capacity does not always correspond with display of the WS colony morphology on agar plates.

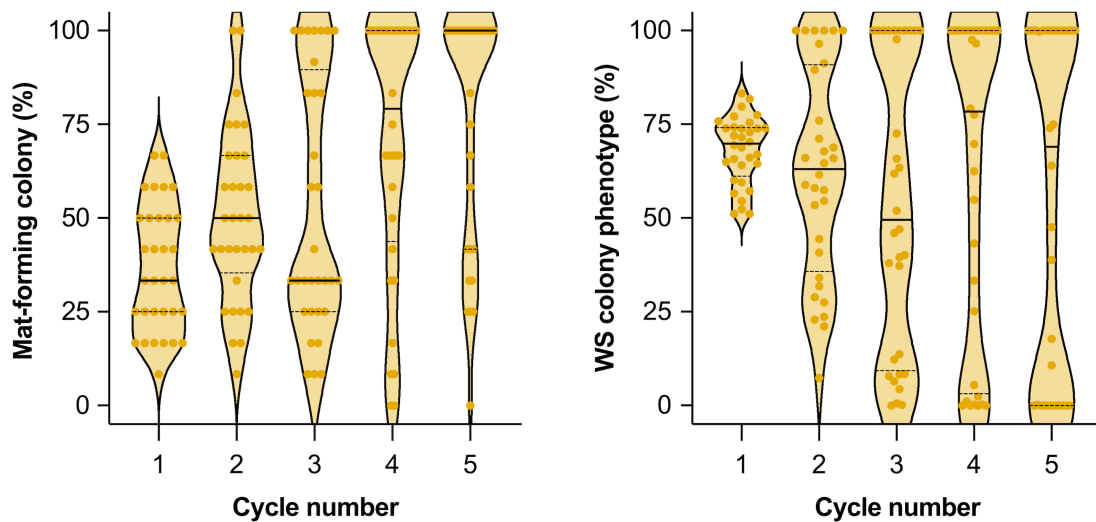


Figure 3.7. Improvement to mat formation does not correspond with the WS phenotype. Phenotypic data from Phase I (Collective) is shown for the 32 replicate lines of the LCE trial, across life cycle numbers 1-5. Left: Mat-forming colony (percentage of colonies that form a mat, of the 12 random colonies selected for each line), during the mat-formation screen. Right: WS colony phenotype (percentage of colonies that display the WS morphology), of the 4 day evolved cultures (PI) plated on agar plates. These data are displayed in a violin plot (medium smoothing), including the median (solid line), quartiles (dotted line), and individual data points.

3.4.4 Phase II – phenotypic analysis

In Phase II (Dispersal), I also observed some improvement to the individual trait of swimming motility, evident in *Figure 3.8 (left)* below. During cycle 1, a large proportion of evolved lineages displayed a short motility distance, with a median of only 10.3 mm (and a mean of 12.3 mm). The lines that went extinct (motility distance less than 10 mm), likely obtained a mutation in the previous phase that locked them in the mat-forming state, and

prevented the production of motile types (e.g. disruption of flagella-associated gene). By cycle 5 the motility of evolved lineages showed some level of improvement, with a median of 15.8 mm observed (mean of 14.5 mm); though a number of lines still performed poorly in the motility screen, and only just passed the threshold of 10 mm. The increase in motility distance did not correlate at all with a larger proportion of individuals having the SM colony phenotype (within each evolved lineage); as shown in *Figure 3.8 (right)* below. In fact very few SM colonies were detected when plating the 6 day evolved PII cultures, with a median of 0% observed for all cycles (mean of 13.6% in cycle 1 & 8.9% in cycle 5). As I showed in the previous *Section 3.4.2*, during the early cycles of the experiment, the single-cell seed for the majority of lines displayed the SM colony morphology (refer to *Figure 3.6 (left)*). This result therefore further demonstrates the ability of the new motility plates to purify for low frequency SM types in a mixed evolved population. While evolved lineages had substantial improvement to mat formation, swimming motility was only marginally improved, with distances achieved far lower than the ancestral SBW25 capacity (~22 mm); this indicates that the use of a stricter motility threshold may be required.

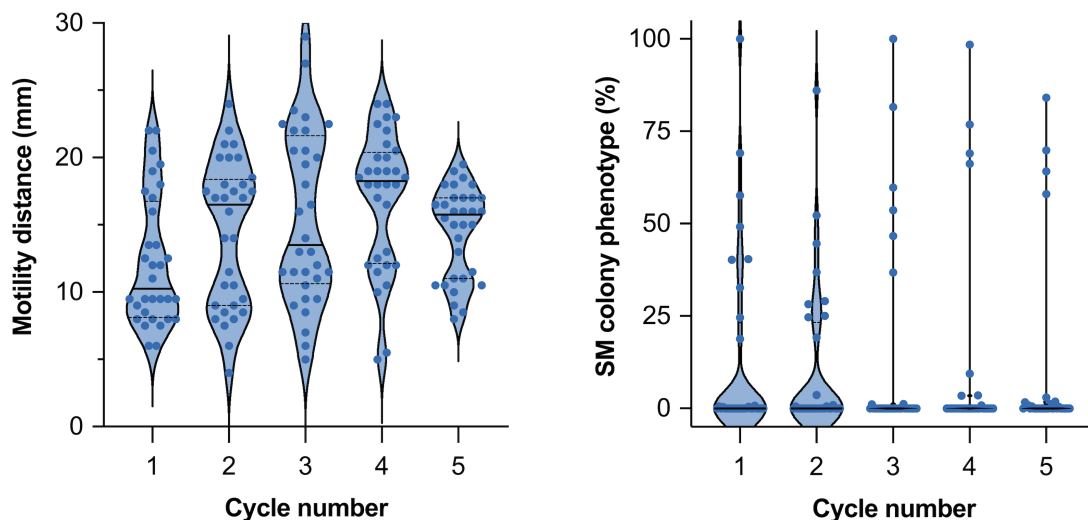


Figure 3.8. Minor improvements to swimming motility and SM phenotypes at low frequency. Phenotypic data from Phase II (Dispersal) is shown for the 32 replicate lines of the LCE trial, across life cycle numbers 1-5. Left: Motility distance (migration diameter in mm, of each evolved population), during the motility screen. Right: SM colony phenotype (percentage of colonies that display the SM morphology), of the 6 day evolved cultures (PII) plated on agar plates. Data displayed as described in [Figure 3.7](#) legend.

3.5 Strategies to transition through the life cycle

After only five generations, evolved lineages showed rapid adaptation to the new LCE regime – for the final surviving lines 87.5% (28 of 32 lines) were both able to form a mat in static

broth, and reach a motility distance of greater than 10 mm. This outcome suggests that these lineages had evolved a means of regulating the life cycle, having obtained some mutation that enabled individuals to readily transition between the mat forming & motile phenotypic states. Sequencing was required to identify the causal mutations that improve these traits, and also to reveal whether developmental regulation had evolved – a mechanism to transition through the life cycle that does not require further mutational change. I carried out whole-genome sequencing of all 32 replicate lineages, from the end of cycle 5 of the LCE trial; the raw sequencing files are available in *Supplementary A-8*. Mutations were then identified using Breseq (Deatherage, & Barrick, 2014), as compared to the SBW25 reference genome; summary of the Breseq output is provided in *Supplementary A-9*. From this I was able to identify a number of unique genotypes that represent different strategies that emerged to transition through the life cycle. Based on the phenotype (capacity to form a mat & motility) and number of mutations present in each lineage, I then categorised these genotypes into the two strategy types – mutational (unable to form mat, with many mutations) and non-mutational (mat-forming & motile, with few mutations). The genealogy of the unique non-mutational strategies & the mutational strategy are displayed in *Figure 3.9* below.

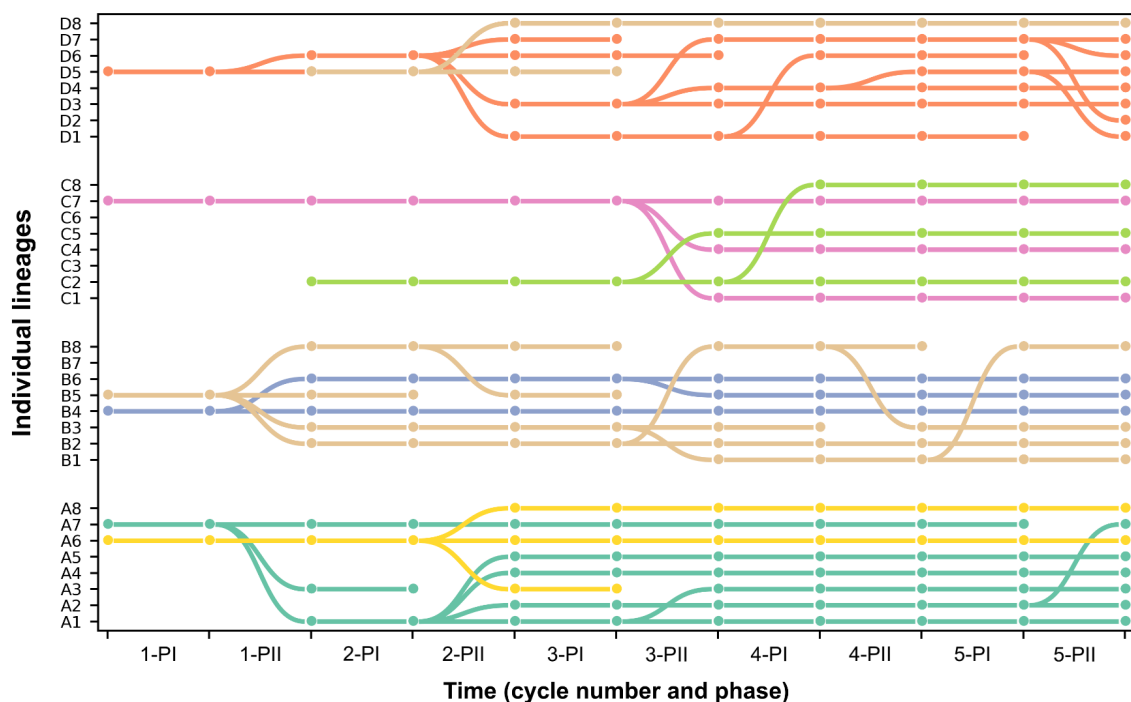


Figure 3.9. Genealogical tree showing unique genotypes & strategies identified in the LCE trial. The parental origin lineage and descendants are given for the genotypes using the mutational strategy (●); and the unique non-mutational strategies: *mwsR* (●), *wspR* (●), *awsR* (●), *pflu0085-bifA* (●), *awsR-pflu0084-pflu0085* (●) & *awsR-wspF-wspA* (●). Genealogy as described in [Figure 3.5](#) legend.

3.5.1 Mutational strategy

The evolved lineages using a mutational strategy to switch between phases of the life cycle contained a lot of coding sequence variation (more than 5 mutations); this corresponds to the transition through each phase by mutation, as observed in the previous experiment of Hammerschmidt et al. (2014). I found that lineages in both rack B and D were using a mutational strategy (●) – see genealogy in previous *Figure 3.9*. The evolved lines B1 (MPB19892) & D8 (MPB19915) were chosen as representative examples of this strategy; the mutations present in these lines are detailed in *Table 3.2* below. Line B1 may be traced back to the parental lineage B5 (from cycle 1), and contains a total of 10 mutations in coding regions; each mutation likely allowed for one phenotypic transition over the five life cycle generations (one mutation required per phase). The majority of these mutations are located within genes previously identified as related to the WS phenotype – the *wsp* operon, *awsR*, *awsX*, *mwsR* & *bifA* (McDonald et al., 2009; Lind et al., 2015), including large deletions within *wspF*, *wspCDE* & *awsX* (refer to *Table 3.2*). This implies that line B1 transitioned through the life cycle by disruptive mutation, each corresponding to the constitutive activation of cellulose overproduction & mat formation (PI), or inactivation for flagella expression & motility (PII). The mutational strategy results in a relatively high extinction rate (see *Figure 3.9*; parental lineage B5 with many extinct nodes), and therefore an associated low lineage fitness – defined as the capacity of a lineage to leave offspring (requires collective-level reproduction and the persistence of offspring lineages).

Parent lineage	Total lines	Gene name	PFLU	Putative product	Nucleotide change	Amino acid change	Protein domain	E-value
B5	4	<i>wspF</i>	1224	chemotaxis-related methyltransferase	150_164del	L51_I55del	REC	1.2e-16
D5	8				352_939del	P118_A313del	CheB	6.5e-55
c4-B1	2	<i>wspCDE</i>	1221-1223	chemotaxis-related methyltransferase	1044[wspC] _827[wspE] del	Q348[wspC] _Q276[wspE] del	-	-
		<i>awsX</i>	5211	membrane protein	223_255del	T75_T85del	YfiR-like	1.4e-32
		<i>mwsR</i>	5329	sensory box protein, GGDEF/EAL domain	2183T>C	V728A	PAS	2.5e-16
					2774G>A	R925H	GGDEF	4.7e-50
		<i>bifA</i>	4858	signaling protein	1661T>A	L554Q	EAL	2.7e-76
					1966G>A	G656S		
<i>pflu5079</i>	5079	integrase	36_39del	S12fs	-	-		
<i>rpsA</i>	1649	30S ribosomal protein	1255A>G	T419A	S1	5.3e-18		

c3-D8	1	<i>awsR</i>	5210	signaling-related membrane protein	875A>G	D292G	GGDEF	1.0e-46
					160C>G	R54G	CHASE8	1.3e-28
		<i>mutY</i>	0323	A/G-specific adenine glycosylase	444T>G	F148L	HhH-GPD	2.4e-19
		<i>wspR</i>	1225	two component system response regulator	746G>T	G249V	GGDEF	4.1e-49
		<i>dipA</i>	0458	hypothetical protein	1825G>A	A609T	GGDEF	1.0e-38
					2309C>A	A770D	EAL	2.6e-73
<i>pflu3936</i>	3936	transporter-like membrane protein	2087G>A	S696N	ACR_tran	0.0		

Table 3.2. Mutational strategy genotypes contain numerous disruptive mutations. The coding sequence variation is given for evolved lines B1 (MPB19892) & D8 (MPB19915) from the LCE trial, that require mutation to transition through the life cycle. Provided for each mutation: Parent lineage (origin from cycle 1, unless stated otherwise; colour corresponding to genotype or strategy), Total lines (number of offspring lines containing the mutation at end of cycle 5), Gene name, PFLU (link to *Pseudomonas* Genome DB entry), Putative protein product, Nucleotide sequence change, Amino acid sequence change, Protein domain the mutation is located within (link to InterPro entry), and *E*-value (Pfam database search).

While the mutational strategy line D8 diverged from the parental lineage D5 during cycle 1 (see [Figure 3.9](#)), first obtaining a deletion in the *wspF* gene. Interestingly, the first mutation obtained by both line B1 & D5 was a deletion in *wspF*; this likely caused loss of WspF methylesterase activity, and constitutive activation of the Wsp pathway (Bantinaki et al., 2007), though it is unclear whether this contributed to the persistence of these lineages. Line D8 then obtained mutations in the genes *wspR*, *awsR*, *dipA*, *pflu3936* & *mutY* (refer to [Table 3.2](#)); disruption to the *wspR* DGC likely prevented further use of the Wsp pathway to transition through the life cycle. *mutY* ([pflu0323](#)) encodes the A/G-specific adenine glycosylase, and functions in the correction of G-A mismatches (to G-C) during DNA replication (Au et al., 1989). For line D8, the *mutY* mutation and disruption to the DNA mismatch repair system may have resulted in an elevation of mutation rate. Although D8 contains a total of only 7 mutations, so I am uncertain whether or not it is a hypermutator; a fluctuation assay would provide insight.

3.5.2 Non-mutational strategies

For the non-mutational strategy, evolved lineages had few mutations (less than 4), also demonstrating the capacity to both form a mat in static broth (within 24 hours) and reach a swimming motility distance of greater than 10 mm. This implies that these lines may have evolved a mechanism for developmental regulation of the life cycle – an ability to transition

through the phenotypic states without dependence on further mutation. I identified a number of unique genotypes using the non-mutational strategy, including single mutants of *mwsR*, *wspR* & *awsR*; the double mutant *pflu0085-bifA*, and triple mutants *awsR-wspF-wspA* & *awsR-pflu0084-pflu0085*. The evolved lines A4 (MPB19887; *mwsR*), A8 (MPB19891; *wspR*), B6 (MPB19897; *awsR*), C2 (MPB19901; *pflu0085-bifA*), C7 (MPB19906; *awsR-pflu0084-pflu0085*) & D1 (MPB19908; *awsR-wspF-wspA*) were selected as representative for each genotype. The mutations present in these select lines are shown in *Table 3.3* below.

Parent lineage	Total lines	Gene name	PFLU	Putative product	Nucleotide change	Amino acid change	Protein domain	E-value
A7	6	<i>mwsR</i>	5329	sensory box protein, GGDEF/EAL domain	3190T>A	W1064R	EAL	1.0e-76
c3-A4	1	<i>pflu1654</i>	1654	hypothetical protein	290C>A	T97N	Glyco_trans	2.2e-5
A6	2	<i>wspR</i>	1225	two component system response regulator	424C>A	Q142K	-	-
B4	3	<i>pflu3595</i>	3595	hypothetical protein	1405C>T	P469S	-	-
c2-D6	7	<i>awsR</i>	5210	signaling-related membrane protein	118G>T	A40S	CHASE8	1.3e-28
	184G>T				A62S			
	167T>G				I56S			
C7	3	<i>pflu0084</i>	0084	endo/exonuclease/ phosphatase	544C>A	Q182*	Exo_endo phos	3.5e-14
C7	8	<i>pflu0085</i>	0085	hypothetical protein	1337A>C	Q446P	-	
c2-C2	3				1846C>T	L616F	GGDEF	1.3e-45
		<i>bifA</i>	4858	signaling protein	910G>A	G304S	GGDEF	7.2e-36
D5	8	<i>wspF</i>	1224	chemotaxis-related methyl-esterase	352_939del	P118_A313 del	CheB	6.5e-55
c2-D6	7	<i>wspA</i>	1219	methyl-accepting chemotaxis protein	1318G>A	G440R	MCPsignal	5.0e-34

Table 3.3. Non-mutational strategy genotypes contain few specific mutations. The coding sequence variation is given for evolved lines A4 (MPB19887), A8 (MPB19891), B6 (MPB19897), C2 (MPB19901), C7 (MPB19906) & D1 (MPB19908), that use a non-mutational strategy to transition through the life cycle. Mutation details as described in *Table 3.2* legend.

3.5.2.1 Generalist strategy

I further categorised the non-mutational strategies based on their swimming motility phenotype – generalist (short motility distance, substantially less than the SBW25 ancestor) & developmental (motility distance comparable to SBW25). The generalist evolved lineages

may have found a way to transition through the life cycle by obtaining a mutation that allowed them to just pass the mat formation & motility screens, but with a relatively mediocre performance in both traits (e.g. forming unstable mats & swimming at a slow pace). A strategy comparable to generalism was observed for two genotypes in rack A – the *mwsR* mutant (●), *wspR* mutant (●); with a mean motility distance of 13.5 mm & 15.8 mm, respectively (compared to 22.8 mm in SBW25). Although these genotypes displayed poor performance in swimming motility, they still managed to fix within rack A, and had a relatively low rate of extinction (see [Figure 3.9](#)).

mwsR ([pflu5329](#)) encodes the dual-domain GGDEF/EAL protein MwsR, that functions as both a DGC & PDE enzyme in the synthesis & degradation of c-di-GMP (Phippen et al., 2014; McDonald et al., 2009); as discussed previously in [Section 1.3.2.3](#). The parental lineage A7 must have obtained the *mwsR* mutation during the first cycle of the experiment; the substitution W1064R in the EAL domain of MwsR likely caused a reduction in PDE function, and a low level of activation of DGC enzymatic activity. The synthesis of c-di-GMP by the semi-active MwsR DGC could then have resulted in activation of cellulose production – enough to allow the formation of a mat, whilst still maintaining a reduced capacity for swimming (McDonald et al., 2009). While *wspR* ([pflu1225](#)) encodes the GGDEF response regulator protein WspR, that functions as a DGC enzyme in the production of c-di-GMP (Goymer et al., 2006); refer to previous [Section 1.3.2.1](#). During cycle 1, the *wspR* mutation was acquired by the parental lineage A6, resulting in the substitution Q142K in the WspR DGC. The *wspR* mutant genotype displays the WS colony phenotype, so must produce a functional WspR protein, as disruptive mutations in *wspR* have been previously observed to suppress the WS phenotype (Spiers et al., 2002; Güvener & Harwood, 2007). This *wspR* mutation must have therefore activated the DGC enzyme, causing an increase in c-di-GMP level & overproduction of cellulose (Malone et al., 2007). Although this is not the common mutational route for activation of the WspR DGC, predominantly occurring by loss-of-function mutation to the WspF negative regulator (McDonald et al., 2009); this implies that this mutation may have a more specific effect on WspR function.

3.5.2.2 Developmental strategy

In the remaining replicate racks, I observed a number of unique genotypes with the capacity to transition through the life cycle by apparent developmental regulation; these include the mutant genotypes *awsR*, *awsR-wspF-wspA*, *pflu0085-pflu0084-awsR* & *pflu0085-bifA*. These

evolved lineages were all able to form a mat in static broth, and had a motility distance comparable to the ancestral SBW25. *awsR* ([pflu5210](#)) encodes the signalling protein AwsR, predicted to function as a DGC enzyme (McDonald et al., 2009; Malone et al., 2010); as discussed in [Section 1.3.2.2](#). In rack B during cycle 1, the parental lineage B4 obtained the substitution A40S in the CHASE8 periplasmic sensor domain of AwsR. Strikingly, the evolved mutants *awsR*, *awsR-wspF-wspA* & *pflu0085-pflu0084-awsR* all contain independent mutations in nearby residues of AwsR – A40S, A62S & I56S, respectively. Rather than constitutive activation of the AwsR DGC by disruption to the AwsX negative regulator, the specific alteration to the sensory domain of AwsR may allow for regulation of DGC activity in response to some environmental stimulus (McDonald et al., 2009; Lind et al., 2017). For the *awsR* (●) genotype in rack B, this mutation conferred developmental regulation of the life cycle; additionally no extinctions were observed in offspring lineages (see [Figure 3.9](#)), indicating a high lineage-level fitness.

For the *awsR-wspF-wspA* mutant genotype, in rack D the parental lineage D5 first acquired a large deletion in the *wspF* gene (p.P118_A313del). *wspF* ([pflu1224](#)) encodes the methylesterase protein WspF, that acts as a negative regulator of the WspR DGC (Bantinaki et al., 2007); as detailed previously in [Section 1.3.2.1](#) & [2.3.4.1](#). Therefore this deletion in the WspF methylesterase most likely caused activation of the WspR DGC, and an increase in c-di-GMP production & mat formation (Goymer et al., 2006). Then during cycle 2, the parental lineage D6 obtained a mutation in *wspA* ([pflu1219](#)), that encodes the membrane-bound methyl-accepting chemotaxis protein WspA; this receptor protein was discussed in extensive detail in [Section 2.3.1](#). The substitution G440R was located within the MCP signalling domain of WspA; remarkably, mutation of the neighbouring residue (V441G) was shown to be responsible for the environmentally-responsive phenotype of TSS-f6 (Summers, 2018). Refer to the revised model for the TSS-f6 phenotype switch in [Section 2.6](#). This specific alteration to the WspA MCP may adjust the sensitivity of the receptor, therefore allowing activation of the Wsp pathway in response to an environmental signal in the static broth (Bantinaki et al., 2007). The *awsR-wspF-wspA* genotype (●) was highly successful in the experiment, and managed to fix within rack D (excluding line D8) (see [Figure 3.9](#)). Although some extinctions occurred in offspring lineages, corresponding to a lower lineage fitness; this may be explained by not all mutations being present during the early cycles, as it is not clear when exactly the *awsR* & *wspA* mutations were obtained.

Within rack C, the two mutant genotypes *pflu0085-pflu0084-awsR* (●) & *pflu0085-bifA* (●) reached fixation, as shown in *Figure 3.9*. Both of these genotypes displayed no further extinction and high lineage fitness; though they were unable to leave more offspring due to competition with other lineages in the rack. During the first cycle, the parental lineage C7 first acquired a mutation in *pflu0085* (p.Q446P). [pflu0085](#) encodes the hypothetical protein Pflu0085, with 52.9% sequence identity to the diguanylate cyclase DgcH in *P. aeruginosa* PAO1 ([PA5487](#); BLASTP *E*-value: 0.0); and contains a GGDEF domain ([PF00990](#); residue: 524-680; *E*-value: 1.3e-45) with an intact motif. Previous studies in *P. aeruginosa* have shown that DgcH functions as a typical DGC enzyme, required for the maintenance of basal levels of intracellular c-di-GMP (Wei et al., 2019). In SBW25, Lind et al. (2015) observed mutations in the same region in Pflu0085 (residues 407-447), predicted to activate the downstream DGC enzyme, resulting in the WS phenotype. Therefore the *pflu0085* mutation likely activated DGC activity, causing an increase in c-di-GMP & mat formation.

Lineage C7 then obtained two additional mutations, including the introduction of a stop codon in the neighbouring gene *pflu0084* (p.Q182*), and a substitution in *awsR* (p.I56S; discussed earlier). [pflu0084](#) encodes the putative endo/exonuclease/phosphatase protein Pflu0084, with 79.2% sequence identity to PA5488 in *P. aeruginosa* PAO1 ([PA5488](#); BLASTP *E*-value: 7e-160). The effect of the *pflu0084* mutation is likely related to the downstream Pflu0085 DGC; though the significance of this combination of mutations in the *pflu0085-pflu0084-awsR* mutant genotype is unclear. While lineage C2, after cycle 2, proceeded to acquire another substitution in *pflu0085* (p.L616F), and a mutation in the *bifA* gene. *bifA* ([pflu4858](#)) encodes signalling protein BifA, predicted to function as a PDE enzyme in the breakdown of c-di-GMP (Kuchma et al., 2007); later discussed in *Section 4.2.5.1*. The substitution G304S in the inactive GGDEF domain of BifA likely resulted in disruption of PDE activity, therefore an increase in c-di-GMP level and cellulose production. For the *pflu0085-bifA* mutant genotype, the effect of the mutation combination is also unclear – recreation of each mutation in the wild-type SBW25 would reveal the contribution of each to developmental regulation of the life cycle.

3.6 Analysis of select evolved lines

I selected a number of evolved lines from the end of cycle 5, to represent the different strategies that lineages had found to transition through the life cycle – mutational lines B1 & D8; generalist lines A4 & A8; and the developmental lines B6, C2, C7 & D1. The genotype

and phenotype of each is summarised in *Table 3.4* below, with the wild-type SBW25 included for comparison.

Line	MPB	Genotype	Mat former	Motility (mm)	Parent lineage	Strategy
SBW25	14218	Wild-type	No	22.8	-	-
A4	19887	<i>mwsR</i> (W1064R) & <i>pflu1654</i> (F120L)	Yes	14.0	A7	Generalist
A8	19891	<i>wspR</i> (Q142K)	Yes	16.5	A6	Generalist
B1	19892	10x mutations	No	20.5	B5	Mutational
B6	19897	<i>awsR</i> (A40S) & <i>pflu3595</i> (P469S)	Yes	18.0	B4	Developmental
C2	19901	<i>pflu0085</i> (Q446P, L616F) & <i>bifA</i> (G304S)	Yes	21.0	C8	Developmental
C7	19906	<i>pflu0085</i> (Q446P), <i>pflu0084</i> (Q182*) & <i>awsR</i> (I56S)	Yes	21.0	C7	Developmental
D1	19908	<i>wspF</i> (P118_A313del), <i>wspA</i> (G440R) & <i>awsR</i> (A62S)	Yes	22.5	D5	Developmental
D8	19915	<i>mutY</i> (F148L) & 6x mutations	Yes	21.5	c3-D8	Mutational

Table 3.4. Genotype & phenotype of selected evolved lines from the LCE trial. Details are given for SBW25, and the following evolved lines from the end of cycle 5 of the LCE trial: A4, A8, B1, B6, C2, C7, D1 & D8. Provided for each: Line name, MPB number, Genotype (genes containing mutation & amino acid change), Mat former (capacity to form a mat in static broth after 24 hours), Motility (migration diameter in mm after 30 hours, of overnight culture inoculated into SSA plate), Parent lineage (origin from cycle 1, unless stated otherwise; colour corresponding to genotype or strategy), and Strategy (predicted strategy to transition through the phases of the life cycle – mutational, generalism or developmental).

3.6.1 Phenotypic characterisation

For the selected evolved lineages, I examined the colony morphology on agar plates incubated at 28°C or room temperature, to investigate if any displayed an environmentally-responsive phenotype. Each genotype was also transformed with the Tn7-Scarlet fluorescent marker (Schlechter et al., 2018) and CdrA-GFP reporter plasmid for c-di-GMP level (Rybtke et al., 2012). The colony morphology and fluorescence at 28°C for the Scarlet-CdrA strains was assessed, as well as mat formation capacity; the results of these phenotypic assays are provided in *Table 3.5* below. I observed that the wild-type SBW25 & line B1 that uses a mutational strategy, were both unable to form a mat in the static broth environment. These strains also displayed the SM colony morphology on agar plates, with an associated low level of c-di-GMP production (no GFP fluorescence with pCdrA reporter).

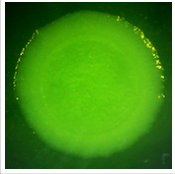
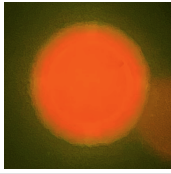
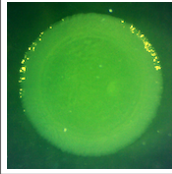
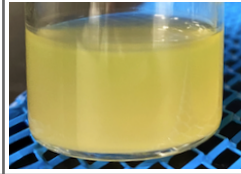
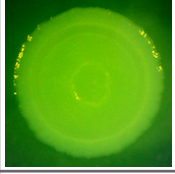
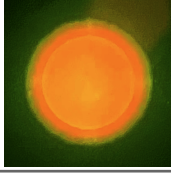
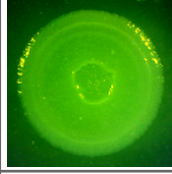

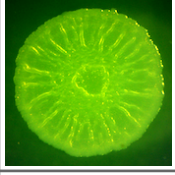
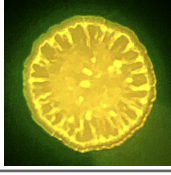
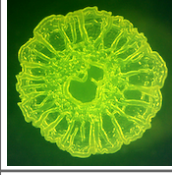
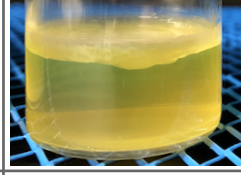
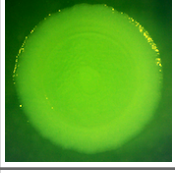
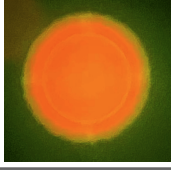
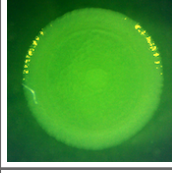
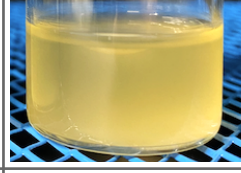
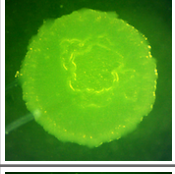
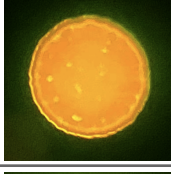
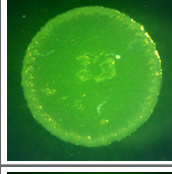
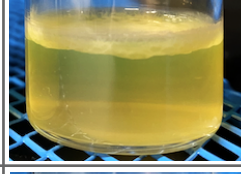
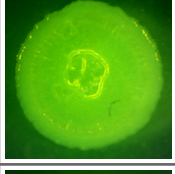
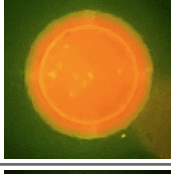
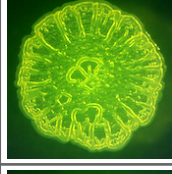
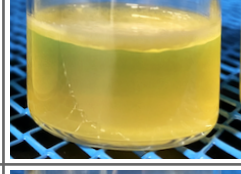
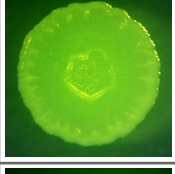
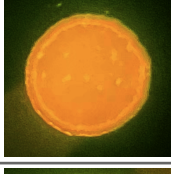
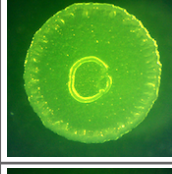
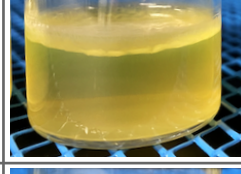
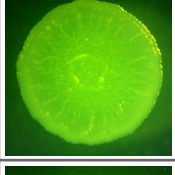
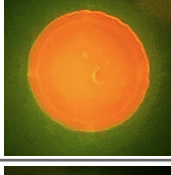
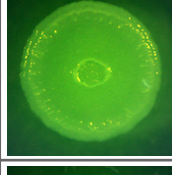

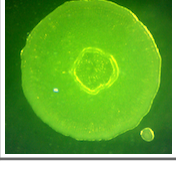
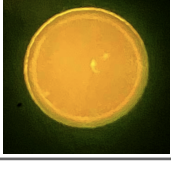
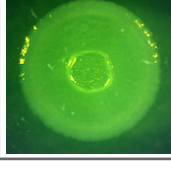

Line	MPB	Genotype	Colony morphology spot			Mat formation
			28°C		Room temp.	
SBW25	14218 17910	WT				
A4	19887 20537	Evolved <i>mwsR</i> * <i>pflu1654</i> *				
A8	19891 20538	Evolved <i>wspR</i> *				
B1	19892 20539	Evolved				
B6	19897 20540	Evolved <i>awsR</i> * <i>pflu3595</i> *				
C2	19901 20541	Evolved <i>pflu0085</i> * <i>bifA</i> *				
C7	19906 20542	Evolved <i>pflu0085</i> * <i>pflu0084</i> * <i>awsR</i> *				
D1	19908 20453	Evolved <i>awsR</i> * <i>wspF</i> * <i>wspA</i> *				
D8	19915 20544	Evolved <i>mutY</i> *				

Table 3.5. Colony morphology & mat formation phenotype of select evolved lineages. Phenotypic images & Genotypes provided for SBW25, and the selected evolved lines from the LCE trial: A4, A8, B1, B6, C2, C7, D1 & D8. Colony morphology spot (imaged with Axiocam) – 5 µL overnight culture spotted on KBA plate and

incubated for 1 day at 28°C or room temperature. For the Scarlet-CdrA strains, GFP & Scarlet fluorescence was imaged using the ChemiDoc. Mat formation (imaged with iPhone 11) – 6 µL overnight culture inoculated into 6 mL KB microcosm (10^{-3} dilution) and incubated under static conditions for 24 hours at 28°C.

While for mutational line D8, and the evolved lineages using a developmental strategy to transition through the life cycle (line A4, A8, B6, C2, C7 & D1), I found that they all formed a substantial mat at the air-liquid interface of the static broth (see images in *Table 3.5*). Line D8 also exhibited an intermediate semi-WS colony morphology at 28°C (high c-di-GMP) & the SM phenotype with a semi-WS centre at room temperature; this indicating that the *mutY* mutant is either a hypermutator allowing for rapid generation of phenotypic states, or that this line acquired a mutation conferring developmental regulation of the life cycle. The generalist strategy line A4 (*mwsR* mutant) displayed the SM phenotype with a slight semi-WS centre at both temperatures & low c-di-GMP levels, and A8 (*wspR* mutant) the strong WS phenotype with high levels of c-di-GMP. The developmental strategy lines B6 (*awsR* mutant), C7 (*pflu0085-pflu0084-awsR* mutant) & D1 (*awsR-wspA-wspF* mutant), all exhibit an intermediate semi-WS phenotype at either incubation temperature, with an associated medium-low c-di-GMP level. Strikingly, I found that the developmental line C2 (*pflu0085-bifA* mutant) displayed a switch in colony morphology with change to temperature – the SM phenotype at 28°C (with low c-di-GMP), and the WS phenotype at room temperature. This result implies that line C2 may achieve developmental regulation of the life cycle by changing phenotype in response to the environment.

3.6.2. Level of c-di-GMP in different environments

To further investigate this, I proceeded to measure the level of c-di-GMP for the selected evolved lineages (A4, A8, B1, B6, C2, C7, D1 & D8) & the WT SBW25 control, of cells grown in two different environments relevant to the life cycle – static broth & motility plate. This was achieved using the pCdrA-GFP reporter for c-di-GMP (Rybtke et al., 2012), with the Scarlet-CdrA transformed strains as previously described. For each genotype, four replicates were grown in the static broth & motility plate environment, and the GFP & Scarlet fluorescence of cells measured by flow cytometry. The mean normalised GFP was then calculated for each sample to approximate the level of intracellular c-di-GMP; the results shown in *Figure 3.10* below. I found that the wild-type SBW25 demonstrates some capacity to regulate c-di-GMP levels, with an increase observed in the static broth environment as compared to the motility plate. This result was not surprising, as the ancestral SBW25 is able to form a feeble mat at the static broth surface; Ardré et al. (2019) previously observed minor

activation of cellulose production at the air-liquid interface, and the formation of surface micro-colonies dependant on the *wsp*, *aws* and *mws* operons. I also previously showed in [Section 2.4.2](#), that deletion of the *wss* operon in SBW25 resulted in loss of the formation of this thin mat at the surface. Therefore the SBW25 ancestor must receive some environmental signal at the air-liquid interface in static broth, which results in a slight increase in c-di-GMP level and therefore some production of cellulose by the Wss pathway (though insufficient to form a proper mat).

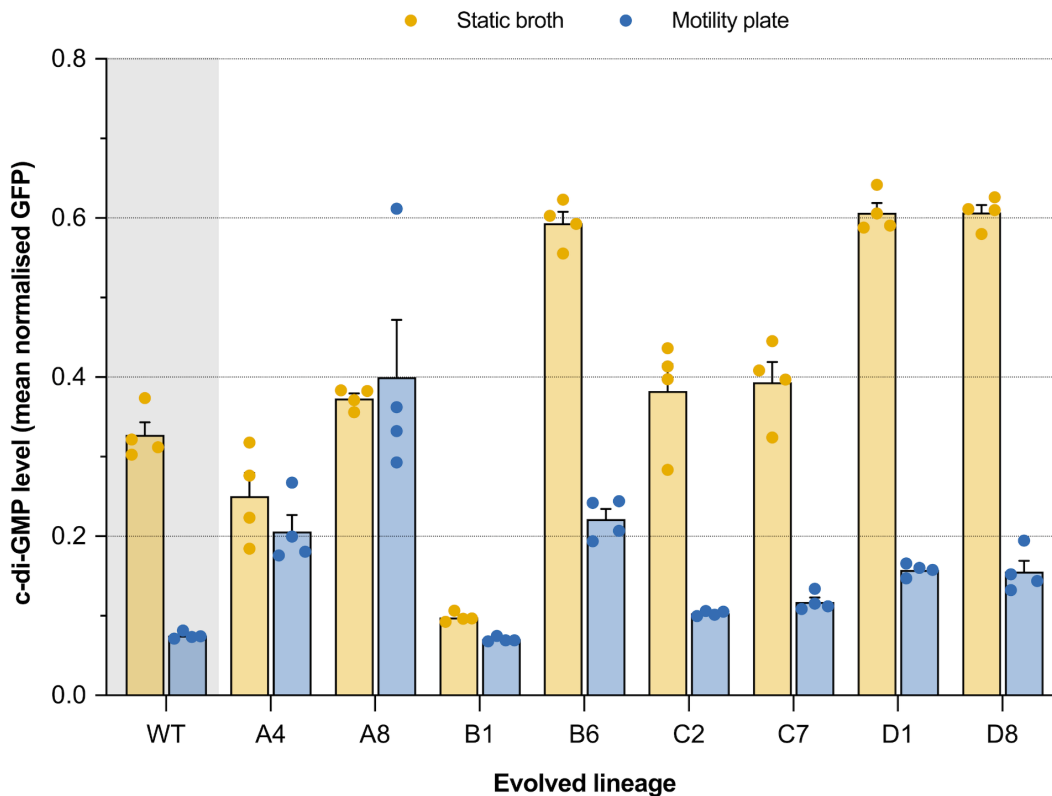


Figure 3.10. Evolved lineages show capacity to further upregulate c-di-GMP level in static broth. Level of c-di-GMP in the static broth & motility plate environment given for the Scarlet-CdrA strains, including the WT SBW25 (MPB17910) and select evolved lineages from the LCE trial: A4 (MPB20537), A8 (MPB20538), B1 (MPB20539), B6 (MPB20540), C2 (MPB20541), C7 (MPB20542), D1 (MPB20543) & D8 (MPB20544). For each genotype, four replicate overnight cultures were each inoculated into an SSA motility plate (0.25% agar & 1% KB) & KB static microcosm, and incubated for 24 hours at 28°C. For each sample, flow cytometry was used to measure the GFP & Scarlet fluorescence of 10,000 cells. The c-di-GMP level was approximated with the mean normalised GFP, this calculated by dividing the mean GFP by the mean Scarlet (cell baseline). Data are displayed on a scatter plot, with bars showing the mean, and error bars the standard error of the mean.

The LCE trial evolved lineages demonstrated varying capacity to upregulate c-di-GMP level in the static broth environment, as shown in [Figure 3.10](#) above. I carried out statistical analysis, to examine for each lineage, whether the increase in c-di-GMP level in static broth

was significantly different from the WT SBW25; the results are provided in *Table 3.6* below. The mutational strategy line B1 demonstrates disruption to c-di-GMP signalling, with low levels of c-di-GMP observed in both environments; the difference significantly lower than in the WT (p -value = 0.000495). This may be explained by the line B1 containing many disruptive mutations (total of 10 mutations), in various genes related to the WS phenotype & c-di-GMP signalling pathway (refer to *Section 3.5.1*). While the generalism strategy lines A4 & A8 displayed an increase in c-di-GMP level in both the static broth & motility plate environments (no statistical difference from the WT). This result confirms that these evolved lineages have not obtained a means of regulating the life cycle, but rather perform as a generalist – increasing c-di-GMP just enough to form a mat and maintain a motility distance over the set threshold of 10 mm.

Line	Static mean increase	Difference to WT		t	df	α	p -value	Significant?	
		Mean	SE						
A4	0.0446	-0.2077	0.0499	-4.1585	3.6872	0.00625	0.016749	No	Equal
A8	-0.0265	-0.2788	0.0748	-3.7254	3.2908	0.00625	0.028729	No	Equal
B1	0.0277	-0.2246	0.0165	-13.5767	3.3314	0.00625	0.000495	Yes	Lower
B6	0.3720	0.1197	0.0266	4.5049	5.6065	0.00625	0.004824	Yes	Higher
C2	0.2796	0.0273	0.0385	0.7097	4.2192	0.00625	0.515146	No	Equal
C7	0.2764	0.0241	0.0296	0.8146	5.1441	0.00625	0.451330	No	Equal
D1	0.4488	0.1966	0.0215	9.1586	5.9059	0.00625	0.000104	Yes	Higher
D8	0.4512	0.1989	0.0213	9.3280	5.8831	0.00625	0.000096	Yes	Higher

Table 3.6. Statistical analysis of the upregulation of c-di-GMP in static broth, comparing evolved lineages to the wild-type SBW25. For each select evolved lineage from the LCE trial (A4, A8, B1, B6, C2, C7, D1 & D8), statistical analysis was carried out to determine whether the mean increase in c-di-GMP level in the static broth environment is different than in the WT SBW25. The increase in c-di-GMP in static broth was first calculated for each sample as: mean normalised GFP (static broth – motility plate). An unpaired Welch’s t-test was then complete for each evolved line to compare the sample means to the WT; this test assumed that samples were independent and means fit a normal distribution (no assumption made regarding equal variance); the α was adjusted for multiple comparisons using the Bonferroni correction. Provided for each test: Line name, Mean increase in c-di-GMP in static broth, Mean difference (evolved – WT), SE (standard error), t (test statistic), df (degrees of freedom), α (adjusted p -value threshold), p -value, Significant? (whether p -value is significant, and the conclusion regarding increase in c-di-GMP level in static broth – equal/higher/lower than in the WT).

The lines that evolved a developmental strategy to transition through the life cycle (A4, A8, B6, C2, C7 & D1), all demonstrate an increase in c-di-GMP level in the static broth as compared to the motility plate environment (see *Figure 3.10*). Although only for lines B6, D1

& D8 was this upregulation in static broth significantly higher than in the WT (p -value: 0.004824, 0.000104 & 0.000096, respectively); for line C2 & C7 there is no statistical difference from the WT SBW25 behaviour. In the evolved line D8 (*mutY* mutant), it is unclear whether this response is due to hypermutability or a form of developmental regulation. While for the lines B6 (*awsR-pflu3595* mutant) & D1 (*awsR-wspF-wspA* mutant), the ability to transition through the life cycle by developmental regulation may be attributed to the modulation of c-di-GMP level in response to the environment. By increasing the level of c-di-GMP in the static broth environment these genotypes are able to activate cellulose production and form a mat, while in the motility plate the decrease in c-di-GMP allows for expression of flagella and dispersal by swimming motility.

3.6.3 Lineage-level fitness

The lines B6 & D1 evolved a mechanism for developmental regulation of the life cycle, able to transition between the two phenotypic states by modulation of c-di-GMP levels (see [Section 3.6.2](#)). The genealogical history of these lineages implies that they have increased lineage-level fitness, with a low rate of extinction observed (see previous [Figure 3.9](#)). To confirm this, the extinction rate was measured of replicate lines taken through an additional life cycle generation, and the capacity to transition without extinction used as an approximation for lineage-level fitness (low extinction rate corresponding to more offspring & high lineage fitness). I did this for the developmental strategy lines B6 & D1, as well as the mutational line B1 & wild-type SBW25 as a negative control; for each genotype one rack (of 8 replicate lines) was taken through life cycle number 6 (or cycle 1 for SBW25), with the extinction rate summarised in [Figure 3.11](#) below. I observed that ancestral SBW25 had a mid-range rate of extinction, with 25% during PI (Collective) & 50% during PII (Dispersal). While the negative control mutational line B1 exhibited a very high extinction rate – 87.5% in PI, with all replicates going extinct in PII. This result demonstrates that using mutation to transition through each phase of the life cycle is an unreliable strategy, and will likely lead to extinction of a lineage. The developmental lines B6 & D1 both displayed a low extinction rate, with 0% during PI, and 12.5% & 25% during PII, respectively; the only extinction observed for these genotypes was due to the falling of mats in PII. Therefore the lines B6 (*awsR-pflu3595*) & D1 (*awsR-wspF-wspA*) demonstrate an increase to lineage-level fitness as compared to the wild-type SBW25. These evolved lineages obtained specific mutations that confer developmental regulation of the collective & dispersal phenotypic states, therefore

allowing reliable transitioning through the life cycle, without a dependence on further mutational change.

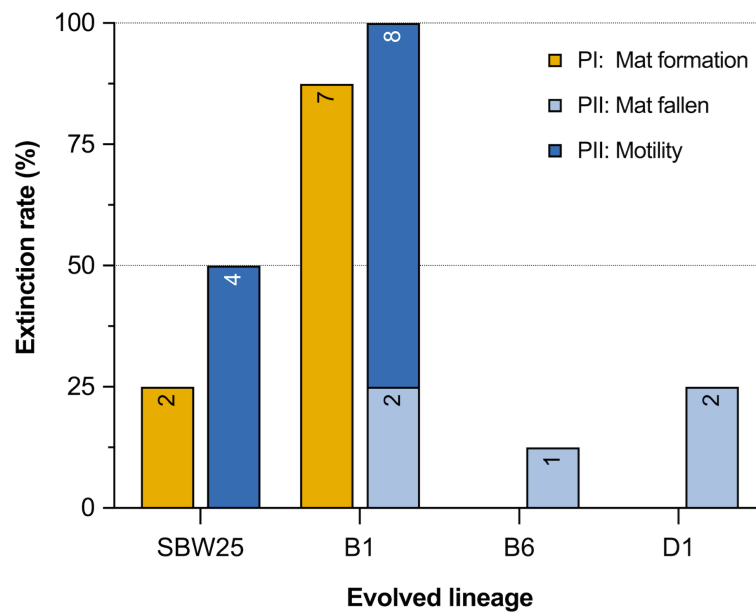


Figure 3.11. Evolved lines B6 & D1 demonstrate an increase in lineage-level fitness. Extinction rate during an additional generation is shown for SBW25 (MPB14218), and the select evolved lines from the LCE trial: B1 (MPB19892), B6 (MPB19897) & D1 (MPB19908). For each genotype, one rack of 8 replicate lines was taken through one life cycle generation (cycle 6, or 1 for SBW25). The extinction rate (percentage of 8 replicates) is shown as a result of – mat formation during PI (failure in mat-formation screen), mat fallen during PII, and swimming motility during PII (failure in motility screen). This data is displayed in a bar graph, with the number of extinct lines provided within the bar.

3.6.3.1 Mutations obtained during additional generation

To confirm that the evolved lines B6 & D1 were indeed transitioning through the life cycle by developmental regulation (and not mutation), I also carried out whole-genome sequencing of the replicate lines after the additional cycle 6 generation; refer to previous [Section 3.6.3](#). Mutations were then identified using Breseq, and the results shown in [Table 3.7](#) below (further detail provided in [Supplementary 4-9](#)). I found for line D1 (*awsR-wspF-wspA* mutant), that no additional mutations were obtained in all 8 replicates; this result confirms that this evolved lineage is using a developmental strategy. While for line B6 (*awsR-pflu3595* mutant), 50% of replicates (4 of 8) acquired no additional mutations, and 25% obtained 1 and 2 mutations each (see details in [Table 3.7](#) below). This also implies that line B6 is able to transition through the life cycle without mutation; though the mutations that were acquired may represent an opportunity to further improve lineage fitness. These include SNPs in *pflu3472*, *pflu3378* & *pflu1084*; [pflu3472](#) encodes the putative citrate lyase subunit beta, and

[pflu3378](#) encodes the putative ferric alcaligin siderophore receptor. The effect of these mutations is unclear, but they do seem to be more closely linked to metabolism than c-di-GMP signalling.

Line	Rep.	#	Gene name	PFLU	Putative product	Nucleotide change	Amino acid change	Protein domain	E-value
B6	No mutations – replicate 1, 3, 7 & 8								
	2	1	pflu3472	3472	citrate lyase subunit β	160T>G	F54V	HpcH/HpaI	2.5e-28
	4	3	pflu3378	3378	ferric alcaligin siderophore receptor	509T>C	V170A	Plug_dom	6.9e-16
	4	2	pflu1084	1084	hypothetical protein	673C>T	P225S	DUF3034	6.2e-109
D1	No mutations – replicate 1-8								

Table 3.7. For evolved lines B6 & D1, replicates obtained few mutations during additional generation. The mutations acquired during an additional life cycle generation are given, for the replicates of evolved lineage B6 (MPB19897) & D1 (MPB19908). Provided for each: Line name, Rep. (replicate line number 1-8; origin of mutation) & # (total number of lines with mutation). Mutation details as described in [Table 3.2](#) legend.

3.7 Conclusions from the trial experiment

The revised LCE regime utilised new selective methods based on the collective trait of mat formation and individual trait of swimming motility, to replace use of the colony morphology proxy. From the results of the LCE trial, I am able to draw a number of conclusions about this new experimental regime, and the objectives for the future. Firstly, from the numerous phenotypic measurements taken during the trial experiment, it has become indisputable for the LCE that colony phenotype is irrelevant. I observed in evolved lineages that the mat formation & motility traits showed no correlation with the SM & WS colony morphology on agar plates. It is evident that for the previous experiment of Hammerschmidt et al. (2014), the use of this proxy was a major limiting factor, and forced lineages to transition through the life cycle phases (and distinct SM & WS phenotypic states) by mutation only. In this way, the previous LCE more closely resembled a mutation accumulation experiment, where the emergence of hypermutators is inevitable.

With the revised experimental regime, I selected directly on traits of ecological relevance to the static broth environment, and to simple multicellular life cycles observed in nature. The new LCE transitioned between the mat-forming collective phase (PI), and motile individual dispersal phase (PII). During the LCE trial, evolved lineages demonstrated rapid adaptation to

the life cycle within five generations; I observed a decrease in extinction rate over time, as well as improvement to the traits of mat formation & swimming motility. Furthermore, I noted the emergence of a number of unique strategies to transition through the life cycle – mutational, generalism & developmental. The mutational strategy (e.g. line B1) required lineages to obtain mutations during each phase, likely resulting in constitutive activation or inactivation of mat formation; this resembling the outcome of the previous experiment (Hammerschmidt et al., 2014). Using mutation to transition through the life cycle corresponded with a high rate of extinction & low lineage-level fitness; I also found that the accumulation of mutations resulted in disruption to c-di-GMP signalling.

In other evolved lineages (e.g. line A4 & A8) the generalism strategy was observed, in which mutations were acquired that allowed for formation of a mat in static broth, but at the expense of swimming motility performance. The presence of generalists prompted an alteration to the selective regime for future experiments, to apply stricter selection on the traits of mat formation & motility – with only 6 colonies (instead of 12) examined in the mat-formation screen, and the motility threshold increased to 15 mm. Most significant was the observation of evolved lineages with unique developmental strategies to transition through the life cycle (e.g. B6, C2, C7 & D1), able to regulate expression of the mat formation & motility phenotypes, without need for further mutation. I also provided evidence for select evolved lineages (B6 & D1), that this developmental regulation could be attributed to the modulation of c-di-GMP level in response to the environment. The developmental lineages B6 & D1 displayed an increase in lineage fitness (low extinction rate), as observed for replicate lines taken through an additional generation; during this extra cycle the majority of replicates also acquired no further mutations. Recreation of the mutations from line B6 (*awsR-pflu3595*) & D1 (*awsR-wspF-wspA*) is an obvious next step, and would reveal the contribution of each to developmental regulation of the life cycle.

Although the trial experiment provided a lot of insight regarding the merit of the new selective methods, it was very limited by the scale, containing only four replicate metapopulation racks. Therefore the critical objective for the future is to run the experiment on a large-scale with many replicate racks, and applying the minor adjustment of the selective methods as discussed. Having a greater number of independent racks will allow for exploration of the different ways to evolve developmental regulation of the life cycle – whether there are many possible mutational pathways, or that it may only be achieved with few specific mutations in select genes. The parallelism observed in the trial experiment with

mutation to nearby residues of the AwsR sensory domain, implies that the latter may be the case. Use of a stricter selective regime will hopefully also push lineages further to improve the collective & dispersal traits, and to evolve even better solutions for regulation of the life cycle.

Chapter IV: Evolution of developmental regulation in a simple multicellular life cycle

4.1 Large-scale life cycle experiment

Following the success of the trial experiment using the revised selective regime (see [Section 3.3](#) & [3.4](#)), I proceeded to conduct the life cycle experiment on a large-scale. This included the minor alterations to the selective method – for the mat-formation screen only six colonies were examined per line, and for the motility screen the threshold was increased to 15 mm. With the stricter assessment of the collective & individual traits, I hoped that this would further push lineages to evolve developmental strategies for regulation of the life cycle, and avoid solutions comparable to generalism (as was observed during the trial, refer to [Section 3.5.2.1](#)). The full experiment consisted of a total of 24 replicate metapopulations evolving in parallel; at this scale the intention was to investigate the possible mutational paths to developmental regulation, as well as examine the results of inter-rack competition – in which successful strategies evolved from independent racks are able to compete with each other to take over an extinct rack. This chapter focuses on analysing the results of the large-scale LCE, and characterising for selected evolved lineages the mechanism underpinning developmental regulation of the simple two-phase life cycle.

To begin the experiment, the 24 metapopulations (rack 1-24) comprised of 8 replicate lines each (1-8; total of 192 lines), were inoculated with the ancestral SBW25 (MPB14218). The lineages were taken through five life cycle generations, with a freezer stock stored of each motile seed at the end of PII every cycle (Cycle 1: MPB20428-20429, 2: MPB20535-20536, 3: MPB20844-20845, 4: MPB21588-21589 & 5: MPB21730-21731). This experiment was carried out with the assistance of technician Norma Rivera from the MPI Plön. All additional data is available in [Supplementary A-12&13](#).

4.1.1 Genealogy over five generations

For the LCE, over five life cycle generations I recorded a total of 640 lineage extinction/replacement events, including the occurrence of 10 metapopulation extinctions. This is summarised with the genealogical tree in [Figure 4.1](#) below, highlighting the coalescence of each surviving lineage – the origin of descent from the parental lineage during the first cycle (Doulcier, 2019). For each independent metapopulation rack, the final lines

may be traced back in most cases to a single parental lineage (in some cases 2 or 3), that has reached fixation within the rack over time. For example, in rack 3 all of the surviving lineages originate from the common ancestor lineage 3.6 from cycle 1 (see *Figure 4.1*). I also observed the clear trend of a decrease in extinction rate over time, with most extinctions occurring during the early cycles, especially during the dispersal phase (note: large number of extinct end nodes & branching points). By cycle 5 there were very few extinctions (note: more nodes connected by parallel opaque lines & fewer transparent lines), except for within the racks 22, 23, and 24. The reduction in extinction is consistent with the evolution of developmental regulation, as lineages may reliably transition through the phenotypic states of the life cycle without requiring rare adaptive mutations.

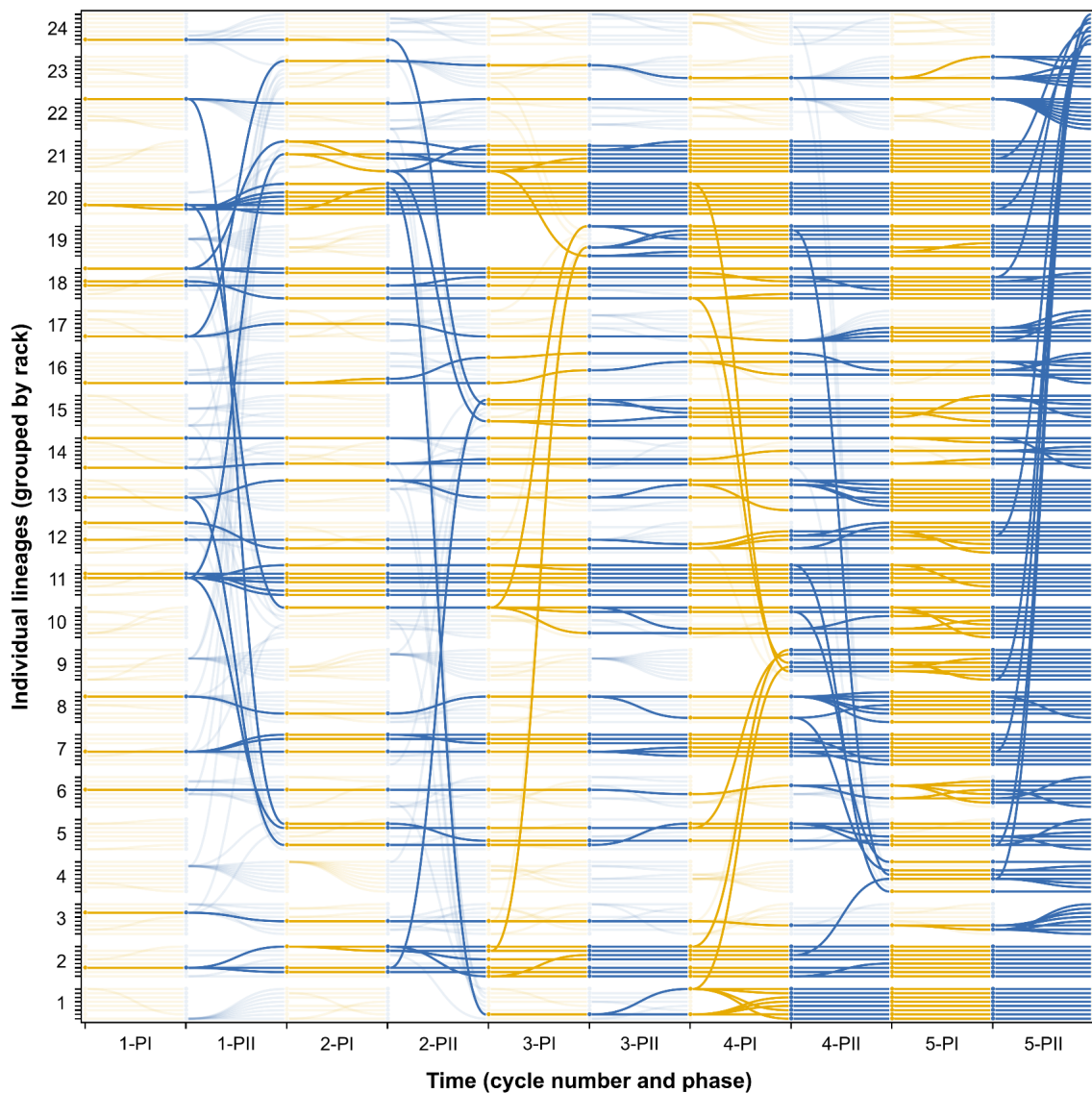


Figure 4.1. Genealogical tree illustrating the coalescence of lineages. Each row displays the genealogy of an individual lineage from the LCE (grouped in racks 1-24, with replicates lines 1-8 each), over time for five life

cycle generations (and phases PI & PII). The circle nodes represent a single lineage in time, and the connections between each node show the history of extinction & replacement during each life cycle phase – an extinction event is illustrated by an end node having no connections, and a group-level reproduction event by a single node having multiple branching connections. The colour shows the phases PI: Collective (●) & PII: Dispersal (●), as well as demonstrating the coalescence of final lines – opaque nodes & connections highlight lineages that survived until the end of cycle 5 (and all parental lines), while transparent nodes & connections show extinct lineages. Figure made using Colgen (Doulcier, 2019).

4.1.2 Rapid decrease in extinction rate

I observed a rapid decrease in the extinction of lineages across five life cycle generations, as shown in *Figure 4.2* below. There was initially a high extinction rate especially in the dispersal phase, with 76.0% of lineages going extinct during PII of cycle 1, the majority as a result of poor performance in swimming motility (failure to reach 15 mm threshold in the motility screen). By cycle 5, the PII extinction rate had decreased substantially, dropping to 26.5%, with only the minority due to failing the motility screen. The number of extinctions during PII as a result of fallen mats was highest in cycle 1 (47 lineages), but then remained relatively consistent in the following cycles (20-30 lineages per cycle). Falling of mats may be explained by the presence of genotypes that produce unstable mats at the broth surface, or as a consequence of random environmental perturbation.

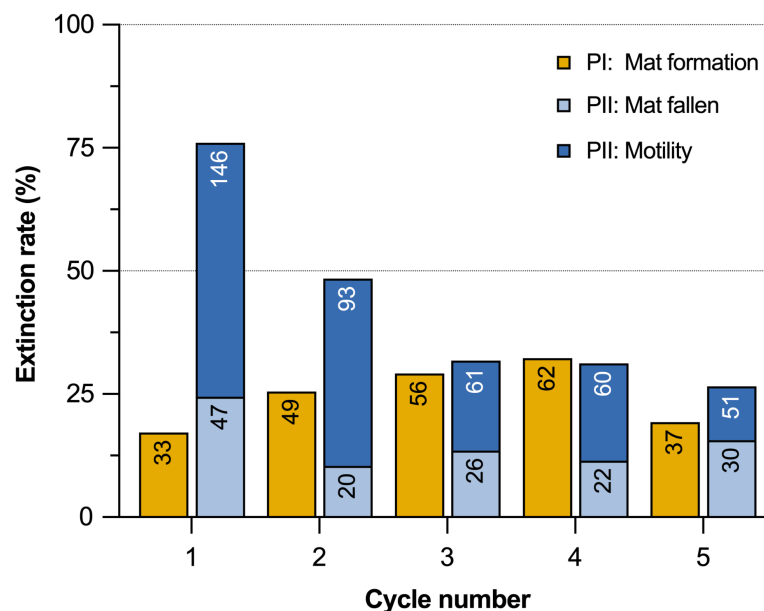


Figure 4.2. Extinction rate of lineages decreases over five generations. The extinction rate is shown of 192 replicate lines from the LCE, across life cycle numbers 1-5; extinction of lines as a result of – Phase I (Collective) mat-formation screen (no mat formers from six random colonies), Phase II (Dispersal) mat fallen (no intact mat in 6 day evolved culture), and the PII motility screen (migration diameter less than 15 mm). These data are displayed with a bar graph, and the number of extinct lines annotated within the bar.

As the extinction rate decreased for the PII dispersal phase, I also observed a slight increase in extinctions during the PI collective phase resulting from failure in the mat formation screen – 17.2% of lineages during cycle 1, to 32.3% in cycle 4. This result implies the existence of a trade-off between the individual trait of motility & collective trait of mat-formation; by strongly selecting in each lineage for the most motile individual during PII, this may also correspond with selection for low mat formation capacity (required during PI). Although by cycle 5, the extinction rate during the collective phase decreased to 19.3% of lineages, perhaps indicating the breaking of this trade-off.

4.1.2.1 Extinction rate within replicate racks

From the LCE genealogical tree, it is evident that the lineage extinction rate is unequally distributed across replicate racks, with some having a large number of extinctions, for example racks 22, 23 & 24 (refer to previous [Figure 4.1](#)). Therefore the total extinction rate may be misleading, as it is skewed by a few metapopulations with poorly-performing lineages. To further examine this distribution, the extinction rate within each rack is displayed in [Figure 4.3](#) below.

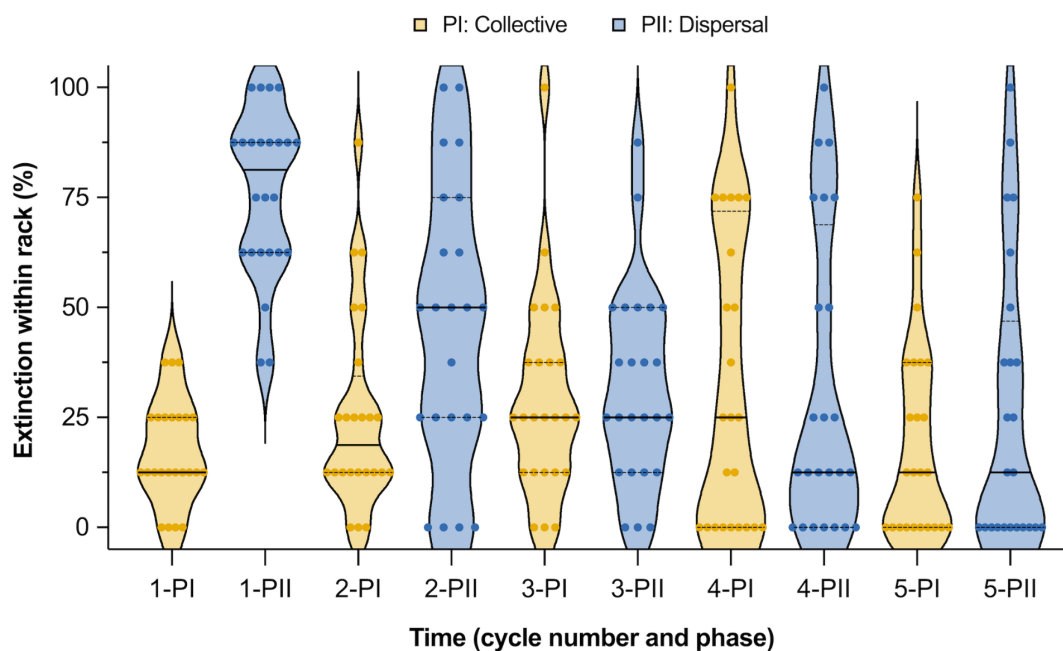


Figure 4.3. Distribution of extinction rate of lineages within each replicate rack. The extinction rate within the rack (percentage of 8 lines) is shown for the 24 replicate racks, across life cycle numbers 1-5, for the Phase I (Collective) & Phase II (Dispersal). These data are displayed with a violin plot (high smoothing), showing the median (solid line), quartiles (dotted line), and individual data points.

During the first cycle, the within rack extinction rate approximated a normal distribution, dispersed around the median of 12.5% of lineages extinct in PI (1 line of 8), and 81.25% during PII (6.5 lines of 8). Then for the collective phase (PI) extinction rate skewed towards higher values, as a result of some racks having many extinct lines; with the median of 25% of lineages extinct in cycle 3, and the distribution becoming bimodal during cycle 4. By cycle 5, the majority of racks have an extinction rate of 0%, with only few racks remaining at a high level of extinction (>40%). While for the dispersal phase (PII), after the first cycle there is a widening of the distribution in within rack extinction rate, which shifts towards lower values across the life cycle generations, with the median of 25% of lineages extinct in cycle 3. By the final cycle, approximately half of the racks have 0% lineage extinction, while the other half have a variable extinction rate from 25-100%. Those racks with minimal extinction may have fixed lineages with a means of developmental regulation of the life cycle, while the remaining racks with a high extinction rate are likely composed of lineages still proceeding by mutation.

4.1.3 Improvement in collective & individual traits

Furthermore, I found that over the five life cycle generations evolved lineages showed substantial improvement to the collective trait of mat formation and individual trait of dispersal by swimming motility. This is displayed in *Figure 4.4* below, which summarises for each replicate rack the measurements taken for each lineage of mat formation capacity in PI and motility distance in PII, over five generations (and of the final surviving lineages). For the mat-formation trait (see *Figure 4.4 (left)*), during cycle 1, 0% of lineages within each rack were able to form a mat, as expected for ancestral SBW25. The proportion of mat-forming lineages rapidly increased over time, and by cycle 5 the majority of racks contained lineages in which 87.5-100% could form a mat. In the final surviving lineages, almost all replicate racks (excluding six) consisted of lineages in which 100% were capable of forming a mat in the static broth within 24 hours – strongly suggesting the emergence of developmental regulation of the life cycle. The remaining racks that contain a low proportion of mat-forming lineages likely correspond with the use of a mutational strategy.

While for the individual trait of swimming motility (see *Figure 4.4 (right)*), I found that the mean motility distance (mean migration diameter of all 192 lineages) increased from 13.83 mm during cycle 1, to 18.53 mm during cycle 5, and 25.46 mm in the final surviving lineages. The improvement to motility was relatively constant over time for replicate racks,

and corresponds with a narrowing of the distribution; although during cycle 4 there was a slight decrease in mean motility distance, as a result of a number of racks containing lineages with low motility (mean of 10-15 mm). During cycle 5, the mean motility distance was also skewed by the presence of a few racks with a very low mean motility (<12 mm) – these include the racks 22, 23 & 24, that are predicted to contain lineages transitioning through the life cycle by mutation.

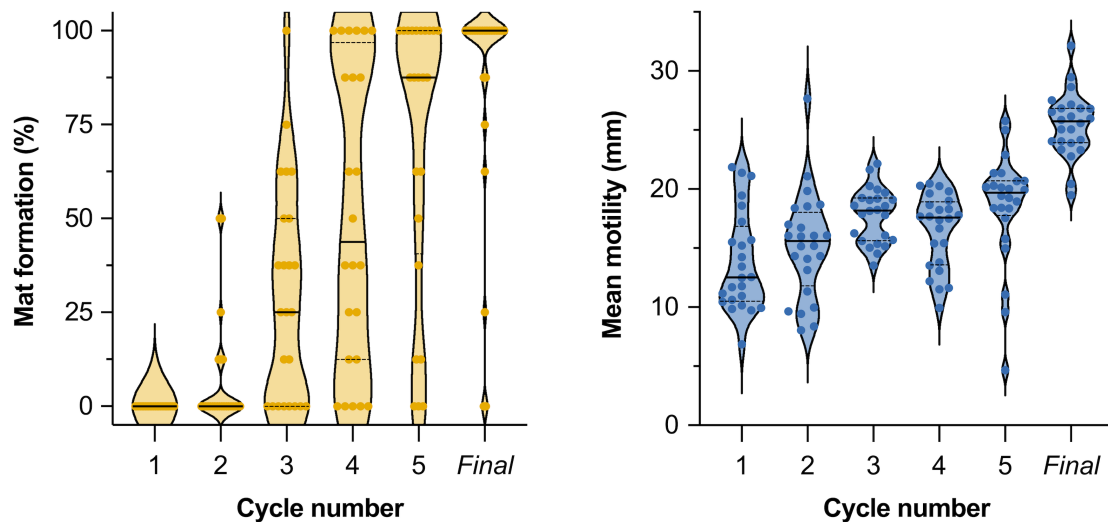


Figure 4.4. Improvement to mat formation & swimming motility observed over five generations. Phenotypic data is shown for the 24 replicate racks (each containing 8 lines), across life cycle numbers 1-5, and of the final surviving lineages. Left: mat formation within rack (percentage of 8 lines), after 24 hours growth in static broth during Phase I (Collective). Right: mean motility within rack (mean migration diameter in mm, of 8 lines), after 30h growth on SSA motility plates. These data are displayed in a violin plot (medium smoothing), showing the median (solid line), quartiles (dotted line), and individual data points.

Overall, these results demonstrate that evolved lineages are rapidly adapting to the life cycle, presumed to have obtained mutations that confer improvement to both the individual and collective phenotypic traits. The improvements to mat formation & motility were greater than that seen during the trial experiment (see [Section 3.4](#)), confirming that the minor alterations to the selective regime were effective. Remarkably, at the end of five life cycle generations, I observed that 84.9% of surviving lineages (163 of total 192) were both motile (>15 mm) and able to form a mat within 24 hours in the static broth environment. This indicates that the majority of lineages have acquired a means of developmental regulation of the life cycle.

4.1.4 Fixation of high fitness lineages

The evolved lineages that had a low extinction rate (due to improvement in mat formation & motility) were able to quickly reach fixation within their rack, by replacing the other lineages

upon extinction. The fitness of a lineage may be defined as its capacity to leave offspring, which depends on the ability of a lineage to persist through time (to transition through the life cycle without extinction), so that it has the opportunity to undergo group-level reproduction (replace extinct lineages). High fitness lineages that rapidly fixed within their rack, were also observed to be successful during inter-rack competitions – where an extinct rack was replaced with a surviving lineage from eight random racks, allowing for these independently-evolved lineages to compete to take over this vacant rack. Examples of this are displayed in *Figure 4.5* below, showing the genealogy of select lineages in rack 2 (●), rack 11 (●), rack 18 (●), rack 20 (●), as well as extinct lineages or racks (●).

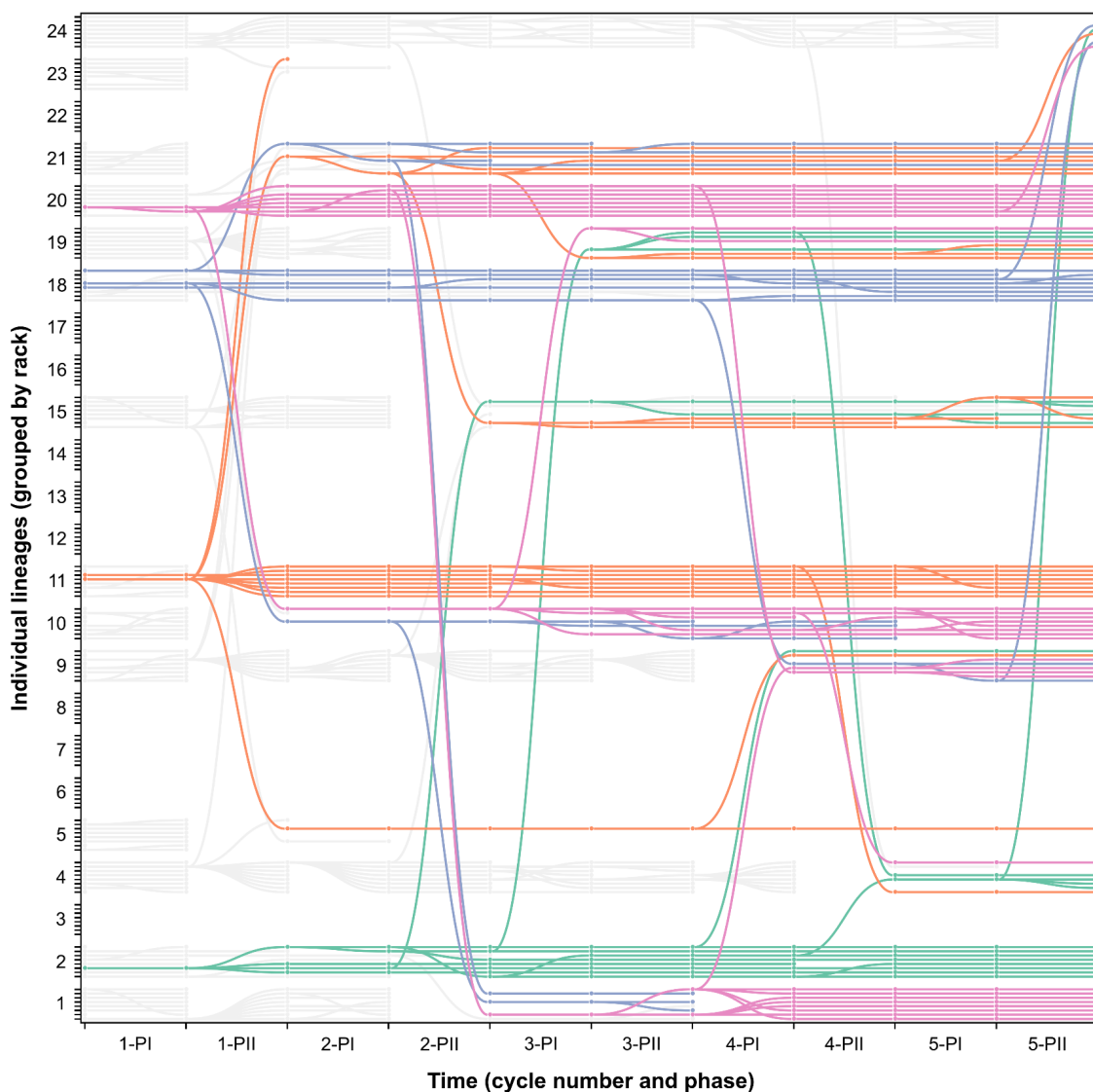


Figure 4.5. Genealogical tree of select lineages that reach fixation within five generations. The descent is shown of select high fitness lineages within rack 2 (●), rack 11 (●), rack 18 (●), and rack 20 (●); extinct lineages or racks are also displayed (●). Genealogy as described in [Figure 4.1](#) legend.

In rack 20 (●), the parental lineage 20.3 (from cycle 1-PI) replaced all other lineages in the rack within two life cycle generations (by cycle 2-PII), and no extinction events occurred in all offspring lineages (note: nodes connected by only parallel lines). This result indicates that this evolved lineage acquired a mutation during the first generation that was strongly beneficial to regulation of the life cycle. Furthermore, this high fitness lineage from rack 20 also managed to reach fixation within the extinct racks 1 & 10 (outcompeting lineages from rack 18 and others), as well as leave offspring in the racks 4, 9, 19 & 24 (see *Figure 4.5* above). While in rack 2 (●), the parental lineage 2.3 fixed within the rack by cycle 3-PII, also leaving offspring in extinct racks 4, 9, 15, 19 & 24, with minimal further extinctions. This evolved lineage likely also gained adaptive mutations early on in the experiment, that mediated the transition through the phenotypic states of the life cycle.

For the racks 11 (●) & 18 (●), multiple independent lineages were maintained over five life cycle generations, originating from the parental lineages 11.5 & 11.6, or 18.4, 18.5 & 18.8, respectively. The time taken for fixation depends on both the fitness of a lineage, and of the other lineages within the rack; if extinction rate is negligible due to the existence of multiple high fitness lineages, then there is minimal opportunity for a lineage to reproduce further. Continuing the experiment for more generations may allow for extinction to occur in racks 11 & 18, and the lineage of highest fitness to be fixed. The observation of coexistence of multiple lineages within a rack also suggests that a number of different viable strategies exist to transition through the life cycle (or that lineages converged on the same solution) – sequencing of the evolved lineages would be required to confirm this. Therefore I decided to pause the experiment after only five generations, so that I could determine the mutations underpinning the capacity of high fitness lineages to regulate the life cycle.

4.2 Strategies to transition through the life cycle

After only five life cycle generations, I observed a rapid decrease in extinction rate (refer to *Section 4.1.2*), improvement to the traits of mat formation & motility (refer to *Section 4.1.3*), as well as the fixation of high fitness lineages. Based on this, I proceeded to carry out whole-genome sequencing of all evolved lines (192 total), from the end of cycle 5 of the experiment. The raw sequencing files are available on the NCBI SRA (Bioproject ID: [PRJNA945835](https://www.ncbi.nlm.nih.gov/bioproject/PRJNA945835)). Mutations were then identified using Breseq (Deatherage, & Barrick, 2014); summary of the output is provided in *Supplementary A-15&16*. From the sequencing results, I was able to identify a number of different strategies that evolved lineages had found to

mediate the transition through the life cycle, categorised into the following – mutational, hypermutation & developmental (see previous discussion of strategy types in [Section 3.5](#)).

The mutational strategy depends on spontaneous mutation to switch between phenotypes (e.g., turning on & off mat formation), with each phenotypic transition generally associated with a single mutation (Hammerschmidt et al., 2014; Rose et al., 2020). This strategy tends to be unreliable, as adaptive mutations are rare, and sometimes will not occur within the timeframe allowed by the experiment (static broth incubation of 4 days in PI & 6 days in PII). Additionally, over subsequent life cycle generations the mutational target size will become smaller, due to the accumulation of disruptive mutations throughout the c-di-GMP signalling network (Barnett, 2022). A solution to this problem is to increase the global mutation rate (hypermutability), this resulting in more genetic variation within a lineage, and therefore a greater chance of acquiring the necessary beneficial mutation to transition through the life cycle (Taddei et al., 1997). The hypermutation strategy may be identified by the presence of mutation to the DNA mismatch repair system (Denamur & Matic, 2006), as well as the total number of mutations exceeding the number of phenotypic transitions. Hammerschmidt et al. (2014) previously observed the evolution of a *mutS*-dependent genetic switch; the elevation of mutation rate allowed for semi-reliable switching between the WS & SM phenotypes by expansion & contraction of a tract of guanine residues in the DGC-encoding *wspR* gene (refer to [Section 1.3.3.2](#)).

Although the use of a hypermutation strategy is not ideal, as most mutations are deleterious, and over time these would accumulate throughout the genome. Arjan et al. (1998) show diminishing returns from an increased supply of beneficial mutations due to elevated mutation rate, and predict that mutator genotypes would only accelerate adaptive evolution in limited circumstances. Other studies performing mutation accumulation experiments in bacteria identified the following disruption to mutator genomes – decrease in genome size (Nilsson et al., 2005), and rapid reduction of GC content (Lind & Andersson, 2008). Therefore while hypermutation may be a reasonable short-term solution, it is unlikely to be feasible in the long-term. Rather than relying on repeated mutation, a better solution would be the evolution of a developmental program to regulate the transition through the life cycle. Such a developmental strategy would require some mechanism of epigenetic regulation of gene expression, likely in response to an environmental signal (Wolpert, 1994; Bonner, 2000; Kaiser, 2001). This would allow for lineages to switch between the phenotypic states of the collective & dispersal phases of the life cycle, without need for further mutational change.

The developmental strategy is made evident by evolved lineages containing far fewer mutations than the number of phenotypic transitions, and demonstrating the capacity to both form a mat in static broth (within 24 hours) and reach a motility distance over 15 mm.

4.2.1 Geneology of different strategies

The different strategies that I observed in evolved lineages for transitioning through the life cycle are displayed in *Figure 4.6* below, including mutational (●), hypermutation (●), and ten unique genotypes for developmental (●:●). I found that only a small number of lineages were proceeding through the life cycle by mutation or elevation of mutation rate, as was previously observed by Hammerschmidt et al. (2014). While the vast majority of lineages had acquired a means for developmental regulation of the life cycle, including ten unique genetic routes present in lines across the independent racks.

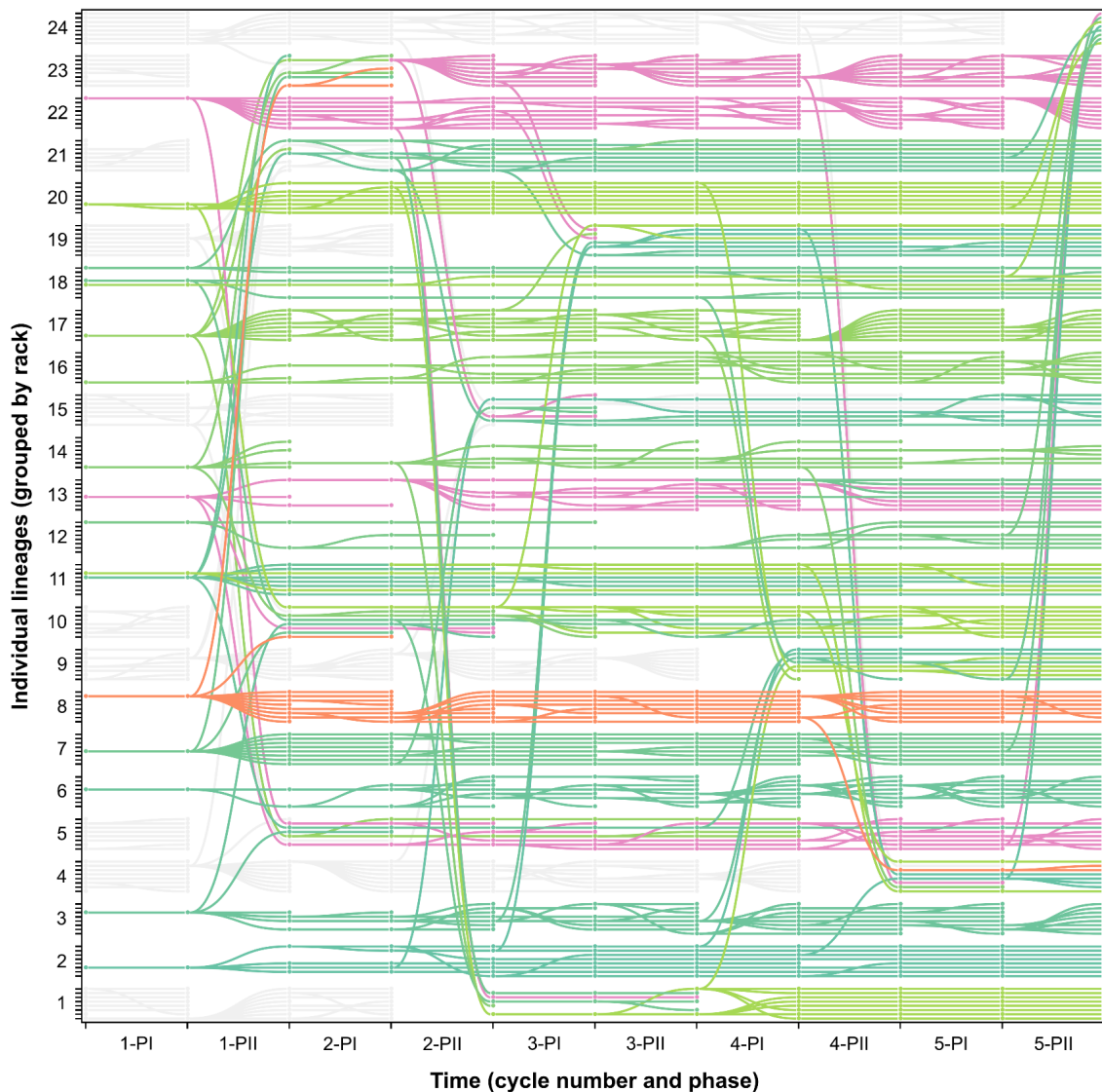


Figure 4.6. Genealogical tree of different strategies to mediate the transition through the life cycle. The parental lineages & offspring are shown for the following strategies – mutational (●), hypermutation (●) & developmental (●:● gradient based on ten genotypes); extinct racks are also shown (○). Genealogy as described in [Figure 4.1](#) legend.

4.2.2 Mutational strategy

The mutational strategy (●) was observed to be used by evolved lineages in racks 22 & 23, and some within racks 13 & 5; refer to previous [Figure 4.6](#). This strategy was associated with a high extinction rate, production of few offspring lineages, and therefore a low lineage-level fitness. For example, all final lines within rack 23 originate from the parental lineage 23.7 during cycle 2 (and 17.2 in cycle 1); at the end of cycle 5 none of the surviving lines were able to form a mat, so would require further mutation to continue through the life cycle. The evolved line 23.7 contains a total of 9 mutations in various genes, including *awsX*, *awsR*, *wspF*, *wspR*, *pflu3956* & *mwsR*; the details provided in [Table 4.1](#) below. The majority of these mutations are located within genes known to be involved in c-di-GMP signalling and regulation of the WS phenotype (McDonald et al., 2009), except for *pflu3956* that encodes a transmembrane transporter protein. Each of these mutations is expected to correspond to a single phenotypic transition during one life cycle phase, resulting in constitutive activation or inactivation (on/off) of cellulose production & mat formation. For example, mutation to the WspF methyltransferase most likely resulted in activation of the Wsp complex, synthesis of c-di-GMP by the WspR DGC & mat formation; while the mutation to WspR probably disrupted DGC activity, decreasing c-di-GMP levels, resulting in no production of cellulose but rather flagellar expression and an increase in swimming motility (Bantinaki et al., 2007; Hickman et al., 2005).

Parent lineage	Total lines	Gene name	PFLU	Putative product	Nucleotide change	Amino acid change	Protein domain	E-value
17.2	16	<i>awsX</i>	5211	hypothetical protein	468C>T	Q157*	YfiR-like	1.4e-32
c2-23.7	8	<i>awsR</i>	5210	signaling-related membrane protein	965G>T	R322L	GGDEF	1.0e-46
		<i>wspF</i>	1224	chemotaxis-specific methyltransferase	476C>T	S159L	CheB methylase	6.5e-55
		<i>wspR</i>	1225	two component system response regulator	513T>G	D171E	GGDEF	4.1e-49
		<i>pflu3956</i>	3956	transmembrane efflux pump protein	1600A>G	T534A	-	-
		<i>mwsR</i>	5329	sensory box protein, GGDEF/EAL domain	3260T>C	V1087A	EAL	1.0e-76

c3-23.3	4				2778G>A	M926I	GGDEF	4.7e-50
					2908T>C	F970L		
					2665_2670 dupTCGACC	L887_R889 dupLD		

Table 4.1. Mutational strategy line 23.7 contains a total of nine mutations. The coding sequence variation is given for evolved line 23.7, which requires mutation to transition through the life cycle. Provided for each mutation: Parent lineage (origin from cycle 1, unless stated otherwise; colour based on strategy), Total lines (number of offspring lines containing the mutation at end of cycle 5), Gene name, PFLU (link to *Pseudomonas* Genome DB entry), Putative protein product, Nucleotide sequence change, Amino acid sequence change, Protein domain the mutation is located within (link to InterPro entry), and *E*-value (Pfam database search).

The mutational strategy lineage 23.7 also displayed a very high rate of extinction, especially during the dispersal phase, in which only 12.5-25% of replicate lines survived each cycle (see [Figure 4.6](#)). This high extinction rate may be explained by the acquisition of loss-of-function mutations in genes necessary for the next phase of the life cycle, for example the cellulose synthase operon (collective phase) or flagella genes (dispersal phase). This may result in a lineage becoming ‘locked’ in either the mat-formation or motility state, thus considered an evolutionary dead end as it is unable to make the next phenotypic transition. Supporting this, Barnett (2022) often observed that extinct lines contained large deletions within the *wss* operon, this being essential for the production of cellulose and the WS phenotype (or mat formation). Furthermore, the primary mutational routes to the WS phenotype include the *Wsp*, *Aws* & *Mws* pathways; with activation of the c-di-GMP synthesising DGC enzymes (*WspR*, *AwsR* & *MwsR*) most frequently occurring by disruption of a negative regulator (*WspF*, *AwsX* or *MwsR*) (McDonald et al., 2009; Lind et al., 2015). Therefore lineages that use a mutational strategy will accumulate loss-of-function mutations in these genes over time, resulting in a reduction in the mutational target size available for activating or inactivating the WS phenotype (Barnett, 2022). Because of this, in later generations evolved lineages will become more likely to take a dead end mutational route, or else require specific rare mutations (e.g. promotor or intergenic activating mutations), or combinations of two or three mutations (Lind et al., 2015). In the evolved line 23.7, mutation to the *WspR* DGC was presumably an easy way to turn off mat formation, although it likely also prevented this pathway from being used for further phenotypic transitions. These results imply that there is a high likelihood that all lineages in rack 23 will soon go extinct if taken through further generations of the life cycle.

4.2.3 Hypermutation strategy

I also found the emergence of hypermutation (●), within lineages in the replicate rack 8; as shown in *Figure 4.6* previously. This strategy was associated with a lower extinction rate than observed for the mutational strategy, but still relatively high during the dispersal phase. In rack 8 all of the final lines may be traced back to the parental lineage 8.7, that obtained a SNP in the *mutS* (*pflu1164*) gene, that encodes the DNA mismatch repair protein MutS; mutation detailed in *Table 4.2* below. In addition, each line contained a huge amount of coding sequence variation – between 105 and 130 mutations each; the details are not provided here but are available in *Supplementary A-16*. The large number of mutations present strongly suggests that the MutS protein is inactive or unable to bind DNA, and that the mismatch repair system is failing to repair DNA replication errors (Oliver et al., 2002). Previous studies in *P. fluorescens* SBW25 report a 309-fold increase in mutation rate (genome-wide base substitutions) in the *mutS* deletion mutant as compared to the wild-type (Long et al., 2018); this is consistent with the number of mutations present in the rack 8 lineages. Use of the hypermutation strategy proved to be far more effective than the mutational, with only few extinctions occurring during the last cycle; during cycle 4-PII, hypermutator lineages from rack 8 were even able to leave offspring in the extinct rack 4. Although this strategy was successful in the short term, it is assumed to be associated with negative long-term effects (as discussed earlier in *Section 4.2*).

Parent lineage	Total lines	Gene name	PFLU	Putative product	Nucleotide change	Amino acid change	Protein domain	E-value
8.7	10	<i>mutS</i>	1164	DNA mismatch repair protein MutS	2051T>G	L684R	MutS_V	7.6e-85

Table 4.2. Hypermutation strategy in line 8.7 due to disruption of the DNA mismatch repair system. The coding sequence variation in the MMR system is given for evolved line 8.7, which uses hypermutation to transition through the life cycle. Mutation details as described in *Table 4.1* legend.

4.2.4 Developmental strategy – single mutant genotypes

More interestingly, I observed that most evolved lineages had found a mechanism for developmental regulation of the life cycle; the ten unique genotypes that I identified will subsequently be discussed in further detail. The most prevalent genotypes were those containing a single nucleotide substitution in the genes *bifA*, *awsR* or *awsX*. The genealogy of these single mutant genotypes is displayed in *Figure 4.7* below, including: *bifA*-T256S (●), *bifA*-G304S (●), *bifA*-A326V (●), *awsR*-E61D (●), *awsR*-A195V (●), and *awsX*-W60C (●).

For each of these genotypes, the parental lineage must have obtained the respective mutation during the first phase of the first cycle (to allow for formation of a mat); with most of these lineages then fixing within their rack, and leaving a large number of offspring – corresponding to a high lineage-level fitness.

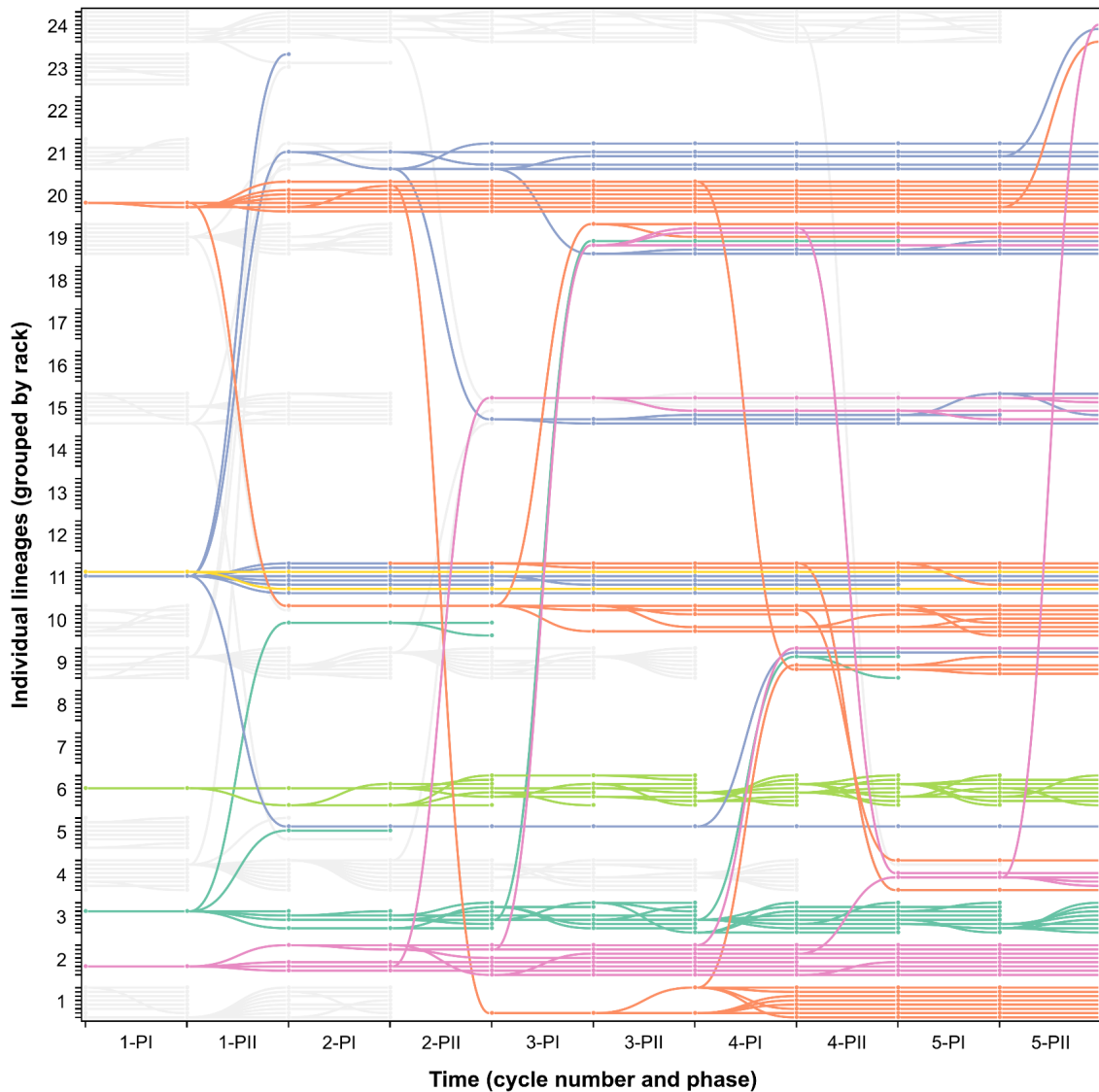


Figure 4.7. Developmental strategy lineages with single mutations in *bifA*, *awsR* or *awsX* dominate. The parental lineages & offspring are shown for the following single mutant genotypes: *bifA*-T256S (●), *bifA*-G304S (●), *bifA*-A326V (●), *awsR*-E61D (●), *awsR*-A195V (●), and *awsX*-W60C (●); extinct racks are also shown (○). Genealogy as described in [Figure 4.1](#) legend.

4.2.4.1 *bifA* mutations

I found that in three independent racks, lineages acquired a single mutation in the *bifA* gene that conferred developmental regulation of the life cycle. These include the single mutant

genotypes *bifA*-T256S in rack 3, *bifA*-G304S in rack 6, and *bifA*-A326V in rack 11; the detail of each mutation is provided in *Table 4.3* below. Notably, BifA mutants were not identified in previous iterations of the life cycle experiment, as despite their capacity to form a mat in static broth they always display the SM phenotype on agar plates. In rack 3, the *bifA*-T256S (●) mutation originated from the parental lineage 3.6, and managed to fix within the rack; although a high rate of extinction was observed for offspring lineages (refer to *Figure 4.7*). A similar trend was observed for *bifA*-G304S (●) in rack 6, originating from the parental lineage 6.5. For these two *bifA* mutants, most extinctions occurred during the collective phase (see cycle 4-PI), as a result of forming mats with poor structural integrity and failure during the mat-formation screen. The low lineage-level fitness is also demonstrated by the inability of the *bifA*-T256S genotype to leave offspring lineages in extinct racks, losing to lineages from other racks in all of the given opportunities of inter-rack competition (see cycle 1-PII, 3-PI & 4-PI). While in rack 11, the *bifA*-A326V (●) mutation was acquired by the parental lineage 11.5, and displayed a far lower extinction rate during the experiment. This lineage left a total of 17 offspring, able to spread from rack 11 into the extinct racks 5, 9, 15, 19, 21 & 24 (see *Figure 4.7*). The *bifA*-A326V mutation appears to have a much higher lineage fitness, resulting from the capacity to form more stable mats that are less prone to falling; though it is unclear how this genotype differs from the other two *bifA* mutant genotypes.

Parent lineage	Total lines	Gene name	PFLU	Putative product	Nucleotide change	Amino acid change	Protein domain	<i>E</i> -value
3.6	8	<i>bifA</i>	4858	signaling protein	767C>G	T256S	GGDEF	7.2e-36
6.5	8				910G>A	G304S		
11.5	17				977C>T	A326V		

Table 4.3. Single mutations in *bifA* allow for developmental regulation in three independent racks. The coding sequence variation is given for the *bifA* mutant genotypes (evolved lines 3.3, 6.3 & 11.5), conferring developmental regulation of the life cycle. Mutation details as described in *Table 4.1* legend.

The *bifA* mutant genotypes provide a striking example of mutational parallelism across replicate racks during the experiment. Lineages from the three independent racks 3, 6 & 11, all acquired a single amino acid substitution in nearby residues in BifA – T256S, G304S & A326V, respectively. *bifA* ([pflu4858](#)) encodes the putative signalling protein BifA (length: 683 amino acids), predicted to localise in the cytoplasmic membrane, and with 81.6% sequence identity to BifA in *P. aeruginosa* PAO1 ([PA4367](#); BLASTP *E*-value: 0.0). The dual-domain protein BifA contains a GGDEF-like domain ([PF00990](#); residue: 250-407;

E-value: $7.2e-36$) and EAL domain ([PF00563](#); residue: 427-662; *E*-value: $2.7e-76$), so may have the associated function of a diguanylate cyclase (DGC) or phosphodiesterase (PDE) enzyme. Although DGC enzymatic activity requires the conserved GG(D/E)EF motif constituting the catalytic active site, while BifA contains the degenerate GGDQF domain, so is unlikely functioning in the synthesis of c-di-GMP (Hengge, 2009; Christen et al., 2006). The conserved EAL motif remains intact, and BifA has previously been demonstrated in *P. aeruginosa* to have PDE enzymatic activity in the degradation of intracellular c-di-GMP; this dependent on conservation of both the GGDQF and EAL motifs (Kuchma et al., 2007). In *P. aeruginosa* PA14, deletion of the *bifA* gene was observed to result in overactivation of biofilm formation, as well as a major defect in swarming motility (Kuchma et al., 2007). Consistent with this, in *P. fluorescens* SBW25 the depletion of BifA using CRISPR interference resulted in a reduction in swarming, and the formation of a thick biofilm with clumping producing a 3D structured architecture (Noirot-Gros et al., 2019). The upregulation of BifA was also observed in SBW25 grown in the plant rhizosphere environment, with *bifA* mutants demonstrating an enhanced root attachment ability (Little et al., 2019).

In the LCE evolved lineages, the identified BifA mutations (T256S, G304S & A326V) are all localised within the GGDEF-like domain. The behaviour of these lineages indicates that the mutations are unlikely to result in complete loss of PDE function – only an unstable mat is formed (no constitutive activation of the WS phenotype), and no reduction to swimming motility; while deletion mutants display the hyper-biofilm phenotype and reduced swarming capacity (Little et al., 2019; Noirot-Gros et al., 2019). The observed *bifA* mutations in the inactive GGDEF domain could rather be altering the way in which BifA interacts with an environmental signal, and responds with the PDE activity of breaking down c-di-GMP (Hengge, 2009). In *Caulobacter crescentus*, a GGDEF/EAL dual-domain protein was identified that controls PDE activity by the binding of GTP to the degenerate GGDEF motif (Christen et al., 2005); a similar form of regulation may be possible in SBW25. Further work is required to figure out exactly how these *bifA* mutations allow for developmental regulation of the life cycle.

4.2.4.2 *awsR* & *awsX* mutations

The most successful lineages in the experiment contained a single mutation in the genes *awsR* or *awsX*, including *awsR*-E61D in rack 20, *awsR*-A195V in rack 11, and *awsX*-W60C in rack 2; these mutations are detailed in *Table 4.4* below. The *awsR*-E61D (●) mutation originated in

the parental lineage 20.3 during the first cycle, and managed to rapidly fix within rack 20 (by cycle 2-PII), as well as in the extinct racks 1 & 10. This genotype demonstrated the highest lineage-level fitness, leaving a total of 36 offspring by the end of cycle 5 (Note: minor inconsistency with presence in rack 11, likely a contamination error when replacing lineage 11.8 during cycle 2). Another independent *awsR* single mutant genotype was identified in rack 11, with the *awsR*-A195V (●) mutation acquired by lineage 11.6; although this mutation did not fix within the rack due to competition with other high fitness lineages (see [Figure 4.7](#)). While in rack 2, the *awsX*-W60C (●) mutation originated in the parental lineage 2.3, managing to reach fixation in the rack and spread to a number of extinct racks – leaving a total of 21 offspring at the end of the experiment. These *awsR* & *awsX* single mutant genotypes displayed a very low rate of extinction in the experiment, with almost no extinction of offspring lineages observed. How exactly these mutations confer developmental regulation of the life cycle requires further investigation.

Parent lineage	Total lines	Gene name	PFLU	Putative product	Nucleotide change	Amino acid change	Protein domain	E-value
20.3	36	<i>awsR</i>	5210	signaling-related membrane protein	183A>T	E61D	CHASE8	1.3e-28
11.6	2				584C>T	A195V	HAMP	1.3e-4
2.3	21	<i>awsX</i>	5211	hypothetical protein	180G>C	W60C	YfiR-like	1.4e-32

Table 4.4. Single mutations in *awsR* or *awsX* confer developmental regulation. The coding sequence variation is given for the *awsR* (evolved lines 20.3 & 11.6) & *awsX* (evolved line 2.1) mutant genotypes, conferring developmental regulation of the life cycle. Mutation details as described in [Table 4.1](#) legend.

The *awsR* ([pflu5210](#)) gene was previously discussed in [Section 1.3.2.2](#); similar mutations were also observed in AwsR during the LCE trial – A40S, A62S & I56S (refer to [Section 3.5.2.2](#)). AwsR contains a CHASE8 sensor domain (residue 41-142), and GGDEF domain (residue 245-398) with an intact catalytic motif. In *P. aeruginosa*, the ortholog YfiN has been shown to function as a membrane-bound DGC enzyme in the synthesis of c-di-GMP, under the control of the small periplasmic protein YfiN (ortholog of AwsX) (Ueda & Wood, 2009; Malone et al., 2010, 2012). *awsX* ([pflu5211](#)) encodes the hypothetical protein AwsX (length: 190 amino acids), with 52.6% sequence identity to YfiR ([PA1121](#)) in *P. aeruginosa* PAO1 (BLASTP; E-value: 2e-61), and contains a YfiR-like domain (PF13689; residue: 45-184; E-value: 1.4e-32) of unknown function. In SBW25, McDonald et al. (2009) demonstrated that AwsX acts as a negative regulator of the AwsR DGC enzyme; disruption to AwsX was observed to result in constitutive activation of AwsR, and therefore the WS phenotype.

The *awsR* mutations identified in LCE evolved lineages are most likely to result in activation of the DGC activity of AwsR, as they allow for the formation of a mat in static broth; similar activating mutations have been previously observed (McDonald et al., 2009; Lind et al., 2017). The *awsR*-E61D single mutant genotype contains the substitution E61D in the CHASE8 sensor domain of AwsR; mutation of the neighbouring residue (A62S) was observed during the LCE trial. In *P. aeruginosa* PAO1, Malone et al. (2012) carried out an extensive screen for mutations in *yfiN* that activate the small colony variant (SCV) phenotype; these mutations were localised in the N-terminal of the PAS domain (residues 51-87), C-terminal of the HAMP domain (residues 204-232), and specific residues of the transmembrane helices. Furthermore, the majority of these mutations were observed to no longer bind to the YfiR repressor, indicating that the YfiN protein had changed conformation to an active state in which binding of the repressor was blocked (Malone et al., 2012). Based on this, Malone et al. (2012) proposed the highly conserved ‘AAVVF’ motif (residues 66-70) in the PAS periplasmic sensor domain of YfiN as a potential binding site of YfiR. Remarkably, the *awsR*-E61D mutant that I identified has alteration of the residue adjacent to this motif (E/D-AAVVF) in AwsR; this may modify the binding of the AwsX repressor and therefore the DGC activity of AwsR. While the *awsR*-195V mutant genotype contains the substitution A195V in the HAMP domain, also resulting in activation of the AwsR DGC, though exactly how is unclear.

The *awsX*-W60C mutant genotype contains the substitution W60C in the YfiR-like domain of AwsX. Previous studies of the YfiB_{NR} system in *P. aeruginosa* PAO1 have shown that the periplasmic YfiR protein allosterically inhibits the DGC activity of YfiN by binding to the PAS domain, this repression released by the sequestration of YfiR by the YfiB lipoprotein in the outer membrane (Malone et al., 2012; Giardina et al., 2013). Malone et al. (2012) also provided evidence that YfiN may be activated in response to the redox state of the periplasm (independently of YfiB), due to misfolding of the YfiR protein. Investigation of the YfiR crystal structure revealed the importance of the Cys145-Cys152 disulfide bond, with formation of the Cys71-Cys110 disulfide bond observed under oxidative conditions (Yang et al., 2015). The *awsX*-W60C genotype evolved during the LCE must result in some level of activation of the AwsR DGC, though it differs in phenotype from the *yfiN* deletion mutant in PAO1 that displays severe impairment to swimming motility (Malone et al., 2010). Mutations that compensate for *yfiN* activating mutants were observed within the C-terminal region of YfiR and nearby residues of the conserved region (including R60H & K63E), these mutations

were found to restore interaction between YfiN and YfiR (Malone et al., 2012). Therefore the substitution W60C in AwsX, rather than causing constitutive activation of AwsR, may also alter the interaction between the AwsX repressor and AwsR DGC. It is also possible that the *awsR* & *awsX* mutant genotypes may have the capacity to adjust this AwsR-AwsX interaction in response to the environment. This may be mediated by response of the membrane-localised lipoprotein AwsO (*pflu5209*; YfiB ortholog) to external signals (e.g. cell wall stress), or periplasmic AwsX to reducing/oxidising conditions.

4.2.5 Developmental strategy – double & triple mutant genotypes

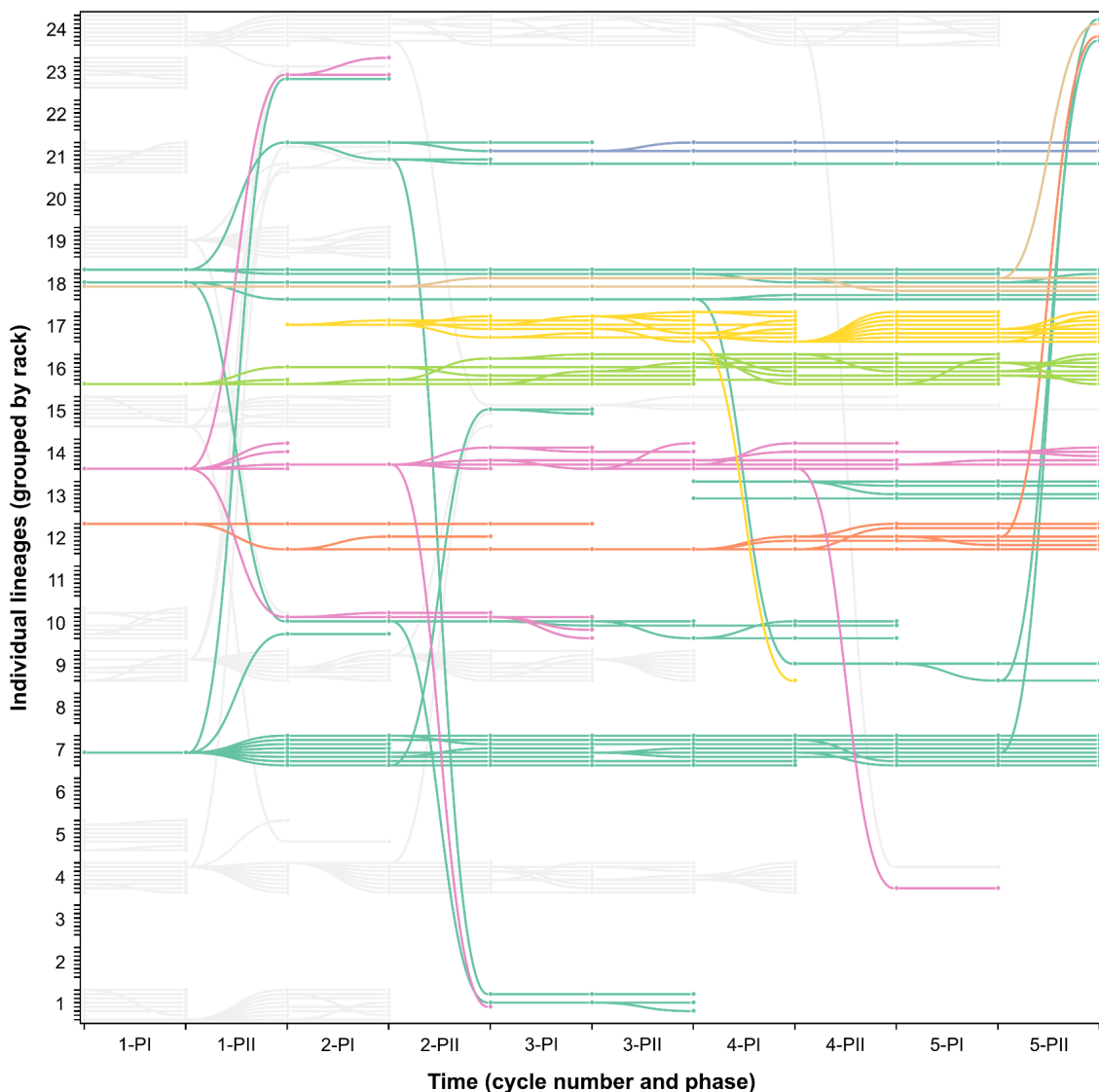


Figure 4.8. Developmental strategy lineages with a combination of mutations in two or three genes. The parental lineages & offspring are shown for the following double/triple mutant genotypes: *awsR-pflu0956* (●), *awsR-mwsR* (●), *awsR-mwsR-dipA* (●), *awsX-awsR-mwsR* (●), *sadB-awsX* (●), *sadB-awsR* (●), and *pflu0185-wspA* (●); extinct racks are also shown (○). Genealogy as described in [Figure 4.1](#) legend.

I also identified a number of lineages with developmental regulation of the life cycle resulting from combinations of mutations in two or three genes. These include the mutant genotypes of *awsR-pflu0956* (●), *awsR-mwsR* (●), *awsR-mwsR-dipA* (●), *awsX-awsR-mwsR* (●), *sadB-awsX* (●), *sadB-awsR* (●) & *pflu0185-wspA* (●); the genealogy of each is displayed in *Figure 4.8* above. In comparison to the single mutant genotypes, the double & triple mutants were not as successful, producing fewer offspring lineages over five life cycle generations. This may be explained by these genotypes having a lower lineage-level fitness, or as a result of having fewer opportunities to reproduce, as it took a longer time to obtain the necessary combination of mutations for developmental regulation of the life cycle. While the single mutants obtained the required mutation during the first cycle, and therefore were quickly able to reach fixation within their rack, as well as leave offspring in other extinct racks (refer to previous *Figure 4.7*).

4.2.5.1 *awsR-pflu0956* mutant

In rack 14, the *awsR-pflu0956* (●) mutant genotype originated from the parental lineage 14.1, and displays a high rate of extinction, corresponding to a low lineage-level fitness (see *Figure 4.8*). This lineage also performed poorly during all inter-rack competitions, outcompeted each time by evolved lineages from other racks (see cycle 1-P11, 2-P11 & 4-P11). The *awsR-pflu0956* genotype contains two mutations in the *awsR* gene and one in *pflu0956*, the details provided in *Table 4.5* below. *awsR* ([pflu5210](#)) encodes the signalling protein AwsR, that functions as a DGC enzyme in the synthesis of c-di-GMP, under negative regulation by the AwsX repressor (McDonald et al., 2009); refer to previous discussion in *Section 1.3.2.2* & *4.2.4.2*. Interestingly, this genotype contains the substitution A63V in the ‘AAVVF’ motif of AwsR, which has been predicted as the binding site for AwsX (Malone et al., 2012); this mutation is very similar to the substitution E61D identified in rack 20 (see *Section 4.2.4.2*). Although the subsequent frameshift mutation in the GGDEF domain of AwsR (L267fs) likely resulted in production of a non-functional DGC enzyme.

Parent lineage	Total lines	Gene name	PFLU	Putative product	Nucleotide change	Amino acid change	Protein domain	E-value
14.1	5	<i>awsR</i>	5210	signaling-related membrane protein	188C>T	A63V	CHASE8	1.3e-28
					801_805dup TGCGC	L267fs	GGDEF	1.0e-46
		<i>pflu0956</i>	0956	hypothetical protein	124A>T	S42C	Cache	1.2e-12

Table 4.5. Mutations present in evolved *awsR-pflu0956* mutant genotype. The coding sequence variation is given for the *awsR-pflu0956* genotype (evolved line 14.2), conferring developmental regulation of the life cycle. Mutation details as described in [Table 4.1](#) legend.

[pflu0956](#) encodes the hypothetical protein Pflu0956 (length: 497 amino acids), with predicted localisation in the inner membrane, and 62.3% sequence identity shared with GcbC in *P. fluorescens* Pf0-1 ([PF101_4666](#); BLASTP; *E*-value: 0.0). Pflu0956 contains a GGDEF domain ([PF00990](#); residue: 332-490; *E*-value: $2.5e-48$) with an intact GGEEF motif, and a double Cache domain ([PF02743](#); residue: 42-278; *E*-value: $1.2e-12$). In *P. fluorescens* Pf0-1, GcbC has been shown to function as a DGC enzyme; deletion of *gcbC* was found to cause a decrease in biofilm formation and increased swimming motility distance (Newell et al., 2011). Lind et al. (2015) also observed the WS phenotype as a result of activating mutations in the promoter region of *pflu0956* (54-57 bp upstream). For the evolved *awsR-pflu0956* mutant genotype, the substitution S42C in Pflu0956 is located within the first residue of the double Cache domain; this extracellular sensory domain is predicted to function as a receptor in the binding of small molecules (Anantharaman & Aravind, 2000; Randal et al., 2022). Giacalone et al. (2015) found in *P. fluorescens* Pf0-1, that presence of the organic acid citrate enhances biofilm formation, dependent on the presence of GcbC and the Cache domain ‘RXYF’ motif (specifically residue R139). Therefore the mutation in the sensory domain of Pflu0956 may alter the binding of a ligand from the environment (e.g. an amino acid or sugar), and the corresponding Pflu0956 DGC activity (Randal et al., 2022). Such a mechanism could allow the *awsR-pflu0956* genotype to regulate the phenotypic states of the life cycle in response to the environment; though it is unclear whether the *awsR* mutations are also required.

4.2.5.2 *awsR-mwsR* mutants

The *awsR-mwsR* (●) double mutant genotype evolved in a number of independent lineages, within racks 7, 13 & 18 (see [Figure 4.8](#)). This genotype displays a mid-range lineage fitness, only reaching fixation within rack 7, and with a number of extinctions occurring during the dispersal phase. These lineages also had a relatively poor performance during inter-rack competition, and in most cases were unable to leave offspring in extinct racks; this perhaps indicates that they were initially transitioning through the life cycle by mutation. The *awsR-mwsR* genotypes contain different combinations of mutations in the *awsR* and *mwsR* genes, detailed in [Table 4.6](#) below. In rack 7, the parental lineage 7.4 first acquired the substitution M926I in the GGDEF domain of MwsR; the offspring lineages then obtained a

second nearby substitution in MwsR (S975R or H899Q), as well as a single mutation in AwsR (D68E, H193R or A195V). In rack 13, the lineage 13.4 first obtained the substitution R54L in the CHASE8 sensor domain of AwsR, followed by the substitution D895N in the GGDEF domain of MwsR and the nonsense mutation S615* in MwsR. While in rack 18, during cycle 1 the parental lineages 18.5/18.8 acquired the substitution T27P in AwsR; and the offspring lineages then obtained either two mutations in MwsR (W794R & M1157I), or the substitutions M724I in MwsR and E89Q in AwsR. These different combinations of mutations in AwsR & MwsR all conferred developmental regulation of the life cycle; the observation of multiple mutational routes implies that there is some redundancy in the function of these two proteins.

Parent lineage	Total lines	Gene name	PFLU	Putative product	Nucleotide change	Amino acid change	Protein domain	E-value
18.5/8	11	<i>awsR</i>	5210	signaling- related membrane protein	79A>C	T27P	-	-
13.4	16				161G>T	R54L	CHASE8	1.3e-28
c2-7.4	5				204C>G	D68E		
c2-18.7	2				265G>C	E89Q		
c2-7.7	2				578A>G	H193R	HAMP	1.3e-4
c2-7.8	2				584C>T	A195V		
c3-13.8	3	<i>mwsR</i>	5329	sensory box protein, GGDEF/EAL domain	1844C>A	S615*	PAS	2.5e-16
c2-18.7	2				2172G>A	M724I		
c2-18.1	5				2380T>A	W794R		
c2-13.8	8				2683G>A	D895N	GGDEF	4.7e-50
c2-7.7/8	4				2697C>A	H899Q		
7.4	9				2778G>A	M926I		
c2-7.4	5				2925T>A	S975R		
c2-18.1	5				3471G>A	M1157I	EAL	1.0e-76

Table 4.6. Mutations present in evolved *awsR-mwsR* mutant genotypes. The coding sequence variation is given for the *awsR-mwsR* mutant genotypes (evolved lines 7.5, 7.7, 7.8, 13.5, 18.1 & 18.5), conferring developmental regulation of the life cycle. Mutation details as described in [Table 4.1](#) legend.

awsR ([pflu5210](#)) encodes the DGC enzyme AwsR (McDonald et al., 2009), as detailed in [Section 1.3.2.2](#) & [4.2.4.2](#). The *mwsR* ([pflu5329](#)) gene was also previously discussed in [Section 1.3.2.3](#), encoding the large dual-function DGC & PDE enzyme MwsR (Phippen et al., 2014; McDonald et al., 2009). MwsR contains both a GGDEF domain (residue: 848-1009) & EAL domain (residue: 1029-1264) with intact catalytic motifs, as well as a PAS fold (residue: 478-569) & two PAS sensory domains. In *P. aeruginosa*, the ortholog MorA was shown to

regulate motility & biofilm formation, with the capacity for both synthesis and degradation of c-di-GMP (Choy et al., 2004; Phippen et al., 2014). For the various independently evolved *awsR-mwsR* mutant genotypes, the effect of each mutation is unclear. It is possible that the first two mutations acquired (e.g. *mwsR*-M926I & S975R in evolved line 7.5) simply resulted in activation & inactivation of the AwsR or MwsR DGC, thus turning on/off mat formation for the phenotypic transition. Therefore it may be only the mutations obtained later (e.g. *awsR*-D68E in evolved line 7.5) that allowed for developmental regulation of the life cycle; genetic dissection of each genotype would be required to confirm exactly which mutations are necessary.

4.2.5.3 *awsR-mwsR-dipA* mutant

In rack 21, the *awsR-mwsR-dipA* (●) mutant genotype diverged from rack 18 during cycle 1-PII (see [Figure 4.8](#)); the parental lineage 18.8 first obtaining the substitution T27P in AwsR, and T997S in the GGDEF domain of MwsR. During cycle 2, the parental lineage 21.8 then acquired the substitution M1L in the first residue of MwsR, followed by lineage 21.6 obtaining a *dipA* mutation from cycle 3 onwards; each mutation is detailed in [Table 4.7](#) below. The *awsR-mwsR-dipA* genotype demonstrates a high lineage-level fitness, with no extinction occurring after the origin in cycle 3; although due to competition with other lineages in rack 21, this genotype was not given the opportunity to produce more offspring or spread to other extinct racks.

Parent lineage	Total lines	Gene name	PFLU	Putative product	Nucleotide change	Amino acid change	Protein domain	E-value
18.8	11	<i>awsR</i>	5210	signaling- related membrane protein	79A>C	T27P	-	-
18.8	4	<i>mwsR</i>	5329	sensory box protein, GGDEF/EAL domain	2990C>G	T997S	GGDEF	4.7e-50
c2-21.8	2				3G>A	M1L	-	-
c3-21.6	2	<i>dipA</i>	0458	hypothetical protein	1399T>A	Y467N	GGDEF	1.0e-38

Table 4.7. Mutations present in evolved *awsR-mwsR-dipA* mutant genotype. The coding sequence variation is given for the *awsR-mwsR-dipA* mutant genotype (evolved line 21.6), conferring developmental regulation of the life cycle. Mutation details as described in [Table 4.1](#) legend.

The effect of the first two mutations in *awsR* & *mwsR* are not obvious (as detailed in [Section 4.2.5.2](#)). Although if this lineage was indeed initially proceeding through the life cycle using a mutational strategy, then these likely correspond to the turning on/off of mat formation; for example, the *awsR*-T27P mutation may have activated the DGC activity of AwsR, and the

mwsR-T997S mutation caused an increase in the PDE activity of MwsR. Interestingly, the second mutation in MwsR is synonymous, and results in alteration of the translation start codon leucine (DNA: TTG→TTA; mRNA: UUG→UUA). In prokaryotes, translation initiation may be achieved from a number of alternative codons; an extensive analysis of bacterial genomes found that the start codons AUG, GUG & UUG are utilised for 80.1%, 11.6% & 7.8% of annotated genes, respectively (Villegas & Kropinski, 2008). For the evolved *awsR-mwsR-dipA* genotype, it is not evident whether the UUA codon (replacing UUG) may initiate translation of the MwsR protein. The observation of such a specific mutation in *mwsR* (rather than any other disruptive mutation), does imply that it has a particular effect on MwsR function, and is not simply a loss-of-function mutation. Hecht et al. (2017) demonstrated in *E. coli* that translation initiation was possible from a number of non-cognate start codons (including UUA), with protein expression observed of 0.007 to 3%, relative to the cognate AUG codon. Therefore MwsR may still be translated at low levels with the UUA start codon.

In *P. aeruginosa*, the high guanine & cystine (GC) content of the genome (~67.2%) corresponds with strong bias in synonymous codon usage (West & Iglewski, 1988). For the amino acid leucine (Leu), the codons UUG & UUA are rarely observed, with a relative synonymous codon usage (RSCU) of 0.42 & 0.01, respectively (across 5548 genes) (Grocock & Sharp, 2002). In the SBW25 genome, Leu is preferentially encoded by the CTG codon (57.7% across all genes), while the codon TTG is used 19.5% of the time, and TTA only 1.8% (statistics obtained using Geneious Prime). Codon usage bias may reflect the availability of transfer RNAs (tRNAs) in the cytoplasmic pool, with preference for the codon that is recognised by the most abundant tRNA anticodon (Ikemura, 1981). Furthermore, Dong et al. (1996) determined in *E. coli* that tRNA abundance is optimised for maximal translation efficiency during exponential growth – the major tRNAs (common codons) increase in concentration as growth rate increases, while the abundance remains relatively unchanged for low concentration tRNAs (rare codons) (Grocock & Sharp, 2002). Dittmar et al. (2005) also observed selective charging (amino acid attachment) of rare codon tRNAs under amino acid starvation conditions, with the tRNA^{Leu} isoacceptor for the UUG & UUA/G codons remaining ~20% charged after leucine starvation, compared to the common CUG codon that was only 2-9% charged. Therefore for the *awsR-mwsR-dipA* genotype, the synonymous *mwsR* mutation may also cause differential expression of the MwsR PDE/DGC depending on environmental conditions. For example, when leucine is limited this could

result in preferential aminoacylation of tRNAs for the rare UUA codon, and therefore an increase in translation initiation of the MwsR protein (Dittmar et al., 2005).

While *dipA* ([pflu0458](#)) encodes the hypothetical protein DipA, with predicted function as a membrane-bound PDE enzyme in the degradation of c-di-GMP (Roy et al., 2012), as earlier discussed in [Section 2.3.2](#). The DipA protein contains a degenerate GGDEF domain (residue: 466-619), EAL domain (residue: 640-875) with an intact enzymatic motif, as well as a GAF regulatory domain (residue: 193-328) & PAS sensor domain (residue: 352-454). For the *awsR-mwsR-dipA* mutant genotype, the substitution Y467N is located at the start of the inactive GGDEF domain of DipA. This mutation may have a similar effect to that predicted for the *bifA* mutation (see [Section 4.2.4.1](#)), altering the PDE activity of DipA in response to the environment; this is also supported by the presence of a PAS sensory domain in DipA. In *P. aeruginosa*, Roy et al. (2012) showed that DipA was essential for nutrient-induced dispersion (by addition of glutamate, ammonium chloride or nitric oxide). Mattingly et al. (2018) also demonstrated that the DipA PDE is required for flagella-based motility in minimal medium, but not rich medium (e.g. LB). Therefore the *awsR-mwsR-dipA* genotype may allow for developmental regulation of the life cycle by modulating the activities of both the DipA PDE and MwsR PDE/DGC; though further work would be required to disentangle the contribution of each individual mutation.

4.2.5.4 *awsX-awsR-mwsR* mutant

The *awsX-awsR-mwsR* (●) triple mutant genotype originated in rack 17 (see [Figure 4.8](#)), with the parental lineage 17.2 first acquiring the nonsense mutation Q157* in AwsX. From cycle 2 onwards, the lineage 17.5 then obtained a number of mutations in AwsR (A192V & D214G) and MwsR (E795K & Q876*); the details provided in [Table 4.8](#) below. This lineage displayed a high extinction rate throughout the experiment, with rack 17 almost going extinct during cycle 4-PII (only one surviving line), therefore corresponding to a low lineage-level fitness. It is unclear which of the five mutations were necessary for the *awsX-awsR-mwsR* genotype and regulation of the life cycle, as this lineage likely used mutation for the early phenotypic transitions. The stop codon mutations in AwsX & MwsR are expected to result in non-functional proteins, and disruption to the AwsX repressor resulting in activation of the AwsR DGC (McDonald et al., 2009). The substitution A192V in AwsR shows strong similarity to the *awsR-A195V* single mutant genotype (see [Section 4.2.4.2](#)); although the effect of these two mutations in the HAMP domain of AwsR is unknown.

Parent lineage	Total lines	Gene name	PFLU	Putative product	Nucleotide change	Amino acid change	Protein domain	E-value
17.2	16	<i>awsX</i>	5211	hypothetical protein	468C>T	Q157*	YfiR-like	1.4e-32
c2-17.5	8	<i>awsR</i>	5210	signaling- related membrane protein	575C>T	A192V	HAMP	1.3e-4
					641A>G	D214G		
		<i>mwsR</i>	5329	sensory box protein, GGDEF/EAL domain	2383G>A	E795K	PAS	2.5e-16
					2626C>T	Q876*	GGDEF	4.7e-50

Table 4.8. Mutations present in evolved *awsX-awsR-mwsR* mutant genotype. The coding sequence variation is given for the *awsX-awsR-mwsR* mutant genotype (evolved line 17.1), conferring developmental regulation of the life cycle. Mutation details as described in [Table 4.1](#) legend.

4.2.5.5 *sadB-awsX* & *sadB-awsR* mutants

I identified combinations of mutations in *sadB* & *awsX* or *awsR* in two independent racks, that conferred developmental regulation of the life cycle. The *sadB-awsX* (●) mutant genotype originated in the parental lineage 12.8, and managed to fix within rack 12 (excluding line 12.6) over five life cycle generations (see [Figure 4.8](#)). This lineage had a relatively low extinction rate, but was by chance not given the opportunity to leave offspring in extinct racks. While the *sadB-awsR* (●) genotype emerged in rack 18 from the parental lineage 18.4, and although it displayed a high lineage-level fitness (no extinctions occurring) it was only able to leave four offspring lineages due to competition within the rack. The mutations underpinning these two genotypes are detailed in [Table 4.9](#) below.

Parent lineage	Total lines	Gene name	PFLU	Putative product	Nucleotide change	Amino acid change	Protein domain	E-value
12.8	7	<i>awsX</i>	5211	hypothetical protein	166A>T	S56C	YfiR-like	1.4e-32
		<i>sadB</i>	6004	hypothetical protein	706G>C	A236P	HDOD	1.3e-46
938_944dup AGCGCCC	P313fs							
18.4	4	<i>awsR</i>	5210	signaling-related membrane protein	235_237delAAT	I79del	CHASE8	1.3e-28

Table 4.9. Mutations present in evolved *sadB-awsX* & *sadB-awsR* mutant genotypes. The coding sequence variation is given for the *sadB-awsX* (evolved line 12.2) & *sadB-awsR* (evolved line 18.4) mutant genotypes, conferring developmental regulation of the life cycle. Mutation details as described in [Table 4.1](#) legend.

sadB ([pflu6004](#)) encodes the hypothetical protein SadB (length: 466 amino acids), predicted to localise in cytoplasm, with 74.7% sequence identity to SadB in *P. aeruginosa* PAO1 ([PA5346](#); BLASTP *E*-value: 0.0). SadB contains a YbaK-like aminoacyl-tRNA synthetase domain ([PF04073](#); residue: 29-140; *E*-value: 2.9e-14), and HDOD signal output domain

([PF08668](#); residue: 194-394; *E*-value: $1.3e-46$). In *P. aeruginosa*, SadB was shown to be necessary for surface attachment during biofilm formation, with high protein levels observed for cells grown in arginine-supplemented minimal medium that promotes biofilm production (but not glucose) (Caiazza & O'Toole, 2004). Caiazza et al. (2005) also found that SadB functions in the modulation of swarming motility in response to rhamnolipid surfactants; with *sadB* mutants displaying both defects in biofilm structure, and an altered swarming phenotype with broader tendrils. Caiazza et al. (2007) propose that SadB inversely regulates biofilm formation & swarming motility upon attachment to a solid surface, by controlling production of the Pel exopolysaccharide, and the rate of flagellar reversals through the chemotaxis cluster IV (including PilJ & ChpB). The function of SadB has also been linked to sensing of intracellular c-di-GMP, and the corresponding activity of the upstream BifA PDE and SadC DGC enzymes (Kuchma et al., 2007; Merritt et al., 2007). Furthermore, in *P. fluorescens* F113, it was shown that SadB inhibits swimming motility & flagella synthesis by repressing transcription of the *fleQ* gene (through the AlgU-AmrZ pathway), predicted to be in response to high c-di-GMP levels (Navazo et al., 2009; Martínez-Granero et al., 2012). In a recent study, Muriel et al. (2019) demonstrated the binding of c-di-GMP to the SadB protein, presumed to occur at the C-terminal HDOD domain. Therefore SadB likely has a similar function in SBW25, binding c-di-GMP synthesised by a DGC enzyme, and responding with the activation of mat formation (e.g. by the Wss cellulose synthase pathway) and inhibition of flagella expression.

For the *sadB-awsX* mutant genotype, the substitution S56C in AwsX likely altered the interaction between the AwsX repressor & AwsR, causing activation of c-di-GMP synthesis by the AwsR DGC enzyme; this mutation is similar to that observed for the *awsX-W60C* single mutant genotype (refer to [Section 4.2.4.2](#)). The substitution A236P in the HDOD domain of SadB may have changed the binding affinity for c-di-GMP, therefore altering the regulation of mat formation & motility. It is also possible that the activity of SadB is responsive to environmental conditions, with an increased expression observed in *P. aeruginosa* during the formation of a biofilm in minimal arginine medium (Caiazza & O'Toole, 2004). While for the *sadB-awsR* mutant genotype, the small in-frame deletion (I79del) in the CHASE8 sensor domain of AwsR may have also adjusted the interaction with the AwsX repressor; with similarity to other identified mutations in *awsR* (see [Section 4.2.4.2](#) & [4.2.5.2](#)). The frame-shift mutation (P313fs) in the HDOD domain of SadB is expected to result in disruption of protein function, and therefore loss of the regulation of biofilm

formation & motility by SadB. For both *sadB* mutant genotypes, recreation of each mutation would reveal how they allow for developmental regulation of the life cycle.

4.2.5.6 *pflu0185-wspA* mutant

In rack 16, the *pflu0185-wspA* (●) mutant genotype originated from the parental lineage 16.1, and was able to reach fixation in the rack, though displaying a relatively high extinction rate throughout the experiment (see [Figure 4.8](#)). This lineage obtained two mutations in *pflu0185*, and one in *wspA*, as detailed in [Table 4.10](#) below. The *wspA* gene ([pflu1219](#)) was extensively discussed in [Section 2.3.1](#), encoding the WspA MCP that functions as the receptor of the Wsp signalling pathway, predicted to sense an environmental signal associated with cell envelope stress (Bantinaki et al., 2007; O’Neal et al., 2022). For the *pflu0185-wspA* mutant genotype, the substitution A381T in the MCP signalling domain of WspA may alter the interaction with the WspE kinase, this located five residues upstream of the predicted adaptor/kinase binding site (LLSxxxxIExEK) (Ortega et al., 2017). Though the effect of this together with mutations in Pflu0185 is unclear; I previously only identified mutations in the WspA MCP in combination with disruption of the WspF methyltransferase (refer to [Section 2.6](#) & [3.5.2.2](#)).

Parent lineage	Total lines	Gene name	PFLU	Putative product	Nucleotide change	Amino acid change	Protein domain	E-value
16.1	8	<i>pflu0185</i>	0185	sensory box protein, GGDEF/EAL domain	205T>C	W69R	-	-
					1388C>T	A463V	EAL	4.0e-76
		<i>wspA</i>	1219	methyl-accepting chemotaxis protein	1142C>T	A381T	MCPsignal	5.0e-34

Table 4.10. Mutations present in evolved *pflu0185-wspA* mutant genotype. The coding sequence variation is given for the *pflu0185-wspA* mutant genotype (evolved line 16.6), conferring developmental regulation of the life cycle. Mutation details as described in [Table 4.1](#) legend.

pflu0185 encodes the putative sensory box protein Pflu0185 (length: 662 amino acids), with predicted localisation in the inner membrane, and 56.6% sequence identity to the phosphodiesterase PipA in *P. aeruginosa* PAO1 ([PA0285](#); BLASTP *E*-value: 0.0). Pflu0185 contains a PAS sensor domain ([PF13426](#); residue: 120-221; *E*-value: 6.5e-14), GGDEF domain ([PF00990](#); residue: 234-390; *E*-value: 1.6e-46), and EAL domain ([PF00563](#); residue: 411-646; *E*-value: 4.0e-76); both the GGDEF & EAL domain with an intact catalytic motif. In *Pseudomonas aeruginosa*, PA0285 was shown to function as a PDE enzyme, important for the maintenance of basal levels of c-di-GMP; with deletion of this gene resulting in an increase in Psl production & biofilm formation (Wei et al., 2019). Cai et al. (2022) further

confirmed that PipA has PDE activity in the degradation of c-di-GMP, additionally detecting involvement in positive regulation of the Pf4 prophage cluster. For the *pflu0185-wspA* mutant genotype, the substitution A463V in the EAL domain of Pflu0185 likely disrupted PDE enzymatic activity, this neighbouring the conserved residue E464 in close proximity to the active sites (Römling et al., 2013). The effect in combination with the other *pflu0185* mutation (p.W69R) is unclear, as well as the alteration to the WspA MCP.

4.2.6 Concluding remarks

The sequencing results revealed that within five life cycle generations, developmental regulation could be achieved with the acquisition of few mutations; in fact in the majority of cases a single substitution in the genes *bifA*, *awsR* or *awsX* was sufficient. This was a surprising observation, that seemingly minor mutational change allowed for a major phenotypic effect, and that developmental strategies readily emerged from the life cycle. The single mutant genotypes displayed the highest lineage-level fitness; by virtue of the mutation being acquired during the first phase of cycle 1, these lineages rapidly reached fixation within their rack, and were therefore given more opportunity to leave offspring lineages in other extinct racks (see [Section 4.2.4](#)). While for the double & triple mutant genotypes most demonstrated a high extinction rate (especially during the early life cycle generations), and production of fewer offspring lineages; this perhaps reflecting the delay in obtaining the necessary combination of mutations, or that these lineages were first transitioning through the life cycle by mutation (see [Section 4.2.5](#)).

I also found that the mutations acquired for developmental regulation of the life cycle were not simply loss-of-function mutations distributed throughout the coding sequence, but rather displayed strong patterns of distribution and localisation within particular functional genes and residues. This implies that these mutations were having a distinct effect on phenotype, rather than just disrupting the protein function. The single mutant genotypes involved point mutation to specific residues in AwsX (W60C) or the CHASE8 sensor domain of AwsR (E61D), that were predicted to alter the interaction between the AwsX repressor & AwsR DGC; or substitutions in the inactive GGDEF domain of BifA (T256S, G304S or A326V), proposed to reduce PDE enzymatic activity in response to the environment. And the double/triple mutant genotypes were the result of combinations of mutations in the AwsR DGC & MwsR DGC/PDE enzyme, in addition to mutations in the DipA PDE, AwsX repressor, SadB regulatory protein, or Pflu0185 PDE; recreating these mutations individually

would reveal the importance of each for the developmental strategy. In general, when considering the complexity of the c-di-GMP signalling network, the mutations conferring developmental regulation of the life cycle were confined to only a small fraction of genes. For example, the Mws & Aws pathway demonstrated strong potential for regulation of the mat-formation & motility traits, while the Wsp pathway did not.

4.3 Analysis of select evolved lines

Based on the sequencing results, I selected a number of evolved lines from the end of cycle 5, to represent the various developmental strategies found by independent racks to transition through the life cycle, including: rack- 2, 6, 7, 11, 12, 14, 16, 18, 20, & 21. The ancestral SBW25 and mutational strategy rack-23 were also examined for comparison to a mutational-based strategy. From this point onwards these evolved lines will be referred to by the name describing their rack of origin during the experiment (e.g. rack-2 for evolved line 2.1, *awsX*-W60C mutant); the genotype and phenotype of each is summarised in *Table 4.11* below. The selected evolved lines with developmental regulation of the life cycle, all demonstrate the capacity to form a mat in the static broth environment, as well as a motility distance equivalent to (or greater than) the wild-type SBW25. Most also display the WS colony morphology on agar plates, excluding rack-6 (*bifA*-G304S mutant) and rack-21 (*awsR*-*mwsR*-*dipA* mutant). While the mutational strategy evolved line rack-23 is motile, but unable to form a mat within 24 hours, and displays the SM colony morphology.

Name	Line	MPB	Genotype	Mat former	Motility (mm)	Colony morph.	Parent lineage
WT	-	14218	Wild-type SBW25 ancestor	No	22.8	SM	-
rack-2	2.1	23200	<i>awsX</i> (W60C)	Yes	23.4	WS	2.3
rack-6	6.3	23203	<i>bifA</i> (G304S)	Yes	23.0	SM	6.5
rack-7	7.5	23206	<i>awsR</i> (D68E), <i>mwsR</i> (M926I & S975R)	Yes	22.6	WS	7.4
rack-11	11.6	23209	<i>awsR</i> (A195V)	Yes	24.6	WS	11.6
rack-12	12.2	23210	<i>sadB</i> (A236P), <i>awsX</i> (S56C)	Yes	30.2	WS	12.8
rack-14	14.2	23213	<i>awsR</i> (A63V & L267fs), <i>pflu0956</i> (S42L)	Yes	22.4	WS	14.1
rack-16	16.6	23215	<i>pflu0185</i> (W69R & A463V), <i>wspA</i> (A381T)	Yes	20.1	WS	16.1
rack-18	18.4	23218	<i>sadB</i> (P313fs), <i>awsR</i> (I79del)	Yes	31.2	WS	18.4
rack-20	20.3	23221	<i>awsR</i> (E61D)	Yes	27.2	WS	20.3

rack-21	21.6	23222	<i>awsR</i> (T27P), <i>mwsR</i> (M1L & T997S), <i>dipA</i> (Y467N)	Yes	30.7	SM	c3-21.6
rack-23	23.7	23224	10x mutations	No	23.0	SM	c2-23.7

Table 4.11. Genotype & phenotype of selected evolved lines. The evolved lines rack-2, rack-6, rack-7, rack-11, rack-12, rack-14, rack-16, rack-18, rack-20 & rack-21 were selected to represent unique developmental strategies to transition through the life cycle. Also shown for comparison is the mutational strategy rack-23, and the WT SBW25. Provided for each: Name (describing rack of origin), Line (evolved line from end of cycle 5), MPB number, Genotype (genes containing mutation & amino acid change), Mat former (capacity to form a mat in static broth after 24 hours), Motility (migration diameter in mm after 30 hours, of overnight culture inoculated into SSA plate), Colony morph. (colony morphology on agar plate), and Parent lineage (origin from cycle 1, unless stated otherwise).

4.3.1 Measuring fitness

For the previous experiment, Hammerschmidt et al. (2014) measured fitness of evolved lines at the level of the collective and of the individual cell, to investigate whether ‘fitness decoupling’ had occurred (refer to [Section 1.3.3.1](#)). Michod & Nedelcu (2003) propose that individuality may emerge at a new hierarchical level as a result of the fitness of groups becoming decoupled from the lower-level cell; fitness decoupling therefore considered a marker for evolutionary transitions in individuality. To measure fitness, evolved lines were taken through an additional life cycle generation, and cell fitness defined as the total number of cells in the mat (end of Phase I), and lineage fitness as the proportion of WS offspring relative to the ancestral SBW25 competitor (end of Phase II). From this, ‘fitness decoupling’ was detected – an increase in lineage-level fitness that came at the cost of individual cell fitness, indicating that selection had shifted towards acting at the collective level (Hammerschmidt et al., 2014; Rose et al., 2020). Although the concept of fitness is a relatively contentious topic (Doebeli et al., 2017), and it is not always clear what it means, or the best way to measure it at different levels of biological organisation. Furthermore, Bourrat (2015) argues that the observation of fitness decoupling is simply an artefact of measuring fitness over different time scales. In more recent work, the emphasis was rather placed on the importance of ‘trade-off breaking’ for evolutionary transitions in individuality; in which the constraint on a set of traits due to the underlying genetic architecture is broken, for example between cell growth and collective persistence (Bourrat et al., 2022). Therefore although the ‘fitness decoupling’ metaphor is not necessarily useful, measuring the fitness of evolved lines may still reveal if a trade-off between these traits has been broken.

4.3.2 Lineage-level fitness

For the lineage-level fitness, I defined this as the ability to leave offspring lineages, which corresponds to the capacity of a genotype to reliably transition through the life cycle without extinction. To approximate the lineage-level fitness, I measured the survival rate of replicate lines during an additional life cycle generation (equivalent to the number of offspring); with a high survival rate (or low extinction) indicating a high lineage-level fitness. For each selected evolved line (detailed in [Table 4.11](#)), three replicate racks (A, B & C, with replicate lines 1-8 each) were taken through the sixth life cycle generation (or cycle 1 for SBW25); the within rack survival rate is shown in [Figure 4.9](#) below. I found that the wild-type SBW25 had a mid-high rate of survival, with a mean of 91.7% during the collective phase (PI) and 45.8% during the dispersal phase (PII); this is consistent with the extinction rate observed during cycle 1 of the experiment (refer to [Section 4.1.2](#)). While the mutational strategy rack-23 displayed a decrease in lineage-level fitness as compared to SBW25, with a mean survival rate of 75% during PI, and only 4.2% during PII, with two replicate racks going extinct. This result confirms that using mutation to transition through the life cycle is not a feasible long-term solution, and that this rack would quickly go extinct if the experiment was continued for further generations; see previous discussion in [Section 4.2.2](#).

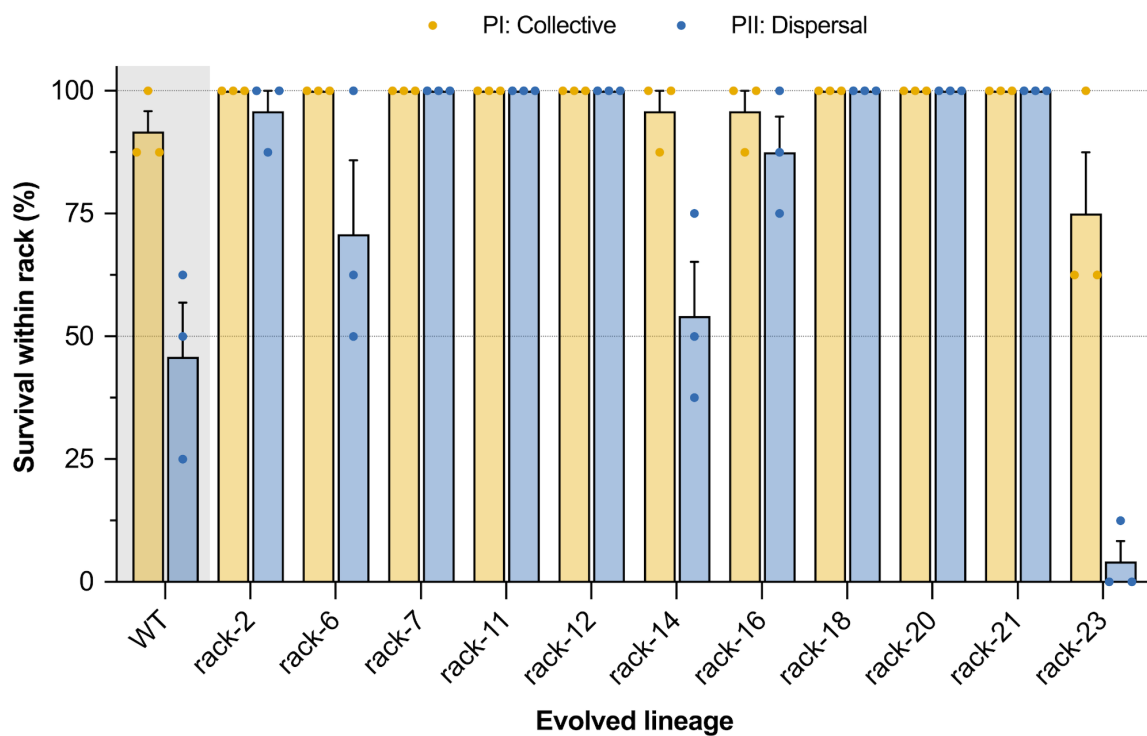


Figure 4.9. Evolved lineages using a developmental strategy have an increase in lineage-level fitness. The lineage-level fitness was approximated by measuring the survival rate during an additional life cycle generation.

For each selected evolved line & the WT SBW25 (detailed in [Table 4.11](#)), three replicate racks (with 8 replicate lines each) were taken through cycle 6 of the experiment (or cycle 1 for SBW25), and the percentage survival within each replicate rack was recorded for the collective (PI) and dispersal (PII) phases. These data are displayed on a scatter plot with bars showing the mean, and error bars the standard error of the mean.

I also found that all evolved lineages with developmental regulation of the life cycle, had an increase in lineage-level fitness as compared to the ancestral SBW25 and mutational strategy rack-23. For almost all genotypes, there was a 100% survival rate during the PI collective phase (except for a single extinct line in rack-14 & rack-16); this indicates strong improvement to the collective trait of mat formation. During the PII dispersal phase, a high survival rate was also observed, with a mean of 100% for rack- 7, 11, 12, 18, 20 & 21, 95.8% for rack-2, 87.5% for rack-16, and 70.8% for rack-6. While rack-14 (*awsR-pflu0956* mutant) had a survival rate similar to the WT SBW25, with a mean of only 54.2%. For the evolved lineages, all extinctions occurring during PII were the result of falling mats and not the motility screen, suggesting substantial improvement to the individual trait of swimming motility. Although it is unclear if this increase in lineage-level fitness is associated with a decrease in the individual-level fitness of the constituent cells.

4.3.3 Individual-level fitness

To measure individual-level cell fitness, I used shaken broth competitive fitness assays, with evolved genotypes competed against the wild-type SBW25. For each selected evolved line (detailed in [Table 4.11](#)), four replicate shaken cultures were grown (for both the GFP & Scarlet fluorescent marker, total of 8 cultures), and then mixed with an equal ratio of the WT SBW25 containing the opposite marker. To test if there was a fitness effect of the different fluorescent proteins, SBW25 with the GFP marker was also competed against SBW25 with the Scarlet marker. Flow cytometry was used to determine the initial (T0) and final (T1) ratio of fluorescent cells for each replicate, and then relative fitness calculated as the ratio of the Malthusian parameter of the evolved line over the WT competitor (Lenski & Travisano, 1994). The results of this competitive fitness assay are shown in [Figure 4.10](#) below; the raw data & analysis is also available in [Supplementary A-17](#).

The relative fitness of the WT SBW25 with either the GFP or Scarlet fluorescent marker approximated 1.0, indicating that there was no strong marker effect. To test whether there was a difference in the mean relative fitness for the WT labelled with the GFP or Scarlet marker, I carried out an unpaired Welch's t-test; the results are shown in [Table 4.12](#) below. From this,

there was no statistical difference observed between the GFP & Scarlet fluorescently labelled strain (p -value = 0.668641), confirming that the marker effect is negligible.

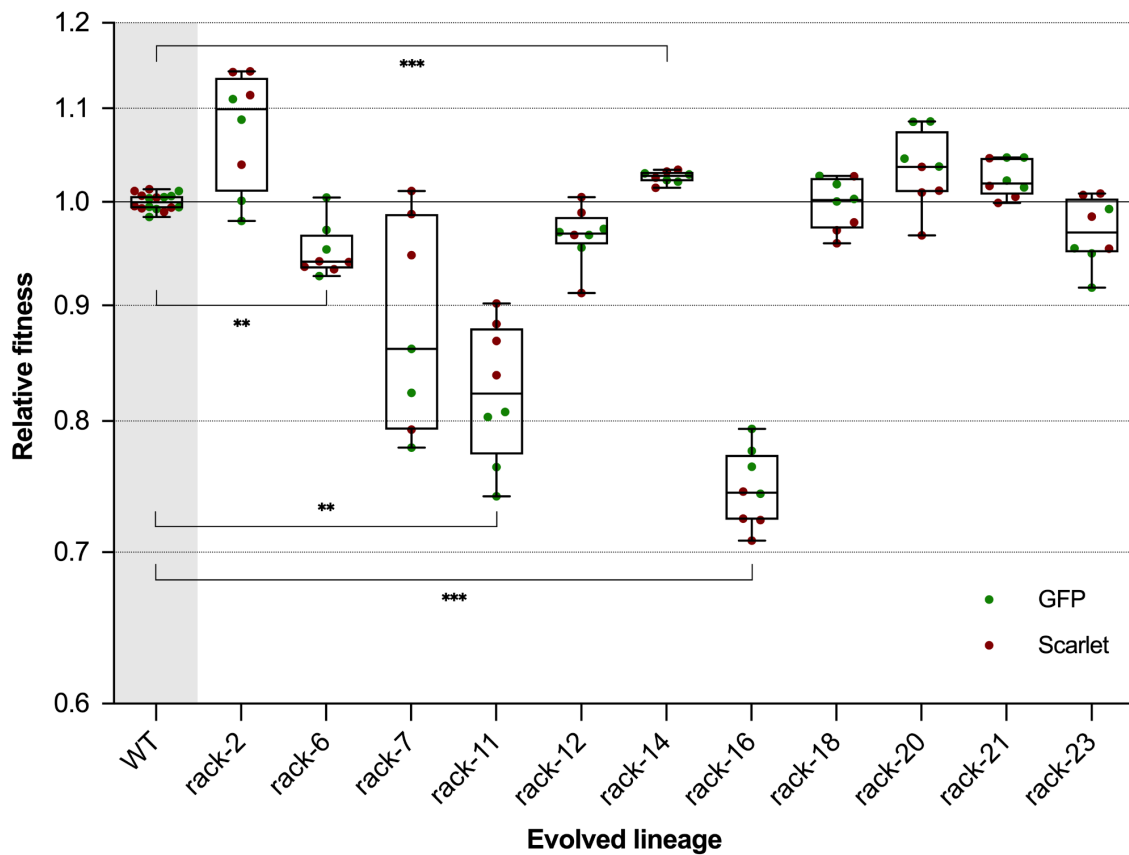


Figure 4.10. Select evolved lineages have an equal or higher individual-level fitness. Individual cell fitness was measured using competitive fitness assays in shaken broth, with evolved genotypes competing against the ancestral SBW25. For each selected evolved line & the WT SBW25 (detailed in [Table 4.11](#)), four replicate shaken cultures were grown (containing the GFP or Scarlet marker, total of 8 replicates), and then mixed at a 1:1 ratio with the WT competitor (containing the other marker). Flow cytometry was used to count 50,000 cells per sample, to determine the initial (T0) and final (T1) ratio of cells; relative fitness was then calculated as the ratio of the Malthusian parameter (evolved line/WT). These data are displayed in a box and whiskers plot, showing the mean, 95% confidence interval, and individual data points (colour indicates GFP or Scarlet marker). The evolved lines with a significant difference from the WT are indicated; refer to statistical analysis in [Table 4.13](#).

Name	Relative fitness		Difference		t	df	α	p -value	Significant?	
	Mean	Log	Mean	SE					No	Equal
WT-GFP	0.9991	-0.0004	-0.0008	0.0019	-0.4372	13.9978	0.00625	0.668641	No	Equal
WT-Scarlet	1.0010	0.0004								

Table 4.12. Statistical analysis of GFP & Scarlet fluorescent marker in the WT SBW25. To compare the mean relative fitness of the wild-type SBW25 containing the GFP or Scarlet marker, an unpaired Welch's t-test was carried out. Assumptions were made that the samples are independent, and means fit a normal distribution; no assumption about equal variance. The p -value threshold (α) was adjusted for multiple comparisons using the

Bonferroni correction method. Provided for each: Name, Mean relative fitness (and mean of log transformed values), Mean difference (mean relative fitness of log values: GFP – Scarlet), SE (Standard error of the difference), t (test statistic), df (degrees of freedom), α (adjusted p -value threshold), p -value, Significant? (whether p -value is significant, and the conclusion regarding the mean relative fitness – equal, higher or lower).

I observed for the selected evolved lines, that some showed a decrease in mean relative fitness (<1), including the developmental strategy rack- 6, 7, 11, 12 & 16, and the mutational strategy rack-23; others showed an increase or no change (≥ 1), including rack- 2, 14, 18, 20 & 21. To test whether the mean relative fitness for each evolved line was different from the WT SBW25, I carried out statistical analysis using multiple unpaired Welch’s t-tests; the results are provided in *Table 4.13* below. I found that the mean relative fitness of the evolved line rack-14 was significantly higher than the WT (p -value = 0.000004); no statistical difference was observed for rack- 2, 7, 12, 18, 20, 21 & 23. While the mean relative fitness of the evolved lines rack- 6, 11 & 16 was significantly lower than the WT (p -value = 0.000702, 0.000090 & <0.000001 , respectively). Therefore for rack-6, rack-11 & rack-16, the increase in lineage-level fitness is associated with a decrease in individual-level fitness. For the other evolved lines with a high lineage fitness, this does not correspond with a decline in cell fitness, including rack-2, rack-18, rack-20 & rack-21.

Name	Relative fitness		Difference to WT		t	df	α	p -value	Significant?	
	Mean	Log	Mean	SE					No	Equal
rack-2	1.0768	0.0315	0.0315	0.0091	3.4497	7.2237	0.01000	0.010183	No	Equal
rack-6	0.9512	-0.0219	-0.0220	0.0043	-5.0592	8.9129	0.00625	0.000702	Yes	Lower
rack-7	0.8858	-0.0548	-0.0549	0.0176	-3.1121	6.0897	0.00625	0.020393	No	Equal
rack-11	0.8257	-0.0841	-0.0842	0.0109	-7.7578	7.2796	0.00625	0.000090	Yes	Lower
rack-12	0.9670	-0.0147	-0.0149	0.0046	-3.2066	8.6622	0.00625	0.011258	No	Equal
rack-14	1.0258	0.0110	0.0111	0.0015	7.4285	13.5722	0.01000	0.000004	Yes	Higher
rack-16	0.7470	-0.1269	-0.1271	0.0061	-20.7362	7.9136	0.00625	<0.000001	Yes	Lower
rack-18	0.9976	-0.0011	-0.0011	0.0041	-0.2638	8.1811	0.01000	0.798461	No	Equal
rack-20	1.0341	0.0143	0.0144	0.0059	2.4286	7.5470	0.01000	0.043056	No	Equal
rack-21	1.0245	0.0105	0.0103	0.0033	3.1744	10.6150	0.00625	0.009229	No	Equal
rack-23	0.9708	-0.0131	-0.0132	0.0054	-2.4504	8.2000	0.00625	0.039206	No	Equal

Table 4.13. Statistical analysis comparing the relative fitness of evolved lines to the WT. For each of the selected evolved lines (detailed in *Table 4.11*), an unpaired Welch's t-test was carried out to examine whether the mean relative fitness is different from the WT ancestor. As described in *Table 4.12* legend, except for Mean difference (evolved – WT); the different values for α reflect experiments with a varying number of comparisons.

4.3.4 Trade-off breaking observations

From the measurements of lineage and individual-level fitness, conclusions may be drawn regarding the trade-off between cell growth and collective persistence. Bourrat et al. (2022) outline a trait-based scenario for an evolutionary transition in individuality, with the following phases: (1) formation of the collective, (2) optimisation of traits within ancestral constraints (optional phase, may result in observation of ‘fitness decoupling’), and (3) trade-off breaking, in which rare mutations are obtained that expand the accessible trait values. The evolved lineages that displayed an increase in lineage-level fitness with no decrease to cell fitness (including rack- 2, 18 20 & 21), may well have broken the trade-off between short-term growth rate and long-term survival.

For the mutational strategy rack-23, both the lineage & individual-level fitness was found to be lower than the WT SBW25; this indicates that by proceeding through the life cycle by mutation, no improvement was made to either trait. While for the developmental strategy lineages, I observed that most showed a substantial increase in lineage-level fitness. For rack-6 (*bifA*-G304S) & rack-14 (*awsR-pflu0956* mutant) only a minor increase to lineage fitness was observed, and in rack-6 this also corresponded with a significant decrease to cell fitness. The evolved lines rack-7 (*awsR-mwsR* mutant), rack-11 (*awsR*-A195V), rack-12 (*awsX-sadB* mutant), rack-16 (*pflu0185-wspA* mutant) & rack-18 (*awsR-sadB* mutant) all displayed a strong increase to lineage fitness, but this was associated with a decrease or no change to cell fitness. For these genotypes it may be concluded that the collective & individual traits are still under the ancestral constraint of the trade-off, and therefore are likely only in the early stages of an evolutionary transition (Bourrat et al., 2022). More interestingly, for rack-2 (*awsX*-W60C), rack-20 (*awsR*-E61D) & rack-21 (*awsR-mwsR-dipA* mutant), I detected a high lineage-level fitness in combination with an increase in individual-level fitness, implying that the trade-off between cell growth and collective persistence had been broken. This observation of trade-off breaking in evolved lineages of the LCE indicates that they are in the later stages of an evolutionary transition in individuality (Bourrat et al., 2022).

4.3.5 Level of c-di-GMP in different environments

I previously discussed the mutations that confer developmental regulation of the life cycle in a number of evolved lineages (refer to [Section 4.2.4](#) & [4.2.5](#)); although the mechanism underpinning this requires further investigation. The collective trait of mat formation and individual trait of swimming motility are inversely regulated by the c-di-GMP signalling

network – high levels of c-di-GMP corresponding with activation of biofilm formation and the downregulation of flagella expression (Hengge, 2009). Based on this, it may be hypothesised that a mechanism for developmental regulation may involve the modulation of c-di-GMP levels in response to environmental conditions. For example, if a lineage acquired the capacity to sense a signal in the static broth environment and respond by increasing the level of intracellular c-di-GMP, this would allow for the transition between the mat-formation & motility phenotypic states without mutation. For the evolved lines rack-2, rack-20 & rack-21, such a regulatory process may also mediate the breaking of the trade-off between cell growth and collective persistence.

To examine whether the selected evolved lines are able to modulate c-di-GMP levels depending on the environment, I proceeded to measure intracellular c-di-GMP in the static broth, motility plate & shaken broth environments. This was achieved using the pCdrA-GFP reporter plasmid, which is under the control of the c-di-GMP responsive *cdrA* promoter from *P. aeruginosa* (Rybtke et al., 2012). Each genotype was additionally tagged using a constitutively expressed Scarlet fluorescent protein that integrates at the *attTn7* locus (Schlechter et al., 2018), to use as a baseline of cell density for normalisation of the GFP fluorescence. For each selected evolved line (detailed in [Table 4.11](#)), four replicate shaken cultures were inoculated into the three environments – static broth, SSA motility plate & shaken broth. After 24 hours of growth in the respective environment, cells were extracted, and then the GFP & Scarlet fluorescence measured by flow cytometry. The mean normalised GFP was then calculated as an approximation of the c-di-GMP level, with the results shown in [Figure 4.11](#) below; the raw data is also available in [Supplementary A-17](#).

As was recognised during the LCE trial, the WT SBW25 has some capacity to increase c-di-GMP levels in static broth as compared to the motility plate or shaken broth environments; refer to previous discussion in [Section 3.6.2](#). Unexpectedly, I observed that the mutational strategy rack-23 had an increase in c-di-GMP level in static broth, even though this genotype is unable to form a mat. The explanation for this result is unclear, though it is likely due to the extensive disruption of the c-di-GMP signalling pathway (see [Section 4.2.2](#)).

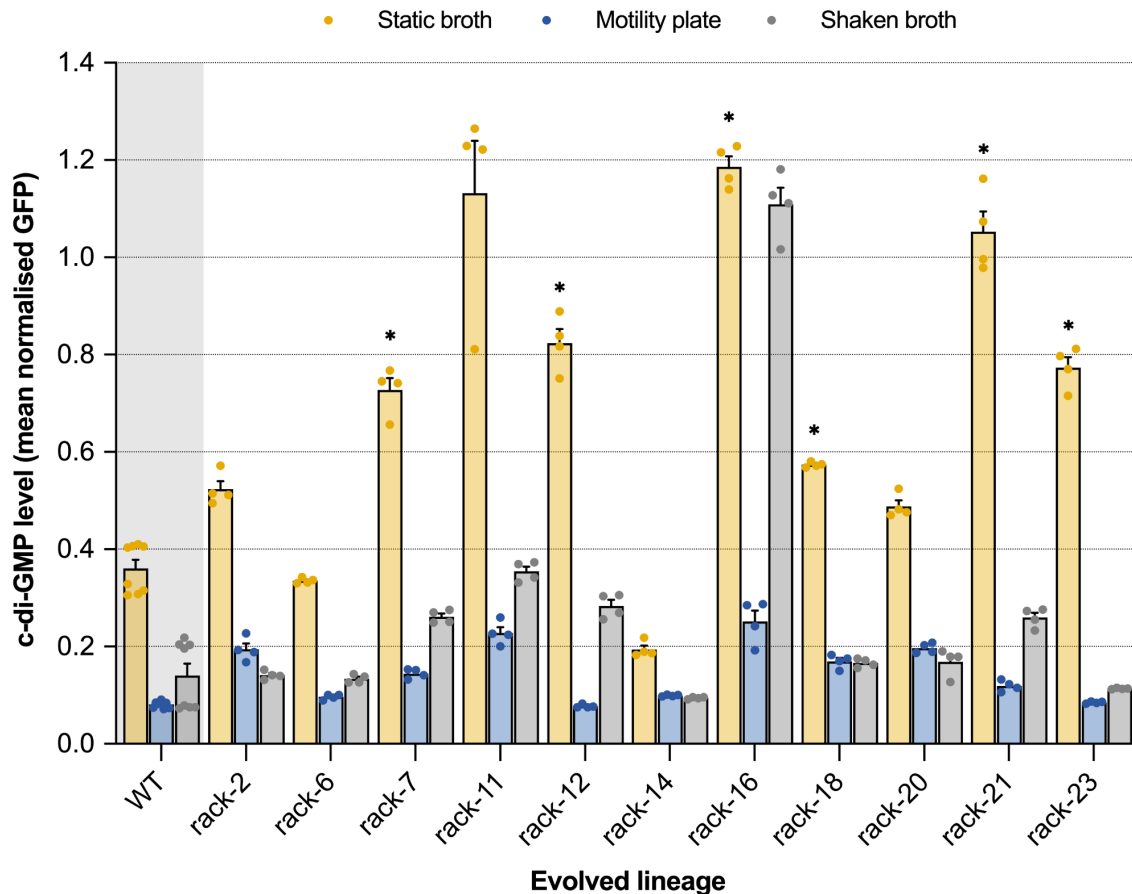


Figure 4.11. Select evolved lineages upregulate c-di-GMP in the static broth environment. The level of c-di-GMP was measured in the static broth, motility plate & shaken broth environments for the following Scarlet-pCdrA strains: WT SBW25 (MPB17910), rack-2 (MPB23337), rack-6 (MPB23340), rack-7 (MPB23343), rack-11 (MPB23346), rack-12 (MPB23347), rack-14 (MPB23350), rack-16 (MPB23352), rack-18 (MPB23355), rack-20 (MPB23358), rack-21 (MPB23359) & rack-23 (MPB23361). For each genotype, four replicate shaken cultures (grown for 24 hours with gentamicin) were each inoculated into an SSA motility plate (0.25% agar & 1% KB), KB static microcosm & shaken microcosm. After 24 hours incubation, cells were extracted from each environment, samples sonicated to minimise cell clumping, and flow cytometry used to measure the GFP & Scarlet fluorescence of 20,000 cells. The c-di-GMP level for each sample was approximated with the mean normalised GFP, this calculated by dividing the mean GFP by the mean Scarlet baseline. These data are displayed on a scatter plot, with bars showing the mean, and error bars the standard error of the mean. The evolved lines with a significant increase in c-di-GMP in static broth as compared to the WT are indicated (*); refer to statistical analysis in [Table 4.14](#).

For the developmental strategy evolved lineages, I found that rack-6 & rack-14 only marginally increased the level of c-di-GMP level in the static broth environment, with a similar behaviour to ancestral SBW25. While for the majority of lineages, substantial upregulation of c-di-GMP was observed in static broth, especially rack-11, rack-16 & rack-21. Interestingly, for rack-16 (*pflu0185-wspA* mutant) the increase in c-di-GMP was also evident in shaken broth; this result indicates that for this genotype the signal to increase

c-di-GMP production is related to the KB medium (e.g. nutrient composition) and not to the spatial structure of the static broth environment. To test whether the mean increase in c-di-GMP level in static broth (as compared to the motility plate) was different for the evolved lineages and the wild-type SBW25, I carried out statistical analysis using multiple unpaired Welch's t-tests; the results are shown in *Table 4.14* below. I observed that rack-6 & rack-14 had a significantly lower mean increase in c-di-GMP level in static broth as compared to the WT (p -value = 0.001129 & 0.000056, respectively); while rack-2, rack-11 & rack-20 had no statistical difference from the WT. The remaining evolved lineages displayed a significantly higher mean increase in c-di-GMP than the WT SBW25, including rack-7, rack-12, rack-16, rack-18 & rack-21 (p -value = 0.001129, 0.000551, <0.000001, <0.000001 & 0.000918, respectively). For these genotypes, it may be concluded that the capacity to developmentally regulate the life cycle is achieved by modulation of c-di-GMP levels in response to the environment.

Name	Mean increase	Difference to WT		t	df	α	p -value	Significant?	
		Mean	SE						
rack-2	0.3293	0.0990	0.0246	4.0260	3.2310	0.00714	0.023932	No	Equal
rack-6	0.2389	-0.0900	0.0054	-16.7044	3.9800	0.00714	0.000078	Yes	Lower
rack-7	0.5831	0.2542	0.0236	10.7905	3.2805	0.00714	0.001129	Yes	Higher
rack-11	0.9044	0.5755	0.0993	5.7925	3.0151	0.00714	0.010095	No	Equal
rack-12	0.7467	0.4179	0.0293	14.2375	3.1780	0.00714	0.000551	Yes	Higher
rack-14	0.0948	-0.1354	0.0098	-13.8520	4.6851	0.00714	0.000056	Yes	Lower
rack-16	0.9350	0.6061	0.0077	78.8202	5.8505	0.00714	<0.000001	Yes	Higher
rack-18	0.4042	0.1740	0.0071	24.3457	5.9146	0.00714	<0.000001	Yes	Higher
rack-20	0.2916	0.0613	0.0165	3.7122	3.5339	0.00714	0.025638	No	Equal
rack-21	0.9332	0.6044	0.0472	12.8089	3.0677	0.00714	0.000918	Yes	Higher
rack-23	0.6887	0.3598	0.0223	16.1473	3.3152	0.00714	0.000288	Yes	Higher

Table 4.14. Statistical analysis of the upregulation of c-di-GMP level in static broth, of evolved lineages as compared to the WT SBW25. For each of the selected evolved lineages (detailed in *Table 4.11*), an unpaired Welch's t-test was carried out to examine whether the mean increase in c-di-GMP level in static broth (compared to the motility plate) is different than in the WT SBW25. Statistical analysis as described in *Table 3.6* legend.

4.4 Mutational steps to rack-21 genotype

From the various phenotypic measurements, I identified the significant evolved line rack-21 (*awsR-mwsR-dipA* mutant), that displays an increase in lineage fitness & cell fitness, as well

as the capacity to upregulate c-di-GMP in static broth to a greater extent than ancestral SBW25. For developmental regulation of the life cycle, this lineage appears to have broken the trade off between cell growth and collective persistence, by modulating c-di-GMP level in response to the environment. The rack-21 genotype includes a total of four point mutations in the *dipA*, *awsR* & *mwsR* genes; each was previously discussed in detail in [Section 4.2.5.3](#). Although it is unclear which of these mutations contributed to breaking the trade off – whether all mutational steps were important, or just one of the later acquired mutations.

Based on the genealogical history of this lineage, I was able to determine the order in which the mutations were obtained – *awsR*-T27P & *mwsR*-T997S during cycle 1, followed by *mwsR*-M1L during cycle 2, and finally *dipA*-Y467N from cycle 3 onwards. As freezer stocks were stored at the end of each cycle, I could also revive each parental lineage representing the mutational steps to the rack-21 genotype – WT SBW25 (MPB14218) cycle-1 line-21.8 (MPB32222), cycle-2 line-21.6 (MPB32223), and cycle-5 line-21.6 (MPB23222); the genotype & phenotype of each is summarised in [Table 4.15](#) below, and from this point onwards each mutational step will be referred to by the name describing the cycle number (e.g. cycle-1 for cycle-1-line-21.8).

Name	Line	MPB	Genotype	Mat former	Motility (mm)
WT	-	14218	Wild-type SBW25 ancestor	No	22.8
cycle-1	c1-21.8	32222	<i>awsR</i> (T27P), <i>mwsR</i> (T997S)	No	28.8
cycle-2	c2-21.6	32223	<i>awsR</i> (T27P), <i>mwsR</i> (M1L & T997S)	Yes	23.0
cycle-5	c5-21.6	23222	<i>dipA</i> (Y467N), <i>awsR</i> (T27P), <i>mwsR</i> (M1L & T997S)	Yes	24.8

Table 4.15. Genotype & phenotype of mutational steps to rack-21 genotype. The evolved lines cycle-1 line-21.8, cycle-2 line-21.6, cycle-5 line-21.6, and the wild-type SBW25 represent the mutational steps to the final rack-21 genotype (*awsR*-*mwsR*-*dipA* mutant). Details as described in [Table 4.11](#) legend; except for the evolved lines cycle- 1, 2 & 5: Motility (migration diameter in mm after 30 hours, of 6 day evolved culture inoculated into SSA plate), as recorded during the experiment.

From the phenotypic measures, it may already be concluded that the mutational step cycle-1 (*awsR*-T27P & *mwsR*-T997S) was insufficient for developmental regulation of the life cycle, as this evolved line is motile but unable to form a mat. While the second mutational step cycle-2 (*mwsR*-M1L) was important for realisation of the final rack-21 phenotype, and the effect of the final step cycle-5 (*dipA*-Y467N) is unclear.

4.4.1 Lineage & individual-level fitness

To investigate the importance of each mutation step to the rack-21 genotype, I proceeded to measure the lineage-level and individual-level fitness of each (as previously described in Section 4.3.2 & 4.3.3); the results are displayed in Figure 4.12 below.

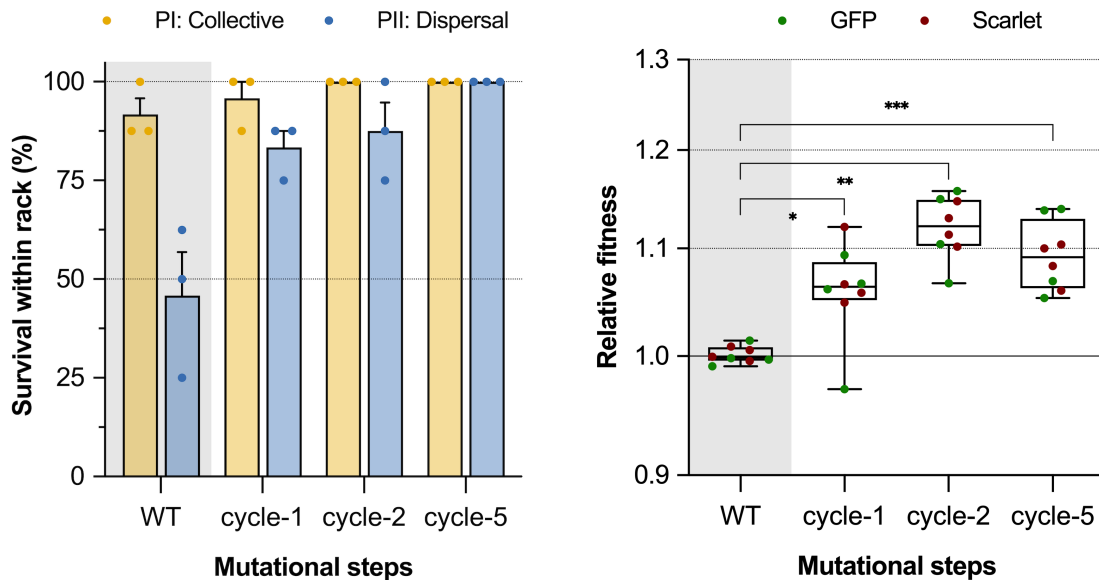


Figure 4.12. All mutational steps to rack-21 genotype have an increase in lineage-level & cell fitness. Fitness was measured for the following mutational steps to the rack-21 genotype (*dipA-awsR-mwsR*): WT, cycle-1, cycle-2 & cycle-5 (detailed in Table 4.15). Left: lineage-level fitness was approximated by measuring the survival rate during an additional life cycle generation, with three replicate racks each. As described in Figure 4.9 legend. Right: cell fitness was measured using competitive fitness assays in shaken broth, evolved genotypes competing against the ancestral SBW25, with four replicates per fluorescent marker. As described in Figure 4.10 legend, except refer to statistical analysis in Table 4.16.

Surprisingly, for all mutational steps I observed an increase in lineage-level fitness as compared to the WT SBW25, with high mean survival rates during both the collective & dispersal phases for cycle-1, cycle-2 & cycle-5; see Figure 4.12 (left) above. For the first mutational step, cycle-1 is unable to form a mat, so requires mutation to proceed through at least the next phase of the life cycle; although I found that this genotype transitioned through the additional life cycle generation with relatively few extinctions. This implies that the mutations present in cycle-1 (*awsR-T27P* & *mwsR-T997S*) may prime this lineage to more reliably acquire mutations for the subsequent phenotypic transitions. The second mutational step cycle-2 had a further increase in lineage-level fitness; but the final step cycle-5 demonstrated the greatest improvement, with a 100% survival rate observed for all replicates during PI & PII. The increase in lineage-level fitness also corresponded with an increase in

individual cell fitness for all mutational steps – cycle-1, cycle-2 & cycle-5 displaying an increase in relative fitness as compared to the WT; see *Figure 4.12 (right)* above. I also carried out statistical analysis to test whether the mean relative fitness was different from the WT, using multiple unpaired Welch’s t-tests; the results are shown in *Table 4.16* below. I found that the mutational steps cycle-1, cycle-2 & cycle-5 all had a mean relative fitness significantly higher than the WT (p -value = 0.006007, 0.000280 & 0.000048, respectively). The increase in both lineage and individual-level fitness for each mutational step was somewhat unexpected, and indicates that it was not just the final mutation that resulted in breaking of the tradeoff, but rather that each may have contributed.

Line	Relative fitness		Difference to WT		t	df	α	p -value	Significant?	
	Mean	Log	Mean	SE					Yes	Higher
cycle-1	1.0930	0.0252	0.0247	0.0065	3.7960	7.4521	0.0125	0.006007	Yes	Higher
cycle-2	1.0606	0.0561	0.0556	0.0085	6.5237	7.2606	0.0125	0.000280	Yes	Higher
cycle-5	1.1395	0.0385	0.0380	0.0047	8.0038	7.8744	0.0125	0.000048	Yes	Higher

Table 4.16. Statistical analysis comparing the relative fitness of rack-21 mutational steps to the WT. For each mutational step to the rack-21 genotype (cycle-1, cycle-2 & cycle-5), an unpaired Welch’s t-test was carried out to examine whether the mean relative fitness is different from the WT ancestor. Statistical analysis as described in [Table 4.12](#) legend, except for Mean difference (evolved – WT).

4.4.2 Level of c-di-GMP in different environments

To further investigate the effect of each mutational step to the rack-21 genotype, I also measured the level of c-di-GMP in the static broth, motility plate & shaken broth environments (as described in [Section 4.3.5](#)); the results are displayed in *Figure 4.13* below. I found that for the first mutational step cycle-1, the behaviour resembled the WT SBW25, with only a minor increase of c-di-GMP level observed in the static broth environment; this corresponds with the inability to form a mat. While both the cycle-2 & cycle-5 mutational steps show a substantial upregulation of c-di-GMP in static broth as compared to the WT, and low levels in both the motility plate & shaken broth environments. Statistical analysis was also carried out to examine whether the increase in c-di-GMP level in static broth (mean normalised GFP (static broth – motility plate)) differs from the WT for each mutational step to the rack-21 genotype. This was achieved using multiple unpaired Welch’s t-tests, and the results provided in *Table 3.16* below. As was expected, cycle-1 displayed no statistical difference from the WT, and cycle-2 & cycle-5 both had a significantly higher mean increase in c-di-GMP level in static broth (p -value = 0.000614 & 0.006316, respectively). This result

indicates that it was the second mutational step cycle-2 (*mwsR*-M1L) that allowed for rack-21 to modulate c-di-GMP in response to the environment; while the last mutational step cycle-5 (*dipA*-Y467N) had no major influence on the observed c-di-GMP levels.

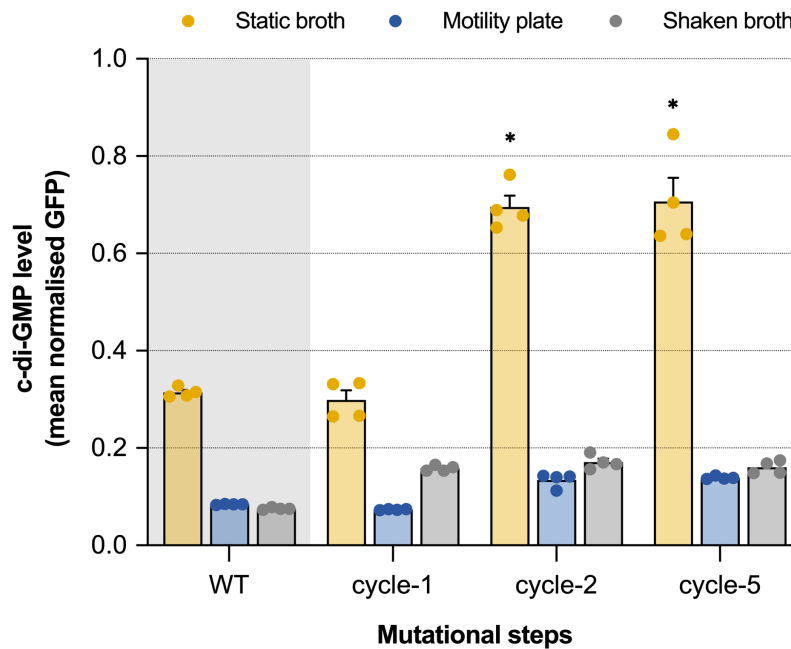


Figure 4.13. The mutational steps cycle-2 & cycle-5 upregulate c-di-GMP in the static broth environment. The level of c-di-GMP was measured in the static broth, motility plate & shaken broth environments for the following Scarlet-pCdrA strains: WT SBW25 (MPB17910), cycle-1 (MPB32578), cycle-2 (MPB32579) & cycle-5 (MPB23359). As described in [Figure 4.11](#) legend, except refer to statistical analysis in [Table 4.17](#).

Line	Mean increase	Difference to WT		<i>t</i>	<i>df</i>	α	<i>p</i> -value	Significant?	
		Mean	SE						
cycle-1	0.2254	-0.0048	0.0199	-0.2407	3.3580	0.00714	0.823737	No	Equal
cycle-2	0.5610	0.3308	0.0247	13.3889	3.2289	0.00714	0.000614	Yes	Higher
cycle-5	0.5677	0.3375	0.0501	6.7346	3.0541	0.00714	0.006316	Yes	Higher

Table 4.17. Statistical analysis of the upregulation of c-di-GMP level in static broth, of mutational steps to rack-21 genotype as compared to the WT SBW25. For each mutational step to the rack-21 genotype (cycle-1, cycle-2 & cycle-5), an unpaired Welch t-test was carried out to determine whether the mean increase in c-di-GMP level in static broth (compared to the motility plate) is different than in the WT SBW25. Statistical analysis as described in [Table 3.6](#) legend.

4.4.3 Conclusions regarding trade-off breaking

The rack-21 genotype (*awsR*-*mwsR*-*dipA* mutant) showed strong evidence of having broken the trade-off between cell growth and persistence, with an increase observed in both lineage-level and individual cell fitness. Unexpectedly, the trade-off breaking was not

associated with a single mutational step, with the mutations obtained during each cycle resulting in consecutive improvement to lineage & cell fitness. The first mutational step cycle-1 (*awsR*-T27P & *mwsR*-T997S) had an intermediary phenotype, demonstrating high fitness but unable to form a mat or transition through the life cycle without further mutation. The substitutions T27P in *AwsR* & T997S in the GGDEF domain of *MwsR* were expected to turn on/off mat formation by activation of the *AwsR* DGC & *MwsR* PDE activity; though it is evident that this high-fitness intermediate step was also important for realisation of the final rack-21 phenotype. The second step cycle-2 (*mwsR*-M1L) conferred developmental regulation of the life cycle, by a mechanism allowing modulation of c-di-GMP levels in response to the environment (c-di-GMP upregulated in static broth), and therefore improvement to both the mat-formation & motility traits. This significant mutation in the first residue of *MwsR* resulted in a synonymous change to the start codon leucine (UUG→UUA), which was predicted to alter translation of the *MwsR* DGC/PDE depending on environmental conditions; refer to discussion of mutation in [Section 4.2.5.3](#). While the final mutational step cycle-5 (*dipA*-Y467N) further improved lineage-level fitness; the substitution Y467N in the GGDEF domain of *DipA* predicted to modify PDE enzymatic activity.

For the rack-21 genotype, it is not obvious how these results fit into the adaptive scenario for an evolutionary transition in individuality, proposed by Doulcier et al. (2022). The cycle-1 intermediate phenotype did not appear to be bound by ancestral constraints of the trade-off, with no observation of ‘fitness decoupling’; though these mutations were not sufficient for developmental regulation of the life cycle. The mutation obtained during cycle-2 (*mwsR*-M1L) had the most significant effect, but were seemingly reliant on the presence of the former mutations; while the final mutation (*dipA*-Y467N) allowed for further optimisation of lineage-level fitness. Therefore the trade-off breaking cannot be attributed to a single mutational event, but rather a cumulative effect of mutations; this begs the question – did this trade off between cell growth and collective persistence ever exist? For the rack-21 evolved lineage, it appears that the fitness of the individual cell and of the lineage was aligned from the beginning; this commands a need for reassessment of the model and how we think about evolutionary transitions in individuality.

4.5 Mutations obtained during additional generation

To approximate the lineage-level fitness, selected evolved lines & SBW25 were run through an additional life cycle generation with three replicate racks each (A, B & C, each with 8

replicate lines); refer to previous [Section 4.3.2](#). To confirm that these lineages were indeed using a developmental strategy to transition through the life cycle (no further mutation required), I proceeded to sequence these evolved lines after the additional generation (cycle 6, or 1 for SBW25). If mutations were obtained during this cycle, I was also interested in examining whether there was some pattern to their distribution; it is possible that these represent secondary adaptive mutations allowing for further adaptation to the life cycle, or improvement to the collective & individual traits. Whole-genome sequencing was carried out for each replicate line at the end of cycle 6, and the unique mutations identified using Breseq (Deatherage, & Barrick, 2014); summary of the output is provided in [Supplementary A-18](#). The results of this are displayed in [Figure 4.14](#) below, which shows for each genotype the number of coding sequence mutations acquired by lines within each replicate rack.

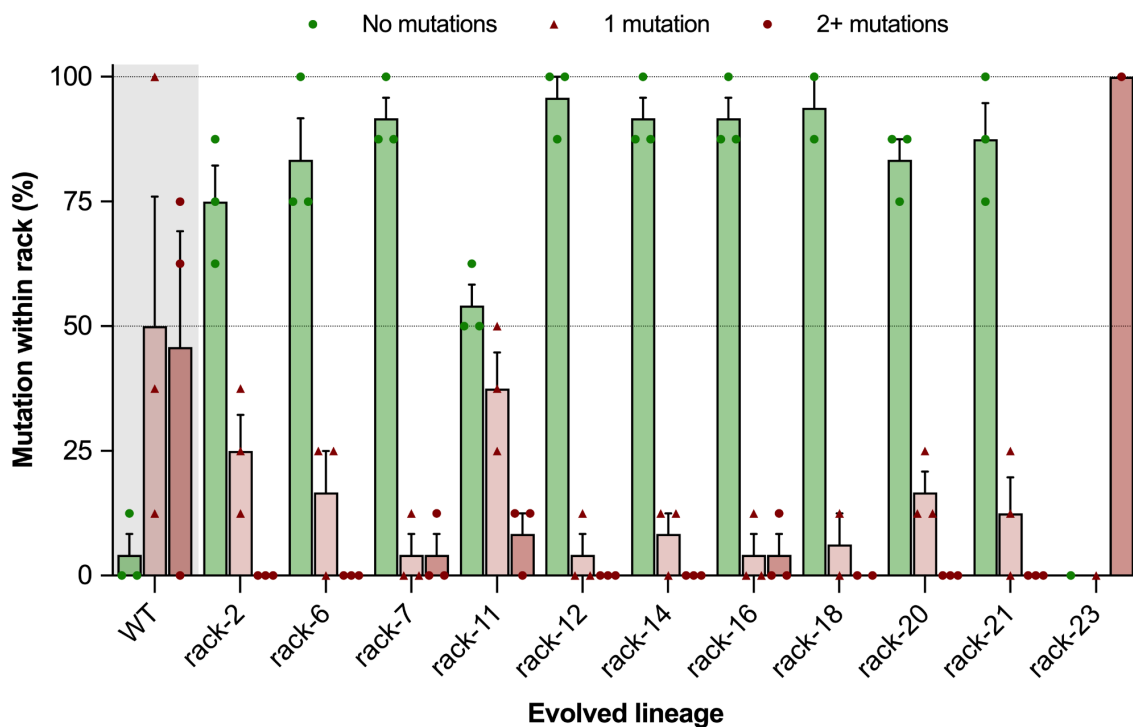


Figure 4.14. Evolved lineages using a developmental strategy acquire few mutations during an additional life cycle generation. For each selected evolved line & the WT SBW25 (detailed in [Table 4.11](#)), three replicate racks (with 8 replicate lines each) were taken through cycle 6 of the experiment (or cycle 1 for SBW25). Whole-genome sequencing revealed the unique mutations obtained by each replicate line during this additional generation. From this result, for each replicate rack the number of mutations acquired by each line was determined – No mutation, 1 mutation, or 2+ mutations (2 or more). These data are displayed on a scatter plot with bars showing the mean, and error bars the standard error of the mean.

For the wild-type SBW25, I found that over the course of one life cycle generation approximately half of the replicate lines obtained one mutation, and the other half two or

more mutations. The observation of two mutations is consistent with the use of a mutational strategy to transition through the life cycle, while the single mutations may indicate that developmental regulation has already emerged. I was relatively surprised to find that the single mutant genotypes were already dominating after only a single generation with the WT SBW25; the identity of these mutations are discussed in the following section. For the mutational strategy rack-23, all replicate lines in the only surviving rack acquired two mutations to transition through the additional generation. While for the majority of the developmental strategy genotypes (rack- 2, 6, 7, 12, 14, 16, 18, 20 & 21), in most replicates no additional mutations were obtained. For rack-11 (*awsR*-A195V), many of the replicate lines obtained 1 or 2 mutations; this may be explained by this genotype having a low individual-level fitness (refer to [Section 4.3.3](#)), and these being compensatory mutations. Overall, the observation of so few mutations confirms that these evolved lineages are transitioning through the life cycle by developmental regulation.

4.5.1 WT SBW25 mutations

The WT SBW25 was run through an additional life cycle generation (cycle 1), as a comparison for the evolved mutational & developmental strategy lineages. The mutations obtained by replicate lines of SBW25 during this cycle are detailed in [Table 4.18](#) below. Many replicates acquired two (or three) mutations in genes with known function in c-di-GMP signalling & the WS phenotype, including *wspA*, *wspE*, *wspF*, *wspR*, *awsR*, *awsX* & *mwsR* (McDonald et al., 2009); corresponding to the mutational strategy of turning on/off mat formation by disruptive mutation. Remarkably, I also observed single mutant genotypes of *bifA* & *awsR* with strong similarity to those found at the end of cycle 5 of the experiment. The replicate line A5 acquired the substitution R327Q in the GGDEF domain of BifA; this mutation is in the neighbouring residue to the *bifA*-A326V single mutant genotype (see [Section 4.2.4.1](#)). While the replicate line B4 obtained the substitution A195V in *AwsR*, that is identical to the *awsR* mutant from rack-11; refer to previous [Section 4.2.4.2](#). This result highlights that these single mutant genotypes conferring developmental regulation of the life cycle repeatedly emerge from the WT SBW25.

Rep.	#	Gene name	PFLU	Putative product	Nucleotide change	Amino acid change	Protein domain	E-value
B7	1	<i>wspA</i>	1219	methyl-accepting chemotaxis protein	1009C>T	Q337*	MCPsignal	5.0e-34
B3	3				1024A>G	M342V		
C1	2				1259C>T	A420V		

C3	1				1537T>C	S513P		
B3	1	<i>wspE</i>	1223	two-component system, sensor kinase	1064_1099 del	L355_R367 del	HATPase	2.1e-11
C3	2	<i>wspF</i>	1224	chemotaxis-related methylesterase	151_165del	L51_I55del	REC	1.2e-16
B6, C1	3	<i>wspR</i>	1225	two component system response regulator	467_469 delCAG	Q156del	GGDEF	1.2e-55
C5	1	<i>awsR</i>	5210	signaling-related membrane protein	545C>G	T182S	HAMP	1.3e-4
B4	3				584C>T	A195V		
A2	4	<i>awsX</i>	5211	hypothetical protein	524T>C	I175T	YfiR-like	1.4e-32
C8	1				530C>T	P177L		
C8	1	<i>mwsR</i>	5329	sensory box protein, GGDEF/EAL domain	2172G>A	M724I	PAS	2.5e-16
A5	4	<i>bifA</i>	4858	signaling protein	980G>A	R327Q	GGDEF	7.2e-36
B2	1	<i>amrZ</i>	4744	DNA-binding protein	233T>C	L78P	-	-
B1	2	<i>tufB</i>	5529	elongation factor Tu	1054G>C	E352Q	GTP_EFTU	2.0e-39
C3	2	<i>lysC</i>	4747	aspartate kinase	475G>A	G159S	AA kinase	4.7e-50
C5	1	<i>pflu2506</i>	2506	AraC family transcriptional regulator	679G>C	A227P	HTH AraC	2.8e-19
C6	1	<i>pflu1809</i>	1809	hypothetical protein	977T>C	F326S	-	-

Table 4.18. Mutations obtained in replicate lines of WT SBW25 during additional generation. The WT SBW25 was taken through an additional life cycle generation (cycle 1), with three replicate racks (A, B & C, each with 8 replicate lines). The unique coding sequence mutations acquired during this cycle are shown. Provided for each: Rep. (Replicate number), and # (number of replicates with the mutation). Mutation details as described in [Table 4.1](#) legend.

4.5.2 Mutational strategy rack-23 mutations

For the evolved lineage rack-23 that uses a mutational strategy, a very high extinction rate was observed during the additional life cycle generation (see [Section 4.3.3](#)). During the dispersal phase (PII) two replicate racks went completely extinct, and for the remaining rack only a single lineage survived; the mutations acquired by the final lines in rack B are provided in [Table 4.19](#) below. Interestingly, during PI the replicate line B4 must have repaired the duplication in the GGDEF domain of MwsR (p.L887_R889dup), likely resulting in restoration of the MwsR DGC activity & formation of a mat. The observation that only this lineage survived the additional generation implies that the remaining mutational target size for this phenotypic transition was very small. During PII, each replicate line then acquired another mutation in *mwsR*; this was expected to disrupt function of the MwsR DGC, turning

off mat formation, thus allowing for dispersal by swimming motility. These included a frameshift or nonsense mutation at the start of MwsR (Q43* & Q49fs), substitution in the GGDEF domain (A848S, A848T & D996N), or an in-frame deletion in the EAL domain (E1150_L1151del). This result demonstrates that the MwsR protein contains a lot of potential for turning on/off mat formation by mutation, particularly with these reversible in-frame duplications & deletions, and substitution within particular residues (e.g. residue 848). Although this rack-23 mutational strategy is clearly infeasible long-term, with the high rate of extinction observed.

Rep.	#	Gene name	PFLU	Putative product	Nucleotide change	Amino acid change	Protein domain	E-value
B6	1	<i>mwsR</i>	5329	sensory box protein, GGDEF/EAL domain	127C>T	Q43*	-	-
B7	1				145_146insCTGC	Q49fs		
B1	1				2542G>T	A848S	GGDEF	4.7e-50
B2	3				2542G>A	A848T		
B4	8				2665_2670 delTCGACC	L887_D888 delLD		
	1				2986G>A	D996N		
B3	1				3448_3453 delGAGCTG	E1150_L1151 delEL	EAL	1.0e-76

Table 4.19. Mutations obtained during additional generation for rack-23 using mutational strategy. The evolved line rack-23 that uses a mutational strategy to transition through the life cycle, was taken through an additional generation (cycle 6), with three replicate racks (A, B & C, each with 8 replicate lines). The unique coding sequence mutations acquired during this cycle are shown, for replicate lines in the surviving rack B. Provided for each: Rep. (Replicate number), and # (number of replicates with the mutation). Mutation details as described in [Table 4.1](#) legend.

4.5.3 Developmental strategy mutations

For the evolved lineages using a developmental strategy (rack- 2, 6, 7, 11, 12, 14, 16, 18, 20 & 21), the mutations obtained during the additional life cycle generation are shown in [Table 4.20](#) below. In general, the mutations acquired in these genotypes are very distinct from those obtained by the WT SBW25 or rack-23 (see [Table 4.18](#) & [4.19](#)); only a small number are within genes encoding GGDEF or EAL domains (e.g. *pflu5698*, *mwsR* & *pflu3650*), or directly related to c-di-GMP signalling or the WS phenotype. Therefore these may represent secondary adaptive mutations that further increase the fitness of lineages, as they no longer require mutation to transition through the life cycle. I found that for the high-fitness rack-2 (*awsX-W60C*) & rack-21 (*awsR-mwsR-dipA* mutant) genotypes, in three independent lines

mutations were acquired in the *fleN* gene (p.S29F, p.L201F & p.V264A). *fleN* ([pflu4418](#)) encodes the ATPase FleN, involved in flagellar assembly (previously discussed in [Section 2.4.5.3](#)); in *P. aeruginosa* PAO1, *fleN* insertion mutants were shown to display multiple polar flagella and reduction in motility (Dasgupta et al., 2000, 2003). Furthermore, FleN binds to the FleQ transcriptional regulator, and this complex controls the expression of flagella & exopolysaccharide genes, depending on the level of intracellular c-di-GMP (Baraquet et al., 2012). Therefore the exact effect of these *fleN* mutations in rack-2 & rack-21 is not obvious, but may result in alteration to the assembly of flagella & thus swimming motility.

Line-Rep.	#	Gene name	PFLU	Putative product	Nucleotide change	Amino acid change	Protein domain	E-value
rack-2-B1	1	<i>fleN</i>	4418	ParA family ATPase	86C>T	S29F	FleN	3.8e-22
rack-21-C1	1				601C>T	L201F		
rack-21-A8	1				791T>C	V264A	-	
rack-11-A8 B2, 5, & 7 C2, 3, & 4	8	<i>pflu3094</i>	3094	transmembrane permease	208G>T	G70C	AA permease	2.8e-23
rack-2-A2, A7, C5	3	<i>viscB</i>	2553	non-ribosomal peptide synthetase	4988A>G	D1663G	AMP binding	5.8e-104
rack-20-A6, C5	2	<i>aruE</i>	4751	succinylglutamate desuccinylase	737C>T	P246L	AstE AspA	1.9e-71
rack-11-A6, C3	2	<i>cyaA</i>	5940	adenylate cyclase	2223C>A	H741Q	Adenylate cyclase	1.2e-117
rack-2-A4	1	<i>pflu5698</i>	5698	GGDEF/EAL domain regulatory protein	116T>C	V39A	Response reg	2.0e-25
rack-2-C8	1	<i>pflu0364</i>	0364	ABC transporter membrane protein	823G>C	G275R	-	-
rack-6-A2	1	<i>pflu5344</i>	5344	hypothetical protein	63C>T	R21R	DUF2474	1.5e-20
rack-6-A3	1	<i>pflu2984</i>	2984	hypothetical protein	171G>A	R57R	-	-
rack-6-B4	2	<i>pflu3179</i>	3179A	LysR family transcriptional regulator	718A>C	T240P	LysR substrate	9.9e-37
rack-7-B2	1	<i>pflu1654</i>	1654	hypothetical protein	619_620insT	S207fs	-	-
		<i>pflu3066</i>	3066	aminotransferase	406G>A	A136T	Aminotran	1.3e-42
rack-7-C3	1	<i>pflu4621</i>	4621	hypothetical protein	418A>C	T140P	Kinase PPPase	5.0e-76
rack-11-A2	1	<i>metN</i>	0070	methionine transporter, ATP-binding subunit	19G>A	V7I	-	-
rack-11-A6	1	<i>cueR</i>	0657	HTH-type copper-efflux transcriptional regulator	235G>A	D79N	MerR DNA bind	1.3e-19
rack-11-B8	1	<i>glcG</i>	1804	hypothetical protein	300T>G	G100G	GlcC-like	5.8e-26

rack-11-C1	1	<i>phnL</i>	1786	phosphonate ABC transporter ATP-binding	660C>T	A220A	AAA+ ATPase	2.7e-8
rack-12-A8	1	<i>pflu0615</i>	0615	hypothetical protein	248A>C	D83A	-	-
rack-14-B6	1	<i>pflu0829</i>	0829	two-component system sensor kinase	311T>C	V104A	-	-
rack-14-C3	1	<i>mwsR</i>	5329	sensory box protein, GGDEF/EAL domain	2910C>A	F970L	GGDEF	4.7e-50
rack-16-A1	1	<i>pflu3088</i>	3088	IcIR family transcriptional regulator	340A>G	S114G	-	-
		<i>pflu3650</i>	3650	transmembrane sensory box GGDEF domain	915G>C	L305F	GGDEF	4.3e-42
rack-16-B7	1	<i>cysB</i>	1710	transcriptional regulator CysB	666C>T	F222F	LysR substrate	6.1e-42
rack-18-B4	1	<i>pflu2000</i>	2000	hypothetical protein	862T>G	L288V	-	-
rack-20-B3	1	<i>pflu3909</i>	3909	hypothetical protein	303C>T	N101N	Transcrip reg	9.5e-68
rack-20-B8	1	<i>relA</i>	4505	GTP pyrophosphokinase	686T>C	L229P	-	-
rack-21-A7	1	<i>csrA</i>	4165	carbon storage regulator	161G>A	R54H	CsrA	1.4e-27

Table 4.20. Mutations obtained during additional generation for evolved lineages using developmental strategy. The evolved lines rack- 2, 6, 7, 11, 12, 14, 16, 18, 20 & 21 were taken through an additional life cycle generation (cycle 6), with three replicate racks each (A, B & C, each with 8 replicate lines). The unique coding sequence mutations acquired during this cycle are shown. Provided for each: Line-Rep. (Line name & Replicate number) & # (number of replicates with the mutation). Mutation details as described in [Table 4.1](#) legend.

There were some other obvious patterns in the mutations acquired during this additional generation, including substitutions in genes encoding transcriptional regulators (rack-6: *pflu3179A*, rack-11: *cueR*, rack-16: *pflu3088* & *cysB*), and transporter proteins (rack-2: *pflu0364*, rack-11: *pflu3094*, *metN* & *phnL*). Further work would be required to investigate the effect of each of these mutations, but I feel confident that these results testify to the potential for future adaptation to the life cycle.

4.6 Conclusions

The transition to multicellularity required the emergence of Darwinian properties at the new hierarchical level of the collective, which cannot be assumed to simply transfer from the lower level of the cells (Libby & Rainey, 2013a; Godfrey-Smith, 2009). This would allow the nascent multicellular organism to become a unit of selection in its own right, and therefore participate in the process of evolution by natural selection (Lewontin, 1970). The major question remains – for simple multicellular groups, how exactly did a mechanism of

reproduction come about? Answering this question is difficult to do without assuming the existence of group-level traits, which paradoxically infers the result of the process that is itself being explained (Rainey & Kerr, 2010; Griesemer, 2000). Rainey et al. (2017) postulate that ecology plays an important role, and that Darwinian properties may be exogenously imposed on simple groups of cells by virtue of the structure of the environment. Ecological scaffolding permits selection to act over two timescales – the shorter timescale of cell doubling, and longer timescale of the collective generation (Black et al., 2020). These Darwinian properties could then become endogenous, for example by the evolution of a developmentally-controlled life cycle, in which the collective determines its own reproduction and is no longer reliant on the scaffold (Rainey et al., 2017; Okasha, 2021; Bonner, 2000). Michod & Nedelcu (2003) argue that this evolutionary transition in individuality is marked by the observation of ‘fitness decoupling’, where the fitness of the collective increases, at the expense of the fitness of constituent cells. While Bourrat et al. (2022) rather emphasise the importance of trade-off breaking – rare events in which the ancestral constraint on a set of traits is broken (e.g. cell growth & collective persistence), which may result in the observation of an increase in both collective and individual-level fitness.

In the LCE, Hammerschmidt et al. (2014) evolved bacterial populations of *P. fluorescens* SBW25 through a simple two-phase life cycle, that transitioned between the WS collective (‘soma’) and SM individual cell (‘germ-line’) phases. This experiment partitioned variation between lineages with the ecology of the glass microcosm, and enforced a lineage-level death-birth process over the longer timescale, with selection for those lineages who could reliably transition through the phases of the life cycle (Hammerschmidt et al., 2014; Black et al., 2020). After ten generations, they observed ‘fitness decoupling’ – an increase in fitness of evolved lineages that corresponded with a decrease in individual cell fitness. Furthermore, they discovered the evolution of a simple genetic switch, that allowed for semi-reliable switching between the WS & SM phenotypic states by the expansion & contraction of a G tract in the DGC-encoding *wspR*; although this was dependant on an elevation of mutation rate due to disruption of the MMR system (Hammerschmidt et al., 2014). The LCE regime used the proxy of colony morphology for adaptation to each phase, resulting in a life cycle proceeding only by mutation – required to generate the stable WS or SM phenotype on the agar plate. By applying screening methods outside the selective environment of the static

broth microcosm, this original experimental regime actually precluded the evolution of a developmental program.

As discussed in Chapter II, evolved genotypes were identified with the capacity to switch between the WS & SM phenotype in response to the environment (observed with temperature) (Summers, 2018), therefore developmental regulation of the life cycle is possible. I was able to recreate this phenotype switch in the wild-type SBW25 with minimal genetic manipulation, requiring only three point mutations, indicating that this solution is readily accessible to selection. These mutations involved simple rewiring of the Wsp system, including disruption to the WspF methylesterase (negative regulator of the WspR DGC), and substitutions in the WspA MCP signalling domain (4HB) & HAMP domain predicted to alter the sensitivity of the receptor to an environmental signal (e.g. membrane stress). The existence (and subsequent purging) of this environmentally-responsive phenotype further emphasised the limitations of the LCE selective regime, and the need for a redesign of the experiment. In Chapter III, I describe the production of a revised LCE selective regime, that eliminates the problematic use of a colony morphology proxy. This includes new methods for screening based on the collective trait of mat formation and individual trait of dispersal by swimming motility. I also present the results from a small-scale trial experiment that demonstrated the efficiency of the revised selective regime. Within five generations evolved lineages displayed rapid adaptation to the life cycle, and the evolution of various strategies to mediate the transition – mutational, generalism & developmental.

In Chapter IV, I discuss the results of a large-scale experiment carried out using the new LCE regime; this consisted of 24 metapopulations (racks), each containing 8 replicate lines (total of 192). By applying minor alteration to the selective methods I was able to enforce stricter selection on the collective & individual traits, thus avoiding the emergence of generalists. I found that after only five life cycle generations, evolved lineages exhibited a major decrease in extinction rate, as well as substantial improvements to both mat formation & motility (exceeding the capacity of ancestral SBW25). Furthermore, the sequencing of evolved lines at the end of cycle 5 revealed a number of unique strategies to mediate the transition through the life cycle. I observed that lineages within a few racks were using a mutational strategy (including rack-23), and for each phenotypic transition required a mutation that resulted in constitutive activation or inactivation of mat formation. Hypermutation also emerged in one lineage, due to a mutation in the *mutS* gene, similar to that underpinning the genetic switch found by Hammerschmidt et al. (2014). The mutational-based strategies were unreliable and

associated with a high extinction rate, as they were dependent on the acquisition of rare adaptive mutations during each phase; the mutational target size was also further reduced over time (Barnett, 2022).

Remarkably, the majority of evolved lineages had found a means of developmental regulation – able to switch between the phenotypic states in response to the environment, with no further mutation necessary. These lineages could reliably transition through the life cycle with a low extinction rate, therefore able to persist through the generations and given more opportunity to produce offspring lineages. I also found that developmental strategies evolved from various genetic routes, including ten distinct genotypes across the independent racks. The most successful lineages were those that acquired a single mutation during the first cycle of the experiment; among these were point mutations in the inactive GGDEF domain of BifA (T256S, G304S or A326V), or in specific residues of AwsR (E61D or A195V) and AwsX (W60C). The *bifA* mutations were predicted to reduce the PDE enzymatic activity of BifA, and the *awsR* & *awsX* mutations to alter the interaction between the AwsR DGC enzyme & AwsX repressor, depending on environmental conditions. Other lineages contained a combination of mutations to two or three genes, particularly in *awsR* & *mwsR*, or *sadB* & *awsR* or *awsX*. The rack-21 genotype was especially interesting; this lineage first obtained substitutions in *awsR* & *awsX*, followed by the mutation *mwsR*-M1L and then *dipA*-Y467N. The synonymous mutation in the first residue of MwsR altered the start codon leucine (UUG→UUA), this was expected to have a major effect on the translation of the MwsR DGC/PDE enzyme. While the substitution Y467N in the inactive GGDEF domain of DipA was predicted to modify the PDE activity (in a manner similar to the BifA mutants).

I proceeded to further characterise these unique developmental strategies, with measurements of the lineage-level & individual-level fitness of representative evolved lines, as well as the mutational strategy rack-23 & ancestral SBW25 for comparison. From this I found that the strategy based on mutation had a decrease in both lineage & cell fitness as compared to SBW25. While the developmental strategies all displayed an increase in lineage-level fitness, and for some this was also associated with an increase in cell fitness (including rack- 2, 20 & 21). This result suggests that the trade-off between cell growth & collective persistence had been broken, and that these evolved lineages may be in the later stages of an evolutionary transition in individuality (Bourrat et al., 2022). Furthermore, I was able to elucidate the mechanism underpinning developmental regulation of the life cycle, with many of these genotypes demonstrating significant upregulation of c-di-GMP level in the static broth

environment (activating mat formation) and downregulation in the motility plate (allowing flagella expression & swimming motility). The rack-21 genotype (*awsR-mwsR-dipA* mutant) displayed the strongest evidence for trade-off breaking and modulation of c-di-GMP level in response to the environment, prompting investigation of the mutational steps from – cycle 1 (*awsR-T27P* & *mwsR-T997S*), cycle 2 (*mwsR-M1L*) & cycle-5 (*dipA-Y467N*). Surprisingly, I found that each mutational step contributed to the consecutive increase in both lineage-level & cell fitness, and that the trade-off breaking could not be attributed to a single mutation. Although the synonymous mutation in the start codon of *mwsR* had the most significant effect, it conferred developmental regulation of the life cycle and the capacity to modulate c-di-GMP. These results highlight that ‘fitness decoupling’ need not occur for an evolutionary transition in individuality; rather what seems important is the alignment of fitness of the individual & collective, and the breaking of trade-offs that impose a constraint on traits realised at each level.

The most remarkable finding from my research is that a developmental program readily emerged for this simple bacterial life cycle. All that this required was ecological scaffolding to impose Darwinian properties on nascent multicellular groups, and a death-birth process of lineages enforced over a longer timescale (Rainey et al., 2017; Black et al., 2020). The observation that developmental regulation was achieved with so few mutations from the ancestral state was also a revelation. This likely reflects the redundancy of the underlying c-di-GMP signalling network, and the need for the SBW25 bacterium to respond to a large diversity of environmental signals in nature for the transition between a motile and sessile lifestyle (Hengge, 2009). It is not simply coincidence that this network is so complex, and that there are 39 putative DGC enzymes encoded by the SBW25 genome. Perhaps this multicellular group is closer to an evolutionary transition in individuality than initially thought; and based on this I would definitely agree with the classification by Grosberg & Strathmann (2007) of the evolution of multicellularity as a ‘minor major’ transition.

4.6.1 Future perspectives

I have a number of plans for the future to move this project forward (some already in motion), that use the new LCE selective regime as a foundation. If the experiment was continued on for many more generations, I would be interested to see whether selection at the lower level of the cell may begin to overcome that at the higher level; or rather if secondary adaptive mutations would emerge that further improve both the collective & individual traits.

A critical factor to consider regards the importance of death – after only five life cycle generations the extinction rate of evolved lineages was negligible, therefore selection likely became less prevalent at the longer timescale of lineage persistence (as fewer death-birth events were occurring). The extinction of lineages could be enforced, either in a stochastic way (e.g. randomly chosen 50% of lineages undergo extinction), or in a selective way (e.g. 50% of lineages with the shortest motility distance). The experimental regime can also be easily adapted to apply more strict selection on the traits of mat formation & motility, which may push lineages further to evolve even better solutions for regulation of the life cycle. It is also possible that pushing them too far may force lineages to again proceed through the life cycle using a mutational strategy. I am very excited for the future of this experiment, and strongly believe that it is a valuable tool to ask and explore a diverse range of evolutionary questions.

Chapter V: Materials & Methods

5.1 Bacterial strains, culturing & reagents

Pseudomonas fluorescens (*P. fluorescens*) strains were cultured at 28°C in King's Medium B (KB). To obtain single colonies, strains were streaked on KB plates containing 1.5% agar, and incubated inverted for 1-2 days. Liquid broth cultures were inoculated from a single colony, and grown in 6 mL of KB (in a 25 mL glass microcosm). These were incubated under static conditions for 1-6 days (28°C room), or shaken overnight for 16-24 hours at 220 rpm (New Brunswick: Innova 44 incubator shaker). Swimming motility assays were made with semi-solid agar (SSA) plates containing 1% KB and 0.25% agar, and incubated upright for 24-30 hours (Heraeus: Function Line B20 Incubator). For cloning, *Escherichia coli* (*E. coli*) strains were grown at 37°C in Lysogeny broth (LB). Freezer stocks of overnight cultures were made in 35% glycerol, and stored indefinitely at -80°C.

5.1.1 *P. fluorescens* strains

The details of *P. fluorescens* strains used in this study are provided in *Table 5.1* below.

MPB	Name	Description	Parent	Reference
14218	SBW25	Wild-type <i>Pseudomonas fluorescens</i> SBW25, isolated from sugar beet phyllosphere; SM phenotype	-	Rainey & Bailey, 1996
13887	LSWS	LSWS (large spreading wrinkly spreader), evolved from SBW25 in static broth; <i>wspF</i> mutation (g.901A>C; p.S301R); WS phenotype	-	Bantinaki et al., 2007
13896	L17- <i>mutS</i> -WT	Line 17 evolved from life cycle experiment (generation 11), with <i>mutS</i> gene restored to wild-type; WS phenotype	-	Hammerschmidt et al., 2014
13893	f2 ancestor	Replicate line-f2 (PE-7-WT-f2) evolved from continuation of LCE with L17- <i>mutS</i> -WT for six generations (end of cycle 6 - phase II); ancestor to TSS-f6; WS phenotype	-	Summers, 2018
13890	TSS-f6	Replicate line-f6 evolved from continuation of LCE with L17- <i>mutS</i> -WT for seven generations (end of cycle 7 - phase II); temperature sensitive switcher – SM phenotype at 28°C & WS phenotype at 20°C	-	Summers, 2018
<i>Mutational pathways to WS phenotype</i>				
15442	WS-1	WS pathway 1 (<i>pflu4313-4308*</i>) – deletion of 4672 bp resulting in gene fusion of <i>pflu4313</i> (M1-F115) to <i>pflu4308</i> (A189-R820), recreated in SBW25	-	Lind et al., 2015
15443	WS-2	WS pathway 2 (<i>pflu0956*</i>) – <i>pflu0956</i> promoter mutation (g.-54T>G), recreated in SBW25	-	Lind et al., 2015

15444	WS-3	WS pathway 3 (<i>pflu1349*</i>) – <i>pflu1349</i> promoter mutation (g.-47_48insTC), recreated in SBW25	-	Lind et al., 2015
15445	WS-4	WS pathway 4 (<i>pflu3448*</i>) – <i>pflu3448</i> mutation (g.599C>T; p.A200T), recreated in SBW25	-	Lind et al., 2015
15446	WS-5	WS pathway 5 (<i>pflu5960*</i>) – <i>pflu5960</i> mutation (g.479T>C; p.D160G), recreated in SBW25	-	Lind et al., 2015
15447	WS-6	WS pathway 6 (<i>pflu0085*</i>) – <i>pflu0085</i> deletion (g.1309_1374del; p.R437_A458del), recreated in SBW25	-	Lind et al., 2015
15448	WS-7	WS pathway 7 (<i>pflu4305-4306*</i>) – deletion of 482 bp resulting in gene fusion of <i>pflu4305</i> (M1-Y340) to <i>pflu4306</i> (S21-G489), recreated in SBW25	-	Lind et al., 2015
15449	WS-8	WS pathway 8 (<i>pflu3571*</i>) – <i>pflu3571</i> mutation (g.37T>C; p.W13R), recreated in SBW25	-	Lind et al., 2015
15450	WS-9	WS pathway 9 (<i>pflu5698*</i>) – <i>pflu5698</i> promoter mutation (g.-73C>T), recreated in SBW25	-	Lind et al., 2015
15451	WS-10	WS pathway 10 (<i>dipA*-pflu0621*</i>) – double mutant: <i>dipA</i> (g.2504A>C; p.I835S) & <i>pflu0621</i> promoter (g.-51C>T), recreated in SBW25	-	Lind et al., 2015
15452	WS-11	WS pathway 11 (<i>dipA*-amrZ*</i>) – double mutant: <i>dipA</i> nonsense (g.208C>A; p.E45*) & <i>amrZ</i> (g.116G>A; p.S39N), recreated in SBW25	-	Lind et al., 2015
15453	WS-12	WS pathway 12 (<i>pflu4414*-fleQ*-amrZ*</i>) – triple mutant: <i>pflu4414</i> (p.Y652fs), <i>fleQ</i> nonsense (g.1192C>A; p.E398*) & <i>amrZ</i> (g.131T>C; p.I44T), recreated in SBW25	-	Lind et al., 2015
15454	WS-13	WS pathway 13 (<i>pflu0184-0183*</i>) – gene fusion of <i>pflu0184</i> (M1-T328) to <i>pflu0183</i> (A29-G335), recreated in SBW25	-	Lind et al., 2015
15455	WS-14	WS pathway 14 (<i>wspF*</i>) – <i>wspF</i> deletion (g.677_826del; p.G225_T274), recreated in SBW25	-	McDonald et al., 2009
15456	WS-15	WS pathway 15 (<i>awsX*</i>) – <i>awsX</i> deletion (g.229_261del; p.Y77_Q87del), recreated in SBW25	-	McDonald et al., 2009
15457	WS-16	WS pathway 16 (<i>mwsR*</i>) – <i>mwsR</i> mutation (g.2183T>C; p.V272A), recreated in SBW25	-	McDonald et al., 2009
<i>Gene deletion & mutation reconstruction</i>				
16047	TSS-f6- <i>wspA</i> -mut1-WT	TSS-f6 with <i>wspA</i> mutation (p.V441G) reverted to wild-type (allelic exchange with MPB15680)	13890	This study
14105	TSS-f6-WspE* (WS)- Δ <i>wspE</i>	TSS-f6 with insertion in WspE (189 bp transposon scar at residue 660) resulting in WS phenotype, with <i>wspE</i> gene deleted (allelic exchange with MPB14086)	13598	This study
14106	TSS-f6-WspE* (SM)- Δ <i>wspE</i>	TSS-f6 with insertion in WspE (189 bp transposon scar at residue 81) resulting in SM phenotype, with <i>wspE</i> gene deleted (allelic exchange with MPB14086)	13596	This study
14082	SBW25- Δ <i>wspE</i>	SBW25 with <i>wspE</i> gene deleted (allelic exchange with MPB14086)	14218	This study

14083	TSS-f6- Δ <i>wspE</i>	TSS-f6 with <i>wspE</i> gene deleted, by allelic exchange with MPB14086	13890	This study
14424	SBW25- Δ <i>wss</i>	SBW25 with entire <i>wss</i> operon (<i>wssA-wssJ</i>) deleted (allelic exchange with MPB12616)	14218	This study
14425	TSS-f6- Δ <i>wss</i>	TSS-f6 with entire <i>wss</i> operon (<i>wssA-wssJ</i>) deleted (allelic exchange with MPB12616)	13890	This study
14426	f2- Δ <i>wss</i>	f2 ancestor with entire <i>wss</i> operon (<i>wssA-wssJ</i>) deleted (allelic exchange with MPB12616)	13893	This study
14084	SBW25- Δ 5960	SBW25 with <i>pflu5960</i> gene deleted (allelic exchange with MPB14087)	14218	This study
14085	TSS-f6- Δ 5960	TSS-f6 with <i>pflu5960</i> gene deleted (allelic exchange with MPB14087)	13890	This study
14634	f2- Δ 5960	f2 ancestor with <i>pflu5960</i> gene deleted (allelic exchange with MPB14087)	13893	This study
14627	SBW25-5960-EAL-mut	SBW25 with mutation (p.E328A) inserted in <i>pflu5960</i> EAL motif (allelic exchange with MPB14586)	14218	This study
14628	TSS-f6-5960-EAL-mut	TSS-f6 with mutation (p.E328A) inserted in <i>pflu5960</i> EAL motif (allelic exchange with MPB14586)	13890	This study
14629	f2-5960-EAL-mut	f2 ancestor with mutation (p.E328A) inserted in <i>pflu5960</i> EAL motif (allelic exchange with MPB14586)	13893	This study
14246	SBW25- Δ <i>amrZ</i>	SBW25 with <i>amrZ</i> (<i>pflu4744</i>) gene deleted (allelic exchange with MPB14195)	14218	This study
14247	TSS-f6- Δ <i>amrZ</i>	TSS-f6 with <i>amrZ</i> (<i>pflu4744</i>) gene deleted (allelic exchange with MPB14195)	13890	This study
14478	SBW25- Δ CA	SBW25 with entire colonic acid (CA) operon (<i>wcaJ-wzb</i>) deleted (allelic exchange with MPB00460)	14218	This study
14479	TSS-f6- Δ CA	TSS-f6 with entire colonic acid operon (<i>wcaJ-wzb</i>) deleted (allelic exchange with MPB00460)	13890	This study
14480	f2- Δ CA	f2 ancestor with entire colonic acid operon (<i>wcaJ-wzb</i>) deleted (allelic exchange with MPB00460)	13893	This study
14131	SBW25- <i>wspA</i> -mut1	<i>wspA</i> mutation 1 from TSS-f6 (p.V441G), recreated in SBW25 (allelic exchange with MPB14102)	14218	This study
14133	f2- <i>wspA</i> -mut1	f2 ancestor with insertion of <i>wspA</i> mutation 1 (allelic exchange with MPB14103)	13893	This study
14609	SBW25- <i>wspA</i> -mut2	<i>wspA</i> mutation 2 from f2 ancestor (p.T104N), recreated in SBW25 (allelic exchange with MPB14554)	14218	This study
14610	L17- <i>mutS</i> -WT- <i>wspA</i> -mut2	L17- <i>mutS</i> -WT with insertion of <i>wspA</i> mutation 2 (allelic exchange with MPB14554)	13896	This study
14624	SBW25- <i>wspE</i> -mut	<i>wspE</i> mutation from f2 ancestor (p.H70L), recreated in SBW25 (allelic exchange with MPB14581)	14218	This study
14626	L17- <i>mutS</i> -WT- <i>wspE</i> -mut	L17- <i>mutS</i> -WT with insertion of <i>wspE</i> mutation (allelic exchange with MPB14581)	13896	This study
14625	SBW25- <i>wspF</i> -mut	<i>wspF</i> mutation from L17- <i>mutS</i> -WT (p.I295S), recreated in SBW25 (allelic exchange with MPB14582)	14218	This study
14623	SBW25- <i>wspA</i> -mut3	<i>wspA</i> mutation 3 from L17- <i>mutS</i> -WT (p.D253Y), recreated in SBW25 (allelic exchange with MPB14580)	14218	This study

14611	SBW25- <i>wspA</i> -mut1&2	SBW25- <i>wspA</i> -mut1 with insertion of <i>wspA</i> mutation 2 (allelic exchange with MPB14554)	14131	This study
14990	SBW25- <i>wspA</i> -mut1- <i>wspF</i> -mut	SBW25- <i>wspA</i> -mut1 with insertion of <i>wspF</i> mutation (allelic exchange with MPB14582)	14131	This study
16050	SBW25- <i>wspA</i> -mut2- <i>wspF</i> -mut	SBW25- <i>wspA</i> -mut2 with insertion of <i>wspF</i> mutation (allelic exchange with MPB14582)	14609	This study
16051	SBW25- <i>wspA</i> -mut1&2- <i>wspF</i> -mut	SBW25- <i>wspA</i> -mut1&2 with insertion of <i>wspF</i> mutation (allelic exchange with MPB14582); temperature sensitive switcher – SM at 28°C & WS at 20°C	14611	This study
<i>Transposon mutants</i>				
13591	TSS-f6: WS Tn- <i>wspE</i>	TSS-f6 transposon mutant (suppressing SM at 28°C), with insertion in <i>wspE</i> (residue 660); WS phenotype	13890	Summers, 2018
13588	TSS-f6: SM Tn- <i>wspE</i>	TSS-f6 transposon mutant (suppressing WS at 20°C), with insertion in <i>wspE</i> (residue 81); SM phenotype	13890	Summers, 2018
13598	TSS-f6- <i>WspE</i> *(WS)	TSS-f6 WS Tn- <i>wspE</i> with transposon removed (conjugation with MPB13623), leaving 189 bp scar in <i>WspE</i> at residue 660; WS phenotype	13591	Summers, 2018
13596	TSS-f6- <i>WspE</i> *(SM)	TSS-f6 SM Tn- <i>wspE</i> with transposon removed (conjugation with MPB13623), leaving 189 bp scar in <i>WspE</i> at residue 81; SM phenotype	13588	Summers, 2018
14801-14817	TSS-f6- Δ 5960 Tn1-17	TSS-f6- Δ <i>pflu5960</i> transposon mutants 1-17, suppressing WS phenotype at 28°C (mutagenesis with MPB14720); Km ^R ; SM phenotype	14085	This study
14833-14855	SBW25- Δ 5960 Tn1-23	SBW25- Δ <i>pflu5960</i> transposon mutants 1-23, suppressing WS phenotype at 28°C (mutagenesis with MPB14720); Km ^R ; SM phenotype	14084	This study
14856-14880	SBW25- Δ 5960 Tn24-48	SBW25- Δ 5960 transposon mutants 24-48, further suppressing SM phenotype at 28°C (mutagenesis with MPB14720); Km ^R ; WS phenotype	14084	This study
14788-14800	TSS-f6- Δ <i>amrZ</i> Tn1-13	TSS-f6- Δ <i>amrZ</i> transposon mutants 1-13, suppressing WS phenotype at 28°C (mutagenesis with MPB14720); Km ^R ; SM phenotype	14247	This study
14818-14825; 15018-15053	SBW25- Δ <i>amrZ</i> Tn1-44	SBW25- Δ <i>amrZ</i> transposon mutants 1-44, suppressing WS phenotype at 28°C (mutagenesis with MPB14720); Km ^R ; SM phenotype	14246	This study
<i>Trial life cycle experiment</i>				
19884-19915	LCE trial-cycle 5: A1-D8	LCE trial evolved lines, SBW25 taken through five generations with new experimental regime (end of cycle 5 - phase II); rack A, B, C & D, with replicate lines 1-8 each	14218	This study
19887	LCE-trial: A4	LCE trial select evolved line A4, from end of cycle 5	14218	This study
19891	LCE-trial: A8	LCE trial select evolved line A8, from end of cycle 5	14218	This study
19892	LCE-trial: B1	LCE trial select evolved line B1, from end of cycle 5	14218	This study
19897	LCE-trial: B6	LCE trial select evolved line B6, from end of cycle 5	14218	This study
19901	LCE-trial: C2	LCE trial select evolved line C2, from end of cycle 5	14218	This study
19906	LCE-trial: C7	LCE trial select evolved line C7, from end of cycle 5	14218	This study

19908	LCE-trial: D1	LCE trial select evolved line D1, from end of cycle 5	14218	This study
19915	LCE-trial: D8	LCE trial select evolved line D8, from end of cycle 5	14218	This study
21753-21760	LCE-trial-c6 B6: 1-8	LCE trial line B6, with replicate lines 1-8 taken through an additional generation (end of cycle 6)	19897	This study
21761-21768	LCE-trial-c6 D1: 1-8	LCE trial line D1, with replicate lines 1-8 taken through an additional generation (end of cycle 6)	19908	This study
21745-21752	LCE-trial-c1 SBW25: 1-8	SBW25 control, with replicate lines 1-8 taken through life cycle generation (end of cycle 1)	14218	This study
<i>Life cycle experiment</i>				
20428; 20429	LCE-cycle-1: 1.1-24.8	Life cycle experiment evolved lines 1.1-24.8 (motile seed from end of cycle 1 - phase II), inoculated with SBW25; racks 1-24, with replicate lines 1-8 each	14218	This study
20535; 20536	LCE-cycle-2: 1.1-24.8	LCE evolved lines 1.1-24.8 (racks 1-24, replicate lines 1-8 each), from end of cycle 2	20428 20429	This study
20844; 20845	LCE-cycle-3: 1.1-24.8	LCE evolved lines 1.1-24.8 (racks 1-24, replicate lines 1-8 each), from end of cycle 3	20844 20845	This study
21588; 21589	LCE-cycle-4: 1.1-24.8	LCE evolved lines 1.1-24.8 (racks 1-24, replicate lines 1-8 each), from end of cycle 4	21588 21589	This study
21730; 21731	LCE-cycle-5: 1.1-24.8	LCE evolved lines 1.1-24.8 (racks 1-24, replicate lines 1-8 each), from end of cycle 5	21730 21731	This study
23200	LCE-c5: rack-2	LCE select evolved line 2.1, from end of cycle 5; representing rack-2 genotype (<i>awsX-W60C</i>)	14218	This study
23203	LCE-c5: rack-6	LCE select evolved line 6.3, from end of cycle 5; representing rack-16 genotype (<i>bifA-G304S</i>)	14218	This study
23206	LCE-c5: rack-7	LCE select evolved line 7.5, from end of cycle 5; representing rack-7 genotype (<i>awsR-mwsR</i>)	14218	This study
23209	LCE-c5: rack-11	LCE select evolved line 11.6, from end of cycle 5; representing rack-11 genotype (<i>awsR-A195V</i>)	14218	This study
23210	LCE-c5: rack-12	LCE select evolved line 12.2, from end of cycle 5; representing rack-12 genotype (<i>sadB-awsX</i>)	14218	This study
23213	LCE-c5: rack-14	LCE select evolved line 14.2, from end of cycle 5; representing rack-14 genotype (<i>awsR-pflu0956</i>)	14218	This study
23215	LCE-c5: rack-16	LCE select evolved line 16.6, from end of cycle 5; representing rack-16 genotype (<i>pflu0185-wspA</i>)	14218	This study
23218	LCE-c5: rack-18	LCE select evolved line 18.4, from end of cycle 5; representing rack-18 genotype (<i>sadB-awsR</i>)	14218	This study
23221	LCE-c5: rack-20	LCE select evolved line 20.3, from end of cycle 5; representing rack-20 genotype (<i>awsR-E61D</i>)	14218	This study
23222	LCE-c5: rack-21	LCE select evolved line 21.6, from end of cycle 5; representing rack-21 genotype (<i>awsR-mwsR-dipA</i>)	14218	This study
23224	LCE-c5: rack-23	LCE select evolved line 23.7, from end of cycle 5; representing rack-23 genotype (mutational strategy)	14218	This study
32222	LCE-cycle-1: 21.8	LCE select evolved line 21.8, from end of cycle 1; ancestor to rack-21 (<i>awsR-T27P, mwsR-T997S</i>)	14218	This study
32223	LCE-cycle-2: 21.6	LCE select evolved line 21.6, from end of cycle 2; ancestor to rack-21 (<i>awsR-T27P, mwsR-T997S-M1L</i>)	14218	This study

24366	LCE-c6-rack-6: A1-C8	LCE-c5 rack-6 (line 6.3), with replicate lines A1-C8 (racks A, B & C; replicates 1-8 each) taken through additional generation (end of cycle 6)	23203	This study
	LCE-c6-rack-7: A1-C8	LCE-c5 rack-7 (line 7.5), with replicate lines A1-C8 taken through additional generation (end of cycle 6)	23206	This study
	LCE-c6-rack-11: A1-C8	LCE-c5 rack-11 (line 11.6), with replicate lines A1-C8 taken through additional generation (end of cycle 6)	23209	This study
	LCE-c6-rack-12: A1-C8	LCE-c5 rack-12 (line 12.2), with replicate lines A1-C8 taken through additional generation (end of cycle 6)	23210	This study
24367	LCE-c6-rack-16: A1-C8	LCE-c5 rack-16 (line 16.6), with replicate lines A1-C8 taken through additional generation (end of cycle 6)	23215	This study
	LCE-c6-rack-21: A1-C8	LCE-c5 rack-21 (line 21.6), with replicate lines A1-C8 taken through additional generation (end of cycle 6)	23222	This study
	LCE-c6-rack-23: A1-C8	LCE-c5 rack-23 (line 23.7), with replicate lines A1-C8 taken through additional generation (end of cycle 6)	23224	This study
	LCE-c1-SBW25: A1-C8	SBW25 ancestor control, with replicate lines A1-C8 taken through life cycle generation (end of cycle 1)	14218	This study
33309	LCE-c6-rack-2: A1-C8	LCE-c5 rack-2 (line 2.1), with replicate lines A1-C8 taken through additional generation (end of cycle 6)	23200	This study
	LCE-c6-rack-14: A1-C8	LCE-c5 rack-14 (line 14.2), with replicate lines A1-C8 taken through additional generation (end of cycle 6)	23213	This study
	LCE-c6-rack-18: A1-C8	LCE-c5 rack-18 (line 18.4), with replicate lines A1-C8 taken through additional generation (end of cycle 6)	23218	This study
	LCE-c6-rack-20: A1-C8	LCE-c5 rack-20 (line 20.3), with replicate lines A1-C8 taken through additional generation (end of cycle 6)	23221	This study
33310	LCE-c2-cycle1-21.8: A1-C8	LCE-cycle-1 line 21.8, with replicate lines A1-C8 taken through additional generation (end of cycle 2)	32222	This study
	LCE-c3-cycle2-21.6: A1-C8	LCE-cycle-2 line 21.6, with replicate lines A1-C8 taken through additional generation (end of cycle 3)	32223	This study
<i>Fluorescent marked strains</i>				
15850	SBW25-GFP	SBW25 with Tn7-GFP-Km fluorescent marker, achieved by conjugation with MPB15811; Km ^R	14218	E. McConnell, unpublished
15852	SBW25-Scarlet	SBW25 with Tn7-Scarlet-Km fluorescent marker, achieved by conjugation with MPB15815; Km ^R	14218	E. McConnell, unpublished
17910	SBW25-Scarlet-pCdrA	SBW25-Scarlet with pCdrA-GFP fluorescent reporter (for intracellular c-di-GMP level), achieved by electroporation with plasmid MPB16772; Km ^R & Gm ^R	15852	E. McConnell, unpublished
20513	LCE-trial: A4-Scarlet	LCE trial cycle 5 evolved line A4, with Tn7-Scarlet marker (MPB15815); Km ^R	19887	This study
20514	LCE-trial: A8-Scarlet	LCE trial cycle 5 evolved line A8, with Tn7-Scarlet marker (MPB15815); Km ^R	19891	This study
20515	LCE-trial: B1-Scarlet	LCE trial cycle 5 evolved line B1, with Tn7-Scarlet marker (MPB15815); Km ^R	19892	This study
20516	LCE-trial: B6-Scarlet	LCE trial cycle 5 evolved line B6, with Tn7-Scarlet marker (MPB15815); Km ^R	19897	This study
20517	LCE-trial: C2-Scarlet	LCE trial cycle 5 evolved line C2, with Tn7-Scarlet marker (MPB15815); Km ^R	19901	This study

20518	LCE-trial: C7-Scarlet	LCE trial cycle 5 evolved line C7, with Tn7-Scarlet marker (MPB15815); Km ^R	19906	This study
20519	LCE-trial: D1-Scarlet	LCE trial cycle 5 evolved line D1, with Tn7-Scarlet marker (MPB15815); Km ^R	19908	This study
20520	LCE-trial: D8-Scarlet	LCE trial cycle 5 evolved line D8, with Tn7-Scarlet marker (MPB15815); Km ^R	19915	This study
20537	LCE-trial: A4-Scarlet-CdrA	LCE trial A4-Scarlet with pCdrA-GFP reporter for c-di-GMP (MPB16772); Km ^R & Gm ^R	20513	This study
20538	LCE-trial: A8-Scarlet-pCdrA	LCE trial A8-Scarlet with pCdrA-GFP reporter for c-di-GMP (MPB16772); Km ^R & Gm ^R	20514	This study
20539	LCE-trial: B1-Scarlet-pCdrA	LCE trial B1-Scarlet with pCdrA-GFP reporter for c-di-GMP (MPB16772); Km ^R & Gm ^R	20515	This study
20540	LCE-trial: B6-Scarlet-pCdrA	LCE trial B6-Scarlet with pCdrA-GFP reporter for c-di-GMP (MPB16772); Km ^R & Gm ^R	20516	This study
20541	LCE-trial: C2-Scarlet-pCdrA	LCE trial C2-Scarlet with pCdrA-GFP reporter for c-di-GMP (MPB16772); Km ^R & Gm ^R	20517	This study
20542	LCE-trial: C7-Scarlet-pCdrA	LCE trial C7-Scarlet with pCdrA-GFP reporter for c-di-GMP (MPB16772); Km ^R & Gm ^R	20518	This study
20543	LCE-trial: D1-Scarlet-pCdrA	LCE trial D1-Scarlet with pCdrA-GFP reporter for c-di-GMP (MPB16772); Km ^R & Gm ^R	20519	This study
20544	LCE-trial: D8-Scarlet-pCdrA	LCE trial D8-Scarlet with pCdrA-GFP reporter for c-di-GMP (MPB16772); Km ^R & Gm ^R	20520	This study
32228	LCE: rack-2-GFP	LCE cycle 5 evolved lineage rack-2 (line 2.1), with Tn7-GFP marker (MPB15811); Km ^R	23200	This study
25230	LCE: rack-6-GFP	LCE cycle 5 evolved lineage rack-6 (line 6.3), with Tn7-GFP marker (MPB15811); Km ^R	23203	This study
25231	LCE: rack-7-GFP	LCE cycle 5 evolved lineage rack-7 (line 7.5), with Tn7-GFP marker (MPB15811); Km ^R	23206	This study
25232	LCE: rack-11-GFP	LCE cycle 5 evolved lineage rack-11 (line 11.6), with Tn7-GFP marker (MPB15811); Km ^R	23209	This study
25233	LCE: rack-12-GFP	LCE cycle 5 evolved lineage rack-12 (line 12.2), with Tn7-GFP marker (MPB15811); Km ^R	23210	This study
32229	LCE: rack-14-GFP	LCE cycle 5 evolved lineage rack-14 (line 14.2), with Tn7-GFP marker (MPB15811); Km ^R	23213	This study
25234	LCE: rack-16-GFP	LCE cycle 5 evolved lineage rack-16 (line 16.6), with Tn7-GFP marker (MPB15811); Km ^R	23215	This study
32230	LCE: rack-18-GFP	LCE cycle 5 evolved lineage rack-12 (line 18.4), with Tn7-GFP marker (MPB15811); Km ^R	23218	This study
32231	LCE: rack-20-GFP	LCE cycle 5 evolved lineage rack-12 (line 20.3), with Tn7-GFP marker (MPB15811); Km ^R	23221	This study
25235	LCE: rack-21-GFP	LCE cycle 5 evolved lineage rack-21 (line 21.6), with Tn7-GFP marker (MPB15811); Km ^R	23222	This study
25236	LCE: rack-23-GFP	LCE cycle 5 evolved lineage rack-23 (line 23.7), with Tn7-GFP marker (MPB15811); Km ^R	23224	This study
23306	LCE: rack-2-Scarlet	LCE cycle 5 evolved lineage rack-2 (line 2.1), with Tn7-Scarlet marker (MPB15815); Km ^R	23200	This study

23309	LCE: rack-6-Scarlet	LCE cycle 5 evolved lineage rack-6 (line 6.3), with Tn7-Scarlet marker (MPB15815); Km ^R	23203	This study
23312	LCE: rack-7-Scarlet	LCE cycle 5 evolved lineage rack-7 (line 7.5), with Tn7-Scarlet marker (MPB15815); Km ^R	23206	This study
23315	LCE: rack-11-Scarlet	LCE cycle 5 evolved lineage rack-11 (line 11.6), with Tn7-Scarlet marker (MPB15815); Km ^R	23209	This study
23316	LCE: rack-12-Scarlet	LCE cycle 5 evolved lineage rack-12 (line 12.2), with Tn7-Scarlet marker (MPB15815); Km ^R	23210	This study
23319	LCE: rack-14-Scarlet	LCE cycle 5 evolved lineage rack-14 (line 14.2), with Tn7-Scarlet marker (MPB15815); Km ^R	23213	This study
23321	LCE: rack-16-Scarlet	LCE cycle 5 evolved lineage rack-16 (line 16.6), with Tn7-Scarlet marker (MPB15815); Km ^R	23215	This study
23324	LCE: rack-18-Scarlet	LCE cycle 5 evolved lineage rack-12 (line 18.4), with Tn7-Scarlet marker (MPB15815); Km ^R	23218	This study
23327	LCE: rack-20-Scarlet	LCE cycle 5 evolved lineage rack-12 (line 20.3), with Tn7-Scarlet marker (MPB15815); Km ^R	23221	This study
23328	LCE: rack-21-Scarlet	LCE cycle 5 evolved lineage rack-21 (line 21.6), with Tn7-Scarlet marker (MPB15815); Km ^R	23222	This study
23330	LCE: rack-23-Scarlet	LCE cycle 5 evolved lineage rack-23 (line 23.7), with Tn7-Scarlet marker (MPB15815); Km ^R	23224	This study
23337	LCE: rack-2-Scarlet-pCdrA	LCE rack-2-Scarlet with pCdrA-GFP reporter for c-di-GMP (MPB16772); Km ^R & Gm ^R	23306	This study
23340	LCE: rack-6-Scarlet-pCdrA	LCE rack-6-Scarlet with pCdrA-GFP reporter for c-di-GMP (MPB16772); Km ^R & Gm ^R	23309	This study
23343	LCE: rack-7-Scarlet-pCdrA	LCE rack-7-Scarlet with pCdrA-GFP reporter for c-di-GMP (MPB16772); Km ^R & Gm ^R	23312	This study
23346	LCE: rack-11-Scarlet-pCdrA	LCE rack-11-Scarlet with pCdrA-GFP reporter for c-di-GMP (MPB16772); Km ^R & Gm ^R	23315	This study
23347	LCE: rack-12-Scarlet-pCdrA	LCE rack-12-Scarlet with pCdrA-GFP reporter for c-di-GMP (MPB16772); Km ^R & Gm ^R	23316	This study
23350	LCE: rack-14-Scarlet-pCdrA	LCE rack-14-Scarlet with pCdrA-GFP reporter for c-di-GMP (MPB16772); Km ^R & Gm ^R	23319	This study
23352	LCE: rack-16-Scarlet-pCdrA	LCE rack-16-Scarlet with pCdrA-GFP reporter for c-di-GMP (MPB16772); Km ^R & Gm ^R	23321	This study
23355	LCE: rack-18-Scarlet-pCdrA	LCE rack-18-Scarlet with pCdrA-GFP reporter for c-di-GMP (MPB16772); Km ^R & Gm ^R	23324	This study
23358	LCE: rack-20-Scarlet-pCdrA	LCE rack-20-Scarlet with pCdrA-GFP reporter for c-di-GMP (MPB16772); Km ^R & Gm ^R	23327	This study
23359	LCE: rack-21-Scarlet-pCdrA	LCE rack-21-Scarlet with pCdrA-GFP reporter for c-di-GMP (MPB16772); Km ^R & Gm ^R	23328	This study
23361	LCE: rack-23-Scarlet-pCdrA	LCE rack-23-Scarlet with pCdrA-GFP reporter for c-di-GMP (MPB16772); Km ^R & Gm ^R	23330	This study
32224	LCE: c1-21.8-GFP	LCE cycle 1 evolved line 21.8 (rack-21 ancestor), with Tn7-GFP marker (MPB15811); Km ^R	32222	This study
32225	LCE: c2-21.6-GFP	LCE cycle 2 evolved line 21.6 (rack-21 ancestor), with Tn7-GFP marker (MPB15811); Km ^R	32223	This study

32226	LCE: c1-21.8-Scarlet	LCE cycle 1 evolved line 21.8 (rack-21 ancestor), with Tn7-Scarlet marker (MPB15815); Km ^R	32222	This study
32227	LCE: c2-21.6-Scarlet	LCE cycle 2 evolved line 21.6 (rack-21 ancestor), with Tn7-Scarlet marker (MPB15815); Km ^R	32223	This study
32578	LCE: c1-21.8-Scarlet-pCdrA	LCE c1-21.8-Scarlet with CdrA-GFP reporter plasmid for c-di-GMP level (MPB16772); Km ^R & Gm ^R	32226	This study
32579	LCE: c2-21.6-Scarlet-pCdrA	LCE c2-21.6-Scarlet with CdrA-GFP reporter plasmid for c-di-GMP level (MPB16772); Km ^R & Gm ^R	32227	This study

Table 5.1. Strains of *P. fluorescens* used in this study. Provided for each *P. fluorescens* strain: MPB (strain storage number), Name, Description (Origin of strain; genotype & phenotype where applicable), Parent (MPB number of parental strain), and Reference.

5.1.2 *E. coli* strains

The details of *E. coli* strains used in this study are provided in Table 5.2 below.

Name	Genotype	Reference
DH5 α	F ⁻ , ϕ 80 <i>lacZ</i> Δ M15, Δ (<i>lacZYA-argF</i>)U169, <i>recA1</i> , <i>endA1</i> , <i>hsdR17</i> , <i>phoA</i> , <i>supE44</i> , λ ⁻ <i>thi-1</i> , <i>gyrA96</i> , <i>relA1</i>	Invitrogen
DH5 α - λ pir	F ⁻ , ϕ 80 <i>lacZ</i> Δ M15, Δ (<i>lacZYA-argF</i>)U169, <i>recA1</i> , <i>endA1</i> , <i>hsdR17</i> , <i>supE44</i> , <i>thi-1</i> , <i>gyrA96</i> , <i>relA1</i> , <i>zdg-232::Tn10</i> , <i>uidA::pir</i> ⁺	Invitrogen
SM10- λ pir	F ⁻ , <i>thi</i> , <i>thr</i> , <i>leu</i> , <i>tonA</i> , <i>lacY</i> , <i>supE</i> , <i>recA</i> , RP4-2-Tc::Mu, Km ^R , λ pir	Simon et al., 1983
S17-1- λ pir	F ⁻ , <i>thi</i> , <i>pro</i> , <i>res</i> ⁻ , <i>mod</i> ⁺ , <i>recA</i> , <i>hsdR-M</i> ⁺ , RP4-2-Tc:Mu-Km::Tn7, Tp ^R , Sm ^R , λ pir	Simon et al., 1983
TOP10	F ⁻ , <i>mcrA</i> , Δ (<i>mrr-hsdRMS-mcrBC</i>), ϕ 80 <i>lacZ</i> Δ M15, Δ <i>lacX74</i> , <i>recA1</i> , <i>araD139</i> , Δ (<i>ara-leu</i>)7697, <i>galU</i> , <i>galK</i> , λ ⁻ <i>rpsL</i> (Str ^R), <i>endA1</i> , <i>nupG</i>	Invitrogen

Table 5.2. Strains of *E. coli* used in this study. Details provided for the *E. coli* competent cells used in transformation and molecular cloning. Provided for each: Name, Genotype, and Reference.

5.1.3 Plasmids and transposons

The plasmids and transposons used in this study are listed in Table 5.3 below. The sequence of mutation constructs are also provided in [Supplementary A-5](#). pMRE-Tn7-152 (MPB15811) & pMRE-Tn7-155 (MPB15815) was a gift from Mitja Remus-Emsermann (Addgene: plasmid [#118566](#) & [#118569](#)). pCdrA-gfpC (MPB16772) was a gift from Tim Tolker-Nielsen (Addgene: plasmid [#111614](#)).

MPB	Name	Strain	Description	Reference
13957	pUIC3	DH5 α - λ pir	pUIC3 integration vector with promoterless- <i>lacZ</i> gene & <i>mob</i> gene; Tc ^R	Rainey, 1999

13966	pUIC3-mini	DH5 α - λ pir	pUIC3-mini-GFP integration vector – combination of pSEVA511 (de Lorenzo) & pBG42-msfGFP; MCS replaced with Gibson landing; Tc ^R	D. Rogers, unpublished
13960	prK2013	DH5 α	prK2013 helper plasmid for tri-parental conjugation; <i>tra</i> & <i>mob</i> genes; Km ^R	Ditta et al., 1980
14720	pSCR001	SM10- λ pir	pSCR001 donor plasmid with IS- Ω -Km/hah transposon for mutagenesis; IE, <i>nptII</i> promoter, OE, <i>loxP</i> recombination sites, ColE1 <i>ori</i> ; Km ^R	Giddens et al., 2007
13623	pCre	S17-1- λ pir	pCre donor plasmid for Cre- <i>loxP</i> -mediated excision of IS- Ω -Km/hah transposon, leaving 189 bp scar at insertion site; phage P1 <i>cre</i> gene in pUT; Am ^R	Bailey & Manoil, 2002
15811	pMRE-Tn7-GFP-Km	S17-1- λ pir	pMRE-Tn7-GFP-Km (Addgene: 118566) – fluorescent marker with site-specific transposon, used for flow cytometry; plasmid MRE-pSC101ori-oriT-Tn7-AraC-Pbad-tnsABCD-PntpII-sGFP2 ; Km ^R & Am ^R	Schlechter et al., 2018
15815	pMRE-Tn7-Scarlet-Km	S17-1- λ pir	pMRE-Tn7-Scarlet-Km (Addgene: 118569) – fluorescent marker with site-specific transposon, for use in flow cytometry; plasmid MRE-pSC101ori-oriT-Tn7-AraC-Pbad-tnsABCD-PntpII-mScarlet-I; Km ^R & Am ^R	Schlechter et al., 2018
16772	pCdrA-GFP	DH5 α	pCdrA-GFP (Addgene: 111614) – fluorescent reporter for intracellular c-di-GMP level; plasmid <i>cdrA</i> -RBSII-gfp(Mut3)-T0-T1, pRO1600, <i>oriV</i> ; Gm ^R & Am ^R	Rybtke et al., 2012
<i>Mutation constructs</i>				
15680	pUIC3mini- <i>wspA</i> -WT	TOP10	Construct for reversion of <i>wspA</i> mutation 1 from TSS-f6 to wild-type (p.G441V), assembled in pUIC3-mini by PCR (P15/16 & 17/18) & Gibson assembly; Tc ^R	This study
14086	pUIC3- Δ <i>wspE</i>	DH5 α - λ pir	Construct for deletion of <i>wspE</i> gene (1889 bp deleted), assembled in pGEM-T then pUIC3 by SOE-PCR (P19/20 & 21/22) & ligation; Tc ^R	This study
12616	pUIC3- Δ <i>wss</i>	DH5 α - λ pir	Construct for deletion of entire <i>wss</i> operon (<i>wssA-wssJ</i>), assembled in pUIC3; Tc ^R	Gallie, 2010
00460	pUIC3- Δ CA	DH5 α - λ pir	Construct for deletion of entire colanic acid (CA) operon (<i>wcaJ-wzb</i>), assembled in pUIC3; Tc ^R	Gallie et al., 2015
14087	pUIC3- Δ 5960	DH5 α - λ pir	Construct for deletion of <i>pflu5960</i> gene (1687 bp deleted), assembled in pGEM-T then pUIC3 by SOE-PCR (P23/24 & 25/26) & ligation; Tc ^R	This study
14583	pUIC3mini-5960-EAL-mut	DH5 α - λ pir	Construct for <i>pflu5960</i> EAL motif mutation (E328A; EAL \rightarrow AAL), assembled in pUIC3-mini by PCR (P27/28 & 29/30) & Gibson assembly; Tc ^R	This study
14195	pUIC3mini- Δ <i>amrZ</i>	DH5 α - λ pir	Construct for deletion of <i>amrZ</i> gene (440 bp deleted), assembled in pUIC3-mini by PCR (P31/32 & 33/34) & Gibson assembly; Tc ^R	This study
14102	pUIC3- <i>wspA</i> (WT)-mut1	DH5 α - λ pir	Construct for recreation of <i>wspA</i> mutation 1 from TSS-f6 (p.V441G), assembled in pGEM-T then pUIC3 by SOE-PCR (P35/36 & 37/38; using WT gDNA template) & ligation; Tc ^R	This study
14103	pUIC3- <i>wspA</i> (f2)-mut1	DH5 α - λ pir	Construct for recreation of <i>wspA</i> mutation 1 from TSS-f6 (p.V441G), assembled in pGEM-T then pUIC3 by SOE-PCR (P35/36 & 37/38; using f2 ancestor gDNA template) & ligation; Tc ^R	This study

14554	pUIC3-mini- <i>wspA</i> -mut2	DH5 α - λ pir	Construct for recreation of <i>wspA</i> mutation 2 from f2 ancestor (p.T104N), assembled in pUIC3-mini by PCR (P39/40 & 41/42) & Gibson assembly; Tc ^R	This study
14581	pUIC3-mini- <i>wspE</i> -mut	DH5 α - λ pir	Construct for recreation of <i>wspE</i> mutation from f2 ancestor (p.H70L), assembled in pUIC3-mini by PCR (P43/44 & 45/46) & Gibson assembly; Tc ^R	This study
15679	pUIC3-mini- <i>wspA</i> -mut3	TOP10	Construct for recreation of <i>wspA</i> mutation 3 from L17 <i>mutS</i> -WT (p.D253Y), assembled in pUIC3-mini by PCR (P47/48 & 49/50) & Gibson assembly; Tc ^R	This study
14582	pUIC3-mini- <i>wspF</i> -mut	DH5 α - λ pir	Construct for recreation of <i>wspF</i> mutation from L17- <i>mutS</i> -WT (p.I295S), assembled in pUIC3-mini by PCR (P51/52 & 53/54) & Gibson assembly; Tc ^R	This study

Table 5.3. Plasmids & transposons used in this study. Information provided for plasmids and transposons used for molecular cloning. Provided for each: MPB, Name, Strain (*E. coli* competent cells; refer to Table 5.2), Description (Details of genotype and/or method of construction), and Reference.

5.1.4 Primers

The primers used in this study are listed in Table 5.4 below. Primers were designed specific to particular regions of the SBW25 genome (GenBank: [AM181176.4](#)), using Geneious Prime version 2020.0.3 (with a modified version of Primer3), as well as NEBuilder for Gibson assembly primers. All DNA oligos were ordered from Integrated DNA Technologies (25 nmole & standard purification).

P#	Name	Sequence (5' → 3')	Target region
<i>Transposon mutagenesis</i>			
1	TnphoA II	GTGCAGTAATATCGCCCTGAGCA	IS- Ω -Km/hah transposon
2	CEKG 2A	GGCCACGCGTCGACTAGTACNNNNNNNNNNAGAG	Non specific; 5' anchor
3	CEKG 2B	GGCCACGCGTCGACTAGTACNNNNNNNNNNACGCC	
4	CEKG 2C	GGCCACGCGTCGACTAGTACNNNNNNNNNNGATAT	
5	Hah-1	ATCCCCCTGGATGGAAAACGG	IS- Ω -Km/hah transposon
6	CEKG 4	GGCCACGCGTCGACTAGTAC	5' end of CEGK 2 A/B/C
<i>Plasmid vector sequencing</i>			
7	M13-F	GTAAAACGACGGCCAG	pGem-T – upstream/ downstream MCS
8	M13-R	CAGGAAACAGCTATGAC	
9	MLG-21	CAGGGTTATTGTCTCATGAGC	pUIC3 – upstream/ downstream SpeI site
10	MLG-22	TGGGATTAAGTGC GCGTCGCC	
11	pUIC3-seq-F	ATTTGTCCTACTCAGGAGAGCGTTC	pUIC3-mini – upstream/ downstream Gibson site
12	pUIC3-seq-R	AGCGTTCTGAACAAATCCAGATG	
<i>Mutation & gene deletion construction</i>			

13	pUIC3-mini-F	AGCACTACATCAACTGACTA	pUIC3-mini – for PCR of backbone
14	pUIC3-mini-R	CTGAACCAAGATAGCTGTAC	
15	<i>wspA</i> -WT-1F	gtacagctatcttggtcagCACGTCCAAGCAGCAACAG	<i>wspA</i> -G441V mutation upstream flank; pUIC3-mini
16	<i>wspA</i> -WT-2R	gtccatgccATCACCCCGCAGACACTG	
17	<i>wspA</i> -WT-3F	cgggggtgatGGGCATGGACAAGTTCTC	<i>wspA</i> -G441V (WT) mutation downstream flank; pUIC3-mini
18	<i>wspA</i> -WT-4R	tagtcagttgatgtagtctCTTGAGGGCATAGCGTTC	
19	<i>wspE</i> -del-1F	<u>ACTAGTTGTTTTACTGGCTGGGGCT</u>	<i>wspE</i> gene upstream flank; SpeI
20	<i>wspE</i> -del-2R	taaggagcaaGCTGAACAATTCCAGCAG	
21	<i>wspE</i> -del-3F	attgttcagcTTGCTCCTTAATCGTGGT	<i>wspE</i> gene downstream flank; SpeI
22	<i>wspE</i> -del-4R	<u>ACTAGTCGAACACTTGGTCCACATG</u>	
23	<i>5960</i> -del-1F	<u>ACTAGTGCCAACTACCTGCTCAACCA</u>	<i>pflu5960</i> gene upstream flank; SpeI
24	<i>5960</i> -del-2R	atcttcgagaAACCCAATCAACATGTGG	
25	<i>5960</i> -del-3F	tgattgggtTCTGCAAGATTCGTTGG	<i>pflu5960</i> gene downstream flank; SpeI
26	<i>5960</i> -del-4R	<u>ACTAGTCGATCAGCATTTTCACCAGC</u>	
27	<i>5960</i> -mut-1F	gtacagctatcttggtcagCAGGCTGTTGAGGTGCACGAAC	<i>pflu5960</i> -E328A mutation upstream flank; pUIC3-mini
28	<i>5960</i> -mut-2R	catatcgtcGTCTCGCGGCCCTGGTGC	
29	<i>5960</i> -mut-3F	gccgcgagacCGACGATATGCCATCGTC	<i>pflu5960</i> -E328A mutation downstream flank; pUIC3-mini
30	<i>5960</i> -mut-4R	tagtcagttgatgtagtctTGATCCTGCAAGTGGTCTC	
31	<i>amrZ</i> -del-1F	gtacagctatcttggtcagCGCCTTACCTTATGTCGCC	<i>amrZ</i> gene upstream flank; pUIC3-mini
32	<i>amrZ</i> -del-2R	ccaggcaaaaAGGGGAGCGGTTTTTGAATTG	
33	<i>amrZ</i> -del-3F	ccgctcccTTTTTGCCTGGGATTTGGTG	<i>amrZ</i> gene downstream flank; pUIC3-mini
34	<i>amrZ</i> -del-4R	tagtcagttgatgtagtctCCTGATAAACGGCCTGGTG	
35	<i>wspA</i> -mut1-1F	<u>ACTAGTCCTGCCGGGCGGAATCAAT</u>	<i>wspA</i> -V441G mutation 1 upstream flank; SpeI
36	<i>wspA</i> -mut1-2R	gtccatgccATCCCCCGCAGACACT	
37	<i>wspA</i> -mut1-3F	cgggggggatGGGCATGGACAAGTTCTC	<i>wspA</i> -V441G mutation 1 downstream flank; SpeI
38	<i>wspA</i> -mut1-4R	<u>ACTAGTGCTGCCAGTATTCGCCCGGC</u>	
39	<i>wspA</i> -mut2-1F	gtacagctatcttggtcagGAGCGTTCTATCCGATAAC	<i>wspA</i> -T104N mutation 2 upstream flank; pUIC3-mini
40	<i>wspA</i> -mut2-2R	tgccatgaaTGTTTTTTTCGTAGTTGGC	
41	<i>wspA</i> -mut2-3F	gaaaaaacaTTCATGGCCAAGCTGACC	<i>wspA</i> -T104N mutation 2 downstream flank; pUIC3-mini
42	<i>wspA</i> -mut2-4R	tagtcagttgatgtagtctCTCCAGGTTAAGGCGTTTG	
43	<i>wspE</i> -mut-1F	gtacagctatcttggtcagGTGGTGCCGGTGGATGAAG	<i>wspE</i> -H70L mutation upstream flank; pUIC3-mini
44	<i>wspE</i> -mut-2R	ccatgacgagGGACACGCTGACCCCGGC	
45	<i>wspE</i> -mut-3F	cagcgtgtccCTCGTCATGGAGGATTGC	<i>wspE</i> -H70L mutation downstream flank; pUIC3-mini
46	<i>wspE</i> -mut-4R	tagtcagttgatgtagtctATCCCCTGGCTTTGAATG	

47	<i>wspA</i> -mut3-1F	gtacagctatcttggtcagAACTACAACAAAGTGCTGG	<i>wspA</i> -D253Y mutation 3 upstream flank; pUIC3-mini
48	<i>wspA</i> -mut3-2R	ggctcatcatgTAGTTAAAGCCGGTTTCG	
49	<i>wspA</i> -mut3-3F	gctttaactaCATGATGACCGAGCTCAC	<i>wspA</i> -D253Y mutation 3 downstream flank; pUIC3-mini
50	<i>wspA</i> -mut3-4R	tagtcagttgatgtagtgctGCTTTTTCCGCTTCGATG	
51	<i>wspF</i> -mut-1F	gtacagctatcttggtcagAACGTCAAAGCCTGGTGG	<i>wspF</i> -I295S mutation upstream flank; pUIC3-mini
52	<i>wspF</i> -mut-2R	tttgctgacCTGGGCGCTGGTCAAATAAC	
53	<i>wspF</i> -mut-3F	cagcgcccagGATCAGCAAAGCTCGGCG	<i>wspF</i> -I295S mutation downstream flank; pUIC3-mini
54	<i>wspF</i> -mut-4R	tagtcagttgatgtagtgctTGGTGGAAAGCACGATGATC	
<i>Mutation sequencing confirmation</i>			
55	<i>wspA</i> -wt-seq-F	AGCAAACGCCTTAACCTGGA	<i>wspA</i> -G441V mutation upstream/downstream
56	<i>wspA</i> -wt-seq-R	GCGTCGGGTGGTAATTGAC	
57	<i>wspEdel</i> -seq-1F	GCGCCGATTCAGCTAAACC	<i>wspE</i> gene deletion upstream/downstream
58	<i>wspEdel</i> -seq-2F	TGCAACCGATCCATTCCCTG	
59	<i>wspEdel</i> -seq-R	CGAATGTGGTGGTTGGTGC	
60	<i>wssdel</i> -seq-1F	TGAGCCCCGACACCACATAAC	<i>wss</i> operon deletion upstream/downstream
61	<i>wssdel</i> -seq-2F	AGGATGACGAATGGCTGAGC	
62	<i>wssdel</i> -seq-R	GTTGCGGCGTGATGAGAATG	
63	<i>CAdel</i> -seq-1F	CAAAGGATCATGACAGCGCG	Colonic acid (CA) operon deletion upstream/downstream
64	<i>CAdel</i> -seq-2F	ACCCTGCCTATCAACACACG	
65	<i>CAdel</i> -seq-R	CTTTCTCAGCGGTAAGTGC	
66	<i>5960del</i> -seq-1F	CCCGGTTTCCTGAGCTTCAT	<i>pflu5960</i> gene deletion upstream/downstream
67	<i>5960del</i> -seq-2F	CTGCATTCGTGGGCTGAAAG	
68	<i>5960del</i> -seq-R	GTCCTTGAGCAGCATCAGGT	
69	<i>5960mut</i> -seq-F	TCCAGGTTGAGGTTGTGAGC	<i>pflu5960</i> -E328A (EAL motif) mutation upstream/downstream
70	<i>5960mut</i> -seq-R	TGGACCTCGATAACTTCCGC	
71	<i>amrZdel</i> -seq-F	GATTGTGGGTCGTCGGATCA	<i>amrZ</i> gene deletion upstream/downstream
72	<i>amrZdel</i> -seq-R	TTACCATGATTGTGCGTGCG	
73	<i>wspA</i> mut1-seq-F	TACAACAAAGTGCTGGCCCA	<i>wspA</i> -V441G mutation 1 upstream/downstream
74	<i>wspA</i> mut1-seq-R	GTCGCAAAGGATTCGGGGTA	
75	<i>wspA</i> mut2-seq-F	GGGTGCGTGGGTTGTATCTT	<i>wspA</i> -T104N mutation 2 upstream/downstream
76	<i>wspA</i> mut2-seq-R	CGACGTAGCACCGATCTCAG	
77	<i>wspEmut</i> -seq-F	TTGCAACCGATCCATTCCCT	<i>wspE</i> -H70L mutation upstream/downstream
78	<i>wspEmut</i> -seq-R	CTGGGCTTCGCTCAACAAAC	
79	<i>wspA</i> mut3-seq-F	GCGACGACAAAACCTTCACC	<i>wspA</i> -D253Y mutation 3 upstream/downstream
80	<i>wspA</i> mut3-seq-R	CCACTTGCTGCACTTCGAAC	
81	<i>wspF</i> mut-seq-F	TCCTCAATATCGGCTGGCTG	<i>wspF</i> -I295S mutation upstream/downstream

82	<i>wspF</i> mut-seq-R	CATGTAGGAGCGCGAGTGAT	
----	-----------------------	----------------------	--

Table 5.4. Primers used in this study. Provided for each primer: P# (primer number), Name, Sequence (5' → 3'; overhang in lowercase & restriction site underlined), and Target region.

5.1.5 Culture medium

Media was prepared with assistance from technicians of the Microbial Population Biology Department (MPI Plön), as well as the disposal of waste. All culture medium was made with Milli-Q ultrapure water (H₂O; purified using Milli-Q Advantage A10), and sterilised by autoclaving at 121°C for 15 minutes. For growth of bacteria, King's Medium B (KB) (King et al., 1954) and Lysogeny Broth (LB) (Bertani, 1951) were used, as detailed below.

KB contained (1 L total volume in H₂O):

10 mL	Glycerol	(Sigma-Aldrich: G9012)
20 g	Bacto Proteose Peptone No. 3	(US Biological: P9113-22)
1.5 g	K ₂ PO ₄ (anhydrous)	(Merck: 105104)
1.5 g	MgSO ₄ ·7H ₂ O	(Fisher Scientific: M/1050/53)

LB contained (1 L total volume in H₂O):

10 g	Tryptone	(VWR: J859)
5 g	Yeast extract	(VWR: J850)
10 g	NaCl	(Sigma-Aldrich: 31434)

To minimise autofluorescence of SBW25, when applicable the iron supplement FeSO₄·7H₂O (0.45 mM) (Sigma-Aldrich: [F8263](#)) was added to media before autoclaving.

For liquid media: KB or LB was prepared as described above, autoclaved in Schott bottles or 25 mL glass microcosms (for 6 mL cultures), and stored at room temperature. For solid agar plates (1.5%): 15 g of Agar (VWR: [J637](#)) was added to 1 L of liquid media before autoclaving; after autoclaving the agar was cooled to 55-60°C in a shaking water bath (Julabo SW23), antibiotics added if required, and then poured into petri dishes (20-30 mL per plate). KBA or LBA plates were left to set before inverting, dried in stacks overnight at 28°C, and stored at room temperature for short term use (or 4°C for long term use). For semi-solid agar (SSA) plates (0.25%): 1 g of Agar was added to 400 mL of 1% KB (4 mL liquid KB in 400 mL total volume H₂O), autoclaved in 500 mL Schott bottles, cooled to 55°C in a water bath, and poured thick into petri dishes (~40 mL per plate; 10 plates per 400 mL). SSA plates were left to set for 2-3 hours, dried upright in stacks of 4-8 at room temperature overnight, and

used the following day for motility assays. For preparation of large batches of agar plates, the plate pouring machine was utilised (Integra MediaClave 10 & MediaJet).

For transformation, the liquid recovery medium Super Optimal Broth (SOB) or Super Optimal broth with Catabolite repression (SOC) (Hanahan, 1983) was used, as detailed below.

SOB contained (1 L total volume in H₂O):

20 g Tryptone
 5 g Yeast extract
 0.58 g NaCl (10 mM)
 0.19 g KCl (2.5 mM) (Sigma-Aldrich: [P3911](#))

Before autoclaving SOB, the pH level was adjusted to 7.0 by addition of 1 M NaOH (Carl Roth: [6771.3](#)). After autoclaving, 10 mL each of sterile 1 M MgCl₂ (anhydrous) (10 mM) (Sigma-Aldrich: [M8266](#)) & 1 M MgSO₄·7H₂O (10 mM) were added to SOB. To make SOC, 20 mL of sterile 1 M Glucose (20 mM) (Carl Roth: [X997.2](#)) was additionally added to SOB.

For freezer storage of bacterial stocks, glycerol/saline contained (1 L total volume in H₂O): 700 mL Glycerol (70%) & 8.5 g NaCl. To prepare electrocompetent cells, glycerol/HEPES contained (1 L total volume in H₂O): 100 mL Glycerol (10%) & 10 mL 1 M HEPES (10 mM) (VWR: [J848](#)). For making dilutions, Ringer's contained: 1x Ringer's solution 1/4 strength tablet (Sigma-Aldrich: [96724](#)) in 500 mL H₂O. For flow cytometry, Phosphate-Buffered Saline (PBS) contained: 1x PBS tablet (Gibco: [18912014](#)) in 500 mL H₂O.

5.1.6 Antibiotics & reagents

The details of antibiotics and reagents used in this study are provided in *Table 5.5* below. To make stock solutions, antibiotics were first dissolved in UltraPure distilled water (UP dH₂O; Invitrogen: [10977-049](#)) at the required concentration, and then sterilised using a 0.2 µm cellulose filter (Whatman FP 30/0.2). Where applicable, the solvent Ethanol denatured (EtOH) (Carl Roth: [K928.1](#)), Dimethyl sulfoxide (DMSO) (Carl Roth: [4720.1](#)) or N,N-Dimethylformamide (DMF) (Thermo Scientific: [20673](#)) were also used.

Name	Abb.	Solvent	Stock conc. (mg/mL)	Storage	Final conc. (µg/mL)	Supplier
Kanamycin	Km	H ₂ O	50.0	-20°C	50.0	TRC: K137500
Tetracycline	Tc	50% EtOH	12.5	-20°C*	12.5	Sigma-Aldrich: T7660

Ampicillin	Am	H ₂ O	100.0	-20°C	100.0	Carl Roth: K029.1
Gentamicin	Gm	H ₂ O	20.0	-20°C	20.0	TRC: G360600
Nitrofurantoin	Nf	DMSO	-	unstable	100.0	TCI: N0883
D-cycloserine	DCS	H ₂ O	-	unstable	800.0	Sigma-Aldrich: C6880
Isopropyl β-D-1-thiogalactopyranoside	IPTG	H ₂ O	238.0	-20°C	238.0	Fisher Scientific: BP1755-1
5-Bromo-4-chloro-3-indolyl-β-D-galactoside	X-gal	DMF	40.0	4°C	80.0	VWR: 37-2610

Table 5.5. Antibiotics & reagents used in this study. Details provided: Name, Abb. (abbreviation), Solvent, Stock concentration (mg/mL), Storage (temperature stock solution was stored; * indicates light sensitivity; unstable stocks made fresh before use), Final concentration (μg/mL), and Supplier (with catalogue number and link to specific product).

5.1.7 Enzymes & kits

The details of enzymes and kits used in this study are provided in *Table 5.6* below. For all molecular cloning, the diluent UP dH₂O (DNase & RNase free) was used.

Name	Description	Supplier
TopTaq Master Mix Kit	Taq thermo-stable DNA polymerase master mix for standard PCR	Qiagen: 200403
Taq 2X Master Mix		NEB: M0270
Phusion High-Fidelity PCR Master Mix	High-fidelity polymerase master mix for mutation construction and cloning	Thermo Scientific: F531L
Q5 High-Fidelity 2X Master Mix		NEB: M0492
SAP-Exo Kit	Kits for purification of PCR products	Jena Bioscience: PP-218
QIAquick PCR Purification Kit		Qiagen: 28106
SureClean Plus		Bioline: BIO-37047
SpeI-HF	For digestion of plasmid vectors for cloning	NEB: R3133
DpnI	For digestion of plasmid PCR template	NEB: R0176
TaKaRa Taq DNA Polymerase	Taq polymerase for AP-PCR	Takara: R001
dNTP mix (10 mM)	dNTP mix for AP-PCR	Thermo Scientific: R0191
Exonuclease I	Enzymes for purification of AP-PCR products	NEB: M0293
Antarctic Phosphatase		NEB: M0289
dATP (100 mM)	dATP for addition of 3'-adenine overhang	Thermo Scientific: R0141
pGEM-T Easy Vector Systems	For cloning of SOE-PCR product into intermediate pGem-T vector	Promega: A1360
T4 DNA Ligase	For ligation into pUIC3 vector	NEB: M0202
NEBuilder HiFi DNA Assembly Master Mix	For Gibson assembly of DNA fragments in pUIC3-mini vector	NEB: E2621

Wizard Genomic DNA Purification Kit	Kits for extraction of genomic DNA	Promega: A1125
DNeasy Blood & Tissue Kit		Qiagen: 69506
Proteinase K	Enzymes for digestion of protease & RNA during gDNA extraction	Qiagen: 19133
RNase A		Qiagen: 19101
QIAprep Spin Miniprep Kit	Kit for extraction of plasmid DNA	Qiagen: 27106
QIAEX II Gel Extraction Kit	Kit for extraction of DNA from gels	Qiagen: 20021
Qubit dsDNA BR Assay Kits	Kit for quantification of DNA	Invitrogen: Q32853
BigDye Terminator v3.1 Cycle Sequencing Kit	Kit for Sanger sequencing reaction	Applied Biosystems: 4337455
BigDye XTerminator Purification Kit	For cleanup of Sanger sequencing reaction	Applied Biosystems: 4376486
Nextera DNA Flex Library Preparation Kit	Kits for library preparation & tagmentation, and with index adaptors for multiplexing of samples; for whole-genome sequencing of gDNA with Illumina NextSeq	Illumina: 20018704
Nextera XT DNA Library Preparation Kit		Illumina: FC-131-1096
Nextera DNA CD Indexes		Illumina: 20018707
Nextera XT Index Kit v2 Set B		Illumina: FC-131-2002
Agencourt AMPure XP	Magnetic beads for cleanup & size selection of PCR products before sequencing	Beckman Coulter: A63880

Table 5.6. Enzymes and kits used in this study. Details provided: Name, Description (application of enzyme or kit), and Supplier (with catalogue number and link to specific product).

5.2 Phenotypic analysis

The phenotype of derived *P. fluorescens* SBW25 strains was analysed, including colony morphology on agar plates, mat formation capacity in static broth and swimming motility in semi-solid agar. The methods used to examine these phenotypic traits are described in the following section. All phenotypic images were edited using Preview (MacOS), only to adjust image brightness and crop to size.

5.2.1 Colony morphology

For the examination of morphology of single colonies, overnight cultures were diluted (10^{-6} or 10^{-7}) in Ringer's solution, and then 50-100 μ L spread on a KBA plate using 4 mm glass beads. For colony spot plates, 5 μ L of overnight culture was spotted on KBA plates, and allowed to be absorbed into the agar. All plates were then inverted and incubated at 28°C or 20°C for 1-2 days (or longer where applicable). Colony morphology was imaged from the

bottom of the petri dish, using the Axiocam ERc 5s camera attached to the Stemi 305 stereomicroscope (Zeiss), or ChemiDoc MP Imaging System (Bio-Rad).

5.2.2 Mat formation

Mat formation in static broth was inspected, by the inoculation of 6 μL vortexed overnight culture into 6 mL KB (1/1000 dilution) in a 25 mL glass microcosm. The microcosms were incubated at 28°C under static conditions (shelf with vibration stabilised) for 24 hours. Mats were then examined – requiring coverage at the surface and attachment to the sides of the glass microcosm (minor cell clumping at the centre of the ALI not considered a mat). Images were taken from the side of the microcosm, using the iPhone 11 camera.

5.2.3 Swimming motility

This protocol was adapted from Ha et al. (2014a). SSA motility plates (0.25% agar & 1% KB) were prepared fresh the day before use, as described in [Section 5.1.5](#). Overnight cultures were first thoroughly vortexed (5-10 seconds on high), and then 50-100 μL transferred to a centrifuge tube or 96-well plate, allowing the cell clumps to settle to the bottom. The tip of a sterile toothpick was then dipped ~1-2 mm into the culture (checking that no cell clumps transfer), and then stabbed into the centre of the SSA plate at a right degree angle, to the bottom of the agar layer. Motility plates were then incubated upright at 28°C for 30 hours, in an incubator with natural convection (Heraeus Function line B20). The migration diameter of swimming motility was then measured using a digital caliper (Mitutoyo: [IP67 Absolute](#)).

5.3 Polymerase Chain Reaction

Polymerase chain reaction (PCR) was used for the amplification of specific DNA sequences, with primers complementary to the region of interest; see [Section 5.1.3](#) for details of the primers utilised. To calculate the optimal annealing temperature of primer sets, the NEB Tm Calculator was used. PCR reactions were carried out with the Labcycler Basic/Gradient thermal cycler (SensoQuest). Gel electrophoresis was performed on all PCR products, before proceeding with sequencing or cloning.

5.3.1 Standard PCR

For general applications, standard PCR was carried out using Taq DNA polymerase (Qiagen TopTaq Master Mix or NEB Taq Master Mix), as detailed below.

Taq PCR contained (total 25 μL in dH_2O):

Taq Master Mix (2x)	12.5 μL
Primer (10 mM) – Forward	0.625 μL
Reverse	0.625 μL
Template	2.0 μL
DMSO	0.75 μL

The DNA template used for PCR was either genomic or plasmid DNA (50 $\text{ng}/\mu\text{L}$), or bacterial cells taken from an overnight culture (10^{-1} dilution) or from a single colony on an agar plate (tip of toothpick or 10 μL pipette tip gently touched to colony, then shaken directly into the PCR reaction). The cycling conditions used for Taq PCR were: initial denaturation at 94°C for 3-10 mins (longer time for cell templates); 35 cycles of – denaturation at 94°C for 30 seconds, annealing at the primer-specific temperature for 30 seconds, and extension at 72°C for approximately 1 minute per kb of DNA; and final extension at 72°C for 10 minutes. The reaction product was stored at $4\text{-}12^\circ\text{C}$ (or -20°C long term). All PCR products were purified before Sanger sequencing, with the SAP-Exo Kit (as specified in manufacturer's protocol).

For molecular cloning and mutation construction, the Phusion or Q5 high-fidelity polymerase was used (Thermo Scientific Phusion Master Mix or NEB Q5 Master Mix), as detailed below.

Phusion PCR contained (total 50 μL in dH_2O):

Phusion Master Mix (2x)	25.0 μL
Primer (10 mM) – Forward	2.5 μL
Reverse	2.5 μL
Template – gDNA (50 $\text{ng}/\mu\text{L}$)	2.0 μL

When applicable, 1.5 μL of DMSO was also added to the reaction, to aid in strand separation. The cycling conditions used for Phusion PCR were: initial denaturation at 98°C for 30 seconds; 35 cycles of – denaturation at 98°C for 10 seconds, primer-specific annealing for 15 seconds, and extension at 72°C for ~ 30 seconds per kb of DNA; final extension at 72°C for 5 minutes; and hold at 4°C . For cloning purposes, all PCR products were first purified using the QIAquick PCR Purification Kit (as specified in manufacturer's protocol).

5.3.2 Strand Overlap Extension

Strand Overlap Extension PCR (SOE-PCR) was used for site-directed mutagenesis and the production of mutation constructs (Ho et al., 1989). Primers were designed to amplify the flanking region ~350-800 bp upstream (1F & 2R) and downstream (3F & 4R) of the mutation of interest (or gene deletion), with a ~20 bp sequence complementary to the genome (Heckman, & Pease, 2007). For the recreation of point mutations, the variant base pair was also included towards the 5' end of this sequence, for one of the inner primers (2R or 3F). The 5' end of each inner primer (2R & 3F) also contained a ~9 bp sequence complementary to the other (total ~18 bp overlap), and the outer primers (1F & 4R) a SpeI restriction site. For SOE-PCR, the first reactions separately amplify the upstream and downstream flanking regions; while the second reaction anneals the two products together at the complementary sequence, amplifying the full-length product (containing the specified mutation or deletion of gene region). All reactions utilised the Phusion (or Q5) High-Fidelity DNA polymerase, to minimise polymerase copying error and prevent introduction of mutations into the amplicon sequence. Following digestion with the SpeI restriction enzyme, the mutation construct may then be inserted into a plasmid vector for subsequent cloning.

The first reactions followed the Phusion PCR protocol and cycling conditions as detailed in [Section 5.3.1](#), using the primer sets 1F/2R & 3F/4R, and template of genomic DNA from SBW25 (MPB14218; or other strain where applicable). The size of each product was confirmed by gel electrophoresis, and when required the correct size band purified by gel extraction. The DNA concentration was then measured with the NanoDrop, and normalised to 50 ng/μL by dilution with dH₂O. The second reaction followed the same general protocol and cycling conditions, but used the outer primers 1F & 4R, and the templates of 1 μL of each purified PCR product (50 ng/μL). This was complete in two amplification stages – the first 5 cycles contained no primers, with the overlap-specific annealing temperature used to allow for the complementary regions of each PCR product to anneal; and for the remaining 30 cycles the primers were added, and the primer-specific annealing temperature used to amplify the full-length product. The final PCR product was size verified by gel electrophoresis, if necessary purified by gel extraction, and then stored at -20°C awaiting ligation into the intermediate vector pGem-T.

5.3.3 FastCloning

The FastCloning method was used to produce mutation constructs using only one round of PCR to separately amplify the vector backbone and insert(s), followed by digestion with the restriction enzyme DpnI to remove template plasmid, and direct transformation into competent cells with no ligation step required (Li et al., 2011). Primers were designed as described in *Section 5.3.2* for SOE-PCR, but the outer primers (1F & 4R) contained a ~20 bp sequence complementary to the ends of the pUIC3-mini vector (rather than the SpeI site). To amplify the upstream and downstream flanking regions (of the mutation or gene deletion), Phusion PCR was carried out as detailed in *Section 5.3.1*, using the primer sets 1F/2R & 3F/4R. For amplification of the pUIC3-mini vector (MPB13966), plasmid DNA extracted using the QIAprep Miniprep Kit, and linearised by digestion with the SpeI restriction enzyme, as detailed below.

SpeI digestion (total 10 μ L in dH₂O):

SpeI HF	1.0 μ L
CutSmart Buffer (10x)	1.0 μ L
pUIC3-mini DNA (100 ng/ μ L)	2.0 μ L

The SpeI digestion reaction was incubated at 37°C for 1 hour, and then heat-inactivated at 80°C for 20 minutes. The digested pUIC3-mini was then amplified with Phusion PCR (as detailed in *Section 5.3.1*), using the primers pUIC3-mini-F/R (P13/14), and the template of 1 μ L SpeI digestion product. The PCR product was then digested with DpnI, by direct addition of 1 μ L DpnI to the reaction, and incubation at 37°C for 1 hour. Both the insert and vector backbone PCR products were cleaned up using the QIAquick kit, eluted in 50 μ L dH₂O, and stored at -20°C awaiting Gibson assembly in pUIC3-mini.

5.3.4 Arbitrary Primed-PCR

Arbitrary Primed-PCR (AP-PCR) was used to identify the specific location of transposon insertions, resulting from transposon mutagenesis with IS- Ω -Km/hah (Giddens et al., 2007; Manoil, 2000). AP-PCR allows for amplification of the chromosome-transposon junction with two rounds of PCR – the first round pairing a transposon-specific primer (TnphoA II) with an arbitrary primer set (CEKG 2A/B/C), to amplify from the transposon into the chromosomal region next to the insertion site; and the second round pairing a nested transposon-specific primer (Hah-1) with a primer containing the anchor sequence of the

previous arbitrary primer (CEKG 4), to enrich for only the transposon-chromosome sequences (Saavedra et al., 2017; Das et al., 2005).

AP-PCR 1 contained (total 25 μ L in dH₂O):

Taq polymerase	0.5 μ L
Buffer (10x)	2.5 μ L
MgCl ₂ (50 mM)	0.8 μ L
dNTP mix (10 mM)	1.0 μ L
Primer (10 mM) – TnpA II	2.0 μ L
CEKG 2A/B/C	2.0 μ L
Template	2.0 μ L

The template used for the first round of AP-PCR was a scraping from a single transposon mutant colony resuspended in 50 μ L dH₂O. The cycling conditions used for AP-PCR 1 were: initial denaturation at 94°C for 10 minutes; 5 initial cycles of – denaturation at 94°C for 30 seconds, annealing at 42°C for 30 seconds (decreased by 1°C each cycle), and extension at 72°C for 3 minutes; followed by 25 cycles with annealing at 65°C; and final extension at 72°C for 5 minutes. The PCR product was then diluted with 80 μ L dH₂O, and used a template for the second round of AP-PCR.

AP-PCR 2 contained the same components as AP-PCR 1, except for the primers in which Hah-1 & CEGK 4 were used, and the template being the diluted PCR product of the first round. The following cycling conditions used were: initial denaturation at 94°C for 3 minutes; 30 cycles of – denaturation at 94°C for 30 seconds, annealing at 65°C for 30 seconds, and extension at 72°C for 3 minutes; final extension at 72°C for 5 minutes; and the product stored at 4°C. The product of the two rounds of AP-PCR was checked with gel electrophoresis, but no clean band expected (rather multiple light bands). Before Sanger sequencing, all AP-PCR products were purified with the enzymes Exonuclease I (ExoI) to remove excess primers and template, and Antarctic Phosphatase to dephosphorylate remaining dNTPs. This was achieved by the addition of 0.1 μ L ExoI & 0.2 μ L Antarctic Phosphatase to each 20-25 μ L reaction product, and then incubated at 37°C for 1 hour followed by heat-inactivation at 85°C for 15 minutes. The purified product was stored at 4°C, awaiting Sanger sequencing.

5.3.5 Gel electrophoresis

Gel electrophoresis was used to separate DNA by size, for verification of the success of PCR (including a correct product size), before continuing with cloning or Sanger sequencing. Agarose gels (1.0-1.5%) were prepared by the addition of 0.5-0.75 g of SeaKem LE agarose (Lonza: [50004](#)) to 50 mL of 1x TAE buffer (Bio-Rad: [161-0773](#)), microwaving for 1-3 minutes to dissolve, 5 μ L of SYBR Safe DNA Gel Stain (Invitrogen: [S33102](#)) added after cooling, then the gel poured and left to cool completely. 5 μ L of each PCR product or DNA sample was mixed with 1 μ L of 6x DNA Gel Loading Dye (Thermo Scientific: [R0611](#)), then loaded into a single well of the agarose gel (suspended in TAE buffer), with 5 μ L of the GeneRuler DNA Ladder Mix (Thermo Scientific: [SM0334](#)) loaded in another well. Gels were run at 80-120V using the Biometra PS300TP (Analytik Jena) power supply unit, for ~30 minutes or until the DNA had sufficiently separated. The DNA bands were then visualised and imaged using the UVP GelStudio PLUS (Analytik Jena). For gel extraction of DNA, a larger 1% agarose gel was prepared (~80-100 mL), and the entire PCR product loaded onto the gel. Bands were then excised using a sterile razor blade, and DNA extracted using the QIAEX II Gel Extraction Kit, following the manufacturer's instructions.

5.4 Bacterial transformation

For molecular cloning, mutation construction vectors were assembled by transformation into DH5 α - λ pir or TOP10 chemically competent *E. coli* cells. 50 μ L aliquots of competent cells were first thawed on ice, then 2-4 μ L of DNA added (e.g product from SOE-PCR & ligation, or Gibson assembly), and gently flicked to mix. The cells were incubated on ice for 30 minutes, then heat shocked for 30 seconds at 42°C in the Isotemp GPD 02 water bath (Fisher Scientific), and returned to the ice for ~2 minutes. 250 μ L of room temperature SOC was then added, and the cells incubated for 1 hour at 37°C shaking (300 rpm) using the ThermoMixer C or comfort (Eppendorf). The transformation mix was diluted in LB (10^0 & 10^{-1}), and then 50 μ L of each dilution (as well as the remaining mix) spread on room temperature LBA plates containing the respective antibiotic (e.g. Tc). Plates were incubated at 37°C for 1 day, and then *E. coli* transformant colonies screened for fluorescence (e.g. GFP) using the FastGene LED Transilluminator (Nippon Genetics).

5.4.1 Bi-parental conjugation

For bi-parental conjugation, overnight cultures were grown of the recipient *P. fluorescens* strain in KB, and the donor *E. coli* (e.g. pMRE-Tn7-GFP or Scarlet) in LB with the respective antibiotic (e.g. Km or Tc). 1 mL of the recipient culture was first heat shocked for 20 minutes at 45°C in the water bath. Then 1 mL of heat-shocked recipient and 0.5 mL of donor culture were spun down by centrifugation (6,000 x g for 2-5 minutes), combined in 100 µL LB, and the conjugation mix spotted onto a room temperature LBA plate. Conjugation spot plates were incubated upright at 28°C overnight, then the entire spot scraped from the plate using a 10 µL inoculation loop, and resuspended in 1 mL LB. This was then diluted in LB (10^0 , 10^{-1} & 10^{-2}), and 50 µL of each dilution spread onto a selective LBA plate containing Nf (to select against *E. coli*) & the respective antibiotic (e.g. Km or Tc), and incubated at 28°C for 1-2 days. If required, the *P. fluorescens* transconjugant colonies were then screened for fluorescence (e.g. GFP or Scarlet) using the transilluminator.

5.4.2 Tri-parental conjugation

Tri-parental conjugation was used for donor *E. coli* plasmids that lack the genes for conjugation and DNA transfer (e.g. pSCR001 with IS-Ω-Km/hah transposon, or pUIC3-mini), requiring the presence of a helper strain for mobilisation. This was achieved using the same protocol as described for bi-parental conjugation (see [Section 5.4.1](#)), except 0.5 mL of the helper *E. coli* prK2013 (MPB13960) was also included in the conjugation mix. For transposon mutagenesis the protocol was also slightly adjusted – the conjugation mix resuspended in 60 µL LB, with 15 µL aliquots spotted in a number of separate conjugations (spread to ~1 cm²); the plates were only incubated for 5 hours (to minimise the chance of multiple insertions), then each conjugation spot resuspended in 1 mL KB (with no further dilution), and 50 µL spread on replicate KBA + Nf + Km plates. The *P. fluorescens* transconjugant colonies were then screened based on change to colony morphology (e.g. WS or SM).

5.4.3 Electroporation

Electroporation was used to directly transform strains of *P. fluorescens* with a plasmid (e.g. pCdrA-GFP), without need for conjugation. The donor plasmid was first extracted from an overnight culture of the respective *E. coli* strain using the QIAprep Miniprep Kit, and the concentration normalised to 50 ng/µL by dilution with dH₂O. Overnight cultures were then

grown of the recipient *P. fluorescens* strain in KB, and 1 mL spun down by centrifugation (20,000 x g for 2 minutes) at 4°C. These cells were made electrocompetent by keeping on ice, and washing three times in 500 mL glycerol/HEPES (spun down at 4°C). The cell pellet was resuspended in 50 µL glycerol/HEPES, then 1 µL (50 ng) of plasmid added, and gently flicked to mix. This was then transferred to a single-use Gene Pulser cuvette (Bio-Rad), and electroporated using the MicroPulser electroporator (Bio-Rad) with the 'Bacteria' preset program. 450 µL of room temperature SOC was immediately added to the cuvette after electroporation, then the cells transferred to a new 1 mL microcentrifuge tube and incubated for 1 hour at 28°C shaking on a thermal mixer. The cells were then diluted in LB (10^{-2} , 10^{-3} & 10^{-4}), with 50 µL of each dilution spread on LBA plates containing the respective antibiotic (e.g. Gm), and incubated at 28°C for 1-2 days. *P. fluorescens* transformant colonies were then screened for fluorescence (e.g. GFP) using the transilluminator.

5.5 Transposon mutagenesis

Suppressor analysis by transposon mutagenesis was used to identify the regulatory genes underpinning a particular phenotype (e.g. WS or SM). Transposon mutagenesis was carried out with the IS-Ω-km/hah transposon that inserts randomly in the genome (Giddens et al., 2007; Manoil, 2000). This was achieved by a tri-parental conjugation (detailed in [Section 5.4.2](#)), between the recipient *P. fluorescens* (*pflu5960* or *amrZ* deletion mutant – MPB 14084, 14085, 14246 & 14247), donor *E. coli* pSCR001 (IS-Ω-km/hah; MPB14720), and helper *E. coli* pRK2013 (MPB13960). Transposon mutants were selected using kanamycin resistance, and screened based on a specific change to colony morphology – suppression of WS or SM phenotype. The insertion location of the transposon was identified by AP-PCR (detailed in [Section 5.3.4](#)), followed by Sanger sequencing using the Hah-1 primer (P5).

5.6 Site-directed mutagenesis

Site-directed mutagenesis was used to reconstruct specific mutations or for the deletion of genes. Mutation construct vectors were first produced by either SOE-PCR & ligation into the intermediate vector pGem-T and then pUIC3 (MPB13957), or by FastCloning & Gibson assembly in pUIC3-mini (MPB13966); followed by transformation into chemically competent *E. coli* (Ho et al., 1989; Li et al., 2011; Gibson et al., 2009). Overnight cultures were made (with Tc) of the final mutation construct in *E. coli* (pUIC3 or pUIC3-mini) for the storage of freezer stocks. The mutation was then introduced into *P. fluorescens* by a two-step

allelic exchange – the first homologous recombination event resulting in integration of the entire plasmid vector, and the second rare homologous recombination event looping out the plasmid (including Tc^R & *lacZ*/GFP gene) to leave behind either the wild-type or mutant allele (Hmelo et al., 2015). The first crossover was achieved by tri-parental conjugation, and the second crossover by cycloserine enrichment (Kitten et al., 1998). The presence of the final mutant allele (SNP or gene deletion) was confirmed by Taq colony PCR (see [Section 5.3.1](#)) using primers flanking the mutation construct region (seq-F/R) & Sanger sequencing.

5.6.1 Ligation into pGem-T & pUIC3

The mutation construct insert fragments were first cloned by SOE-PCR, as detailed in [Section 5.3.2](#) (Ho et al., 1989). For TA cloning and ligation into pGem-T, the 3' adenine overhang was first added to the SOE-PCR product, as detailed below.

3'-adenine reaction (total 10 µL):

Taq Polymerase	0.2 µL
Buffer (10x)	1.0 µL
MgCl ₂ (50 mM)	0.3 µL
dATP (10 mM)	0.5 µL
SOE-PCR product	8.0 µL

The 3'-adenine reaction was incubated at 72°C for 30 mins. Ligation was then carried out of the SOE-PCR product into an intermediate vector, using the pGEM-T Easy Vector Systems (Promega), following the manufacturer's instructions; and the product cleaned up with SureClean Plus (Bioline). 4 µL of the ligation product was then transformed into *E. coli* DH5α-λpir chemically competent cells (as described in [Section 5.4](#)), with selection using ampicillin on LBA + X-gal + Amp + IPTG plates. The white transformant colonies were selected (insert disrupting *lacZ* gene, so inactive β-galactosidase), and the presence of the insert in pGem-T confirmed by Taq colony PCR (as described in [Section 5.3.1](#)) using the primers M13-F & M13-R (P7/8), and Sanger sequencing.

Overnight cultures were grown of pGem-T (with the mutation construct insert) & pUIC3 (MPB13957), containing the appropriate antibiotic (Am or Tc), and then plasmids extracted using the QIAprep Miniprep Kit. Both plasmids were separately digested with the SpeI HF restriction enzyme, following the manufacturer's instructions. The mutation construct insert was then purified from the pGem-T plasmid backbone by gel extraction (see [Section 5.3.5](#)).

The Gibson assembly reaction was incubated at 50°C for 1 hour, and then 2 µL transformed into *E. coli* DH5α-λpir or TOP10 chemically competent cells (as described in [Section 5.4](#)), with selection using tetracycline. The GFP fluorescent colonies were selected, and the presence of the insert in pUIC3-mini confirmed by Taq colony PCR (as described in [Section 5.3.1](#)) using the primers pUIC3-seq-F & R (P11/12) or the outer construct primer 1F & 4R, and Sanger sequencing.

5.6.3 Allelic exchange

Allelic exchange was used to introduce mutant alleles into *P. fluorescens*, from the mutant construct vectors cloned in *E. coli* (Hmelo et al., 2015). The first crossover (entire plasmid integrates into the genome) was achieved by tri-parental conjugation (as described in [Section 5.4.1](#) & [5.4.2](#)) between the recipient *P. fluorescens*, donor *E. coli* pUIC3/pUIC3mini (containing mutation construct) & helper *E. coli* pRK2013 (MPB13960), with selection for tetracycline resistance. When using the pUIC3-mini vector, *P. fluorescens* transconjugant colonies were also screened for GFP fluorescence using a transilluminator.

The second crossover (plasmid loops out of the genome) was achieved using cycloserine enrichment for tetracycline sensitivity (Kitten et al., 1998). An overnight culture in LB (with Tc) was made of the first crossover *P. fluorescens* transconjugant, then 20 µL inoculated into 400 mL of LB (in a large Erlenmeyer flask) and incubated at 28°C shaking for 24 hours. 400 µL of this culture was then inoculated into 20 mL LB and incubated for 30 minutes, then 20 µL tetracycline (1000x) was added, and the culture incubated for 2 hours (selecting for presence of pUIC3/pUIC3-mini vector). Following this, 200 µL of D-cycloserine (100x) was added and incubation continued for an additional 4-5 hours (counter-selection, enrichment for loss of vector). 1 mL of culture was then spun down by centrifugation (6,000 x g for 2 minutes), resuspended in 500 µL KB, and 50 µL (undiluted and 10⁻¹ dilution) spread on KBA plates (also containing X-gal for pUIC3). Plates were incubated for 2 days at 28°C, and many white colonies (no *lacZ* for pUIC3 or GFP fluorescence for pUIC3-mini) screened using Taq colony PCR (see [Section 5.3.1](#)) with the relevant flanking primers (seq-F/R). For gene deletions, gel electrophoresis was used to confirm the mutant allele (deletion indicated by DNA band of smaller size); while for the recreation of SNPs, Sanger sequencing was required. Overnight cultures of the final confirmed mutant in *P. fluorescens* were then made for the storage of freezer stocks, awaiting phenotypic analysis.

5.7 DNA extraction & sequencing

Genomic DNA (gDNA) was extracted from overnight shaken cultures (inoculated by a single colony), using the Wizard gDNA Purification Kit (following the manufacturer's protocol for gram-negative bacteria), or DNeasy Blood & Tissue Kit. An adapted protocol was used for the DNeasy kit: spin down 200-500 μL culture by centrifugation (6,000 $\times g$ for 5 minutes), and resuspend in 180 μL Buffer ATL; add 20 μL Proteinase K, and lyse cells for 1-2 hours by incubation at 56°C shaking (>1000 rpm) on a thermal mixer; add 4 μL RNase A, and digest for 5 minutes at room temperature; mix 200 μL each of Buffer ATL & 100% Ethanol, add to sample, immediately vortex and then transfer to DNeasy spin column; incubate for 1 minute at room temperature, spin down, and discard flow through; wash column with 500 μL Buffer AW1, followed by 500 μL Buffer AW2, and then centrifuge at high speed to dry the membrane (20,000 $\times g$ for 3 minutes); elute gDNA in 100 μL dH₂O. Plasmid DNA was extracted from cultures using the QIAprep Miniprep Kit, following the manufacturer's instructions, with elution in dH₂O. The concentration and quality of DNA was measured using the NanoDrop spectrophotometer (Peqlab: NanoDrop ND-1000) & Qubit Fluorometer (Invitrogen: Qubit 3), and all DNA samples stored at -20°C.

5.7.1 Sanger sequencing

Small DNA fragments (e.g. purified PCR product or plasmids) were sequenced by Sanger sequencing, using the 3500xL Genetic Analyzer (24 capillary system; Applied Biosystems). This was carried out in-house by technical staff of the Max Planck Institute for Evolutionary Biology (MPI Plön). The sequencing reaction used the BigDye sequencing kit (Applied Biosystems), as detailed below.

Big Dye reaction (total 10 μL in dH₂O):

BigDye	0.5 μL
Sequencing buffer (5x)	2.0 μL
Primer (10 mM) – seq-F/R	1.0 μL
DNA template	1.0 μL

The Big Dye reaction was carried out in the wells of a MicroAmp Fast 96-well plate (0.1 mL), using the Veriti 96-well Fast Thermal Cycler (Applied Biosystems). With the following cycling conditions: initial denaturation at 96°C for 1 minute; 30 cycles of – denaturation at 96°C for 10 seconds, annealing at 56°C for 15 seconds, and extension at 60°C for 4 minutes;

and hold at 4°C. To remove unbound terminators & salts, the reaction product was then purified using the BigDye purification kit (Applied Biosystems), according to the manufacturer's protocol; the samples were then sequenced.

For site-directed mutagenesis, output DNA sequences (.ab1 files) from Sanger sequencing were then mapped to the mutation construct region using Geneious Prime (version 2020.0.3), to confirm the presence of mutant alleles. For transposon mutagenesis, AP-PCR product sequences were queried against the *P. fluorescens* SBW25 genome with a Megablast nucleotide BLAST search (Morgulis et al., 2008). Genes were then investigated using the *Pseudomonas* Genome database (Winsor et al., 2016); and functional protein domains identified based on Interpro predictions (Paysan-Lafosse et al., 2022), Pfam database search (Finn et al., 2014) & the NCBI Conserved Domains database (Marchler-Bauer et al., 2011).

5.7.2 Whole-genome sequencing

Whole-genome sequencing (with minimum 50x coverage) was used to identify mutations in evolved lines of *P. fluorescens* SBW25. This was carried out in-house at the MPI Plön by Dr. Sven Künzel & technical staff, using the Illumina NextSeq 500/550 system (2x 150 bp paired-end reads). The concentration of gDNA samples were first measured using the Qubit, and normalised to 2 ng/µL by dilution with dH₂O. The protocol used for multiplexed library preparation was adapted from Baym et al. (2015). Tagmentation was achieved using the Nextera XT or DNA Flex library preparation kits, and adaptors added with the Nextera XT v2 (Kit B) or DNA CD kits (Illumina); following the manufacturer's instructions. The reaction products were then cleaned up using the AMPureXP magnetic beads (Beckman Coulter), following the provided protocol with the bead ratio of 0.6x; and the samples then sequenced. For demultiplexing and generation of fastq files, the Illumina bcl2fastq conversion software was used. The sequencing fastq files were then mapped to the SBW25 reference genome (GenBank: [AM181176.4](#)) using Geneious Prime, and mutations identified using Breseq (Deatherage, & Barrick, 2014). Genes were further investigated using the *Pseudomonas* Genome database (Winsor et al., 2016), and protein orthologs in *P. aeruginosa* PAO1 identified with a BLASTP search (Altschul et al., 1990, 1997).

5.8 Life cycle experiment with new selective methods

The aim of revising the LCE experimental regime of Hammerschmidt et al. (2014), was to eliminate the use of the colony morphology proxy for niche preference in static broth. This

was achieved by the design of new screening methods based on mat formation and swimming motility (see discussion in *Section 3.2*). The following section describes in full detail the new experimental design and selective methods. Each life cycle generation requires two weeks, consisting of the Phase I (PI: Collective) & Phase II (PII: Dispersal); freezer stocks were made of each replicate line at the end of each cycle. Replicate lines were organised into racks (or metapopulations) containing 8 replicate lines each; with extinct lines replaced by another random viable line within their rack. In the case of an entire rack extinction (all 8 replicate lines extinct), 8 random racks were selected, and then a random viable line from each chosen to replace the extinct rack (allowing for inter-rack competition).

Day 1 (Week 0 - Thursday): Start of Phase I – for each replicate line a 6 mL KB microcosm was inoculated with a single motile colony (SBW25 during first cycle), vortexed briefly, and then cultures incubated at 28°C static for 4 days (enriching for mat forming types). After 24 hours, mat formation was also assessed (record: P1_1d_mat = 1 or 0), requiring full coverage at the surface and attachment to the glass microcosm wall; this indicating whether lineages had evolved a means of developmental regulation (no mat present if proceeding by mutation).

Day 5 (Week 1 - Monday): Plating of Phase I cultures – each evolved line was vortexed for ~5 seconds at high speed, and then serially diluted to 10^{-6} in Ringer's solution (using 96-well plate & multichannel pipette; 20 μ L culture resuspended in 180 μ L Ringer's, transfer repeated five times for 10^{-6} dilution); 50 μ L was then spread on KBA plates using glass beads (shake beads in stack of 8 plates), and plates incubated at 28°C for 1 day. The plated cultures were then screened for variation in colony morphology phenotype (record: colony_variation = 1 or 0), to indicate whether lineages had fixed a single genotype.

Day 6 (Tuesday - Week 1): Mat formation screen – 200 μ L of KB was added to the wells of a flat-bottom 96-well plate (each rack requiring half a plate or 6 columns); for each line six random individual colonies were selected, then inoculated into each well using a sterile toothpick (gently touch colony on plate with tip of toothpick, and then dip into KB in the well), and plates incubated at 28°C static for 24 hours. The mats were then assessed with the following criteria: must visibly cover the surface of the broth (including connection to the wall at the top edge of the meniscus), and no fallen mat should be visible at the bottom of the well. For each line, the first mat-forming colony was marked (on the lid of the well), or if all 6 colonies were unsuccessful in making a mat then the line was marked as extinct (record:

P1_extinct = 1). Extinct lines were chosen for replacement by a random viable line in the rack (record: P1_replace = 'line#'; e.g. extinct line 2.5 replaced by line 2.2).

Day 7 (Week 1 - Wednesday): Start of Phase II – in the second phase of the experiment each replicate line was inoculated by a single mat forming individual, directly from the mat formation screen. For each line, the selected marked well was mixed by pipetting to resuspend the mat (~5-10 times using P100 pipette); then 6 μ L was transferred into a fresh 6 mL KB microcosm (1/1000 dilution), vortexed briefly, and cultures incubated at 28°C static for 6 days (enriching for motile dispersing types). Extinct lines were replaced, by inoculation from the selected well of the chosen replacement (e.g. for line 2.2 the well containing a single mat forming individual is used to inoculate line 2.2 & 2.5). After 24 hours, mat formation was also assessed as described previously (record: P2_1d_mat = 1 or 0), to confirm the accuracy of the mat formation screen using the 96-well plate format (all lines should form a mat in the microcosm).

Day 12 (Week 2 - Monday): Preparation of motility plates – semi-solid agar (SSA) plates with 1% KB & 0.25% agar were prepared the day before use, as described in [Section 5.1.5](#). The plate-pouring machine was used for large batches: to make ~240 motility plates, 8 litres of media was autoclaved, cooled to 55°C, and 30 mL poured in each petri dish; the plates were left to set in the machine for at least 3 hours, and then left in stacks of 8 at room temperature overnight to dry. Before use, the motility plates were first inspected for excess condensation and these discarded (when using the plate pouring machine ~5-10% of plates were observed to not dry correctly).

Day 13 (Week 2 - Tuesday morning): Mat check & motility screen – the 6 day cultures were first examined to ensure the collective mat remained intact (recorded: P2_6d_mat = 1 or 0); evolved lines with no mat present (or a fallen mat) at day 1 or 6 were marked as extinct (record: P2_extinct_1 = 1), and a replacement line chosen as described previously (record: P2_replace_1 = 'line#'). Each surviving evolved line was then vortexed for 5 seconds to resuspend the mat, and 200 μ L transferred into the well of a 96-well plate (each rack requiring 1 column). This evolved population was then inoculated into a motility plate, by dipping the tip of a sterile toothpick into the culture aliquot ~1-2 mm deep, and then stabbing this into the centre of an SSA plate (at right angle, to the bottom of the agar). Extinct lines were replaced by inoculation of the SSA plate from the chosen replacement line. The motility plates were incubated upright (in stacks of 8) at 28°C for 30 hours.

Day 14 (Week 2 - Wednesday evening): Measurement and streaking of motility plates – the migration diameter of each motility plate was measured using a digital caliper (as described in [Section 5.2.3](#); record: motility_mm = ‘migration diameter’). The minimum motility threshold was set at 15 mm, and those lines that had a migration diameter less than 15 mm were marked as extinct (record: P2_extinct_2 = 1), and a replacement line chosen as described previously (record: P2_replace_2 = ‘line#’). Each surviving evolved line was then streaked from the motility plate to individual colonies, by stabbing a sterile toothpick into the outer edge of the migration area and streaking this on a KBA plate. The streak plates were incubated at 28°C for 1 day.

Day 1 (Week 0 - Thursday): Start of next generation & preparation of freezer stocks – for each line the next life cycle generation was inoculated with a single random colony from the streak plate (using a sterile toothpick), with extinct lines replaced by inoculation with the same colony as the chosen replacement line. Freezer stocks were also made of each evolved line, with overnight cultures grown directly in individual cryogenic tubes of the FluidX 96-well format rack (Azenta Life Sciences: [66-62318-Y6](#)). 300 µL of KB was added to each tube, and then each line inoculated into the respective culture tube from the same colony used to seed the next generation. The racks were then incubated (with no lids on the tubes, just the rack cover) at 28°C for 16-18 hours, shaken at 500 rpm using the Microplate Shaker (Fisher Scientific: [15504070](#)). 300 µL of glycerol/saline was then added to each tube, mixed ~5 times using a multichannel pipette, and the lids added; the racks containing freezer stock were stored at -20°C indefinitely.

5.9 Phenotypic assessment of evolved lines

To assess the phenotype of evolved lines of *P. fluorescens*, mat formation capacity, colony morphology and swimming motility was examined (see methods in [Section 5.2](#)). The c-di-GMP level in different environments, group-level lineage fitness, and individual-level cell fitness were also measured, as described in the following section. For all phenotypic assays, the ancestral SBW25 (MPB14218) was used as a control to compare the behaviour of evolved lines.

5.9.1 c-di-GMP assay using pCdrA reporter

To quantify the intracellular levels of c-di-GMP in evolved lines of *P. fluorescens*, the pCdrA-GFP fluorescent reporter was used (Rybtke et al., 2012). Each genotype was first

transformed with the Tn7-mScarlet-Km^R fluorescent marker (Schlechter et al., 2018), by a bi-parental conjugation with MPB15815 (see [Section 5.4.1](#)), and selection based on kanamycin resistance & Scarlet fluorescence. The Scarlet marked strains were then transformed with the CdrA-GFP-Gm^R plasmid (MPB16772) by electroporation (see [Section 5.4.3](#)), and selected using gentamicin resistance. For all evolved lines, the SBW25-Scarlet-pCdrA (MPB17910) control was used to compare changes in c-di-GMP level in different environments.

For the c-di-GMP assay, each Scarlet-pCdrA line was streaked to single colonies on an LB + Gm plate, with the Scarlet fluorescence double-checked on a transilluminator. Four replicate KB cultures (with Gm) were inoculated with single colonies, and grown shaken overnight at 28°C for 16-24 hours. Each culture was then inoculated into different growth environments – the static broth, shaken broth (where applicable), and semi-solid agar (SSA) motility plate; as previously detailed in [Sections 5.2.2 & 5.2.3](#). These were incubated under the different environmental conditions for 24 hours at 28°C, and then cells extracted from each environment. When required, the static & shaken broth cultures were first sonicated to break apart cell clumps; this was achieved using the Sonopuls Mini20 Ultrasonic Homogenizer (Bandelin), with the 2mm probe and sonication at 80% for 15 seconds (directly in the glass microcosm). The broth cultures were then vortexed, and cells diluted in PBS buffer (total dilution of ~1/2000). For the motility plate, cells were extracted directly from the semi solid agar: ~20-50 µL of agar was pipetted using a 1 mL pipette tip (set at 100 mL), resuspended in a total of 1 mL PBS buffer, and then briefly spun down (1,000 x g for 1 minute). Flow cytometry was used to measure the fluorescence of 10,000-20,000 cells, with the MACSQuant VYB flow cytometer (Miltenyi Biotec) following the instrument user manual. The normalised c-di-GMP level was then calculated for each sample, by dividing the mean GFP (B1-A mean) by the cell baseline of Scarlet (Y2-A mean).

5.9.2 Lineage fitness approximation

The lineage-level fitness of evolved lines of *P. fluorescens* was approximated by the survival rate during an additional life cycle generation; corresponding with the capacity of a lineage to transition through the life cycle without extinction, and to produce group-level offspring. Replicate lines were inoculated with a single genotype (1-3 racks with 8 replicates each), and taken through one life cycle generation (cycle 6 in most cases), as described in [Section 5.8](#).

The extinction and survival rate of replicate lines during PI (Collective) & PII (Dispersal) was recorded, and used to approximate the fitness of the lineage.

5.9.3 *Competitive fitness assays*

The individual-level cell fitness of evolved lines of *P. fluorescens* was measured using competitive growth assays in shaken broth; the GFP/Scarlet fluorescent marked evolved line competing against the corresponding Scarlet/GFP marked wild-type SBW25 ancestor (MPB15852 & MPB15850). Each genotype was first separately transformed with the Tn7-sGFP2-Km^R (MPB15811) & Tn7-mScarlet-Km^R (MPB15815) fluorescent marker (Schlechter et al., 2018), by bi-parental conjugation (see [Section 5.4.1](#)) and selection based on kanamycin resistance & GFP/Scarlet fluorescence.

For the competitive growth assay, Scarlet or GFP lines were first streaked to single colonies on LB + Km plates, and the fluorescence double-checked on a transilluminator. Four replicate KB cultures (with Km) were inoculated with single colonies, for both GFP & Scarlet (total of 8 cultures per genotype), and then grown shaken at 28°C for 24 hours. Each culture was then mixed at a 1:1 ratio with the SBW25 competitor (harbouring the opposite fluorescent marker), with 60 µL of the mix inoculated into a fresh 6 mL KB microcosm (1/100 dilution), and grown shaken for 24 hours at 28°C – T₀ culture. The T₀ cultures were again diluted 1/100 into a fresh microcom, and grown for another 24 hours at 28°C – T₁ culture. Flow cytometry (MACSQuant VYB) was used to measure the ratio of cells in both the T₀ & T₁ culture, with 50,000 fluorescent cells counted for each sample. From this, the relative fitness was calculated as the ratio of the Malthusian parameter of the evolved line over the SBW25 competitor (Lenski & Travisano, 1994).

5.10 Graphing and statistical analysis

Diagrams were created with [BioRender.com](#). Collective-level genealogies were visualised using Colgen (Doulcier, 2019). All other graphs were produced using Prism 9 (v. 9.4.1). Statistical testing was also carried out using Prism 9; with multiple Welch's t-tests conducted to detect differences in relative fitness or mean normalised GFP, comparing evolved lines of *P. fluorescens* to the wild-type SBW25. The *p*-values were adjusted for multiple testing using the Bonferroni correction method (α divided by the number of comparisons).

Supplementary A

Available on Zenodo: [10.5281/zenodo.7681262](https://zenodo.org/doi/10.5281/zenodo.7681262)

1. **Intro_figures.csv** – figures from Chapter I.
2. **TSS_images.zip** – images & figures from Chapter II.
3. **Mutagenesis_5960_amrZ.csv** – summary results of transposon mutagenesis screen with *pflu5960* & *amrZ* deletion mutants; BLAST search & insertion location.
4. **Mutagenesis_sequence.zip** – Sanger sequencing files (.ab1) from AP-PCR with $\Delta pflu5960$ & $\Delta amrZ$ transposon mutants.
5. **Plasmids_sequence.zip** – GenBank files from sequencing of mutation constructs.
6. **LCE_trial_images.zip** – images & figures from Chapter III.
7. **LCE_trial_data.zip** – LCE trial cycle data (records of extinction/replacement & phenotypic measurements) & c-di-GMP assay with pCdrA reporter (flow cytometry raw values of GFP (B1A) and Scarlet (Y2-A) fluorescence & statistical analysis).
8. **LCE_Trial_fastq.zip** – Illumina sequencing files (.fastq) for LCE trial evolved lineages from the end of cycle 5 & after additional generation (cycle 6).
9. **LCE_trial_mutations.csv** – Breseq output summary for LCE trial evolved lineages.
10. **LCE_trial_colgen.zip** – Colgen files for producing LCE trial genealogical trees.
11. **LCE_figures.zip** – figures from Chapter IV.
12. **LCE_cycle_data.zip** – LCE cycle data (records of extinction & replacement).
13. **LCE_summary.csv** – LCE summary data for all lineages (extinction, mat formation & motility over five generations).
14. **LCE_Colgen.zip** – Colgen files for producing LCE genealogical trees.
15. **LCE_mutations.csv** – Breseq summary for LCE lineages at the end of cycle 5.
16. **LCE_hypermutator.csv** – Breseq summary for LCE hypermutator lineages.
17. **LCE_data_analysis.zip** – LCE pCdrA & fitness assay data (flow cytometry raw values & statistical analysis).
18. **LCE_cycle6_mutations.csv** – Breseq summary for LCE replicate lineages after an additional generation (cycle 6; cycle 1 for SBW25 control).

Supplementary B

Raw sequence reads (.fastq) available on the NCBI SRA – LCE cycle 5 lineages: [PRJNA945835](https://www.ncbi.nlm.nih.gov/sra/PRJNA945835); LCE additional generation (cycle 6) replicate lineages: [PRJNA1026500](https://www.ncbi.nlm.nih.gov/sra/PRJNA1026500).

Acknowledgements

I could never have made it alone through this five year PhD journey (pandemic included), I had a strong support system of people around me – to whom I am forever indebted.

Firstly, I would like to thank Paul for convincing me to move to the other side of the world, to a small town in Northern Germany, to do some crazy fun experiments. I appreciate all your support over the years, and for surrounding me with inspiring and high-quality science.

To my mentor and friend Dave, thank you for everything. I have learnt so much under your supervision, and am only the scientist I am today because of your encouragement & wisdom. Whether it was a failed experiment, coffee & chat, moment of crisis, or an urgent need for a good burger – you were always there.

My German-mother Britta, danke schön, for always taking care and looking out for my well-being. I could never make enough baked goods to repay your kindness.

To my house/lab/office-mate Michael, cheers. Appreciate you being my live-in nose for so many years, for taking out the trash, and bringing me pinky donuts. And to all the forever friends that I met in party Plön – Bilal, Bram, Margot, Elena, Charly, Quentin, Ellen, Norma, Gillian, Loukas, Daniel, Devika, Nico, Maria, Eric, Lavisha, Aleksa, Jordan, Elio, Wiola, Gisela, Octavio, et al. Thanks for the beer, food & stories that we have shared; I hope there is more to come in the future. Bilal & Bram, you ain't getting rid of me that easy.

My gratitude goes to all the members of the MPB department, especially our wonderful technicians, your help has been invaluable. And to my office mates past & present – Marc, Norma, Malavika, Lena & Inga; thanks for sharing your snacks.

To my family and friends back home – Mum, Dad, Davina, Rebecca, Isla, Susan, Martin, Ronald, Lyon & Monnie. I miss you, and I will see you soon.

And lastly, to my partner-in-wholesome-crime Roxy. Thank you for your patience.

Bibliography

- Altschul, S. F., Gish, W., Miller, W., Myers, E. W., & Lipman, D. J. (1990). Basic local alignment search tool. *Journal of Molecular Biology*, 215(3), 403-410. doi:[10.1016/S0022-2836\(05\)80360-2](https://doi.org/10.1016/S0022-2836(05)80360-2)
- Altschul, S. F., Madden, T. L., Schäffer, A. A., Zhang, J., Zhang, Z., Miller, W., & Lipman, D. J. (1997). Gapped BLAST and PSI-BLAST: a new generation of protein database search programs. *Nucleic Acids Research*, 25(17), 3389-3402. doi:[10.1093/nar/25.17.3389](https://doi.org/10.1093/nar/25.17.3389)
- Alvarez-Ortega, C., Wiegand, I., Olivares, J., Hancock, R. E., & Martínez, J. L. (2010). Genetic determinants involved in the susceptibility of *Pseudomonas aeruginosa* to beta-lactam antibiotics. *Antimicrobial Agents and Chemotherapy*, 54(10), 4159-4167. doi:[10.1128/AAC.00257-10](https://doi.org/10.1128/AAC.00257-10)
- Anantharaman, V., & Aravind, L. (2000). Cache - a signaling domain common to animal Ca(2+)-channel subunits and a class of prokaryotic chemotaxis receptors. *Trends in Biochemical Sciences*, 25(11), 535-537. doi:[10.1016/s0968-0004\(00\)01672-8](https://doi.org/10.1016/s0968-0004(00)01672-8)
- Andersen, J. B., Sternberg, C., Poulsen, L. K., Bjorn, S. P., Givskov, M., & Molin, S. (1998). New unstable variants of green fluorescent protein for studies of transient gene expression in bacteria. *Applied and Environmental Microbiology*, 64(6), 2240-2246. doi:[10.1128/AEM.64.6.2240-2246.1998](https://doi.org/10.1128/AEM.64.6.2240-2246.1998)
- André, M., Dufour, D., & Rainey, P. B. (2019). Causes and Biophysical Consequences of Cellulose Production by *Pseudomonas fluorescens* SBW25 at the Air-Liquid Interface. *Journal of Bacteriology*, 201(18), e00110-19. doi:[10.1128/JB.00110-19](https://doi.org/10.1128/JB.00110-19)
- Arjan, J. A., Visser, M., Zeyl, C. W., Gerrish, P. J., Blanchard, J. L., & Lenski, R. E. (1999). Diminishing returns from mutation supply rate in asexual populations. *Science*, 283, 404-106. doi:[10.1126/science.283.5400.404](https://doi.org/10.1126/science.283.5400.404)
- Au, K. G., Clark, S., Miller, J. H., & Modrich, P. (1989). *Escherichia coli* mutY gene encodes an adenine glycosylase active on G-A mispairs. *PNAS USA*, 86(22), 8877-8881. doi:[10.1073/pnas.86.22.8877](https://doi.org/10.1073/pnas.86.22.8877)
- Bacik, J. P., Whitworth, G. E., Stubbs, K. A., Yadav, A. K., Martin, D. R., Bailey-Elkin, B. A., Vocadlo, D. J., & Mark, B. L. (2011). Molecular basis of 1,6-anhydro bond cleavage and phosphoryl transfer by *Pseudomonas aeruginosa* 1,6-anhydro-N-acetylmuramic acid kinase. *The Journal of Biological Chemistry*, 286(14), 12283-12291. doi:[10.1074/jbc.M110.198317](https://doi.org/10.1074/jbc.M110.198317)
- Bailey, J., & Manoil, C. (2002). Genome-wide internal tagging of bacterial exported proteins. *Nature Biotechnology*, 20(8), 839-842. doi:[10.1038/nbt715](https://doi.org/10.1038/nbt715)
- Bailey, M. J., Lilley, A. K., Thompson, I. P., Rainey, P. B., & Ellis, R. J. (1995). Site directed chromosomal marking of a fluorescent pseudomonad isolated from the phytosphere of sugar beet; stability and potential for marker gene transfer. *Molecular Ecology*, 4(6), 755-763. doi:[10.1111/j.1365-294x.1995.tb00276.x](https://doi.org/10.1111/j.1365-294x.1995.tb00276.x)

- Bantinaki, E., Kassen, R., Knight, C. G., Robinson, Z., Spiers A. J., & Rainey, P. B. (2007). Adaptive divergence in experimental populations of *Pseudomonas fluorescens*. III. Mutational origins of wrinkly spreader diversity. *Genetics*, *176*, 441-453. doi:[10.1534/genetics.106.069906](https://doi.org/10.1534/genetics.106.069906)
- Baraquet, C., Murakami, K., Parsek, M. R., & Harwood, C. S. (2012). The FleQ protein from *Pseudomonas aeruginosa* functions as both a repressor and an activator to control gene expression from the *pel* operon promoter in response to c-di-GMP. *Nucleic Acids Research*, *40*(15), 7207-7218. doi:[10.1093/nar/gks384](https://doi.org/10.1093/nar/gks384)
- Baraquet, C., & Harwood, C. S. (2016). FleQ DNA binding consensus sequence revealed by studies of FleQ-dependent regulation of biofilm gene expression in *Pseudomonas aeruginosa*. *Journal of Bacteriology*, *198*(1), 178-186. doi:[10.1128/JB.00539-15](https://doi.org/10.1128/JB.00539-15)
- Barnett, M. (2022). *How bias in the production of phenotypic variation shapes and is shaped by adaptive evolution* (PhD thesis, Christian-Albrecht University, Kiel, Germany).
- Baym, M., Kryazhimskiy, S., Lieberman, T. D., Chung, H., Desai, M. M., & Kishony, R. (2015). Inexpensive multiplexed library preparation for megabase-sized genomes. *PLoS One*, *10*(5), e0128036. doi:[10.1371/journal.pone.0128036](https://doi.org/10.1371/journal.pone.0128036)
- Baynham, P. J., Brown, A. L., Hall, L. L., & Wozniak, D. J. (1999). *Pseudomonas aeruginosa* AlgZ, a ribbon-helix-helix DNA-binding protein, is essential for alginate synthesis and *algD* transcriptional activation. *Molecular Microbiology*, *33*(5), 1069-1080. doi:[10.1046/j.1365-2958.1999.01550.x](https://doi.org/10.1046/j.1365-2958.1999.01550.x)
- Baynham, P. J., Ramsey, D. M., Gvozdyev, B. V., Cordonnier, E. M., & Wozniak, D. J. (2006). The *Pseudomonas aeruginosa* ribbon-helix-helix DNA-binding protein AlgZ (AmrZ) controls twitching motility and biogenesis of type IV pili. *Journal of Bacteriology*, *188*(1), 132-140. doi:[10.1128/JB.188.1.132-140.2006](https://doi.org/10.1128/JB.188.1.132-140.2006)
- Beaumont, H. J., Gallie, J., Kost, C., Ferguson, G. C., & Rainey, P. B. (2009). Experimental evolution of bet hedging. *Nature*, *462*(7269), 90-93. doi:[10.1038/nature08504](https://doi.org/10.1038/nature08504)
- Bertani, G. (1951). Studies on lysogenesis. I. The mode of phage liberation by lysogenic *Escherichia coli*. *Journal of Bacteriology*, *62*(3), 293-300. doi:[10.1128/jb.62.3.293-300.1951](https://doi.org/10.1128/jb.62.3.293-300.1951)
- Black, A. J., Bourrat, P. & Rainey, P. B. (2020). Ecological scaffolding and the evolution of individuality. *Nature Ecology & Evolution*, *4*, 426-436. doi:[10.1038/s41559-019-1086-9](https://doi.org/10.1038/s41559-019-1086-9)
- Bonner, J. T. (1998). The origins of multicellularity. *Integrative Biology*, *1*, 27-36. doi:[10.1002/\(SICI\)1520-6602\(1998\)1:1<27::AID-INBI4>3.0.CO;2-6](https://doi.org/10.1002/(SICI)1520-6602(1998)1:1<27::AID-INBI4>3.0.CO;2-6)
- Bonner, J. T. (2000). *First Signals: The Evolution of Multicellular Development*. Princeton, NJ: Princeton University Press. doi:[10.1515/9781400830589](https://doi.org/10.1515/9781400830589)
- Bonner, J. T. (2004). Perspective: the size-complexity rule. *Evolution*, *58*(9), 1883-1890. doi:[10.1111/j.0014-3820.2004.tb00476.x](https://doi.org/10.1111/j.0014-3820.2004.tb00476.x)

- Bouffartigues, E., Si Hadj Mohand, I., Maillot, O., Tortuel, D., Omnes, J., David, A., Tahrioui, A., Duchesne, R., Azuama, C. O., Nusser, M., Brenner-Weiss, G., Bazire, A., Connil, N., Orange, N., Feuilloley, M. G. J., Lesouhaitier, O., Dufour, A., Cornelis, P., & Chevalier, S. (2020). The temperature-regulation of *Pseudomonas aeruginosa* cmaX-cfrX-cmpX operon reveals an intriguing molecular network involving the sigma factors AlgU and SigX. *Frontiers in Microbiology*, *11*, 579495. doi:[10.3389/fmicb.2020.579495](https://doi.org/10.3389/fmicb.2020.579495)
- Bourrat, P., Doulcier, G., Rose, C. J., Rainey, P. B., & Hammerschmidt, H. (2022). Tradeoff breaking as a model of evolutionary transitions in individuality and limits of the fitness-decoupling metaphor. *eLife*, *11*, e73715. doi:[10.7554/eLife.73715](https://doi.org/10.7554/eLife.73715)
- Bourrat, P. (2015). Levels, time and fitness in evolutionary transitions in individuality. *Philosophy Theory and Practice in Biology*, *7*, 1-17. doi:[10.3998/ptb.6959004.0007.001](https://doi.org/10.3998/ptb.6959004.0007.001)
- Bourrat, P. (2022). Evolutionary transitions in individuality by endogenization of scaffolded properties. *The British Journal for the Philosophy of Science*. doi:[10.1086/719118](https://doi.org/10.1086/719118)
- Buss, L. W. (1987). *The Evolution of Individuality*. Princeton University Press.
- Byrd, M. S., Sadovskaya, I., Vinogradov, E., Lu, H., Sprinkle, A. B., Richardson, S. H., Ma, L., Ralston, B., Parsek, M. R., Anderson, E. M., Lam, J. S., & Wozniak, D. J. (2009). Genetic and biochemical analyses of the *Pseudomonas aeruginosa* Psl exopolysaccharide reveal overlapping roles for polysaccharide synthesis enzymes in Psl and LPS production. *Molecular Microbiology*, *73*(4), 622-638. doi:[10.1111/j.1365-2958.2009.06795.x](https://doi.org/10.1111/j.1365-2958.2009.06795.x)
- Cai, Y. M., Yu, K. W., Liu, J. H., Cai, Z., Zhou, Z. H., Liu, Y., Wang, T. F., & Yang, L. (2022). The c-di-GMP phosphodiesterase PipA (PA0285) regulates autoaggregation and Pf4 bacteriophage production in *Pseudomonas aeruginosa* PAO1. *Applied and Environmental Microbiology*, *88*(12), e0003922. doi:[10.1128/aem.00039-22](https://doi.org/10.1128/aem.00039-22)
- Caiazza, N. C., Merritt, J. H., Brothers, K. M., & O'Toole, G. A. (2007). Inverse regulation of biofilm formation and swarming motility by *Pseudomonas aeruginosa* PA14. *Journal of Bacteriology*, *189*(9), 3603-3612. doi:[10.1128/JB.01685-06](https://doi.org/10.1128/JB.01685-06)
- Caiazza, N. C., & O'Toole, G. A. (2004). SadB is required for the transition from reversible to irreversible attachment during biofilm formation by *Pseudomonas aeruginosa* PA14. *Journal of Bacteriology*, *186*(14), 4476-4485. doi:[10.1128/JB.186.14.4476-4485.2004](https://doi.org/10.1128/JB.186.14.4476-4485.2004)
- Caiazza, N. C., Shanks, R. M., & O'Toole, G. A. (2005). Rhamnolipids modulate swarming motility patterns of *Pseudomonas aeruginosa*. *Journal of Bacteriology*, *187*(21), 7351-7361. doi:[10.1128/JB.187.21.7351-7361.2005](https://doi.org/10.1128/JB.187.21.7351-7361.2005)
- Calcott, B., & Sterelny, K. (2011). *The Major Transitions in Evolution Revisited*. The MIT Press.
- Chen, A. I., Dolben, E. F., Okegbe, C., Harty, C. E., Golub, Y., Thao, S., Ha, D. G., Willger, S. D., O'Toole, G. A., Harwood, C. S., Dietrich, L. E., & Hogan, D. A. (2014). *Candida albicans* ethanol stimulates *Pseudomonas aeruginosa* WspR-controlled biofilm formation as part of a cyclic relationship involving phenazines. *PLoS Pathogens*, *10*(10), e1004480. doi:[10.1371/journal.ppat.1004480](https://doi.org/10.1371/journal.ppat.1004480)

- Chen, L., & Duan, K. (2016). A PhoPQ-regulated ABC transporter system exports tetracycline in *Pseudomonas aeruginosa*. *Antimicrobial Agents and Chemotherapy*, *60*(5), 3016-3024. doi:[10.1128/AAC.02986-15](https://doi.org/10.1128/AAC.02986-15)
- Cheng, Q., & Park, J. T. (2002). Substrate specificity of the AmpG permease required for recycling of cell wall anhydro-muropeptides. *Journal of Bacteriology*, *184*(23), 6434-6436. doi:[10.1128/JB.184.23.6434-6436.2002](https://doi.org/10.1128/JB.184.23.6434-6436.2002)
- Choy, W. K., Zhou, L., Syn, C. K., Zhang, L. H., & Swarup, S. (2004). MorA defines a new class of regulators affecting flagellar development and biofilm formation in diverse *Pseudomonas* species. *Journal of Bacteriology*, *186*(21), 7221-7228. doi:[10.1128/JB.186.21.7221-7228.2004](https://doi.org/10.1128/JB.186.21.7221-7228.2004)
- Christen, B., Christen, M., Paul, R., Schmid, F., Folcher, M., Jenoe, P., Meuwly, M., & Jenal, U. (2006). Allosteric control of cyclic di-GMP signalling. *Journal of Biological Chemistry*, *281*(42), 32015-24. doi:[10.1074/jbc.M603589200](https://doi.org/10.1074/jbc.M603589200)
- Christen, M., Christen, B., Folcher, M., Schauerte, A., & Jenal, U. (2005). Identification and characterization of a cyclic di-GMP-specific phosphodiesterase and its allosteric control by GTP. *Journal of Biological Chemistry*, *280*(35), 30829-37. doi:[10.1074/jbc.M504429200](https://doi.org/10.1074/jbc.M504429200)
- D'Argenio, D. A., Calfee, M. W., Rainey, P. B., & Pesci, E. C. (2002). Autolysis and autoaggregation in *Pseudomonas aeruginosa* colony morphology mutants. *Journal of Bacteriology*, *184*(23), 6481-6489. doi:[10.1128/JB.184.23.6481-6489.2002](https://doi.org/10.1128/JB.184.23.6481-6489.2002)
- D'Argenio, D. A., & Miller, S. I. (2004). Cyclic di-GMP as a bacterial second messenger. *Microbiology*, *150*(8), 2497-2502. doi:[10.1099/mic.0.27099-0](https://doi.org/10.1099/mic.0.27099-0)
- Darwin, C. (1859). *On the Origin of Species by Means of Natural Selection* (1st ed.) John Murray.
- Das, S., Noe, J. C., Paik, S., & Kitten, T. (2005). An improved arbitrary primed PCR method for rapid characterization of transposon insertion sites. *Journal of Microbiological Methods*, *63*(1), 89-94. doi:[10.1016/j.mimet.2005.02.011](https://doi.org/10.1016/j.mimet.2005.02.011)
- Dasgupta, N., & Ramphal, R. (2001). Interaction of the antiactivator FleN with the transcriptional activator FleQ regulates flagellar number in *Pseudomonas aeruginosa*. *Journal of Bacteriology*, *183*(22), 6636-6644. doi:[10.1128/JB.183.22.6636-6644.2001](https://doi.org/10.1128/JB.183.22.6636-6644.2001)
- Dasgupta, N., Arora, S. K., & Ramphal, R. (2000). fleN, a gene that regulates flagellar number in *Pseudomonas aeruginosa*. *Journal of Bacteriology*, *182*(2), 357-364. doi:[10.1128/JB.182.2.357-364.2000](https://doi.org/10.1128/JB.182.2.357-364.2000)
- De, N., Pirruccello, M., Krasteva, P. V., Bae, N., Raghavan, R. V., & Sondermann, H. (2008). Phosphorylation-independent regulation of the diguanylate cyclase WspR. *PLoS Biology*, *6*(3), e67. doi:[10.1371/journal.pbio.0060067](https://doi.org/10.1371/journal.pbio.0060067)
- Dean, C. R., & Goldberg, J. B. (2002). *Pseudomonas aeruginosa* galU is required for a complete lipopolysaccharide core and repairs a secondary mutation in a PA103 (serogroup O11) wbpM mutant. *FEMS Microbiology Letters*, *210*(2), 277-283. doi:[10.1111/j.1574-6968.2002.tb11193.x](https://doi.org/10.1111/j.1574-6968.2002.tb11193.x)

- Deatherage, D. E., Barrick, J. E. (2014). Identification of mutations in laboratory-evolved microbes from next-generation sequencing data using breseq. *Methods in Molecular Biology*, 1151, 165-188. doi:[10.1007/978-1-4939-0554-6_12](https://doi.org/10.1007/978-1-4939-0554-6_12)
- De Monte, S., & Rainey, P. B. (2014). Nascent multicellular life and the emergence of individuality. *Journal of Biosciences*, 39(2), 237-248. doi:[10.1007/s12038-014-9420-5](https://doi.org/10.1007/s12038-014-9420-5)
- Denamur, E., & Matic, I. (2006). Evolution of mutation rates in bacteria. *Molecular Microbiology*, 60(4), 820-827. doi:[10.1111/j.1365-2958.2006.05150.x](https://doi.org/10.1111/j.1365-2958.2006.05150.x)
- Ditta, G., Stanfield, S., Corbin, D., & Helinski, D. R. (1980). Broad host range DNA cloning system for gram-negative bacteria: construction of a gene bank of *Rhizobium meliloti*. *PNAS USA*, 77(12), 7347-7351. doi:[10.1073/pnas.77.12.7347](https://doi.org/10.1073/pnas.77.12.7347)
- Dittmar, K. A., Sørensen, M. A., Elf, J., Ehrenberg, M., & Pan, T. (2005). Selective charging of tRNA isoacceptors induced by amino-acid starvation. *EMBO Reports*, 6(2), 151-157. doi:[10.1038/sj.embor.7400341](https://doi.org/10.1038/sj.embor.7400341)
- Doebeli, M., Ispolatov, Y., & Simon, B. (2017) Point of view: Towards a mechanistic foundation of evolutionary theory. *eLife*, 6. doi:[10.7554/eLife.23804](https://doi.org/10.7554/eLife.23804)
- Dombek, K. M., & Ingram, L. O. (1984). Effects of ethanol on the *Escherichia coli* plasma membrane. *Journal of Bacteriology*, 157(1), 233-239. doi:[10.1128/jb.157.1.233-239.1984](https://doi.org/10.1128/jb.157.1.233-239.1984)
- Dong, H., Nilsson, L., & Kurland, C. G. (1996). Co-variation of tRNA abundance and codon usage in *Escherichia coli* at different growth rates. *Journal of Molecular Biology*, 260(5), 649-663. doi:[10.1006/jmbi.1996.0428](https://doi.org/10.1006/jmbi.1996.0428)
- Dötsch, A., Becker, T., Pommerenke, C., Magnowska, Z., Jänsch, L., & Häussler, S. (2009). Genome wide identification of genetic determinants of antimicrobial drug resistance in *Pseudomonas aeruginosa*. *Antimicrobial Agents and Chemotherapy*, 53(6), 2522-2531. doi:[10.1128/AAC.00035-09](https://doi.org/10.1128/AAC.00035-09)
- Doulcier, G. (2019). Colgen, Collective Genealogies Visualisation and Analysis. Zenodo. doi:[10.5281/zenodo.7342768](https://doi.org/10.5281/zenodo.7342768).
- Feng, Q., Ahator, S. D., Zhou, T., Liu, Z., Lin, Q., Liu, Y., Huang, J., Zhou, J., & Zhang, L. H. (2020). Regulation of exopolysaccharide production by ProE, a cyclic-di-GMP phosphodiesterase in *Pseudomonas aeruginosa* PAO1. *Frontiers in Microbiology*, 11, 1226. doi:[10.3389/fmicb.2020.01226](https://doi.org/10.3389/fmicb.2020.01226)
- Ferguson, G. C., Bertels, F., & Rainey, P. B. (2013). Adaptive divergence in experimental populations of *Pseudomonas fluorescens*. V. Insight into the niche specialist fuzzy spreader compels revision of the model *Pseudomonas* radiation. *Genetics*, 195(4), 1319-1335. doi:[10.1534/genetics.113.154948](https://doi.org/10.1534/genetics.113.154948)
- Finn, R. D., Bateman, A., Clements, J., Coggill, P., Eberhardt, R. Y., Eddy, S. R., Heger, A., Hetherington, K., Holm, L., Mistry, J., Sonnhammer, E. L., Tate, J., & Punta, M. (2014). Pfam: the protein families database. *Nucleic Acids Research*, 42, D222-230. doi:[10.1093/nar/gkt1223](https://doi.org/10.1093/nar/gkt1223)

- Gallie, J., Libby, E., Bertels, F., Remigi, P., Jendresen, C. B., Ferguson, G. C., Desprat, N., Buffing, M. F., Sauer, U., Beaumont, H. J., Martinussen, J., Kilstrup, M., & Rainey, P. B. (2015). Bistability in a metabolic network underpins the de novo evolution of colony switching in *Pseudomonas fluorescens*. *PLoS Biology*, *13*(3), e1002109. doi:[10.1371/journal.pbio.1002109](https://doi.org/10.1371/journal.pbio.1002109)
- Gallie, J. (2010). *Evolutionary and molecular origins of a phenotypic switch in Pseudomonas fluorescens SBW25* (PhD thesis, Massey University, Auckland, New Zealand)
- García, V., Godoy, P., Daniels, C., Hurtado, A., Ramos, J. L., & Segura, A. (2010). Functional analysis of new transporters involved in stress tolerance in *Pseudomonas putida* DOT-T1E. *Environmental Microbiology Reports*, *2*(3), 389-395. doi:[10.1111/j.1758-2229.2009.00093.x](https://doi.org/10.1111/j.1758-2229.2009.00093.x)
- Giacalone, D., Smith, T. J., Collins, A. J., Sondermann, H., Koziol, L. J., & O'Toole, G. A. (2018). Ligand-mediated biofilm formation via enhanced physical interaction between a diguanylate cyclase and its receptor. *mBio*, *9*(4), e01254-18. doi:[10.1128/mBio.01254-18](https://doi.org/10.1128/mBio.01254-18)
- Giardina, G., Paiardini, A., Fericola, S., Franceschini, S., Rinaldo, S., Stelitano, V., & Cutruzzolà, F. (2013). Investigating the allosteric regulation of YfiN from *Pseudomonas aeruginosa*: clues from the structure of the catalytic domain. *PLoS One*, *8*(11), e81324. doi:[10.1371/journal.pone.0081324](https://doi.org/10.1371/journal.pone.0081324)
- Gibson, D. G., Young, L., Chuang, R. Y., Venter, J. C., Hutchison, C. A., 3rd, & Smith, H. O. (2009). Enzymatic assembly of DNA molecules up to several hundred kilobases. *Nature Methods*, *6*(5), 343-345. doi:[10.1038/nmeth.1318](https://doi.org/10.1038/nmeth.1318)
- Giddens, S. R., Jackson, R. W., Moon, C. D., Jacobs, M. A., Zhang, X., Gehrig, S. M., & Rainey, P. B. (2007). Mutational activation of niche-specific genes provides insight into regulatory networks and bacterial function in a complex environment. *PNAS*, *104*(46), 18247-18252. doi:[10.1073/pnas.0706739104](https://doi.org/10.1073/pnas.0706739104)
- Gisin, J., Schneider, A., Nägele, B., Borisova, M., & Mayer, C. (2013). A cell wall recycling shortcut that bypasses peptidoglycan de novo biosynthesis. *Nature Chemical Biology*, *9*(8), 491-493. doi:[10.1038/nchembio.1289](https://doi.org/10.1038/nchembio.1289)
- Godfrey-Smith, P. (2009). *Darwinian Populations and Natural Selection*. Oxford University Press.
- Gould, S. J., & Lloyd, E. A. (1999). Individuality and adaptation across levels of selection: how shall we name and generalize the unit of Darwinism? *PNAS USA*, *96*(21), 11904-11909. doi:[10.1073/pnas.96.21.11904](https://doi.org/10.1073/pnas.96.21.11904)
- Gould, S. J. (2002). *The Structure of Evolutionary Theory*. Belknap Press of Harvard University Press.
- Goymer, P., Kahn, S. G., Malone, J. G., Gehrig, S. M., Spiers, A. J., & Rainey, P. B. (2006). Adaptive divergence in experimental populations of *Pseudomonas fluorescens*. II. Role of the GGDEF regulator WspR in evolution and development of the wrinkly spreader phenotype. *Genetics*, *173*, 515-526. doi:[10.1534/genetics.106.055863](https://doi.org/10.1534/genetics.106.055863)
- Griesemer, J. (2000). The units of evolutionary transition. *Selection*, *1*, 67-80 doi:[10.1556/Select.1.2000.1-3.7](https://doi.org/10.1556/Select.1.2000.1-3.7)

- Grocock, R. J., & Sharp, P. M. (2002). Synonymous codon usage in *Pseudomonas aeruginosa* PA01. *Gene*, 289(1-2), 131-139. doi:[10.1016/s0378-1119\(02\)00503-6](https://doi.org/10.1016/s0378-1119(02)00503-6)
- Grosberg, R. K., & Strathmann, R. R. (1998). One cell, two cell, red cell, blue cell: The persistence of a unicellular stage in multicellular life histories. *Trends in Ecology & Evolution*, 13(3), 112-116. doi:[10.1016/S0169-5347\(97\)01313-X](https://doi.org/10.1016/S0169-5347(97)01313-X)
- Grosberg, R. K., & Strathmann, R. R. (2007). The evolution of multicellularity: A minor major transition? *Annual Review of Ecology Evolution and Systematics*, 38(1), 621-654. doi:[10.1146/annurev.ecolsys.36.102403.114735](https://doi.org/10.1146/annurev.ecolsys.36.102403.114735)
- Guttenplan, S. B., & Kearns, D. B. (2013). Regulation of flagellar motility during biofilm formation. *FEMS Microbiology Reviews*, 37(6), 849-871. doi:[10.1111/1574-6976.12018](https://doi.org/10.1111/1574-6976.12018)
- Güvener, Z. T., & Harwood, C. S. (2007). Subcellular location characteristics of the *Pseudomonas aeruginosa* GGDEF protein, WspR, indicate that it produces cyclic-di-GMP in response to growth on surfaces. *Molecular Microbiology*, 66(6), 1459-1473. doi:[10.1111/j.1365-2958.2007.06008.x](https://doi.org/10.1111/j.1365-2958.2007.06008.x)
- Ha, D. G., Kuchma, S. L., O'Toole, G. A. (2014a). Plate-based assay for swimming motility in *Pseudomonas aeruginosa*. *Methods in Molecular Biology*, 1149, 59-65. doi:[10.1007/978-1-4939-0473-0_7](https://doi.org/10.1007/978-1-4939-0473-0_7)
- Ha, D. G., & O'Toole, G. A. (2015). c-di-GMP and its effects on biofilm formation and dispersion: A *Pseudomonas aeruginosa* review. *Microbiology Spectrum*, 3(2). doi:[10.1128/microbiolspec.MB-0003-2014](https://doi.org/10.1128/microbiolspec.MB-0003-2014)
- Ha, D. G., Richman, M. E., & O'Toole, G. A. (2014b). Deletion mutant library for investigation of functional outputs of cyclic diguanylate metabolism in *Pseudomonas aeruginosa* PA14. *Applied and Environmental Microbiology*, 80(11), 3384-3393. doi:[10.1128/AEM.00299-14](https://doi.org/10.1128/AEM.00299-14)
- Hamilton W. D. (1964). The genetical evolution of social behaviour. I. *Journal of Theoretical Biology*, 7(1), 1-16. doi:[10.1016/0022-5193\(64\)90038-4](https://doi.org/10.1016/0022-5193(64)90038-4)
- Hammerschmidt, K., Rose, C. J., Kerr, B., & Rainey, P. B. (2014). Life cycles, fitness decoupling and the evolution of multicellularity. *Nature*, 515, 75-79. doi:[10.1038/nature13884](https://doi.org/10.1038/nature13884)
- Hanahan D. (1983). Studies on transformation of *Escherichia coli* with plasmids. *Journal of Molecular Biology*, 166(4), 557-580. doi:[10.1016/s0022-2836\(83\)80284-8](https://doi.org/10.1016/s0022-2836(83)80284-8)
- Hecht, A., Glasgow, J., Jaschke, P. R., Bawazer, L. A., Munson, M. S., Cochran, J. R., Endy, D., & Salit, M. (2017). Measurements of translation initiation from all 64 codons in *E. coli*. *Nucleic Acids Research*, 45(7), 3615-3626. doi:[10.1093/nar/gkx070](https://doi.org/10.1093/nar/gkx070)
- Hengge, R. (2009). Principles of c-di-GMP signalling in bacteria. *Nature Reviews Microbiology*, 7(4), 263-73. doi:[10.1038/nrmicro2109](https://doi.org/10.1038/nrmicro2109)

- Herron, M. D., Borin, J. M., Boswell, J. C., Walker, J., Chen, I. K., Knox, C. A., Boyd, M., Rosenzweig, F., & Ratcliff, W. C. (2019). De novo origins of multicellularity in response to predation. *Scientific Reports*, *9*(1), 2328. doi:[10.1038/s41598-019-39558-8](https://doi.org/10.1038/s41598-019-39558-8)
- Hickman, J. W., & Harwood, C. S. (2008). Identification of FleQ from *Pseudomonas aeruginosa* as a c-di-GMP-responsive transcription factor. *Molecular Microbiology*, *69*(2), 376-389. doi:[10.1111/j.1365-2958.2008.06281.x](https://doi.org/10.1111/j.1365-2958.2008.06281.x)
- Hickman, J. W., Tifrea, D. F., & Harwood, C. S. (2005). A chemosensory system that regulates biofilm formation through modulation of cyclic diguanylate levels. *PNAS USA*, *102*(40), 14422-14427. doi:[10.1073/pnas.0507170102](https://doi.org/10.1073/pnas.0507170102)
- Hmelo, L. R., Borlee, B. R., Almblad, H., Love, M. E., Randall, T. E., Tseng, B. S., Lin, C., Irie, Y., Storek, K. M., Yang, J. J., Siehnel, R. J., Howell, P. L., Singh, P. K., Tolker-Nielsen, T., Parsek, M. R., Schweizer, H. P., & Harrison, J. J. (2015). Precision-engineering the *Pseudomonas aeruginosa* genome with two-step allelic exchange. *Nature Protocols*, *10*(11), 1820-1841. doi:[10.1038/nprot.2015.115](https://doi.org/10.1038/nprot.2015.115)
- Ho, S. N., Hunt, H. D., Horton, R. M., Pullen, J. K., & Pease, L. R. (1989). Site-directed mutagenesis by overlap extension using the polymerase chain reaction. *Gene*, *77*(1), 51-59. doi:[10.1016/0378-1119\(89\)90358-2](https://doi.org/10.1016/0378-1119(89)90358-2)
- Ikemura T. (1981). Correlation between the abundance of *Escherichia coli* transfer RNAs and the occurrence of the respective codons in its protein genes: a proposal for a synonymous codon choice that is optimal for the *E. coli* translational system. *Journal of Molecular Biology*, *151*(3), 389-409. doi:[10.1016/0022-2836\(81\)90003-6](https://doi.org/10.1016/0022-2836(81)90003-6)
- Jones, C. J., Newsom, D., Kelly, B., Irie, Y., Jennings, L. K., Xu, B., Limoli, D. H., Harrison, J. J., Parsek, M. R., White, P., & Wozniak, D. J. (2014). ChIP-Seq and RNA-Seq reveal an AmrZ-mediated mechanism for cyclic di-GMP synthesis and biofilm development by *Pseudomonas aeruginosa*. *PLoS Pathogens*, *10*(3), e1003984. doi:[10.1371/journal.ppat.1003984](https://doi.org/10.1371/journal.ppat.1003984)
- Jones, C. J., Ryder, C. R., Mann, E. E., & Wozniak, D. J. (2013). AmrZ modulates *Pseudomonas aeruginosa* biofilm architecture by directly repressing transcription of the *psl* operon. *Journal of Bacteriology*, *195*(8), 1637-1644. doi:[10.1128/JB.02190-12](https://doi.org/10.1128/JB.02190-12)
- Jorgenson, M. A., Chen, Y., Yahashiri, A., Popham, D. L., & Weiss, D. S. (2014). The bacterial septal ring protein RlpA is a lytic transglycosylase that contributes to rod shape and daughter cell separation in *Pseudomonas aeruginosa*. *Molecular Microbiology*, *93*(1), 113-128. doi:[10.1111/mmi.12643](https://doi.org/10.1111/mmi.12643)
- Kaiser, D. (2001). Building a multicellular organism. *Annual Review of Genetics*, *35*, 103-23. doi:[10.1146/annurev.genet.35.102401.090145](https://doi.org/10.1146/annurev.genet.35.102401.090145)
- Kato, J., Misra, T. K., & Chakrabarty, A. M. (1990). AlgR3, a protein resembling eukaryotic histone H1, regulates alginate synthesis in *Pseudomonas aeruginosa*. *PNAS USA*, *87*(8), 2887-2891. doi:[10.1073/pnas.87.8.2887](https://doi.org/10.1073/pnas.87.8.2887)

- Kearns, D. B. (2010). A field guide to bacterial swarming motility. *Nature Reviews Microbiology*, 8(9), 634-44. doi:[10.1038/nrmicro2405](https://doi.org/10.1038/nrmicro2405)
- Kessler, C., & Kim, W. (2022). Identification of cyclic-di-GMP-modulating protein residues by bidirectionally evolving a social behaviour in *Pseudomonas fluorescens*. *mSystems*, 7(5), e0073722. doi:[10.1128/msystems.00737-22](https://doi.org/10.1128/msystems.00737-22)
- Kessler, C., Mhatre, E., Cooper, V., & Kim, W. (2021). Evolutionary divergence of the Wsp signal transduction systems in beta- and gammaproteobacteria. *Applied and Environmental Microbiology*, 87(22), e0130621. doi:[10.1128/AEM.01306-21](https://doi.org/10.1128/AEM.01306-21)
- Kim, W., Levy, S. B., & Foster, K. R. (2016). Rapid radiation in bacteria leads to a division of labour. *Nature Communications*, 7, 10508. doi:[10.1038/ncomms10508](https://doi.org/10.1038/ncomms10508)
- King, E. O., Ward, M. K., & Raney, D. E. (1954). Two simple media for the demonstration of pyocyanin and fluorescin. *The Journal of Laboratory and Clinical Medicine*, 44(2), 301-307.
- Kirk D. L. (2001). Germ-soma differentiation in volvox. *Developmental Biology*, 238(2), 213-223. doi:[10.1006/dbio.2001.0402](https://doi.org/10.1006/dbio.2001.0402)
- Kitten, T., Kinscherf, T. G., McEvoy, J. L., & Willis, D. K. (1998). A newly identified regulator is required for virulence and toxin production in *Pseudomonas syringae*. *Molecular Microbiology*, 28(5), 917-929. doi:[10.1046/j.1365-2958.1998.00842.x](https://doi.org/10.1046/j.1365-2958.1998.00842.x)
- Koufopanou, V., & Bell, G. (1993). Soma and germ: an experimental approach using Volvox. *Proceedings of the Royal Society of London Series B*, 254, 107-113. doi:[10.1098/rspb.1993.0134](https://doi.org/10.1098/rspb.1993.0134)
- Kuchma, S. L., Brothers, K. M., Merritt, J. H., Liberati, N. T., Ausubel, F. M., & O'Toole, G. A. (2007). BifA, a cyclic-di-GMP phosphodiesterase, inversely regulates biofilm formation and swarming motility by *Pseudomonas aeruginosa* PA14. *Journal of Bacteriology*, 189(22), 8165-78. doi:[10.1128/JB.00586-07](https://doi.org/10.1128/JB.00586-07)
- Kulasakara, H., Lee, V., Brenic, A., Liberati, N., Urbach, J., Miyata, S., Lee, D. G., Neely, A. N., Hyodo, M., Hayakawa, Y., Ausubel, F. M., & Lory, S. (2006). Analysis of *Pseudomonas aeruginosa* diguanylate cyclases and phosphodiesterases reveals a role for bis-(3'-5')-cyclic-GMP in virulence. *PNAS USA*, 103(8), 2839-2844. doi:[10.1073/pnas.0511090103](https://doi.org/10.1073/pnas.0511090103)
- Lamers, R. P., Nguyen, U. T., Nguyen, Y., Buensuceso, R. N., & Burrows, L. L. (2015). Loss of membrane-bound lytic transglycosylases increases outer membrane permeability and β -lactam sensitivity in *Pseudomonas aeruginosa*. *MicrobiologyOpen*, 4(6), 879-895. doi:[10.1002/mbo3.286](https://doi.org/10.1002/mbo3.286)
- Lau, P. C., Lindhout, T., Beveridge, T. J., Dutcher, J. R., & Lam, J. S. (2009). Differential lipopolysaccharide core capping leads to quantitative and correlated modifications of mechanical and structural properties in *Pseudomonas aeruginosa* biofilms. *Journal of Bacteriology*, 191(21), 6618-6631. doi:[10.1128/JB.00698-09](https://doi.org/10.1128/JB.00698-09)

- Lenski, R. E., & Travisano, M. (1994). Dynamics of adaptation and diversification: A 10,000-generation experiment with bacterial populations. *PNAS USA*, *91*, 6808-6814. doi:[10.1073/pnas.91.15.6808](https://doi.org/10.1073/pnas.91.15.6808)
- Lewontin, R. C. (1970). The units of selection. *Annual Review of Ecology and Systematics*, *1*, 1-18. doi:[10.1146/annurev.es.01.110170.000245](https://doi.org/10.1146/annurev.es.01.110170.000245)
- Li, C., Wen, A., Shen, B., Lu, J., Huang, Y., & Chang, Y. (2011). FastCloning: A highly simplified, purification-free, sequence and ligation-independent PCR cloning method. *BMC Biotechnology*, *11*, 92. doi:[10.1186/1472-6750-11-92](https://doi.org/10.1186/1472-6750-11-92)
- Li, Y., Xia, H., Bai, F., Xu, H., Yang, L., Yao, H., Zhang, L., Zhang, X., Bai, Y., Saris, P. E., Tolker-Nielsen, T., & Qiao, M. (2007). Identification of a new gene PA5017 involved in flagella-mediated motility, chemotaxis and biofilm formation in *Pseudomonas aeruginosa*. *FEMS Microbiology Letters*, *272*(2), 188-195. doi:[10.1111/j.1574-6968.2007.00753.x](https://doi.org/10.1111/j.1574-6968.2007.00753.x)
- Libby, E., & Rainey, P. (2013a). A conceptual framework for the evolutionary origins of multicellularity. *Physical Biology*, *10*(3), 035001. doi:[10.1088/1478-3975/10/3/035001](https://doi.org/10.1088/1478-3975/10/3/035001)
- Libby, E., & Rainey, P. B. (2013b). Eco-evolutionary feedback and the tuning of proto-developmental life cycles. *PloS One*, *8*(12), e82274. doi:[10.1371/journal.pone.0082274](https://doi.org/10.1371/journal.pone.0082274)
- Lind, P. A., & Andersson, D. I. (2008). Whole-genome mutational biases in bacteria. *PNAS*, *105*(46), 17878-17883. doi:[10.1073/pnas.0804445105](https://doi.org/10.1073/pnas.0804445105)
- Lind, P. A., Farr, A. D., & Rainey, P. B. (2015). Experimental evolution reveals hidden diversity in evolutionary pathways. *eLife*, *4*. doi:[10.7554/eLife.07074](https://doi.org/10.7554/eLife.07074)
- Lind, P. A., Farr, A. D., & Rainey, P. B. (2017). Evolutionary convergence in experimental *Pseudomonas* populations. *The ISME Journal*, *11*(3), 589-600. doi:[10.1038/ismej.2016.157](https://doi.org/10.1038/ismej.2016.157)
- Long, H., Miller, S. F., Williams, E., & Lynch, M. (2018). Specificity of the DNA mismatch repair system (MMR) and mutagenesis bias in bacteria. *Molecular Biology and Evolution*, *35*(10), 2414-21. doi:[10.1093/molbev/msy134](https://doi.org/10.1093/molbev/msy134)
- Malone, J. G., Jaeger, T., Manfredi, P., Dötsch, A., Blanka, A., Bos, R., Cornelis, G. R., Häussler, S., & Jenal, U. (2012). The YfiB/NR signal transduction mechanism reveals novel targets for the evolution of persistent *Pseudomonas aeruginosa* in cystic fibrosis airways. *PLoS Pathogens*, *8*(6), e1002760. doi:[10.1371/journal.ppat.1002760](https://doi.org/10.1371/journal.ppat.1002760)
- Malone, J. G., Jaeger, T., Spangler, C., Ritz, D., Spang, A., Arrieumerlou, C., Kaeffer, V., Landmann, R., & Jenal, U. (2010). YfiB/NR mediates cyclic di-GMP dependent small colony variant formation and persistence in *Pseudomonas aeruginosa*. *PLoS Pathogens*, *6*(3), e1000804. doi:[10.1371/journal.ppat.1000804](https://doi.org/10.1371/journal.ppat.1000804)

- Malone, J. G., Williams, R., Christen, M., Jenal, U., Spiers, A. J., & Rainey, P. B. (2007). The structure-function relationship of WspR, a response regulator with a GGDEF output domain. *Microbiology*, *153*(4), 980-994. doi:[10.1099/mic.0.2006/002824-0](https://doi.org/10.1099/mic.0.2006/002824-0)
- Manoil C. (2000). Tagging exported proteins using Escherichia coli alkaline phosphatase gene fusions. *Methods in Enzymology*, *326*, 35-47. doi:[10.1016/s0076-6879\(00\)26045-x](https://doi.org/10.1016/s0076-6879(00)26045-x)
- Marchler-Bauer, A., Lu, S., Anderson, J. B., Chitsaz, F., Derbyshire, M. K., DeWeese-Scott, C., ... Bryant, S. H. (2011). CDD: a Conserved Domain Database for the functional annotation of proteins. *Nucleic Acids Research*, *39*, 225-229. doi:[10.1093/nar/gkq1189](https://doi.org/10.1093/nar/gkq1189)
- Martínez-Granero, F., Navazo, A., Barahona, E., Redondo-Nieto, M., Rivilla, R., & Martín, M. (2012). The Gac-Rsm and SadB signal transduction pathways converge on AlgU to downregulate motility in Pseudomonas fluorescens. *PLoS One*, *7*(2), e31765. doi:[10.1371/journal.pone.0031765](https://doi.org/10.1371/journal.pone.0031765)
- Matsuyama, B. Y., Krasteva, P. V., Baraquet, C., Harwood, C. S., Sondermann, H., & Navarro, M. V. (2015). Mechanistic insights into c-di-GMP-dependent control of the biofilm regulator FleQ from Pseudomonas aeruginosa. *PNAS USA*, *113*(2), E209-E218. doi:[10.1073/pnas.1523148113](https://doi.org/10.1073/pnas.1523148113)
- Mattingly, A. E., Kamatkar, N. G., Morales-Soto, N., Borlee, B. R., & ShROUT, J. D. (2018). Multiple Environmental Factors Influence the Importance of the Phosphodiesterase DipA upon Pseudomonas aeruginosa Swarming. *Applied and Environmental Microbiology*, *84*(7), e02847-17. doi:[10.1128/AEM.02847-17](https://doi.org/10.1128/AEM.02847-17)
- Maynard Smith, J., & Szathmáry, E. (1995). *The Major Transitions in Evolution*. Oxford University Press.
- Maynard Smith, J. (1964). Group selection and kin selection. *Nature*, *201*, 1145-1147. doi:[10.1038/2011145a0](https://doi.org/10.1038/2011145a0)
- Mayr, E. (1982). *The Growth of Biological Thought: Diversity, Evolution, and Inheritance*. Belknap Press of Harvard University Press.
- McDaniel, C., Su, S., Panmanee, W., Lau, G. W., Browne, T., Cox, K., Paul, A. T., Ko, S. H., Mortensen, J. E., Lam, J. S., Muruve, D. A., & Hassett, D. J. (2016). A putative ABC transporter permease is necessary for resistance to acidified nitrite and EDTA in Pseudomonas aeruginosa under aerobic and anaerobic planktonic and biofilm conditions. *Frontiers in Microbiology*, *7*, 291. doi:[10.3389/fmicb.2016.00291](https://doi.org/10.3389/fmicb.2016.00291)
- McDonald, M. J., Gehrig, S. M., Meintjes, P. L., Zhang, X., & Rainey, P. B. (2009). Adaptive divergence in experimental populations of Pseudomonas fluorescens. IV. Genetic constraints guide evolutionary trajectories in a parallel adaptive radiation. *Genetics*, *183*, 1041-1053. doi:[10.1534/genetics.109.107110](https://doi.org/10.1534/genetics.109.107110)
- Merritt, J. H., Brothers, K. M., Kuchma, S. L., & O'Toole, G. A. (2007). SadC reciprocally influences biofilm formation and swarming motility via modulation of exopolysaccharide production and flagellar function. *Journal of Bacteriology*, *189*(22), 8154-8164. doi:[10.1128/JB.00585-07](https://doi.org/10.1128/JB.00585-07)
- Michod, R. E., & Nedelcu, A. M. (2003). On the reorganization of fitness during evolutionary transitions in individuality. *Integrative and Comparative Biology*, *43*(1), 64-73. doi:[10.1093/icb/43.1.64](https://doi.org/10.1093/icb/43.1.64)

- Michod, R. E., & Roze, D. (2001). Cooperation and conflict in the evolution of multicellularity. *Heredity*, 86, 1-7. doi:[10.1046/j.1365-2540.2001.00808.x](https://doi.org/10.1046/j.1365-2540.2001.00808.x)
- Michod, R. E., Nedelcu, A. M., & Roze, D. (2003). Cooperation and conflict in the evolution of individuality. IV. Conflict mediation and evolvability in *Volvox carteri*. *Bio Systems*, 69, 95-114. doi:[10.1016/s0303-2647\(02\)00133-8](https://doi.org/10.1016/s0303-2647(02)00133-8)
- Michod, R. E. (1997). Cooperation and conflict in the evolution of individuality. I. Multilevel selection of the organism. *The American Naturalist*, 149(4), 607-645. doi:[10.1086/286012](https://doi.org/10.1086/286012)
- Michod, R. E. & Roze, D. (1999). Cooperation and conflict in the evolution of individuality. III. Transitions in the unit of fitness. In C. L. Nehaniv (Ed.), *Mathematical and Computational Biology Computational Morphogenesis, Hierarchical Complexity, and Digital Evolution* (pp. 47-92). American Mathematical Society.
- Michod R. E. (1996). Cooperation and conflict in the evolution of individuality. II. Conflict mediation. *Proceedings of the Royal Society B: Biological Sciences*, 263(1372), 813-822. doi:[10.1098/rspb.1996.0121](https://doi.org/10.1098/rspb.1996.0121)
- Minelli, A., & Fusco, G. (2010). Developmental plasticity and the evolution of animal complex life cycles. *Philosophical Transactions of the Royal Society of London. Series B, Biological Sciences*, 365(1540), 631-640. doi:[10.1098/rstb.2009.0268](https://doi.org/10.1098/rstb.2009.0268)
- Moczek, A. P., Sultan, S., Foster, S., Ledón-Rettig, C., Dworkin, I., Nijhout, H. F., Abouheif, E., & Pfennig, D. W. (2011). The role of developmental plasticity in evolutionary innovation. *Proceedings of the Royal Society B: Biological Sciences*, 278(1719), 2705-2713. doi:[10.1098/rspb.2011.0971](https://doi.org/10.1098/rspb.2011.0971)
- Modrich P. (1991). Mechanisms and biological effects of mismatch repair. *Annual Review of Genetics*, 25, 229-253. doi:[10.1146/annurev.ge.25.120191.001305](https://doi.org/10.1146/annurev.ge.25.120191.001305)
- Morgulis, A., Coulouris, G., Raytselis, Y., Madden, T. L., Agarwala, R., & Schäffer, A. A. (2008). Database indexing for production MegaBLAST searches. *Bioinformatics*, 24(16), 1757-1764. doi:[10.1093/bioinformatics/btn322](https://doi.org/10.1093/bioinformatics/btn322)
- Mukhopadhyay, S., Kapatral, V., Xu, W., & Chakrabarty, A. M. (1999). Characterization of a Hank's type serine/threonine kinase and serine/threonine phosphoprotein phosphatase in *Pseudomonas aeruginosa*. *Journal of Bacteriology*, 181(21), 6615-6622. doi:[10.1128/JB.181.21.6615-6622.1999](https://doi.org/10.1128/JB.181.21.6615-6622.1999)
- Muriel, C., Blanco-Romero, E., Trampari, E., Arrebola, E., Durán, D., Redondo-Nieto, M., Malone, J. G., Martín, M., & Rivilla, R. (2019). The diguanylate cyclase AdrA regulates flagellar biosynthesis in *Pseudomonas fluorescens* F113 through SadB. *Scientific Reports*, 9(1), 8096. doi:[10.1038/s41598-019-44554-z](https://doi.org/10.1038/s41598-019-44554-z)
- Navarrete, B., Leal-Morales, A., Serrano-Ron, L., Sarrió, M., Jiménez-Fernández, A., Jiménez-Díaz, L., López-Sánchez, A., & Govantes, F. (2019). Transcriptional organization, regulation and functional analysis of *flhF* and *flhN* in *Pseudomonas putida*. *PloS One*, 14(3), e0214166. doi:[10.1371/journal.pone.0214166](https://doi.org/10.1371/journal.pone.0214166)

- Navazo, A., Barahona, E., Redondo-Nieto, M., Martínez-Granero, F., Rivilla, R., & Martín, M. (2009). Three independent signalling pathways repress motility in *Pseudomonas fluorescens* F113. *Microbial Biotechnology*, 2(4), 489-498. doi:[10.1111/j.1751-7915.2009.00103.x](https://doi.org/10.1111/j.1751-7915.2009.00103.x)
- Newell, P. D., Yoshioka, S., Hvorecny, K. L., Monds, R. D., & O'Toole, G. A. (2011). Systematic analysis of diguanylate cyclases that promote biofilm formation by *Pseudomonas fluorescens* Pf0-1. *Journal of Bacteriology*, 193(18), 4685-4698. doi:[10.1128/JB.05483-11](https://doi.org/10.1128/JB.05483-11)
- Nilsson, A. I., Koskiniemi, S., Eriksson, S., Kugelberg, E., Hinton, J. C. D., & Andersson, D. I. (2005). Bacterial genome size reduction by experimental evolution. *PNAS*, 102(34), 12112-12116. doi:[10.1073/pnas.0503654102](https://doi.org/10.1073/pnas.0503654102)
- Noirot-Gros, M. F., Forrester, S., Malato, G., Larsen, P. E., & Noirot, P. (2019). CRISPR interference to interrogate genes that control biofilm formation in *Pseudomonas fluorescens*. *Scientific Reports*, 9, 15954. doi:[10.1038/s41598-019-52400-5](https://doi.org/10.1038/s41598-019-52400-5)
- Nowak, M. A., Tarnita, C. E., & Wilson, E. O. (2010). The evolution of eusociality. *Nature*, 466(7310), 1057-1062. doi:[10.1038/nature09205](https://doi.org/10.1038/nature09205)
- O'Connor, J. R., Kuwada, N. J., Huangyutitham, V., Wiggins, P. A., & Harwood, C. S. (2012). Surface sensing and lateral subcellular localization of WspA, the receptor in a chemosensory-like system leading to c-di-GMP production. *Molecular Microbiology*, 86(3), 720-729. doi:[10.1111/mmi.12013](https://doi.org/10.1111/mmi.12013)
- O'Neal, L., Baraquet, C., Suo, Z., Dreifus, J. E., Peng, Y., Raivio, T. L., Wozniak, D. J., Harwood, C. S., & Parsek, M. R. (2022). The Wsp system of *Pseudomonas aeruginosa* links surface sensing and cell envelope stress. *PNAS USA*, 119(18), e2117633119. doi:[10.1073/pnas.2117633119](https://doi.org/10.1073/pnas.2117633119)
- O'Toole, G. A., & Kolter, R. (1998). Flagellar and twitching motility are necessary for *Pseudomonas aeruginosa* biofilm development. *Molecular Microbiology*, 30(2), 295-304. doi:[10.1046/j.1365-2958.1998.01062.x](https://doi.org/10.1046/j.1365-2958.1998.01062.x)
- Okasha, S. (2005). Multilevel selection and the major transitions in evolution. *Philosophy of Science*, 72(5), 1013-1025. doi:[10.1086/508102](https://doi.org/10.1086/508102)
- Okasha, S. (2021). The strategy of endogenization in evolutionary biology. *Synthese*, 198, 3413-3435. doi:[10.1007/s11229-018-1832-6](https://doi.org/10.1007/s11229-018-1832-6)
- Oliver, A., Baquero, F., & Blázquez, J. (2002). The mismatch repair system (mutS, mutL and uvrD genes) in *Pseudomonas aeruginosa*: molecular characterization of naturally occurring mutants. *Molecular Microbiology*, 43(6), 1641-50. doi:[10.1046/j.1365-2958.2002.02855.x](https://doi.org/10.1046/j.1365-2958.2002.02855.x)
- Oliver, A., Sánchez, J. M., & Blázquez, J. (2002). Characterization of the GO system of *Pseudomonas aeruginosa*. *FEMS Microbiology Letters*, 217(1), 31-35. doi:[10.1111/j.1574-6968.2002.tb11452.x](https://doi.org/10.1111/j.1574-6968.2002.tb11452.x)
- Ophir, T., & Gutnick, D. L. (1994). A role for exopolysaccharides in the protection of microorganisms from desiccation. *Applied and Environmental Microbiology*, 60(2), 740-745. doi:[10.1128/aem.60.2.740-745.1994](https://doi.org/10.1128/aem.60.2.740-745.1994)

- Ortega, D. R., Fleetwood, A. D., Krell, T., Harwood, C. S., Jensen, G. J., & Zhulin, I. B. (2017). Assigning chemoreceptors to chemosensory pathways in *Pseudomonas aeruginosa*. *PNAS USA*, *114*(48), 12809-12814. doi:[10.1073/pnas.1708842114](https://doi.org/10.1073/pnas.1708842114)
- Oster, G., & Alberch, P. (1982). Evolution and bifurcation of developmental programs. *Evolution*, *36*(3), 444-459. doi:[10.2307/2408093](https://doi.org/10.2307/2408093)
- Paysan-Lafosse, T., Blum, M., Chuguransky, S., Grego, T., Pinto, B. L., Salazar, G. A., Bileschi, M. L., Bork, P., Bridge, A., Colwell, L., Gough, J., Haft, D. H., Letunić, I., Marchler-Bauer, A., Mi, H., Natale, D. A., Orengo, C. A., Pandurangan, A. P., Rivoire, C., Sigrist, C. J. A., ... Bateman, A. (2023). InterPro in 2022. *Nucleic Acids Research*, *51*(D1), D418-427. doi:[10.1093/nar/gkac993](https://doi.org/10.1093/nar/gkac993)
- Pfeiffer, T., & Bonhoeffer, S. (2003). An evolutionary scenario for the transition to undifferentiated multicellularity. *PNAS USA*, *100*(3), 1095-1098. doi:[10.1073/pnas.0335420100](https://doi.org/10.1073/pnas.0335420100)
- Phippen, C. W., Mikolajek, H., Schlaefli, H. G., Keevil, C. W., Webb, J. S., & Tews, I. (2014). Formation and dimerization of the phosphodiesterase active site of the *Pseudomonas aeruginosa* MorA, a bi-functional c-di-GMP regulator. *FEBS Letters*, *588*(24), 4631-4636. doi:[10.1016/j.febslet.2014.11.002](https://doi.org/10.1016/j.febslet.2014.11.002)
- Pichugin, Y., Peña, J., Rainey, P. B., & Traulsen, A. (2017). Fragmentation modes and the evolution of life cycles. *PLoS Computational Biology*, *13*(11), e1005860. doi:[10.1371/journal.pcbi.1005860](https://doi.org/10.1371/journal.pcbi.1005860)
- Poon, K. K., Westman, E. L., Vinogradov, E., Jin, S., & Lam, J. S. (2008). Functional characterization of MigA and WapR: putative rhamnosyltransferases involved in outer core oligosaccharide biosynthesis of *Pseudomonas aeruginosa*. *Journal of Bacteriology*, *190*(6), 1857-1865. doi:[10.1128/JB.01546-07](https://doi.org/10.1128/JB.01546-07)
- Queller, D. C. (1997). Cooperators since life began [Review of the book *The Major Transitions in Evolution*, by J. Maynard Smith & E. Szathmáry]. *The Quarterly Review of Biology*, *72*(2), 184-188.
- Queller D. C. (2000). Relatedness and the fraternal major transitions. *Philosophical Transactions of the Royal Society B: Biological Sciences*, *355*(1403), 1647-1655. doi:[10.1098/rstb.2000.0727](https://doi.org/10.1098/rstb.2000.0727)
- Rainey, P. B., & Bailey, M. J. (1996). Physical and genetic map of the *Pseudomonas fluorescens* SBW25 chromosome. *Molecular Microbiology*, *19*(3), 521-533. doi:[10.1046/j.1365-2958.1996.391926.x](https://doi.org/10.1046/j.1365-2958.1996.391926.x)
- Rainey, P. B., & Kerr, B. (2010). Cheats as first propagules: A new hypothesis for the evolution of individuality during the transition from single cells to multicellularity. *BioEssays*, *32*(10), 872-880. doi:[10.1002/bies.201000039](https://doi.org/10.1002/bies.201000039)
- Rainey, P. B., & Rainey, K. (2003). Evolution of cooperation and conflict in experimental bacterial populations. *Nature*, *425*(6953), 72-74. doi:[10.1038/nature01906](https://doi.org/10.1038/nature01906)
- Rainey, P. B., & Travisano, M. (1998). Adaptive radiation in a heterogeneous environment. *Nature*, *394*(6688), 69-72. doi:[10.1038/27900](https://doi.org/10.1038/27900)

- Rainey, P. B., Remigi, P., Farr, A. D., & Lind, P. A. (2017) Darwin was right: where now for experimental evolution? *Current Opinion in Genetics and Development*, 47, 102-109. doi:[10.1016/j.gde.2017.09.003](https://doi.org/10.1016/j.gde.2017.09.003)
- Rainey, P. B. & De Monte, S. (2014). Resolving conflicts during the evolutionary transition to multicellular life. *Annual Review of Ecology Evolution and Systematics*, 45(1), 599-620. doi:[10.1146/annurev-ecolsys-120213-091740](https://doi.org/10.1146/annurev-ecolsys-120213-091740)
- Rainey P. B. (1999). Adaptation of *Pseudomonas fluorescens* to the plant rhizosphere. *Environmental microbiology*, 1(3), 243-257. doi:[10.1046/j.1462-2920.1999.00040.x](https://doi.org/10.1046/j.1462-2920.1999.00040.x)
- Randall, T. E., Eckardt, K., Kakumanu, S., Price-Whelan, A., Dietrich, L. E. P., & Harrison, J. J. (2022). Sensory perception in bacterial cyclic diguanylate signal transduction. *Journal of Bacteriology*, 204(2), e0043321. doi:[10.1128/JB.00433-21](https://doi.org/10.1128/JB.00433-21)
- Ratcliff, W. C., Herron, M., Conlin, P. L., & Libby, E. (2017). Nascent life cycles and the emergence of higher-level individuality. *Philosophical Transactions of the Royal Society of London. Series B, Biological Sciences*, 372(1735). doi:[10.1098/rstb.2016.0420](https://doi.org/10.1098/rstb.2016.0420)
- Remigi, P., Ferguson, G. C., McConnell, E., De Monte, S., Rogers, D. W., & Rainey, P. B. (2019). Ribosome provisioning activates a bistable switch coupled to fast exit from stationary phase. *Molecular Biology and Evolution*, 36(5), 1056-1070. doi:[10.1093/molbev/msz041](https://doi.org/10.1093/molbev/msz041)
- Römling, U., Galperin, M. Y., & Gomelsky, M. (2013). Cyclic di-GMP: the first 25 years of a universal bacterial second messenger. *Microbiology and Molecular Biology Reviews*, 77(1), 1-52. doi:[10.1128/MMBR.00043-12](https://doi.org/10.1128/MMBR.00043-12)
- Römling, U., Gomelsky, M., & Galperin, M. Y. (2005). C-di-GMP: the dawning of a novel bacterial signalling system. *Molecular Microbiology*, 57(3), 629-639. doi:[10.1111/j.1365-2958.2005.04697.x](https://doi.org/10.1111/j.1365-2958.2005.04697.x)
- Rose, C. J., Hammerschmidt, K., Pichugin, Y., & Rainey, P. B. (2020). Meta-population structure and the evolutionary transition to multicellularity. *Ecology Letters*, 23(9), 1380-1390. doi:[10.1111/ele.13570](https://doi.org/10.1111/ele.13570)
- Rose, C. J. & Hammerschmidt, K. (2021). What do we mean by multicellularity? The evolutionary transitions framework provides answers. *Frontiers in Ecology and Evolution*, 9. doi:[10.3389/fevo.2021.730714](https://doi.org/10.3389/fevo.2021.730714)
- Ross, P., Weinhouse, H., Aloni, Y., Michaeli, D., Weinberger-Ohana, P., Mayer, R., Braun, S., de Vroom, E., van der Marel, G. A., van Boom, J. H., & Benziman, M. (1987). Regulation of cellulose synthesis in *Acetobacter xylinum* by cyclic diguanylic acid. *Nature*, 325(6101), 279-281. doi:[10.1038/325279a0](https://doi.org/10.1038/325279a0)
- Roy, A. B., Petrova, O. E., & Sauer, K. (2012). The phosphodiesterase DipA (PA5017) is essential for *Pseudomonas aeruginosa* biofilm dispersion. *Journal of Bacteriology*, 194(11), 2904-2915. doi:[10.1128/JB.05346-11](https://doi.org/10.1128/JB.05346-11)
- Rybtke, M. T., Borlee, B. R., Murakami, K., Irie, Y., Hentzer, M., Nielsen, T. E., Givskov, M., Parsek, M. R., Tolker-Nielsen, T. (2012). Fluorescence-based reporter for gauging cyclic di-GMP levels in *Pseudomonas aeruginosa*. *Applied Environmental Microbiology*, 78(15), 5060-5069. doi:[10.1128/AEM.00414-12](https://doi.org/10.1128/AEM.00414-12)

- Saavedra, J. T., Schwartzman, J. A., & Gilmore, M. S. (2017). Mapping transposon insertions in bacterial genomes by arbitrarily primed PCR. *Current Protocols in Molecular Biology*, 118. doi:[10.1002/cpmb.38](https://doi.org/10.1002/cpmb.38)
- Sachs, J. L., Mueller, U. G., Wilcox, T. P., & Bull, J. J. (2004). The evolution of cooperation. *The Quarterly Review of Biology*, 79(2), 135-160. doi:[10.1086/383541](https://doi.org/10.1086/383541)
- Schlechter, R. O., Jun, H., Bernach, M., Oso, S., Boyd, E., Muñoz-Lintz, D. A., Dobson, R. C. J., Remus, D. M., Remus-Emsermann, M. N. P. (2018). Chromatic bacteria – A broad host-range plasmid and chromosomal insertion toolbox for fluorescent protein expression in bacteria. *Frontiers in Microbiology*, 9. doi:[10.3389/fmicb.2018.03052](https://doi.org/10.3389/fmicb.2018.03052)
- Schmidt, A. J., Ryjenkov, D. A., & Gomelsky, M. (2005). The ubiquitous protein domain EAL is a cyclic diguanylate-specific phosphodiesterase: enzymatically active and inactive EAL domains. *Journal of Bacteriology*, 187(14), 4774-4781. doi:[10.1128/JB.187.14.4774-4781.2005](https://doi.org/10.1128/JB.187.14.4774-4781.2005)
- Shivaji, S., & Prakash, J. S. (2010). How do bacteria sense and respond to low temperature? *Archives of Microbiology*, 192(2), 85-95. doi:[10.1007/s00203-009-0539-y](https://doi.org/10.1007/s00203-009-0539-y)
- Silby, M. W., Cerdeño-Tárraga, A. M., Vernikos, G. S., Giddens, S. R., Jackson, R. W., Preston, G. M., Zhang, X. X., Moon, C. D., Gehrig, S. M., Godfrey, S. A., Knight, C. G., Malone, J. G., Robinson, Z., Spiers, A. J., Harris, S., Challis, G. L., Yaxley, A. M., Harris, D., Seeger, K., Murphy, L., ... Thomson, N. R. (2009). Genomic and genetic analyses of diversity and plant interactions of *Pseudomonas fluorescens*. *Genome Biology*, 10(5), R51. doi:[10.1186/gb-2009-10-5-r51](https://doi.org/10.1186/gb-2009-10-5-r51)
- Simon, R., Prierer, U., & Puhler, A. (1983). A broad host range mobilization system for in vivo genetic-engineering: Transposon mutagenesis in gram-negative bacteria. *Nature Biotechnology*, 1, 784-791. doi:[10.1038/nbt1183-784](https://doi.org/10.1038/nbt1183-784)
- Sledjeski, D. D., & Gottesman, S. (1996). Osmotic shock induction of capsule synthesis in *Escherichia coli* K-12. *Journal of Bacteriology*, 178(4), 1204-1206. doi:[10.1128/jb.178.4.1204-1206.1996](https://doi.org/10.1128/jb.178.4.1204-1206.1996)
- Sober, E., & Wilson, D. S. (1998). *Unto Others: The Evolution and Psychology of Unselfish Behavior*. Harvard University Press.
- Spiers, A. J., Kahn, S. G., Bohannon, J., Travisano, M., & Rainey, P. B. (2002). Adaptive divergence in experimental populations of *Pseudomonas fluorescens*. I. Genetic and phenotypic bases of wrinkly spreader fitness. *Genetics*, 161, 33-46. doi:[10.1093/genetics/161.1.33](https://doi.org/10.1093/genetics/161.1.33)
- Stevenson, G., Andrianopoulos, K., Hobbs, M., & Reeves, P. R. (1996). Organization of the *Escherichia coli* K-12 gene cluster responsible for production of the extracellular polysaccharide colanic acid. *Journal of Bacteriology*, 178(16), 4885-4893. doi:[10.1128/jb.178.16.4885-4893.1996](https://doi.org/10.1128/jb.178.16.4885-4893.1996)
- Summers, J. A. (2018). *Exploring the origins of multicellularity using experimental populations of Pseudomonas fluorescens SBW25: Deciphering the genetic basis of an environmentally-responsive developmental switch* (Master's thesis, Massey University, Auckland, New Zealand)

- Szathmáry, E., & Maynard Smith, J. (1995). The major evolutionary transitions. *Nature*, *374*(6519), 227-232. doi:[10.1038/374227a0](https://doi.org/10.1038/374227a0)
- Szathmáry E. (2015). Toward major evolutionary transitions theory 2.0. *PNAS USA*, *112*(33), 10104-10111. doi:[10.1073/pnas.1421398112](https://doi.org/10.1073/pnas.1421398112)
- Taddei, F., Radman, M., Maynard-Smith, J., Toupance, B., Gouyon, P. H., & Godelle, B. (1997). Role of mutator alleles in adaptive evolution. *Nature*, *387*, 700-702. doi:[10.1038/42696](https://doi.org/10.1038/42696)
- Tart, A. H., Blanks, M. J., & Wozniak, D. J. (2006). The AlgT-dependent transcriptional regulator AmrZ (AlgZ) inhibits flagellum biosynthesis in mucoid, nonmotile *Pseudomonas aeruginosa* cystic fibrosis isolates. *Journal of Bacteriology*, *188*(18), 6483-6489. doi:[10.1128/JB.00636-06](https://doi.org/10.1128/JB.00636-06)
- Ueda, A., & Wood, T. K. (2009). Connecting quorum sensing, c-di-GMP, pel polysaccharide, and biofilm formation in *Pseudomonas aeruginosa* through tyrosine phosphatase TpbA (PA3885). *PLoS Pathogens*, *5*(6), e1000483. doi:[10.1371/journal.ppat.1000483](https://doi.org/10.1371/journal.ppat.1000483)
- Vaara M. (1992). Agents that increase the permeability of the outer membrane. *Microbiological Reviews*, *56*(3), 395-411. doi:[10.1128/mr.56.3.395-411.1992](https://doi.org/10.1128/mr.56.3.395-411.1992)
- Vásquez-Ponce, F., Higuera-Llantén, S., Pavlov, M. S., Ramírez-Orellana, R., Marshall, S. H., & Olivares-Pacheco, J. (2017). Alginate overproduction and biofilm formation by psychrotolerant *Pseudomonas mandelii* depend on temperature in Antarctic marine sediments. *Electronic Journal of Biotechnology*, *28*, 27-34. doi:[10.1016/j.ejbt.2017.05.001](https://doi.org/10.1016/j.ejbt.2017.05.001)
- Verstraeten, N., Braeken, K., Debkumari, B., Fauvart, M., Fransaer, J., Vermant, J., & Michiels, J. (2008). Living on a surface: swarming and biofilm formation. *Trends in Microbiology*, *16*(10), 496-506. doi:[10.1016/j.tim.2008.07.004](https://doi.org/10.1016/j.tim.2008.07.004)
- Villegas, A., & Kropinski, A. M. (2008). An analysis of initiation codon utilization in the Domain Bacteria - concerns about the quality of bacterial genome annotation. *Microbiology*, *154*(9), 2559-2661. doi:[10.1099/mic.0.2008/021360-0](https://doi.org/10.1099/mic.0.2008/021360-0)
- Waddington, C. H. (1942). Canalization of development and the inheritance of acquired characters. *Nature*, *150*, 563-565. doi:[10.1038/150563a0](https://doi.org/10.1038/150563a0)
- Waddington, C. H. (1959). Canalization of development and genetic assimilation of acquired characters. *Nature*, *183*(4676), 1654-1655. doi:[10.1038/1831654a0](https://doi.org/10.1038/1831654a0)
- Wei, Q., Leclercq, S., Bhasme, P., Xu, A., Zhu, B., Zhang, Y., Zhang, M., Wang, S., & Ma, L. Z. (2019). Diguanylate cyclases and phosphodiesterases required for basal-level c-di-GMP in *Pseudomonas aeruginosa* as revealed by systematic phylogenetic and transcriptomic analyses. *Applied and Environmental Microbiology*, *85*(21), e01194-19. doi:[10.1128/AEM.01194-19](https://doi.org/10.1128/AEM.01194-19)

- West, S. A., Fisher, R. M., Gardner, A., & Kiers, E. T. (2015). Major evolutionary transitions in individuality. *PNAS USA*, *112*(33), 10112-19. doi:[10.1073/pnas.1421402112](https://doi.org/10.1073/pnas.1421402112)
- West, S. E., & Iglewski, B. H. (1988). Codon usage in *Pseudomonas aeruginosa*. *Nucleic Acids Research*, *16*(19), 9323-9335. doi:[10.1093/nar/16.19.9323](https://doi.org/10.1093/nar/16.19.9323)
- West-Eberhard, M. J. (2003). *Developmental Plasticity and Evolution*. Oxford University Press.
- Whitfield, C., & Roberts, I. S. (1999). Structure, assembly and regulation of expression of capsules in *Escherichia coli*. *Molecular Microbiology*, *31*(5), 1307-1319. doi:[10.1046/j.1365-2958.1999.01276.x](https://doi.org/10.1046/j.1365-2958.1999.01276.x)
- Wilson D. S. (1975). A theory of group selection. *PNAS USA*, *72*(1), 143-146. doi:[10.1073/pnas.72.1.143](https://doi.org/10.1073/pnas.72.1.143)
- Winsor, G. L., Griffiths, E. J., Lo, R., Dhillon, B. K., Shay, J. A., & Brinkman, F. S. (2016). Enhanced annotations and features for comparing thousands of *Pseudomonas* genomes in the *Pseudomonas* genome database. *Nucleic Acids Research*, *44*(D1), 646-653. doi:[10.1093/nar/gkv1227](https://doi.org/10.1093/nar/gkv1227)
- Wolpert, L., & Szathmáry, E. (2002). Multicellularity: evolution and the egg. *Nature*, *420*(6917), 745. doi:[10.1038/420745a](https://doi.org/10.1038/420745a)
- Wolpert, L. (1994). The evolutionary origin of development: cycles, patterning, privilege and continuity. *Development Supplement*, 79-84. doi:[10.1242/dev.1994.Supplement.79](https://doi.org/10.1242/dev.1994.Supplement.79)
- Yan, J., Deforet, M., Boyle, K. E., Rahman, R., Liang, R., Okegbe, C., Dietrich, L. E. P., Qiu, W., & Xavier, J. B. (2017). Bow-tie signaling in c-di-GMP: Machine learning in a simple biochemical network. *PLoS Computational Biology*, *13*(8), e1005677. doi:[10.1371/journal.pcbi.1005677](https://doi.org/10.1371/journal.pcbi.1005677)
- Yang, X., Yang, X. A., Xu, M., Zhou, L., Fan, Z., & Jiang, T. (2015). Crystal structures of YfiR from *Pseudomonas aeruginosa* in two redox states. *Biochemical and Biophysical Research Communications*, *461*(1), 14-20. doi:[10.1016/j.bbrc.2015.03.160](https://doi.org/10.1016/j.bbrc.2015.03.160)
- Yero, D., Díaz-Lobo, M., Costenaro, L., Conchillo-Solé, O., Mayo, A., Ferrer-Navarro, M., Vilaseca, M., Gibert, I., & Daura, X. (2021). The *Pseudomonas aeruginosa* substrate-binding protein Ttg2D functions as a general glycerophospholipid transporter across the periplasm. *Communications Biology*, *4*(1), 448. doi:[10.1038/s42003-021-01968-8](https://doi.org/10.1038/s42003-021-01968-8)
- Zhang, Y., Bao, Q., Gagnon, L. A., Huletsky, A., Oliver, A., Jin, S., & Langae, T. (2010). ampG gene of *Pseudomonas aeruginosa* and its role in β -lactamase expression. *Antimicrobial Agents and Chemotherapy*, *54*(11), 4772-4779. doi:[10.1128/AAC.00009-10](https://doi.org/10.1128/AAC.00009-10)